

AD-A145 142

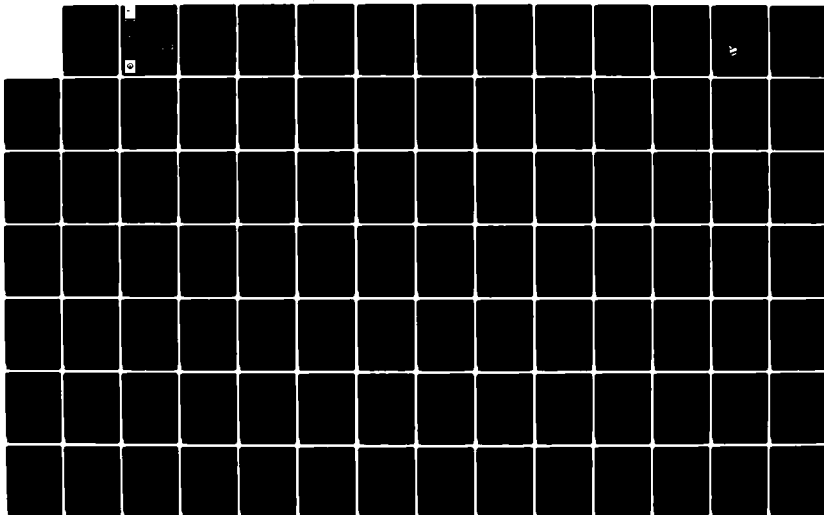
LOS ANGELES AND LONG BEACH HARBORS MODEL STUDY
NUMERICAL ANALYSIS OF TIDA..(U) COASTAL ENGINEERING
RESEARCH CENTER VICKSBURG MS W C SEABERGH ET AL.
JUN 84 CERC-MP-84-5

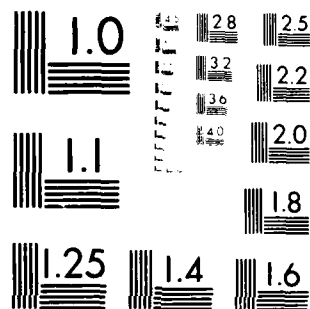
1/3

UNCLASSIFIED

F/G 8/3

NL



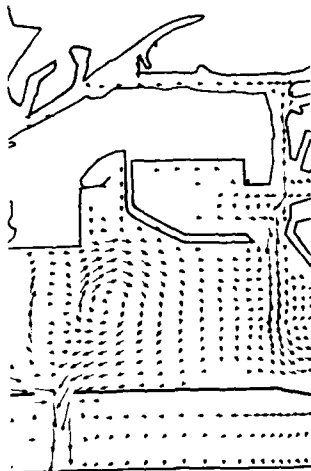


MICROCOPY RESOLUTION TEST CHART
NATIONAL BUREAU OF STANDARDS-1963-A



US Army Corps
of Engineers

AD-A145 142



DTIC FILE COPY

MISCELLANEOUS PAPER CERC-84-5

72

LOS ANGELES AND LONG BEACH HARBORS MODEL STUDY

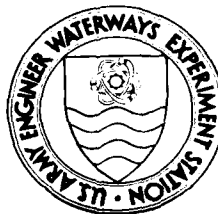
NUMERICAL ANALYSIS OF TIDAL CIRCULATION FOR THE 2020 MASTER PLAN

by

W. C. Seabergh and D. G. Outlaw

Coastal Engineering Research Center

DEPARTMENT OF THE ARMY
Waterways Experiment Station, Corps of Engineers
PO Box 631
Vicksburg, Mississippi 39180



June 1984

Final Report

Approved For Public Release; Distribution Unlimited

DTIC
ELECTE
AUG 3 0 1984
H

Prepared for

US Army Engineer District, Los Angeles
Los Angeles, California 90053

84 08 28 002

Destroy this report when no longer needed. Do not
return it to the originator.

The findings in this report are not to be construed as an
official Department of the Army position unless so
designated by other authorized documents.

The contents of this report are not to be used for
advertising, publication, or promotional purposes.
Citation of trade names does not constitute an
official endorsement or approval of the use of such
commercial products.

Unclassified

SECURITY CLASSIFICATION OF THIS PAGE (When Data Entered)

REPORT DOCUMENTATION PAGE		READ INSTRUCTIONS BEFORE COMPLETING FORM
1. REPORT NUMBER Miscellaneous Paper CERC-84-5	2. GOVT ACCESSION NO. AD-A145142	3. RECIPIENT'S CATALOG NUMBER
4. TITLE (and Subtitle) LOS ANGELES AND LONG BEACH HARBORS MODEL STUDY; NUMERICAL ANALYSIS OF TIDAL CIRCULATION FOR THE 2020 MASTER PLAN		5. TYPE OF REPORT & PERIOD COVERED Final report
7. AUTHOR(s) W. C. Seabergh and D. G. Outlaw		6. PERFORMING ORG. REPORT NUMBER
8. PERFORMING ORGANIZATION NAME AND ADDRESS US Army Engineer Waterways Experiment Station Coastal Engineering Research Center PO Box 631, Vicksburg, Miss. 39180		9. CONTRACT OR GRANT NUMBER(s)
11. CONTROLLING OFFICE NAME AND ADDRESS US Army Engineer District, Los Angeles PO Box 2711 Los Angeles, Calif. 90053		10. PROGRAM ELEMENT, PROJECT, TASK AREA & WORK UNIT NUMBERS
14. MONITORING AGENCY NAME & ADDRESS (if different from Controlling Office)		12. REPORT DATE June 1984
		13. NUMBER OF PAGES 195
		15. SECURITY CLASS. (of this report) Unclassified
		15a. DECLASSIFICATION/DOWNGRADING SCHEDULE
16. DISTRIBUTION STATEMENT (of this Report) Approved for public release; distribution unlimited.		
17. DISTRIBUTION STATEMENT (of the abstract entered in Block 20, if different from Report)		
18. SUPPLEMENTARY NOTES Available from the National Technical Information Service, 5285 Port Royal Road, Springfield, Va. 22161.		
19. KEY WORDS (Continue on reverse side if necessary and identify by block number) Harbors--Hydrodynamics (LC) Mathematical models (LC) Los Angeles (Calif.)--Harbor (LC) 2020 Master Plan (WES) Long Beach (Calif.)--Harbor (LC) Tidal currents (LC)		
20. ABSTRACT (Continue on reverse side if necessary and identify by block number) A study to determine the effect of the proposed 2020 Master Plan on tidal circulation in Los Angeles and Long Beach Harbors was conducted using a numerical model with a two-dimensional depth-averaged formulation of the hydrodynamic equations. The model, which had been verified in a previous study, used an implicit finite-difference scheme to numerically solve the equations. To observe the dispersion of conservative substances, the model also incorporated the two-dimensional conservative constituent transport equations. (Continued)		

DD FORM 1 JAN 73 1473

EDITION OF 1 NOV 65 IS OBSOLETE

Unclassified

SECURITY CLASSIFICATION OF THIS PAGE (When Data Entered)

Unclassified

SECURITY CLASSIFICATION OF THIS PAGE(When Data Entered)

20. ABSTRACT (Concluded)

The 2020 Master Plan consists of placing 2600 acres of landfill at various locations throughout the harbors. Tidal circulation was studied for 70-hr sequences of spring, mean, and neap tides for each of three harbor configurations: (1) existing configuration (1983), (2) landfills placed on existing bathymetry, and (3) landfills placed with increased channel depths.

The 2020 Master Plan produced no changes in tidal elevation or phase throughout the harbors. The tidal prism was reduced by the amount of displacement of the landfill. Flow distribution entering and exiting the harbor through Angel's Gate, Queen's Gate, and the east end were not significantly affected. The net flow in the inner harbor (Main Channel and Cerritos Channel) was reversed from the existing westerly flow to an easterly flow; however, the net flow volumes for both existing and planned conditions were small relative to the total flow volumes. Channel deepening combined with the 2020 Master Plan reduced large horizontal eddies in the outer harbor, permitting more efficient flow into the inner harbor area from Angel's Gate to the Main Channel. Dye tests indicated good flushing and mixing in the outer harbor.

Unclassified

SECURITY CLASSIFICATION OF THIS PAGE(When Data Entered)

PREFACE

Expansion of ship mooring facilities for the Ports of Los Angeles and Long Beach is planned to meet future demand. This report, the eighth to be published by the U. S. Army Engineer Waterways Experiment Station (WES) under the general title Los Angeles and Long Beach Harbors Model Study, presents results of a numerical model tidal circulation study performed for the 2020 Master Plan, which has been designed to provide for future port needs.

This project was administered and funded by the U. S. Army Engineer District, Los Angeles (SPL), under project management of Mr. D. Muslin and under the general direction of Mr. P. Berger, Chief, Coastal Resources Branch. COL P. C. Taylor, CE, was the District Engineer of SPL during the course of this study. General project administration for the U. S. Army Engineer Division, South Pacific, was provided by Messrs. A. E. Wanket and J. R. Edmisten.

This numerical model investigation was initiated by the Wave Dynamics Division (WDD), Hydraulics Laboratory (HL), WES, under the general supervision of Messrs. H. B. Simmons and F. H. Herrmann, Jr., Chief and Assistant Chief, respectively, HL. In July 1983, the Wave Dynamics Division was transferred to the Coastal Engineering Research Center (CERC) under the general supervision of Drs. R. W. Whalin and L. E. Link, Chief and Assistant Chief, respectively, and the direction of Mr. C. E. Chatham, Chief, WDD, and Mr. D. G. Outlaw, Chief, Wave Processes Branch. This report was prepared by Mr. W. C. Seabergh, Project Engineer, and Mr. Outlaw.

Commander and Director of WES during the course of this study and the preparation of this report was COL Tilford C. Creel, CE. Technical Director was Mr. F. R. Brown.

Accession For	
NTIS GRA&I	<input checked="" type="checkbox"/>
DTIC TAB	<input type="checkbox"/>
Unannounced	<input type="checkbox"/>
Justification	
By	
Distribution/	
Availability Codes	
Avail. Codes	
GPO	
A-1	



CONTENTS

	<u>Page</u>
PREFACE	1
CONVERSION FACTORS, INCH-POUND TO METRIC (SI)	
UNITS OF MEASUREMENT	3
PART I: INTRODUCTION	4
Objective	4
Background	4
PART II: NUMERICAL MODEL FORMULATION	8
Hydrodynamic Equations	8
Finite-Difference Formulation	10
Addition of Constituent Transport Equation	11
Application to San Pedro Bay	13
PART III: THE 2020 MASTER PLAN ANALYSIS OF RESULTS	17
Model Data Summary	17
Tidal Elevation and Phase	17
Tidal Velocity	21
Tidal Discharges	23
Tidal Flow Volumes	24
Tidal Circulation--Velocity Vector Plots	28
Dye Movement	34
PART IV: CONCLUSIONS	36
REFERENCES	38
TABLES 1-4	
PLATES 1-153	

CONVERSION FACTORS, INCH-POUND TO METRIC (SI)
UNITS OF MEASUREMENT

Inch-pound units of measurement used in this report can be converted to metric (SI) units as follows:

<u>Multiply</u>	<u>By</u>	<u>To Obtain</u>
acres	4046.856	square metres
cubic feet	0.02831685	cubic metres
cubic feet per second	0.02831685	cubic metres per second
feet	0.3048	metres
feet per second	0.3048	metres per second
miles (U. S. statue)	1.60934	kilometres
square miles (U. S. statue)	2.589998	square kilometres

LOS ANGELES AND LONG BEACH HARBORS MODEL STUDY
NUMERICAL ANALYSIS OF TIDAL CIRCULATION FOR
THE 2020 MASTER PLAN

PART I: INTRODUCTION

Objective

1. The purpose of the numerical analysis described herein was to investigate tidal circulation in existing basins of Los Angeles and Long Beach Harbors for spring, mean, and neap tidal conditions and to evaluate the impact of the 2020 Master Plan on existing harbor circulation for a range of tidal conditions.

Background

2. Los Angeles and Long Beach Harbors are located adjacent to each other and share a common breakwater system that encloses one of the largest harbor systems in the world. Their location on San Pedro Bay along the southern coast of California is shown in Figure 1. The various channels and basins are shown in Figure 2. In order to accommodate increased shipping activities, extensive expansion of facilities is anticipated, and as a result, careful and comprehensive planning is required. As a part of the planning and design process, the Port of Los Angeles, the Port of Long Beach, and the U. S. Army Corps of Engineers are working together to evaluate the effects of expansion on tidal circulation and harbor resonance.

3. A physical model of Los Angeles and Long Beach Harbors was constructed at the U. S. Army Engineer Waterways Experiment Station (WES) to investigate tidal circulation and wave-induced oscillations in the harbors for present conditions and for proposed plans; McAnally (1975) reported on tidal verification. Numerical models also have been used for tidal circulation studies when necessary (Raney 1976 a, b; Outlaw and Raney 1976; Outlaw 1983); these numerical studies were conducted during periods in which harbor resonance wave tests were being conducted in the physical model.

4. The numerical tidal circulation model used during this study is a

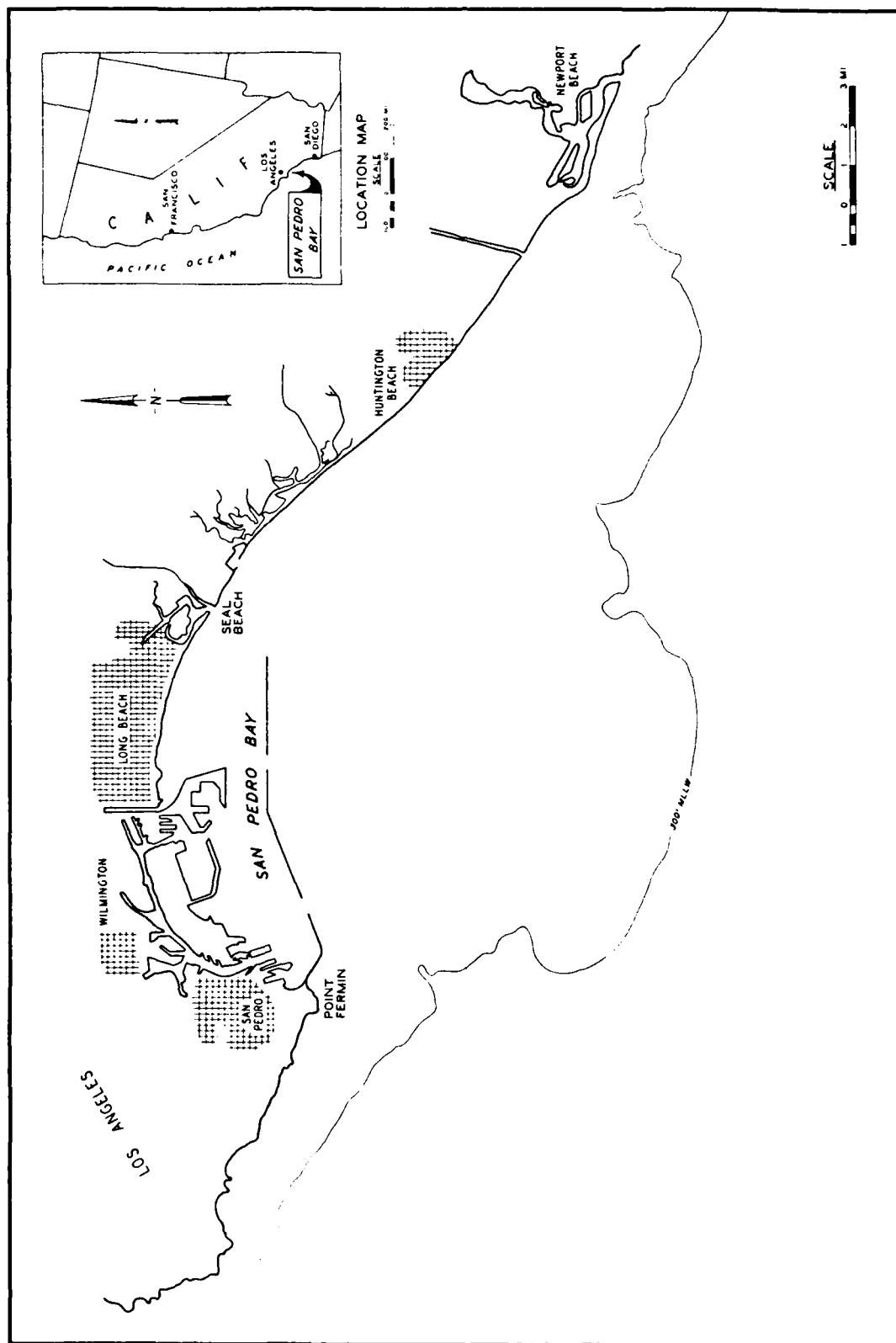


Figure 1. Site map

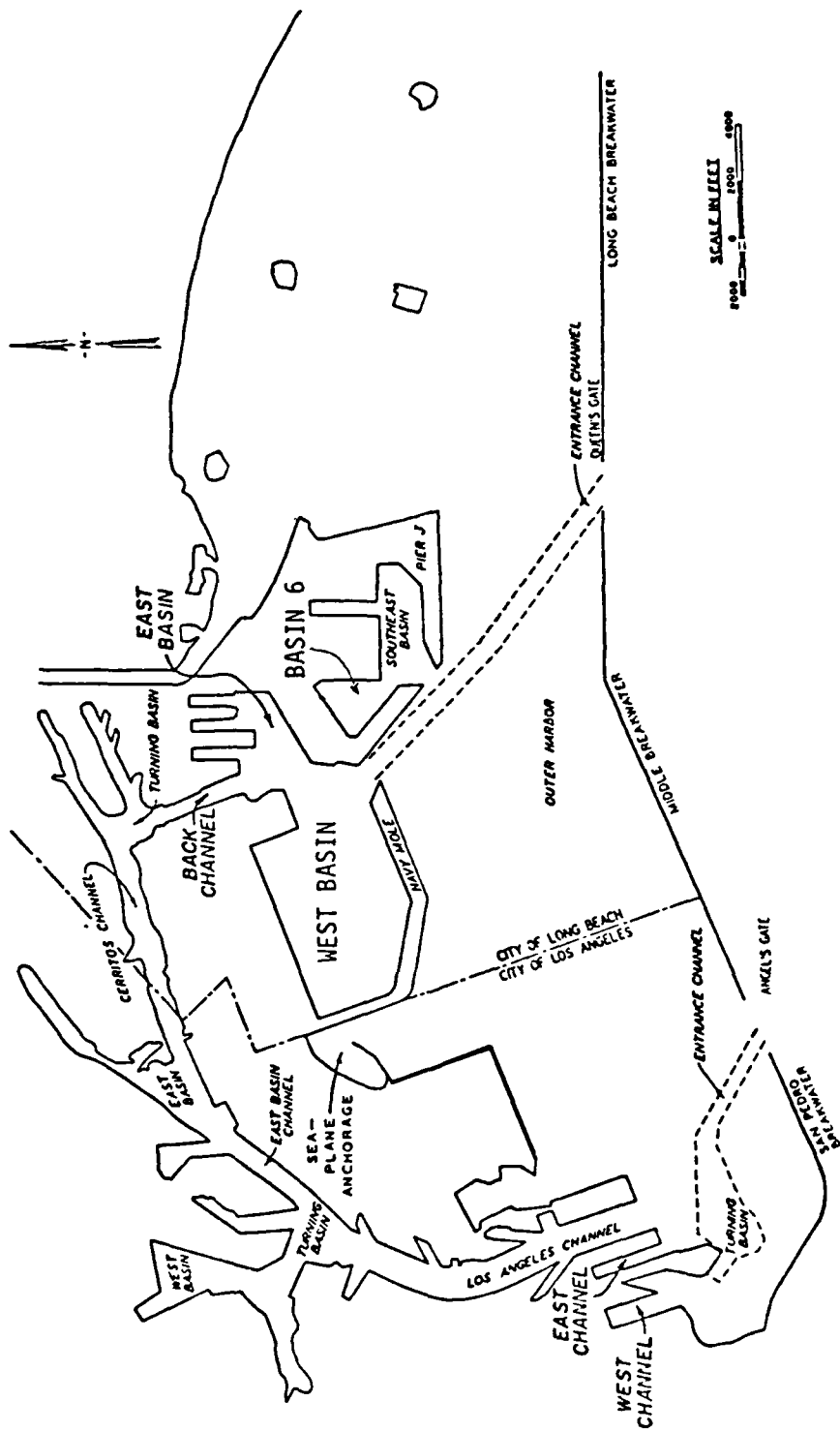


Figure 2. Location of city boundary and various channels and basins in Los Angeles and Long Beach Harbors

two-dimensional, depth-averaged, second order finite-difference solution to the hydrodynamic equations. The model was developed for application requiring the simulation of tidal hydrodynamics and is referred to as the Waterways Experiment Station Implicit Flooding Model (WIFM). Although the model has the capability to allow for flooding of low-lying terrain, this option was not required for the present study.

5. The 2020 Master Plan, illustrated in Figure 3, consists of placing landfills within the harbors where indicated by the shaded regions and increasing basin and channel depths* as indicated. The plan calls for 1104 acres of landfill in Los Angeles Harbor and 1596 acres in Long Beach Harbor. A portion of the landfill (666 acres) is to be located outside the existing harbor breakwater system, requiring construction of an access connector from the large central landfill (1265 acres). A trestle-type connector structure is envisioned between these "island" fills to enhance harbor circulation. The outer harbor trestle (connecting the island outside the breakwater to the large island inside) would contain a swing bridge to permit ship transit between the harbors.

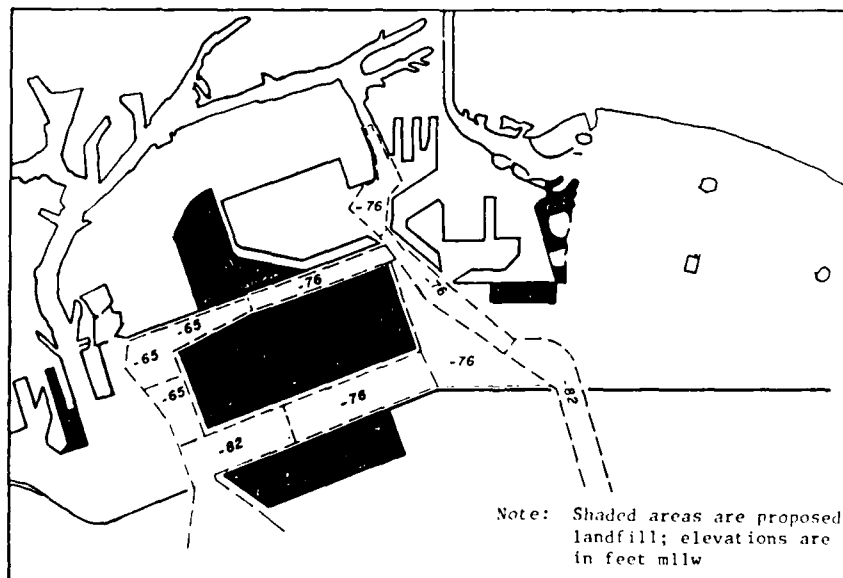


Figure 3. 2020 Master Plan

* A table for converting the inch-pound units of measurement used in this report to metric (SI) units can be found on page 3.

PART II: NUMERICAL MODEL FORMULATION

Hydrodynamic Equations

6. Formulation of the numerical model is described in detail in several reports and papers (Butler 1978 a,b,c and 1980) and is summarized in this section. Equations of fluid flow used in WIFM are derived from the classical Navier-Stokes equations in a Cartesian coordinate system (Figure 4). The familiar two-dimensional form of the equations of momentum and continuity is obtained by assuming that vertical accelerations are small and the fluid is homogeneous and by integrating the flow from sea bottom to water surface. A major advantage of WIFM is its ability to apply a smoothly varying grid to the given study

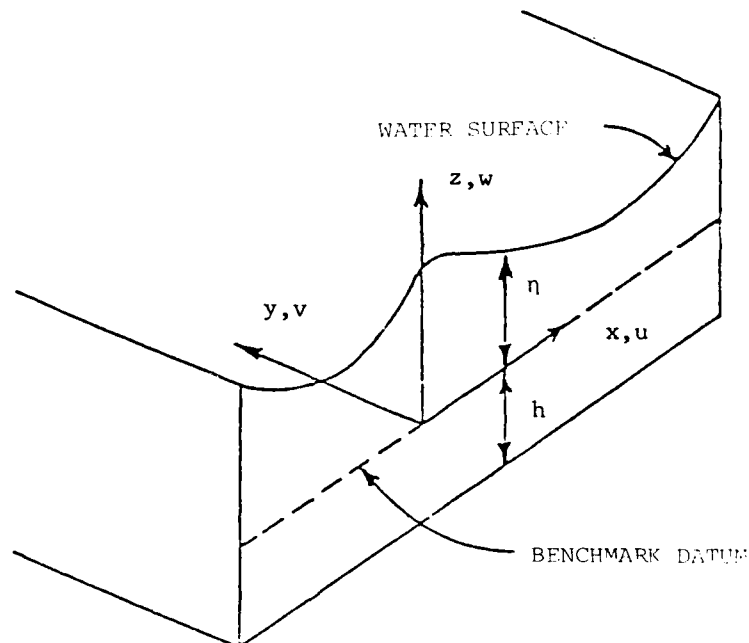


Figure 4. Cartesian coordinate system

region, permitting simulation of a complex landscape by locally increasing grid resolution and/or aligning coordinates along physical boundaries. A piecewise reversible transformation is used for each direction to map prototype or real (x) space into computational (x) space. The transformation takes the form

$$x = a + b \eta_1^c \quad (1)$$

where a , b , and c are arbitrary constants. Application of a smoothly varying grid transformation whose functional as well as its first derivatives are continuous eliminates many stability problems commonly associated with variable grid schemes, provided that all derivatives are centered in ξ -space. By applying transformations patterned on Equation 1 to both the x and y coordinates, the equations of motion in ξ -space can be written as follows for momentum

$$\begin{aligned}
 u_t + \frac{1}{a_1} uu_{\xi_1} + \frac{1}{b_2} vu_{\xi_2} - fv + \frac{g}{a_1} (\eta - \eta_d)_{\xi_1} + \frac{gu}{c_d^2} (u^2 + v^2)^{1/2} \\
 - \left[\left(\frac{1}{a_1} \right)^2 u_{\xi_1 \xi_1} + \frac{1}{a_1} \left(\frac{1}{a_1} \right)_{\xi_1} u_{\xi_1} + \left(\frac{1}{a_2} \right)^2 u_{\xi_2 \xi_2} \right. \\
 \left. + \frac{1}{b_2} \left(\frac{1}{b_2} \right)_{\xi_2} u_{\xi_2} \right] = F_{\xi_1}
 \end{aligned} \quad (2)$$

$$\begin{aligned}
 v_t + \frac{1}{a_1} uv_{\xi_1} + \frac{1}{b_2} vv_{\xi_2} + fu + \frac{g}{b_2} (\eta - \eta_d)_{\xi_2} + \frac{gv}{c_d^2} (u^2 + v^2)^{1/2} \\
 - \left[\left(\frac{1}{a_1} \right)^2 v_{\xi_1 \xi_1} + \frac{1}{a_1} \left(\frac{1}{a_1} \right)_{\xi_1} v_{\xi_1} + \left(\frac{1}{b_2} \right)^2 v_{\xi_2 \xi_2} \right. \\
 \left. + \frac{1}{b_2} \left(\frac{1}{b_2} \right)_{\xi_2} v_{\xi_2} \right] = F_{\xi_2}
 \end{aligned} \quad (3)$$

and for continuity

$$\eta_t + \frac{1}{a_1} (du)_{\xi_1} + \frac{1}{b_2} (dv)_{\xi_2} = R \quad (4)$$

where

u = vertically integrated velocity at time t in the ξ_1 direction

t = time

$a_1 = \frac{\partial x}{\partial \xi_1}$ = quantities stretching the regular-spaced computational grid

$b_2 = \frac{\partial y}{\partial \xi_2}$ in ξ -space to approximate a study region in real space

α_1 = x-direction

α_2 = y-direction

v = vertically integrated velocity at time t in the α_2 direction

f = Coriolis parameter

g = acceleration due to gravity

η = water-surface elevation

η_a = hydrostatic elevation corresponding to the atmospheric pressure anomaly

C = Chezy frictional coefficient

$d = \eta - h$ = total water depth

ϵ = generalized eddy viscosity coefficient

F = external forcing function (e.g. windstress)

R = rate at which additional water is introduced into or taken from the system (e.g. through rainfall or evaporation)

h = still-water elevation

Subscripts α_1 , α_2 , and t denote differentiation with respect to α_1 ,

α_2 , or t (i.e., $u_{\alpha_1} = \frac{\partial u}{\partial \alpha_1}$).

Finite-Difference Formulation

7. A numerical technique is necessary to obtain a solution to the governing nonlinear partial differential equations on a region with highly complex geometry and bathymetry. A variable rectilinear grid is first developed for the model area. Appropriate variables are defined on the grid in a space-staggered fashion as depicted in Figure 5 for a typical cell. The partial differential equations (Equations 2-4) are approximated by difference equations and solved implicitly using an alternating-direction three-time-level scheme.

8. Tidal surface elevations were given as a function of time at the seaward boundary of the computational grid. The water-surface elevation time history applied at the boundary is the forcing function driving the hydrodynamic system.

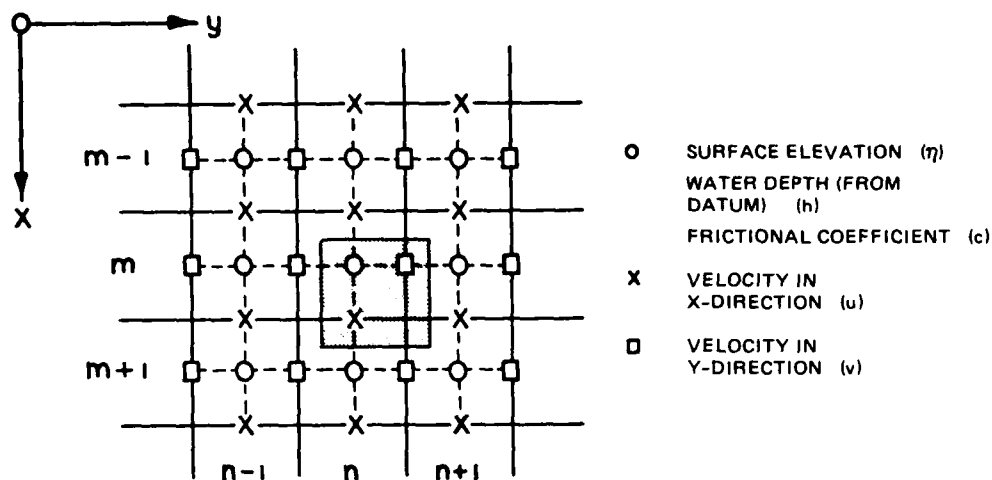


Figure 5. Space-staggered scheme

Addition of Constituent Transport Equation

9. Schmalz (1983) modified WIFM to include a solution to the transport equation. Starting from the three-dimensional passive constituent transport equation for laminar flow, modifications for turbulent flow were made and then the equation was depth integrated and transformed using an exponential mapping analogous to that performed for the hydrodynamic equations.

10. The constituent transport equation is given for laminar flow as

$$\frac{\partial s}{\partial t} + u \frac{\partial s}{\partial x} + v \frac{\partial s}{\partial y} + w \frac{\partial s}{\partial z} = \frac{\partial}{\partial x} \left(D_x \frac{\partial s}{\partial x} \right) + \frac{\partial}{\partial y} \left(D_y \frac{\partial s}{\partial y} \right) + \frac{\partial}{\partial z} \left(D_z \frac{\partial s}{\partial z} \right) \quad (5)$$

where

s = concentration of the material of concern

t = time

u, v, w = velocity components in the x , y , and z directions, respectively

x, y, z = Cartesian coordinates

D_x = molecular diffusion coefficient in the x direction

D_y = molecular diffusion coefficient in the y direction

D_z = molecular diffusion coefficient in the z direction

Eddy dispersion is much greater than molecular diffusion for turbulent flow. Equation 6 holds for turbulent flow where time averaging over the time scale of the turbulence has been performed.

$$\frac{\partial s}{\partial t} + u \frac{\partial s}{\partial x} + v \frac{\partial s}{\partial y} + w \frac{\partial s}{\partial z} = \frac{\partial}{\partial x} K_x \frac{\partial s}{\partial x} + \frac{\partial}{\partial y} K_y \frac{\partial s}{\partial y} + \frac{\partial}{\partial z} K_z \frac{\partial s}{\partial z} \quad (6)$$

where K_x , K_y , and K_z are turbulent eddy dispersion coefficients. Using the continuity equation, Equation 6 may be rewritten as

$$\frac{\partial s}{\partial t} + \frac{\partial (us)}{\partial x} + \frac{\partial (vs)}{\partial y} + \frac{\partial (ws)}{\partial z} = \frac{\partial}{\partial x} K_x \frac{\partial s}{\partial x} + \frac{\partial}{\partial y} K_y \frac{\partial s}{\partial y} + \frac{\partial}{\partial z} K_z \frac{\partial s}{\partial z} \quad (7)$$

Integration of Equation 7 over the depth (described in Schmalz (1983)) yields

$$\frac{\partial}{\partial t} (hs) + \frac{\partial}{\partial x} (hus) + \frac{\partial}{\partial y} (hvs) = \frac{\partial}{\partial x} \left(hK_x^* \frac{\partial s}{\partial x} \right) + \frac{\partial}{\partial y} \left(hK_y^* \frac{\partial s}{\partial y} \right) \quad (8)$$

where h is the water depth and K_x^* and K_y^* are effective dispersion coefficients.

11. Effective dispersion coefficients K_x^* and K_y^* are assumed to have the following forms:

$$K_x^* = C_x \sqrt{g} \frac{|u|h}{C} + D_x \quad (9)$$

$$K_y^* = C_y \sqrt{g} \frac{|v|h}{C} + D_y \quad (10)$$

where

K_x^* , K_y^* = effective dispersion coefficients in the x and y directions, respectively

g = acceleration due to gravity

u, v = velocity components in the x and y directions, respectively

h = water depth

C = Chezy coefficient

C_x, C_y = dispersion factors in the x and y directions, respectively

D_x, D_y = dispersion offsets due to wind effects in the x and y directions, respectively, ($D_x, D_y > 0$)

12. Transforming Equation 8 in x-y space to α_1 - α_2 space produces the following result:

$$(ds)_t + \frac{(dus)_{\alpha_1}}{\mu_1} + \frac{(dvs)_{\alpha_2}}{\mu_2} = \frac{1}{\mu_1} \left[dK_{\alpha_1} \frac{(s)_{\alpha_1}}{\mu_1} \right]_{\alpha_1} + \frac{1}{\mu_2} \left[dK_{\alpha_2} \frac{(s)_{\alpha_2}}{\mu_2} \right]_{\alpha_2} \quad (11)$$

where d is introduced as the depth in place of h and

$$(\)_t = \partial/\partial t$$

$$(\)_{\alpha_1} = \partial/\partial \alpha_1$$

$$(\)_{\alpha_2} = \partial/\partial \alpha_2$$

Equation 11 was approximated by the Flux Corrected Transport Scheme (FCT) as discussed in Schmalz (1983).

Application to San Pedro Bay

13. The study area included in the numerical model is shown in Figure 6. This area was represented by a smoothly varying finite-difference grid with x and y axes parallel to the east-west and north-south model limits, respectively (see Figure 6). The total grid included 128 cells in the x-direction and 94 cells in the y-direction (12,032 total cells). Minimum cell width was 235 ft, and the maximum width was 1463 ft. Smaller cells were concentrated in the outer harbor area and the inner harbor channels to provide better circulation definition for the harbor area, as seen in Figure 7. The grid extended seaward of the middle breakwater approximately 4.2 miles and covered an area of about 146 sq miles. The grid was aligned to coincide with the inner harbor entrance channels.

14. Input data for each cell in the grid included the bottom elevation relative to mean lower low water (mllw), which then was converted to the

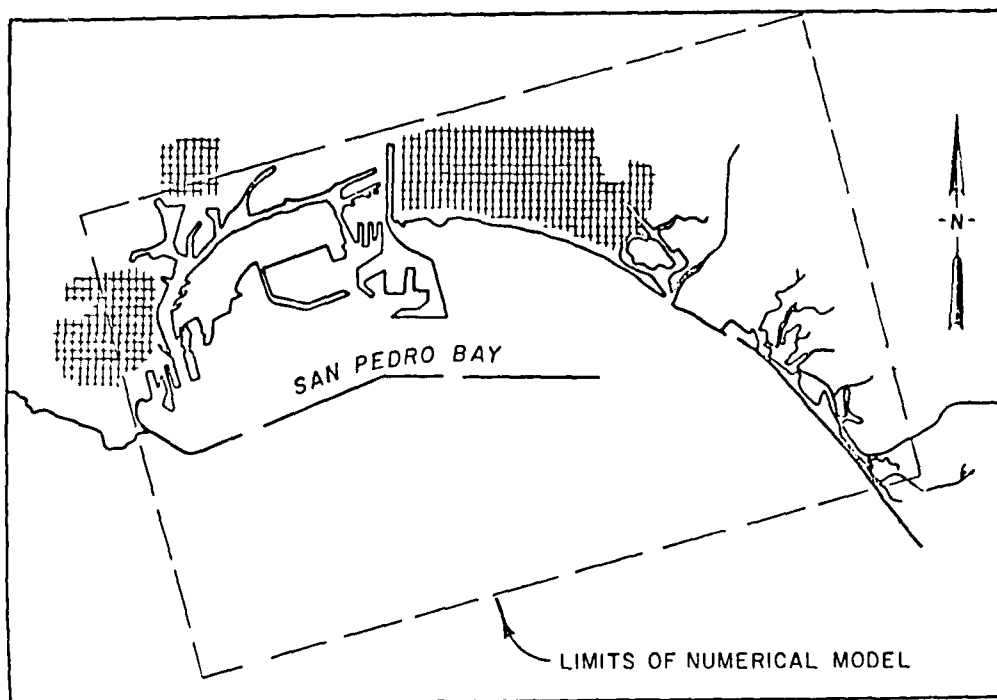


Figure 6. Limits of the model finite-difference grid

National Geodetic Vertical Datum of 1929 (NGVD). NGVD is 2.7 ft above mllw in Los Angeles and Long Beach Harbors. A friction characteristic of each cell was expressed in terms of Manning's n , which then was converted internally to a Chezy frictional coefficient by the relation

$$C = \frac{1.49}{n} d^{1/6}$$

with d equalling the total water depth. Other parameters required for input were the eddy viscosity coefficient, $\nu = 0.25$; dispersion factors C_x and C_y in Equations 9 and 10, chosen as 10.0 for each direction; and items such as gage locations, printout and plot controls, and other logic control parameters. A 90-sec time-step was used for the simulations, and the tide signal was input along the ocean boundary as a function of time. Three sets of tidal input were used, representing typical spring, neap, and mean tide conditions. These input tides were determined by a separate computer program which used 21 tidal elevation constituents to calculate the water surface variation. The tidal constituents had been previously determined by the National Ocean Service. The spring tide, a tide of increased range (relative to the mean) which

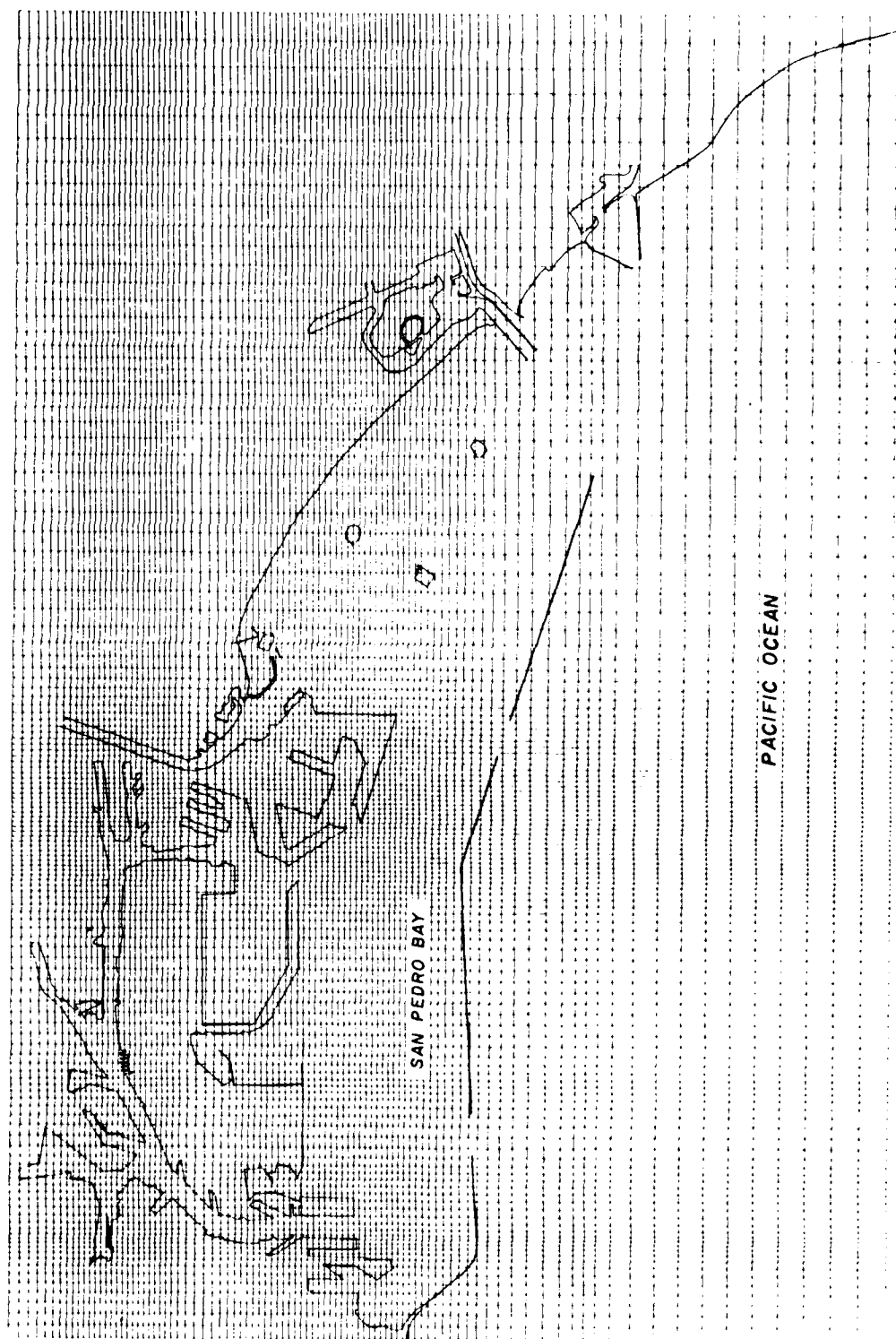


Figure 7. Grid layout over the harbor

occurs semimonthly as a result of the Moon being new or full, had a maximum range of 7.2 ft. The neap tide, a tide of decreased range, occurring semimonthly as a result of the Moon being in quadrature, had a maximum range of 3.5 ft. Finally, the mean tide showed a maximum range of 5.5 ft.

15. The numerical model calculates a water surface elevation and velocity components u and v in the x - and y -directions, respectively, for each grid point (or computational cell, see Figure 5). Plots of these elevations or velocities may be made for any selected cell location. A string of these cells may be used to compute a flow discharge through a given region, such as the entrance at Angel's Gate (see Figure 2), by summing the product of the velocity component perpendicular to the channel cross section and the area through which the velocity flows for all the cells in the string. This produces an instantaneous discharge value with units of cubic feet per second. For this study, discharges are calculated every eight time steps (or every 720 seconds, prototype time). If a discharge value is multiplied by 720 seconds, the volume of water moving through a certain cross-sectional area for the 720-second time period may be computed, having units of cubic feet (since cubic feet per second \times seconds = cubic feet). These flow volumes can be summed over a given time period--usually over one, two, or four tidal cycles--adding flood flow volumes and ebb flow volumes separately, with the difference between the two being net flow volumes. It is important to start and end the summary interval at the same water level so that there is no net storage on one side of the discharge and flow volume cross section.

PART III: THE 2020 MASTER PLAN ANALYSIS OF RESULTS

Model Data Summary

16. Tidal elevation stations, velocity stations, discharge/flow volume ranges, and direction of flow are shown in Figures 8 and 9 for the numerical simulation of tidal hydrodynamics for the existing conditions and two 2020 Master Plan conditions. The two 2020 Master Plan conditions, or configurations, were these:

- a. The landfills (see Figure 3) were placed on the existing depth grid; i.e. on the same depth grid as that used for the existing conditions testing.
- b. The landfills were placed and depths increased to those shown in Figure 3.

Spring, mean, and neap tidal conditions were run for each configuration, making a total of nine simulation runs. Each simulation was 70 hours in duration. At Hour 18 of each simulation a "dye slug" was released at the two locations shown in Figure 10 and allowed to disperse throughout the harbor for the remainder of the test run. Velocity vectors also were computed and plotted for every second computation cell. Selected plots are presented herein; plots made every two hours of the simulation, starting at Hour 18, are on file at WES.

Tidal Elevation and Phase

17. Tide elevation data for existing conditions and both 2020 Master Plan conditions are compared on Plates 1-12 for Stations 9, 10, 16, and 19 (Plates 1-3 show results at Station 9 for the spring, mean, and neap tide conditions, respectively, and results are presented similarly for the other stations). Hourly tidal elevation plots indicate no discernable differences in amplitude or phase. Other tidal elevation stations shown in Figure 8, but not included in this report, also indicated no amplitude or phase change. These data are on file at WES. From these results it can be concluded that the 2020 Master Plan has little effect on tidal elevations or phase throughout the Los Angeles and Long Beach Harbors.

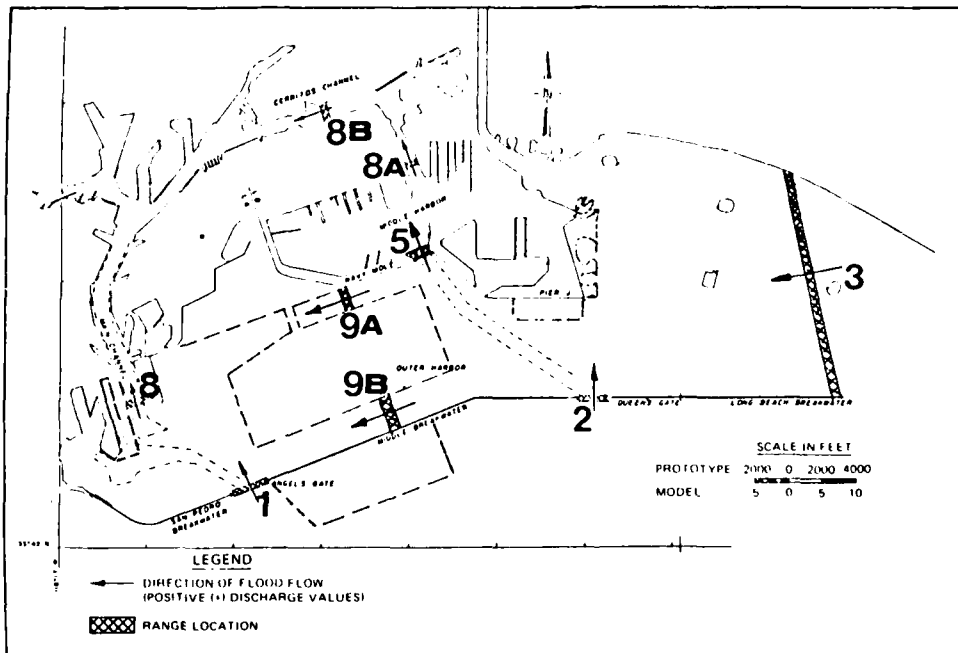


Figure 9. Locations of discharge and flow volume ranges and directions

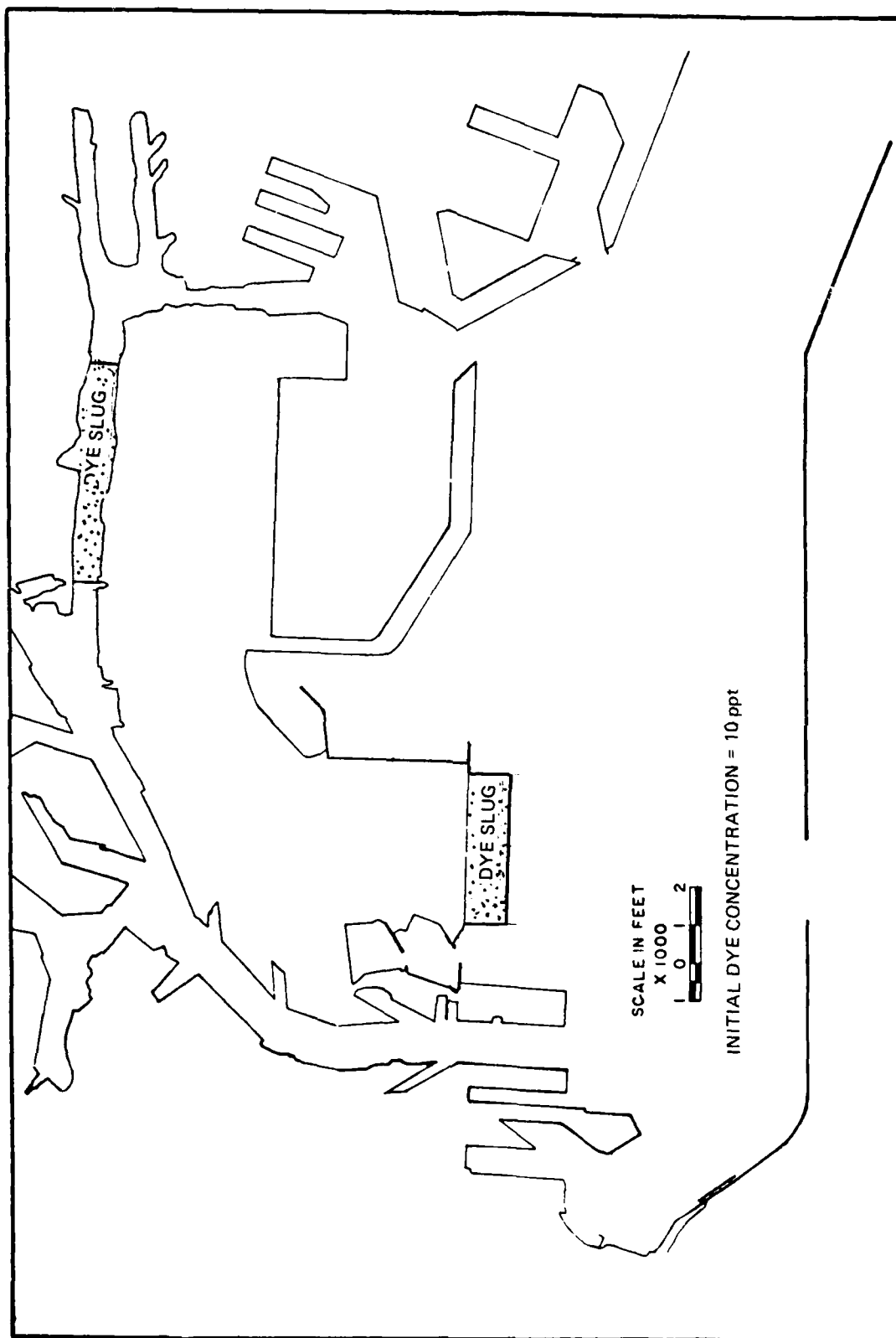


Figure 10. Initial dye slug locations

Tidal Velocity

18. Velocity data are presented in Plates 13-54. Spring, mean, and neap tidal velocities for the center stations at Ranges 1-3, which control the flow into and out of the harbors (see Figure 8 for locations), are shown on Plates 13-21.

19. Velocities at Station 1B (Plates 13-15) located at Angel's Gate indicated, for the most part, reductions in velocity for both of the 2020 Master Plans at this entrance. For the 2020 Plan with existing depths (abbreviated 2020-ED) the reduction was more consistent during ebb velocities, with peak ebb velocity reductions from 0 to 40 percent. Flood velocities were not reduced so much for 2020-ED; and during the flood phase, starting at Hour 50 (for spring tide), flood velocities at Station 1B were greater for 2020-ED than for existing conditions. These flood velocity changes were attributable to the following two effects of the landfill: (a) reduction of the tidal prism which produced slight velocity reductions for 2020-ED; and (b) interruption of the gyre in the outer harbor which reduced the ebb return flow, hence the ebb flow momentum, toward Angel's Gate, permitting initial flood velocities to enter through Angel's Gate more efficiently. This reasoning was further reinforced by the fact that the 2020-ED flood velocities were greater relative to the base after a short ebb tide fall (smaller ebb velocities) than after a long ebb tide fall. The reduction of velocities for the 2020 Plan with dredged channels (2020-DC) was due to the increased cross-sectional area at the velocity range; i.e., the depth increase from -54 ft, NGVD to -85 ft, NGVD provided a cross-sectional area increase of 1.574 times the original area. Velocity reduction due to this factor alone would be about 63 percent, and reductions in velocity on this order occurred for 2020-DC. Mean and neap tide currents at Station 1B followed the same trends as the spring tide data. Maximum spring tide velocities at 1B were:

	<u>Existing</u>	<u>2020-ED</u>	<u>2020-DC</u>
Maximum ebb velocity, ft/sec	0.95	0.75	0.52
Maximum flood velocity, ft/sec	0.88	0.88	0.57

20. Station 2E, the midchannel station at Queen's Gate, had velocity magnitude changes that varied inversely with those at Station 1B. Plate 16 shows that the 2020-ED plan produced a reduction in flood velocities but maintained

almost identical ebb velocity magnitudes. Therefore, Range 2 had captured a portion of the ebb flow of Range 1 but lost some flood flow to Range 1. Mean and neap tide data at Station 2E showed similar responses to the spring tide data (Plates 17 and 18). Maximum spring tide velocities at Station 2E were:

	<u>Existing</u>	<u>2020-ED</u>	<u>2020-DC</u>
Maximum ebb velocity, ft/sec	0.95	0.92	0.60
Maximum flood velocity, ft/sec	0.80	0.67	0.47

21. Station 3H data were representative of the other Range 3 Stations (3G and 3I), indicating only slight change in velocities entering or exiting the harbor from the east opening near Alamitos Bay. Plates 19-21 show the velocities for the three tidal conditions. Maximum spring tide velocities were:

	<u>Existing</u>	<u>2020-ED</u>	<u>2020-DC</u>
Maximum ebb velocity, ft/sec	0.41	0.39	0.35
Maximum flood velocity, ft/sec	0.31	0.28	0.28

22. Station 5M (adjacent to the Navy Mole, see Figure 8) velocities (Plates 22-24) indicated the 2020-ED flood velocities increased over the existing conditions but returned to just below existing condition levels for the 2020-DC configuration. Dredging increased depths from -60 ft to -79 ft, NGVD. Ebb velocities were slightly reduced for the 2020-DC condition, while existing condition and 2020-ED ebb velocities were similar. Maximum spring tide velocities at station 5M were:

	<u>Existing</u>	<u>2020-ED</u>	<u>2020-DC</u>
Maximum ebb velocity, ft/sec	0.54	0.52	0.46
Maximum flood velocity, ft/sec	0.46	0.55	0.40

23. Velocities at Stations 8Y, 8A-P, and 8BR (Plates 25-33) showed very minor changes from one condition to another at these low-velocity values (less than about 0.38 ft/sec), and the analysis of flow variation at the ranges of these stations will be better illustrated by examining the flow volumes through these ranges in a later section of this report.

24. Station 9A (Plates 34-36), located near the middle breakwater in the outer harbor, indicated that for existing conditions there was a constant, low-magnitude (about 0.1 ft/sec), westerly flow along the middle breakwater. The introduction of the 2020-ED plan produced a predominantly eastern flow, since the outer harbor circulation gyre had been interrupted and flood flow through Range 1 was increased. Spring tide maximum velocities were 0.2 ft/sec.

Deepening the channels for 2020-DC reduced the maximum velocities and permitted a reversing flow (i.e. spring tide maximum ebb and flood velocities of 0.1 ft/sec).

25. Plates 37-39 show velocities at Station 9B for both plans, only. This station was adjacent to the west end of the landfill in the outer harbor. Maximum spring tide flood currents were 0.50 ft/sec for 2020-ED and 0.23 ft/sec for 2020-DC. Maximum spring tide ebb currents were 0.32 ft/sec and 0.20 ft/sec for 2020-ED and 2020-DC, respectively. These results indicate strong flood-flow predominance for 2020-ED and more balanced flow for 2020-DC. Neap tide results (Plate 39) indicated very low velocities and no noticeable difference between plans.

26. Station 9C velocities (Plates 40-42) indicated a flood flow predominance at this location east of the main landfill on the edge of the existing channel. Peak spring tide flood velocities were 0.20 ft/sec for 2020-ED and 0.10 ft/sec for 2020-DC, and peak ebb velocities were 0.08 ft/sec for both plans.

27. Station 9D velocities (Plates 43-45) were predominantly eastward along the Navy Mole, with a maximum spring tide magnitude of 0.21 ft/sec for 2020-ED and 0.25 ft/sec for 2020-DC. Velocities for neap tide conditions were low but did have a greater proportion of westward movement than for spring and mean tides, with a maximum of 0.06 ft/sec eastward and 0.04 ft/sec westward.

28. Range 10 velocities are shown on Plates 46-53. Station 10A indicated reduced velocities for the plans (Plates 46-48), though the basic pattern of flow remained the same; i.e., there is essentially a net ebb velocity at this location. Station 10B velocities showed slight increases over base conditions, and Station 10C (Plate 53) indicated a predominant ebb flow for the plans as compared to the more oscillatory flood and ebb for the existing conditions.

Tidal Discharges

29. Hourly tidal discharges for Ranges 1, 2, 3, 5, 8, 8A, 8B, 9A, and 9B (see Figure 9 for locations) are shown in Plates 55-81; the spring, mean, and neap discharges are presented for each range. Maximum ebb and flood peak discharge values are presented in Table 1. Generally, as Plates 55-59 and Table 1 indicate, for Ranges 1 (Angel's Gate) and 2 (Queen's Gate) the 2020 Master Plan with existing depths caused a reduction in discharges on ebb and flood flows; the dredging of channels increased the discharges, but not to

existing condition levels. These reductions are to be expected because of the loss of tidal prism due to the landfills.

30. Range 3 (Plates 61-63) indicates reduced discharges for both plans. Flood discharges for each plan condition remain fairly close to each other, but ebb discharge values are lower for the dredged plan than for the plan with existing depths, indicating a shift of ebb flow from Range 3 to the dredged channels at Ranges 1 and 2.

31. Discharge changes are not visually discernable in plots for Ranges 5, 8, 8A, and 8B (Plates 64-75), but trends can be detected by examining the maximum tidal discharges given in Table 1; detailed analysis of flow in the inner harbor is best examined with flow volume data (see below).

32. Plates 76-81 show discharges at Ranges 9A and 9B. Discharges at Range 9A (Plates 76-78) indicate predominant easterly flow adjacent to the Navy Mole for both plans. Range 9B (Plates 79-81) shows the change from a pre-dominant easterly flow for the 2020 Master Plan with existing channels to an oscillating-direction flow when the channels have been dredged. Evidently, the deepened channels in the vicinity of the Queen's Gate allow greater flood flow penetration between the landfill and the middle breakwater.

Tidal Flow Volumes

33. Total flood, ebb, and net flow volumes are shown in Tables 2 and 3 for each range. Each flow volume is a one-tidal-cycle average of four continuous spring, mean, or neap flood/ebb tidal cycles (approximately 12.5 hours); the initial and final water surface elevations over the averaging period were the same, so there was no net storage. As mentioned above, the 2020 Master Plan will produce a change in tidal prism for the entire harbor. Figure 11 shows that the entire area, bounded by discharge Ranges 1, 2, and 3, contains 561×10^6 sq ft of water surface. The total landfill surface area within the harbor predicted for the 2020 Master Plan is 88.5×10^6 sq ft (total surface area, including outside the harbor, for the 2020 Master Plan is 117×10^6 sq ft). The plan will produce, therefore, a 15.8 percent reduction in water surface area within the harbor; i.e., there will be a loss of tidal prism of the same percentage as a result of the landfill. Using a different approach, when the flood and ebb flow volumes at Ranges 1, 2, and 3 are summed and averaged for a given tidal condition, the tidal prisms are, for one tidal cycle,

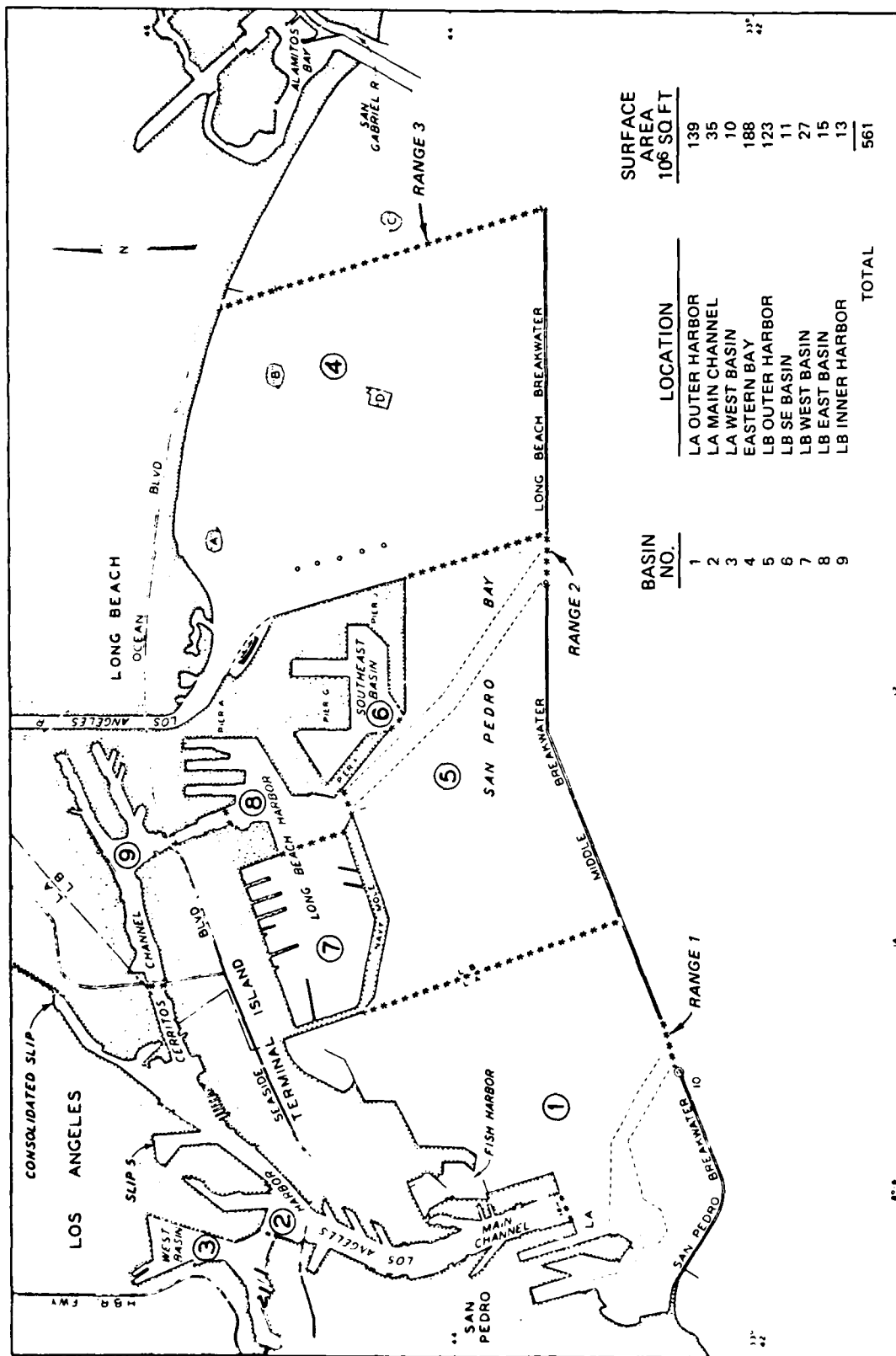


Figure 11. Surface area of the harbors, by basin

	<u>Spring Tide*</u>	<u>Mean Tide*</u>	<u>Neap Tide*</u>
Existing conditions	2740	2263	1017
2020-ED	2246 (-18.0%)**	1874 (-17.2%)	840 (-17.4%)
2020-ED	2244 (-18.1%)	1876 (-17.1%)	839 (-17.5%)

* Quantities given are in cubic feet and should be multiplied by 10^6 .

** Percent change from existing conditions.

The percent changes in the above table are within 2.3 percent of the model's estimate of volume change due to the change in surface area of the harbor. The difference is probably attributable to approximating the landfill boundaries with the finite difference grid. Volume changes between spring, mean, and neap tides do indicate some variation in tidal prism for different tide conditions, but the difference amounts to only a 0.01-ft change in tide range over the entire harbor.

34. Flow distribution changes and magnitudes can be determined using Tables 2, 3, and 4. Table 4 shows the ratio of flood flow volume to ebb flow volume at a given range for the three tide conditions. The overall ocean-harbor circulation pattern was maintained for the plans when compared to the base. That is, flood flow predominates at Ranges 1 and 2 (Angel's Gate and Queen's Gate, respectively), and ebb flow predominates at Range 3, at the east end of the harbor. The following tabulation shows how the flood and ebb flows were distributed among Ranges 1, 2, and 3:

Percent of Total Flood Flow

<u>Range</u>	<u>Spring Tide</u>			<u>Mean Tide</u>			<u>Neap Tide</u>		
	<u>Ex</u>	<u>2020-ED</u>	<u>2020-DC</u>	<u>Ex</u>	<u>2020-ED</u>	<u>2020-DC</u>	<u>Ex</u>	<u>2020-ED</u>	<u>2020-DC</u>
1	47.1	45.7	47.1	48.5	46.7	47.9	51.6	45.8	46.6
2	28.6	29.3	27.3	26.5	27.6	26.2	25.2	28.4	27.5
3	24.3	25.0	25.6	25.0	25.7	25.9	23.2	25.8	25.9
Total	100.0	100.0	100.0	100.0	100.0	100.0	100.0	100.0	100.0

Percent of Total Ebb Flow

<u>Range</u>	<u>Spring Tide</u>			<u>Mean Tide</u>			<u>Neap Tide</u>		
	<u>Ex</u>	<u>2020-ED</u>	<u>2020-DC</u>	<u>Ex</u>	<u>2020-ED</u>	<u>2020-DC</u>	<u>Ex</u>	<u>2020-ED</u>	<u>2020-DC</u>
1	39.6	33.2	37.2	37.5	32.3	36.5	36.9	34.4	38.5
2	19.8	19.4	22.6	21.6	21.1	23.5	23.0	22.0	22.8
3	40.6	47.4	40.2	20.9	46.6	40.0	40.1	43.6	38.7
Total	100.0	100.0	100.0	100.0	100.0	100.0	100.0	100.0	100.0

By reading across the above tabulation, one can see that (a) the proportions of flood flow through Ranges 1, 2, and 3 remained very similar for the existing condition and for both plans for spring and mean tides and (b) more change was indicated for the neap tide condition. The proportion of flood flow at Range 1 for neap tide was reduced by about 5 percent by the plans, and a resulting increase at Ranges 2 and 3 was split evenly. The reason for the percent increase in flood flow for existing conditions at Range 1 as the tide changed from spring to mean to neap condition lies in the reduction of ebb flow momentum toward Range 1. The ebb tide range near Hour 55 following the long ebb tide runout decreased as neap tide conditions approached, essentially maintaining flood flow over a longer duration. The circulation gyre strength was weaker during neap tide conditions due to the smaller neap tide range on flood flow. The distribution of ebb flow indicated a drop in percentage at Ranges 1 and 2 for the plan without the increased depths and an increase of ebb flow percentage at Range 3. With the depths increased for 2020-DC, the ebb flow distribution through Ranges 1, 2, and 3 approached that of existing conditions.

35. Flow volume percentages given in Table 4 for Ranges 5, 8A, and 8B indicate that the percentage of flood flow volume decreased when proceeding (a) from the existing condition, (b) to the 2020-ED Plan, and then (c) to the plan with the increased depth, for the spring and mean tidal ranges. For the neap tidal range, the flow volume percentage was similar for existing conditions and the 2020-ED Plan, but decreased for the 2020-DC Plan. For the spring and mean tide conditions, the flood flow percentage dropped below 50.0 percent for the 2020 Plan with the dredged channels, indicating a change in direction for the net flow, with circulation in the back harbor reversing from east to west (that is, from Long Beach Harbor to Los Angeles Harbor) to west to east. For the neap tide condition, ebb flow predominated at Ranges 5, 8A, and 8B for the existing and plan conditions.

36. At Range 8, in the Main Channel of the Los Angeles Harbor, flood flow volumes showed progressive increases when stepping (a) from existing conditions, (b) to the 2020-ED Plan, (c) to the plan with increased depths. For each tidal condition, the net flow at Range 8 changed from ebb for existing conditions and the 2020 plan with existing depths to flood for the 2020 plan with dredged channels.

37. Flow at Ranges 9A and 9B (see Figure 9 for locations) have been

arbitrarily assigned positive, or flood flow, values for east to west flows. Therefore, for mean tide existing conditions the large central eddy produces almost total ebb flow at Range 9A along the Navy Mole and total flood flow at Range 9B along the middle breakwater (see Tables 2 and 3). The installation of the 2020 Master Plan with existing depths shows a slight reduction in net flow (Table 3); however, when the channel is deepened, the net flow volume increases almost 50 percent from existing mean tide conditions. Range 9B net flow volume reverses for the 2020 Master Plan with existing depths, then reverses again when channels are deepened, though flood and ebb flows are more closely balanced.

Tidal Circulation--Velocity Vector Plots

38. Plates 82-117 show velocity vector plots at every second cell location of the model grid. Four plots for each combination of tide and condition (i.e. existing, 2020-ED, and 2020-DC) are presented. Velocities of less than 0.01 ft/sec drop out of the plots. Velocities within the 0.01- to about 0.15-ft/sec range are difficult to determine because the vector length is within the triangular vector head and does not reproduce well from the video plotter used in the study. Velocities greater than 0.15 ft/sec have the vector stem projecting down from the base of the vector head and easily can be scaled off. Refer to Figure 9 for location of ranges.

39. Plates 82-93 present the tidal circulation patterns for existing conditions. Plates 82 and 83 show tidal circulation during ebb conditions of a 7-ft fall of the tide, and Plates 84 and 85 show velocities during the following rise in spring tide level. The clockwise gyre in the outer harbor was noted as a dominant feature of the circulation developed by flood flow through Range 1 (Plate 85). During the strength of flood flow for this existing spring tide condition, there was flow along the Navy Mole into Range 5 (Plate 85), and it can be noted that the flood flow through Range 2 eddied south of Pier J and did not appear to significantly contribute flow toward Range 5. Flood flow through Range 1, which moved northwesterly, split into two parts: (a) a counterclockwise eddy which returned toward the entrance and (b) a flow which continued into the Main Channel (Range 8). The flow nodal point in the back harbor region occurred in the East Basin Channel. It can be noted that the eddy strength decreased as the tide range decreased and, for neap conditions

(Plates 90-93), only the main gyre in the central portion of the outer harbor was significant. Figure 12 compares maximum flood flow (Plates 85, 88, and 91) for existing conditions.

40. Plates 97 and 109 can be compared directly to Plate 85 (see Figure 13) to examine changes developed by the Master Plans during flood flow. For the 2020 Master Plan with existing channels, the main gyre had been negated by the landfill but a strong flood flow still existed along the Navy Mole to provide inflow into Range 5. Flood currents from Range 2 were moving toward Range 5 also, since flood flow from Range 1 was flowing eastward south of the major harbor landfill and had negated the eddy that circulated along the middle breakwater near Range 2 for existing conditions. The counterclockwise eddy gyre just west of Range 1 had been reduced in magnitude by the filling in of the East Channel slip, and this also possibly aided in providing a slight increase in flood flow through Range 8. The nodal point in the East Basin Channel remained close to the location it had for existing conditions. Circulation inside the Navy Mole (i.e. West Basin) remained the same as for existing conditions.

41. Flood flow for the 2020 Master Plan with dredged channels (Plate 109) produced some smaller changes from the previous undeeened conditions. The greater depths lowered velocities in the region between Range 1 and Range 8, providing smoother flow patterns into Range 8 (which showed an increase in flood flow volume) and further reducing the eddy gyre inside the harbor west of Range 1. Velocities between the Navy Mole and the landfill were increased as they flowed eastward toward Range 5 and appeared to (a) dominate flood flow through Range 5 and (b) reduce the flow approaching Range 5 from Range 2. This in turn reduced eastward flow between the landfill and the middle breakwater. The nodal point in the East Basin Channel may have shifted slightly eastward (on the order of 1000-2000 ft) as indicated by the change in net flow at Range 8B (compare Plates 97 and 103). The greater depths increased the efficiency of flow through Range 8 and Range 9A, but the change at Range 8 predominated and changed the net circulation in the back channels.

42. Ebb velocities for the existing condition (Plate 83, or Figure 14) indicated a strong ebb flow pattern approaching Range 1 from east and west inside the harbor. The large eddy gyre still persisted, with northerly currents about 4000 ft north of the Range 1 entrance. The gyre inside the harbor to the west of Range 1 also persisted and deflected ebb flow from Range 8 slightly

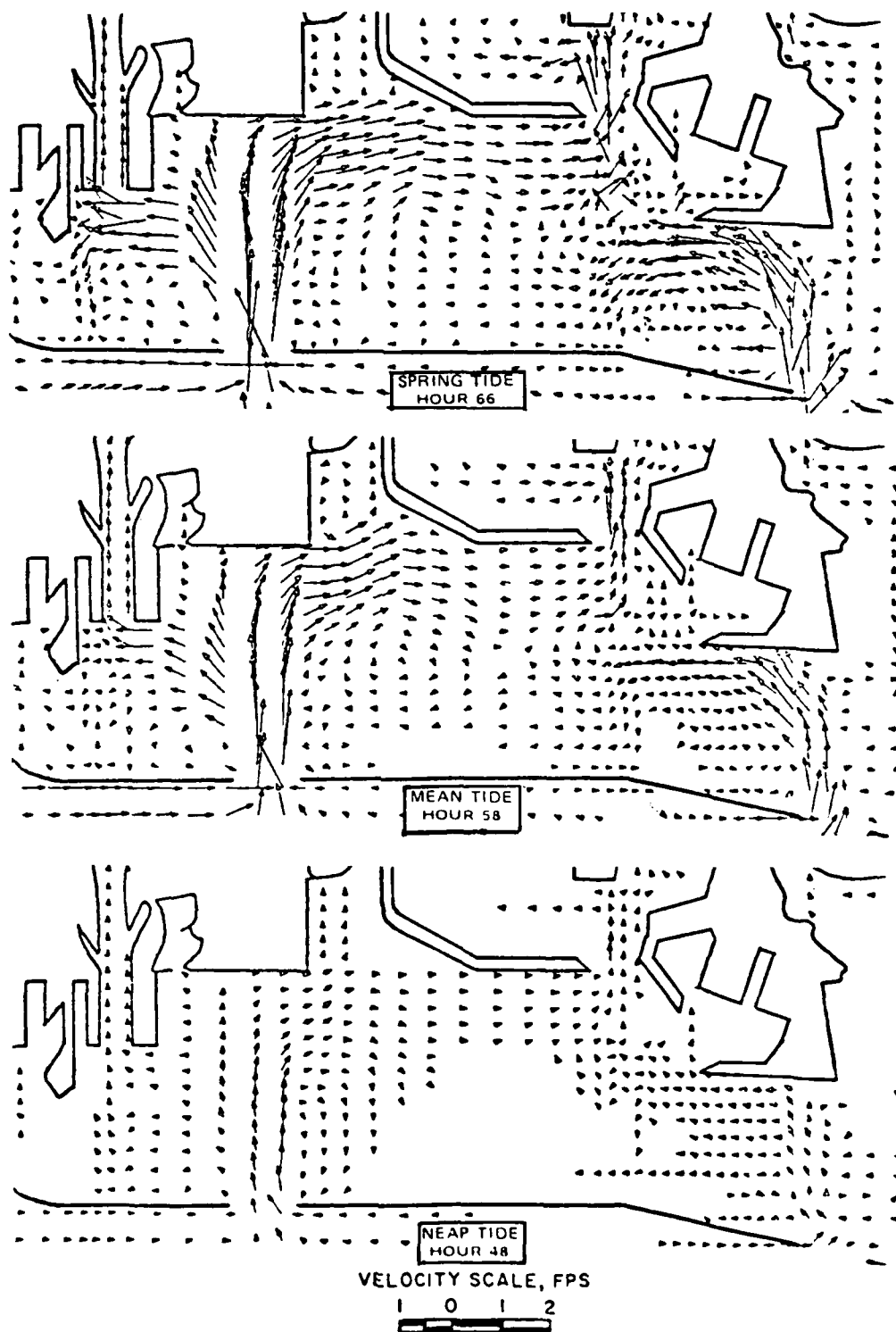


Figure 12. Maximum flood tide velocity vectors for existing conditions
--spring, mean, and neap tides

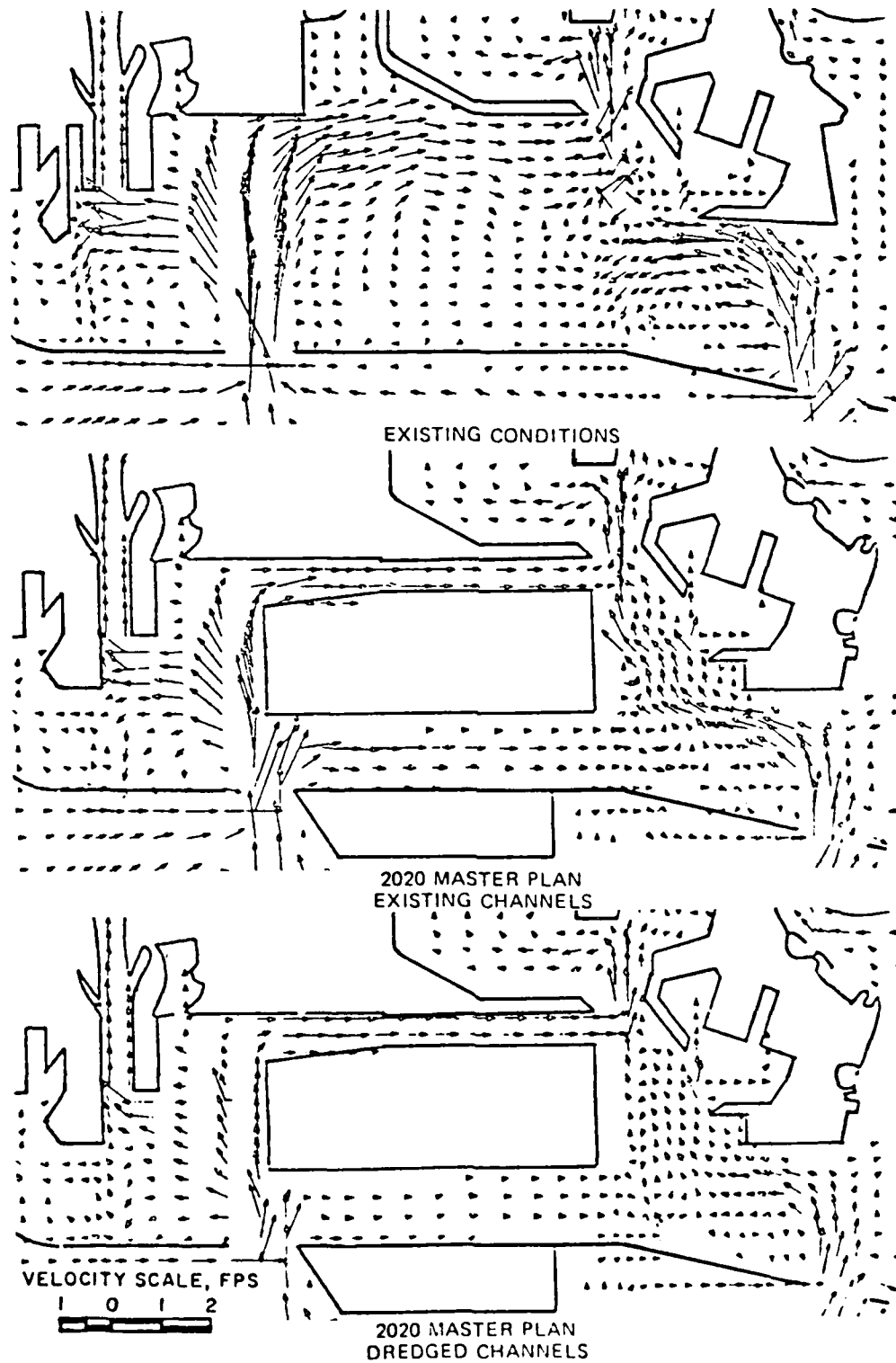


Figure 13. Maximum flood tide velocity vectoes for existing and 2020 Master Plan conditions--spring tide

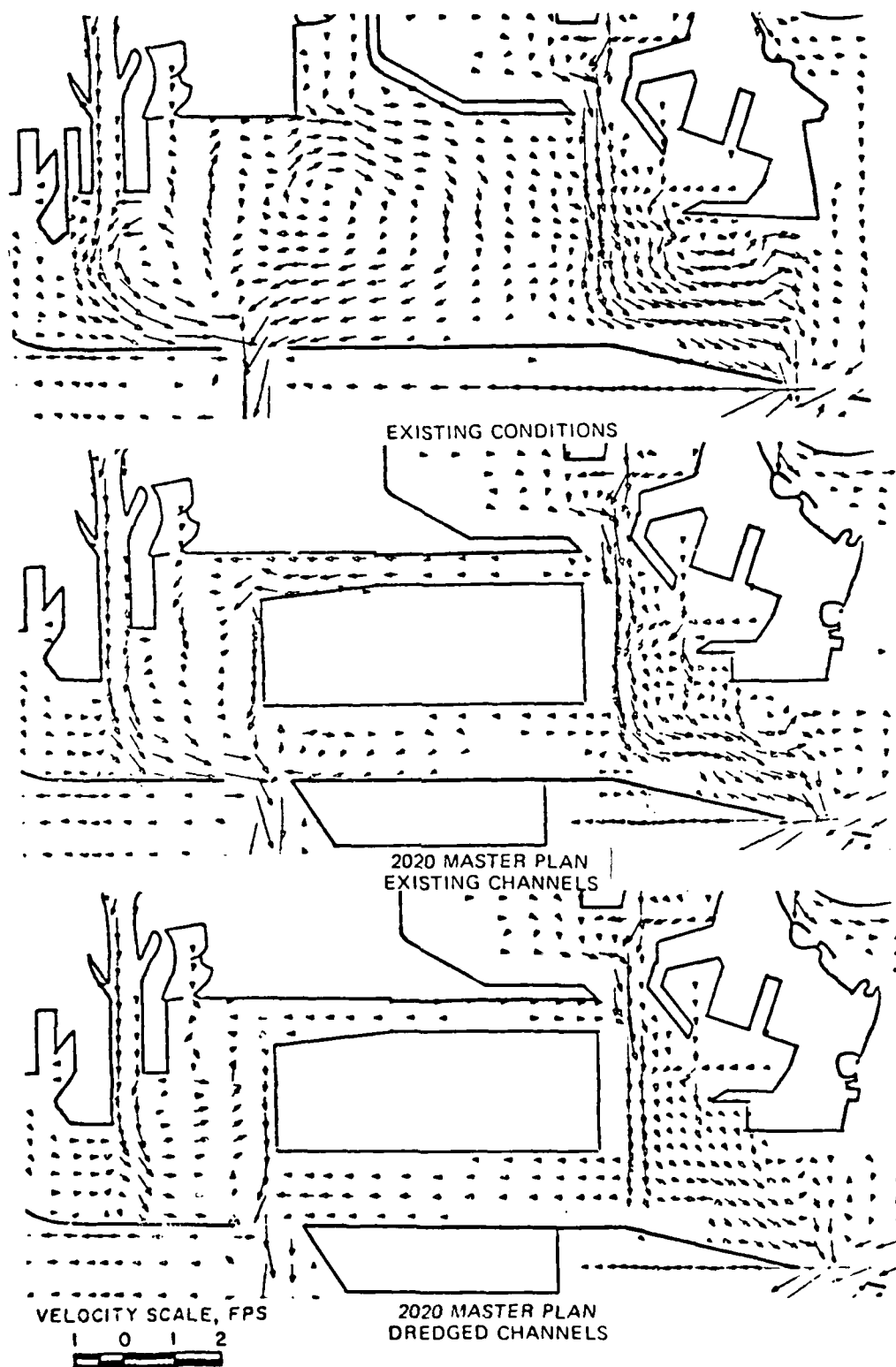


Figure 14. Maximum ebb tide velocity vectors for existing and 2020 Master Plan conditions--spring tide

to the west. Flow off the main gyre split and joined flow ebbing through Range 5 and then exited through Range 2. A strong counterclockwise eddy near Pier J still persisted from flood flow, guiding ebb flow from Range 5 straight toward the breakwater where it then turned eastward to exit Range 2. Current vectors just north of Range 5 eddied into the West Basin before circling back and out through Range 5.

43. With the Master Plan (with existing channels) in place, Plate 94 (or Figure 14) shows the ebb velocities at the time comparable to the existing conditions of Plate 82 (i.e. Hour 58). Currents from Range 8, Main Channel, flowed toward the Angel's Gate (Range 1) similar to the flow under existing conditions; but, due to the lack of an opposing eddy gyre with ebb currents east of Range 1, a portion of the ebb currents flowed east between the major landfill and the middle breakwater, exiting the harbor through Range 2. Currents along the Navy Mole flowed west and did not join the flow ebbing through Range 5, as a small part of currents of the gyre did for existing conditions. The gyre south of the Pier J extension was much smaller.

44. With the increased depths of the Master Plan with dredged channels, velocity magnitudes were reduced in many areas and eddying conditions were reduced. For example, velocities from Range 8 flowed in a straighter path toward Range 1 (Plate 107 or Figure 14). Since there were no eddy remnants from flood flow, ebb flow from Range 8 filled the region between the landfill of East Channel and the west face of the large landfill. This reduced the ebb flow emptying from the region between the landfill and the Navy Mole, and flow in this region split between exiting east and west. Also, the flow just east of the Range 1 entrance was reversed, as ebb currents were not jetting across the region just north of Range 1. Ebb flow patterns from Range 5 had more continuity and smoothness toward Range 2. The congested flow area (for existing conditions and the initial plan) inside the West Basin, just north of Range 5, showed improvement in flow patterns.

45. Trends for the other tide conditions generally follow those discussed above; however, neap tide conditions varied more than spring or mean tide results, as discussed earlier. For example, the main gyre in Plate 90 was not as extensive as for spring tide (Plate 82) and did not contribute any ebb flow toward Range 2; consequently, ebb flow percentage through Range 1 was higher for neap tide conditions (see Table 4). Eddy conditions were considerably reduced as a whole for neap tide conditions, as can be seen when

comparing Plate 90 to Plate 82.

Dye Movement

46. The injection of dye (representing a conservative substance) was simulated at two locations in the harbor as shown in Figure 3. These two "slugs" of dye had a concentration of 10 parts per thousand (ppt) and were injected at Hour 18 of the numerical simulation. The movement of the depth-averaged dye slug was then traced for the remainder of the simulation (through Hour 70). Plates 118-153 show contours of the dye as it dispersed through the harbor for each tide condition (spring, mean, and neap) and for each of the three study conditions (i.e. existing, 2020 Master Plan with existing depths, and 2020 Master Plan with dredged channels). Four plates are shown for each combination of tide and study condition: one each for Hours 31, 37, 56, and 62. In each case, the selected time is either at high water or low water of the tidal cycle.

47. Plates 118-129 present results for existing conditions. Hour 31 (Plate 118) shows the dye concentrations at high water after flood inflow, at 13 hours (or 1 full tidal cycle) after the introduction of the dye. The dye in the outer harbor has split into three zones. One portion has moved toward Fish Harbor and Reservation Point, another part has moved in toward the Sea-plane Basin, and the third part has moved into the middle of the outer harbor, caught in the eddy gyre noted in the velocity vector plots. The dye slug in the Cerritos Channel area has remained concentrated, with dispersion at each end of the slug. At Hour 37 (Plate 119), greater dispersion occurred at all locations previously discussed. By Hour 56 (Plate 120), concentrations have been considerably reduced by the tidal circulation. Some dye had dispersed through Range 5, at the corner of the Navy Mole. Maximum concentration contours in the outer harbor were 1.0 ppt, with most contoured areas between 0.1 and 1.0 ppt. The net migration in the outer harbor was toward the east. Concentrations in the Cerritos Channel region were also reduced. Hour 62 (Plate 121) shows concentrations after the long ebb runout; Fish Harbor has accumulated a slight increase in concentration. The region of highest overall concentration has shifted eastward. Dispersion patterns for the mean tide existing conditions (Plates 122-125) indicate dye movement similar to the spring tide, except that the net movement in the outer harbor was more to the west

along the middle breakwater. Neap tide concentration (Plates 126-129) indicate less dispersion in the outer harbor, with the net circulation in the outer harbor toward the west; dispersion in Cerritos Channel was lower for this low tidal energy condition.

48. The installation of the 2020 Master Plan produced lower concentrations in the Fish Harbor area for all Plan cases (Plates 133, 137, 141, 145, 149, and 153) and less dispersion for that part of the dye slug moving along the Navy Mole due to the confinement of the landfill. However, each plan case indicated good movement through the region between the Navy Mole and the landfill with the dye slug's net movement in each case being easterly. The 0.1-concentration contour in the Navy Mole region is similar for the 2020 Plan with existing channels and with dredged channels for spring and mean tide conditions (compare Plates 133 to 145 and 137 to 149 for spring and mean tide conditions, respectively). The concentration areas within the 0.1 area are higher for the dredged channels due to (a) the greater depths, and thus the larger initial slug, and also (b) the lower velocities, which reduced mixing. However, since the region was not stagnant and showed strong net movement, eventually this water mass would mix with flow in the Range 5 region. The dispersion difference between the dredged channel condition and nondredged condition was slightly greater for neap tide conditions (Plates 141 and 153). In the Cerritos Channel region, the difference in contours between existing conditions and the 2020 Master Plan with existing channels was very slight (compare Plates 121 and 133, Plates 125 and 137, and Plates 129 and 141). In each case, the reversal in net flow in Cerritos Channel was apparent for the 2020 Master Plan with dredged channels, as the contours in Cerritos Channel showed a net shift toward the east (compare Plates 133 to 145, 137 to 149, and 141 to 153).

PART IV: CONCLUSIONS

49. The model simulation revealed no changes in tidal elevation or phases caused by the 2020 Master Plan.

50. Individual velocity magnitude changes were small, with the greatest changes (about 0.3 ft/sec) coming at locations where dredging increased cross-sectional area and reduced velocities. It should be noted that while changes were small, velocity magnitudes throughout the harbor are small (usually less than 1 ft/sec). Percentage changes therefore can be significant and indicate changes in harbor circulation, which are best evaluated by flow volume computations and velocity vector plots.

51. Tidal prism reduction from existing conditions was between 17 and 18 percent (for various tidal conditions and plans), a reduction very nearly equal to the volume displaced by the landfill. This indicates the landfills did not affect the filling of the harbors (also noted by a lack of variation in tidal elevation from existing conditions).

52. Flow enters and exits the harbors through Angel's Gate, Queen's Gate, and the east end. Flood flow distribution through these three locations showed only very slight changes for the plans, with a tendency to increase flood flow on the east side of the harbors. The basic flood flow proportions remained about the same; i.e., Angel's Gate contributed 47 percent of flood flow, Queen's Gate, 27 percent, and east side, 26 percent. Ebb flow distribution indicated a tendency for (a) slight decreases in flow volume at Angel's Gate, (b) slight increases at Queen's Gate, and (c) initial increases at the east end for the 2020 Master Plan without dredging; but there was a return to no change or slight reduction when depths were increased in the central outer harbor, permitting greater ebb flow through Queen's Gate. Typical ebb flow distributions exiting the harbor were Angel's Gate, 37 percent Queen's Gate, 23 percent, and east end, 40 percent.

53. Net circulation in the inner harbor (i.e., Los Angeles Harbor's Main Channel and Long Beach Harbor's Cerritos Channel) showed a reversal from existing conditions and 2020-ED to 2020-DC. The net circulation for existing conditions is from east to west (i.e., from Long Beach to Los Angeles Harbor); the net circulation is reversed for the 2020 Master Plan with dredged channels condition, in fact the net circulation changed from $+8 \times 10^6$ cu ft to -12×10^6 cu ft for the spring tide condition. It should be noted that due to the small

REFERENCES

- Butler, H. Lee. 1978a (Jun). "Numerical Simulation of Tidal Hydrodynamics; Great Egg Harbor and Corson Inlets, New Jersey," Technical Report H-78-11, U. S. Army Engineer Waterways Experiment Station, CE, Vicksburg, Miss.
- _____. 1978b (Aug). "Coastal Flood Simulation in Stretched Coordinates," Proceedings, 16th International Conference on Coastal Engineering, American Society of Civil Engineers, New York, pp 1030-1048.
- _____. 1978c (Dec). "Numerical Simulation of the Coos Bay-South Slough Complex," Technical Report H-78-22, U. S. Army Engineer Waterways Experiment Station, CE, Vicksburg, Miss.
- _____. 1980. "Evolution of a Numerical Model for Simulating Long-Period Wave Behavior in Ocean Estuarine Systems," Estuarine and Wetland Processes: With Emphasis on Modeling; Marine Science, Vol. 11, Plenum Press, New York.
- McAnnally, W. H., Jr. 1975 (Sep). "Los Angeles and Long Beach Harbors Model Study; Report 5: Tidal Verification and Base Circulation Tests," Technical Report H-75-4, U. S. Army Engineer Waterways Experiment Station, CE, Vicksburg, Miss.
- Outlaw, D. G. 1984. "Los Angeles and Long Beach Harbors Model Study; Numerical Analysis of Tidal Circulation for Navigation Channel Improvements," In preparation. U. S. Army Engineer Waterways Experiment Station, CE, Vicksburg, Miss.
- Outlaw, D. G., and Raney, D. G. 1979 (May). "Numerical Analysis of Tidal Circulation for Long Beach Outer Harbor Proposed Landfill," Miscellaneous Paper H-79-5, U. S. Army Engineer Waterways Experiment Station, CE, Vicksburg, Miss.
- Raney, D. C. 1976a (Sep). "Numerical Analysis of Tidal Circulation for Long Beach Harbor; Report 1: Existing Conditions and Alternate Plans for Pier J Completion and Tanker Terminal Study," Miscellaneous Paper H-76-4, U. S. Army Engineer Waterways Experiment Station, CE, Vicksburg, Miss.
- _____. 1976 (Sep). "Numerical Analysis of Tidal Circulation for Long Beach Harbor; Report 3: Existing Conditions and Alternate Plans for Pier J Completion and Tanker Terminal Study with -82 ft Channel," Miscellaneous Paper H-76-4, U. S. Army Engineer Waterways Experiment Station, CE, Vicksburg, Miss.
- Schmalz, R. A., Jr. 1983 (Sep). "The Development of a Numerical Solution to the Transport Equation; Report 1: Methodology, Report 2: Computational Procedures, Report 3: Test Results," Miscellaneous Paper CERC-83-2, U. S. Army Engineer Waterways Experiment Station, CE, Vicksburg, Miss.

differences in tidal elevations which govern these flows, other factors not studied here (such as wind) probably could influence circulation in the back channels (for both existing conditions and the modifications considered herein). Net flow volumes in the inner harbor for both existing and Plan conditions are small relative to the total flow volumes.

54. Velocity vector plots provided information on overall circulation patterns. Existing condition patterns were dominated by large horizontal eddies generated by incoming flood flow through Angel's Gate (Range 1) and Queen's Gate (Range 2). The eddies were strong for spring and mean tide conditions, but only the large central outer harbor eddy was significant during neap tide for existing conditions.

55. The velocity vector plots explained the reversal in net flow in the back channel region. Progressively smoother flow patterns were created between Angel's Gate and the Main Channel in Los Angeles Harbor by the Master Plans, permitting more efficient flow into the back channels from the Los Angeles side of the harbor. The deepening of channels generally reduced eddy strength at various locations in the outer harbor.

56. Dye movement tests indicated good flushing and mixing for the 2020 Master Plan in the vicinity of Fish Harbor and the Navy Mole. Movement of dye in Cerritos Channel in the inner harbor was very similar for existing and plan conditions.

Table 1

Maximum Tidal Discharges

Range	Spring Tide			Mean Tide			Neap Tide		
	Ex *	2020-ED	2020-DC	Ex	2020-ED	2020-DC	Ex	2020-ED	2020-DC
<u>Flood Flow Discharges (cu ft/sec)</u>									
1	106,944	85,000	91,250	85,139	64,583	68,056	38,889	29,583	33,056
2	68,194	59,444	49,585	45,139	38,861	39,028	21,528	18,056	18,889
3	58,333	50,833	50,417	48,194	44,306	43,472	28,056	24,861	24,028
5	27,778	27,083	26,667	23,333	21,806	22,361	10,819	11,000	11,028
8	12,764	13,528	14,167	10,931	11,264	11,597	5,833	5,556	5,736
8A	11,375	10,708	10,014	9,139	8,375	8,347	4,722	4,597	4,139
8B	6,389	5,833	5,431	5,167	4,583	4,514	2,792	2,472	2,361
9A	--	3,319	6,639	919	2,889	5,139	832	1,750	2,917
9B	--	9,569	14,583	5,792	7,597	11,069	1,282	3,681	7,042
<u>Ebb Flow Discharges (cu ft/sec)</u>									
1	95,694	70,694	79,722	75,833	55,833	59,583	51,528	39,028	41,806
2	55,139	44,722	47,917	45,833	36,806	39,028	30,694	25,278	25,278
3	86,389	80,278	72,639	70,139	64,306	57,639	45,278	41,111	36,389
5	29,167	28,472	29,583	19,444	22,778	23,611	15,278	15,417	14,861
8	14,861	15,000	14,167	11,903	11,861	11,708	7,292	8,056	7,417
8A	11,347	10,986	11,917	9,097	8,736	9,694	5,944	5,972	6,208
9A	--	9,292	19,444	5,944	7,500	13,667	2,083	3,694	5,139
9B	--	18,889	12,222	671	15,972	8,125	1,444	5,681	4,972

*

Ex = Existing conditions.

2020-ED = 2020 Master Plan with existing depths.

2020-DC = 2020 Master Plan with dredged channels.

Table 2

Average Flow Volumes for One Tidal Cycle

Range	Spring Tide			Mean Tide			Neap Tide		
	Ex *	2020-ED	2020-DC	Ex	2020-ED	2020-DC	Ex	2020-ED	2020-DC
<u>Flood Flow Volumes (10^6 cu ft)</u>									
1	1307	1071	1072	1106	898	900	502	376	380
2	793	686	621	604	532	492	245	233	224
3	677	585	581	569	495	487	226	211	211
5	335	328	324	278	274	272	122	120	119
8	159	165	171	136	140	143	60	62	62
8A	136	129	124	112	107	104	48	46	46
8B	77	71	66	63	58	55	27	25	27
9A	--	9	6	0	7	7	2	4	11
9B	--	31	159	93	22	119	15	31	57
<u>Ebb Flow Volumes (10^6 cu ft)</u>									
1	1071	713	823	843	588	683	375	283	317
2	536	417	501	486	384	440	234	182	187
3	1096	1020	891	918	850	749	410	363	321
5	330	325	337	277	274	280	121	119	121
8	168	172	160	138	142	133	60	62	59
8A	128	124	136	109	105	113	48	46	49
8B	70	66	78	60	56	65	27	25	27
9A	--	158	300	145	132	228	47	69	86
9B	--	249	104	0	208	99	16	55	41

* Ex = Existing conditions.

2020-ED = 2020 Master Plan with existing depths.

2020-DC = 2020 Master Plan with dredged channels.

Table 3

Average Net Flow Volumes for One Tidal Cycle (10^6 cu ft)*

Range	Spring Tide			Mean Tide			Neap Tide		
	Ex	2020-ED	2020-DC	Ex	2020-ED	2020-DC	Ex	2020-ED	2020-DC
1	236	358	249	263	310	217	127	93	63
2	257	269	120	118	148	52	11	51	37
3	-419	-435	-310	-349	-355	-262	-184	-152	-110
5	5	3	-13	1	0	-8	1	-1	-2
8	-9	-7	11	-2	-2	10	0	0	3
8A	8	5	-12	3	2	-9	0	0	-3
8B	7	5	-12	3	2	-10	0	0	-3
9A	--	-149	-294	-145	-125	-221	-45	-65	-75
9B	--	-218	55	93	-186	20	-1	-24	16

* Negative (-) net volume indicates net ebb flow; positive net volume indicates net flood flow (flow direction is defined in Figure 9).

Ex = Existing conditions.

2020-ED = 2020 Master Plan with existing depths.

2020-DC = 2020 Master Plan with dredged channels.

Table 4

Ratio of Percent of Flood Flow Volume to Percent of Ebb Flow Volume

Range	Ex *	Spring Tide		Ex	Mean Tide		Ex	Neap Tide	
		2020-ED	2020-DC		2020-ED	2020-DC		2020-ED	2020-DC
1	56.2/43.8	60.1/39.9	56.6/43.4	56.8/ 43.2	60.4/39.6	56.9/42.1	57.2/42.8	57.1/42.9	54.5/45.5
2	59.7/40.3	62.2/37.8	55.4/44.6	55.4/ 44.6	58.1/41.9	52.8/47.2	51.1/48.9	56.1/43.9	54.5/45.5
3	38.2/61.8	36.4/63.6	39.4/60.6	38.3/ 61.7	36.8/63.2	39.4/60.6	35.5/64.5	36.8/63.2	39.7/60.3
5	50.4/49.6	50.2/49.8	49.0/51.0	50.2/ 49.8	50.0/50.0	49.2/50.8	50.2/49.8	50.2/49.8	49.6/50.4
8	48.6/51.4	49.0/51.0	51.5/48.5	49.5/ 50.5	49.7/50.3	51.8/48.2	50.0/50.0	50.0/50.0	50.8/49.2
8A	51.4/48.6	50.9/49.1	47.6/52.4	50.6/ 49.4	50.4/49.6	47.8/52.2	50.0/50.0	50.0/50.0	48.4/51.6
8B	52.6/48.4	51.8/48.2	45.9/54.1	51.0/ 49.0	50.8/49.2	45.9/54.1	50.0/50.0	50.0/50.0	47.1/52.9
9A	---	5.0/95.0	2.0/98.0	0.0/100.0	5.4/94.6	2.8/97.2	48.9/51.1	5.5/94.5	11.3/88.7
9B	---	11.1/88.9	60.4/39.6	100.0/ 00.0	9.7/90.3	54.6/45.4	48.4/51.6	36.0/64.0	58.2/41.8

* Ex = Existing conditions.

2020-ED = 2020 Master Plan with existing depths.

2020-DC = 2020 Master Plan with dredged channels.

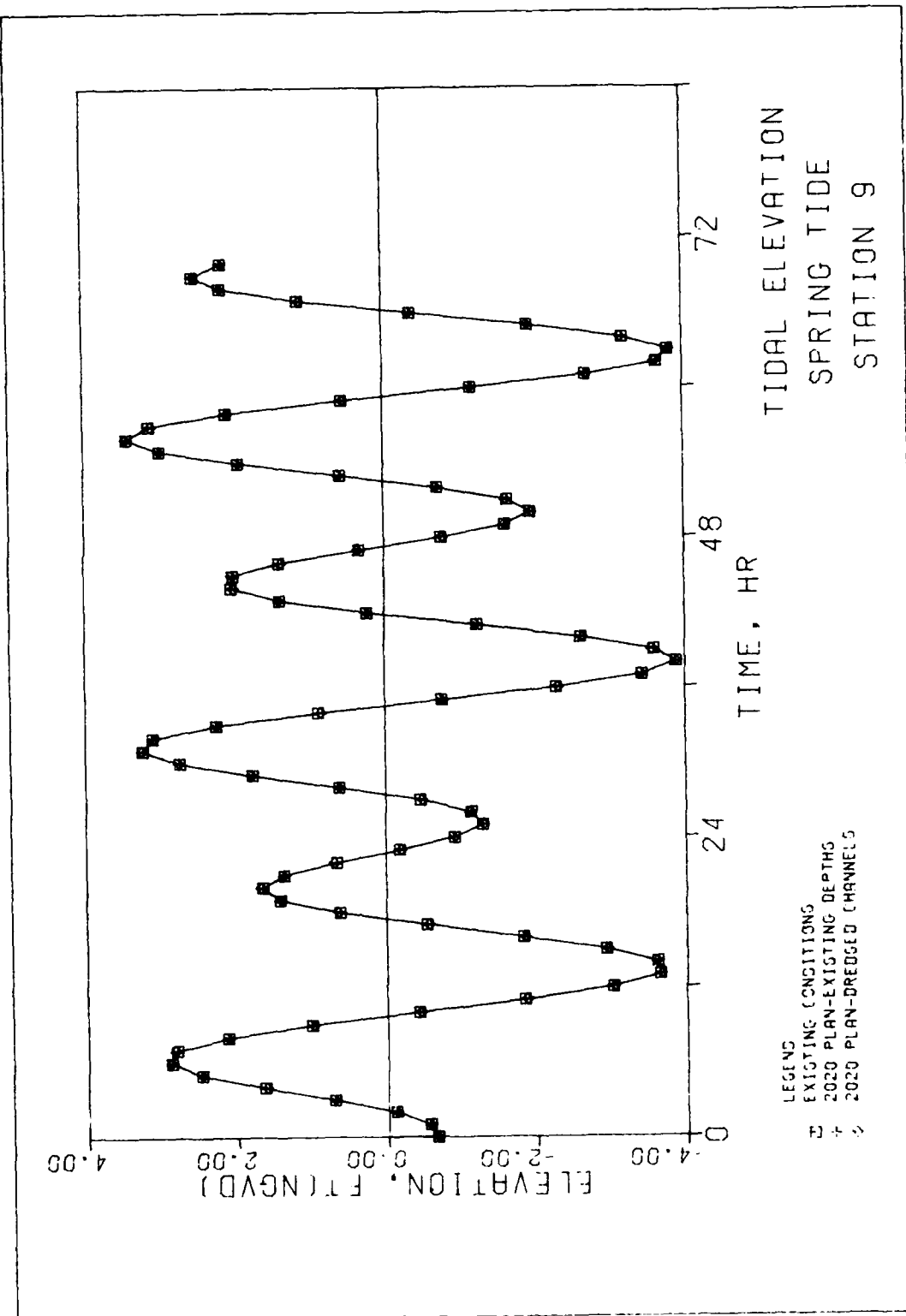


Plate 1

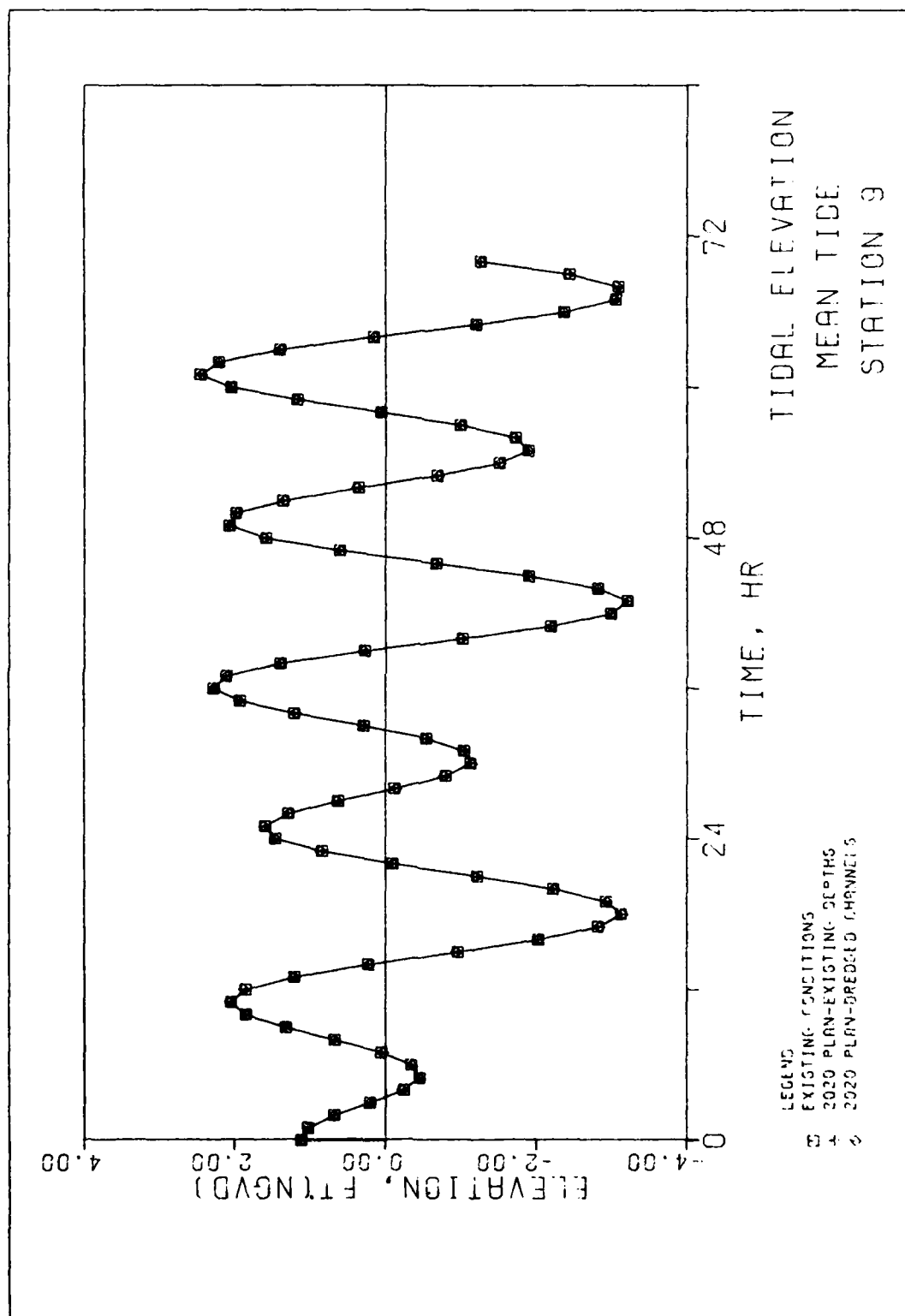


Plate 2

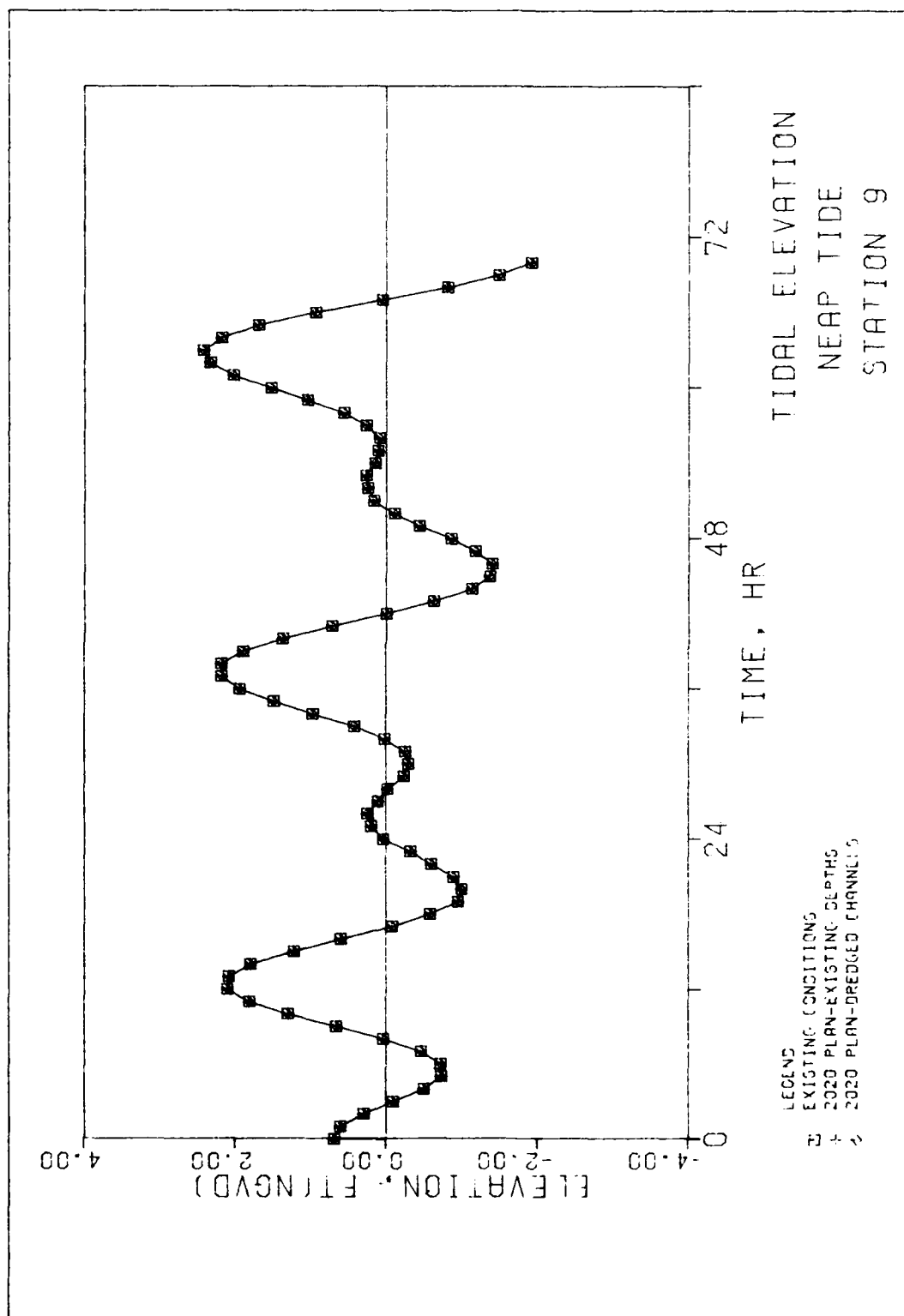


Plate 3

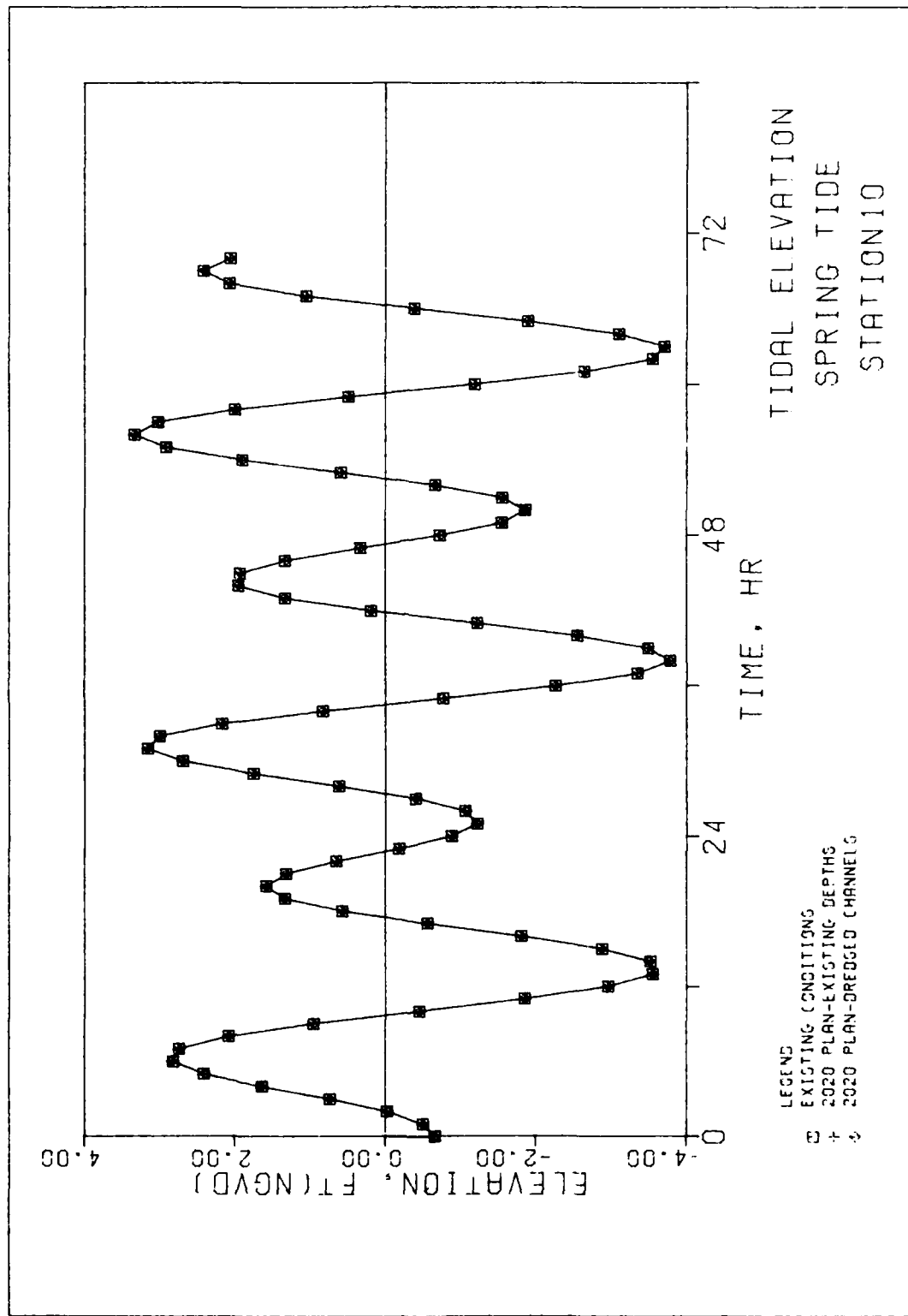


Plate 4

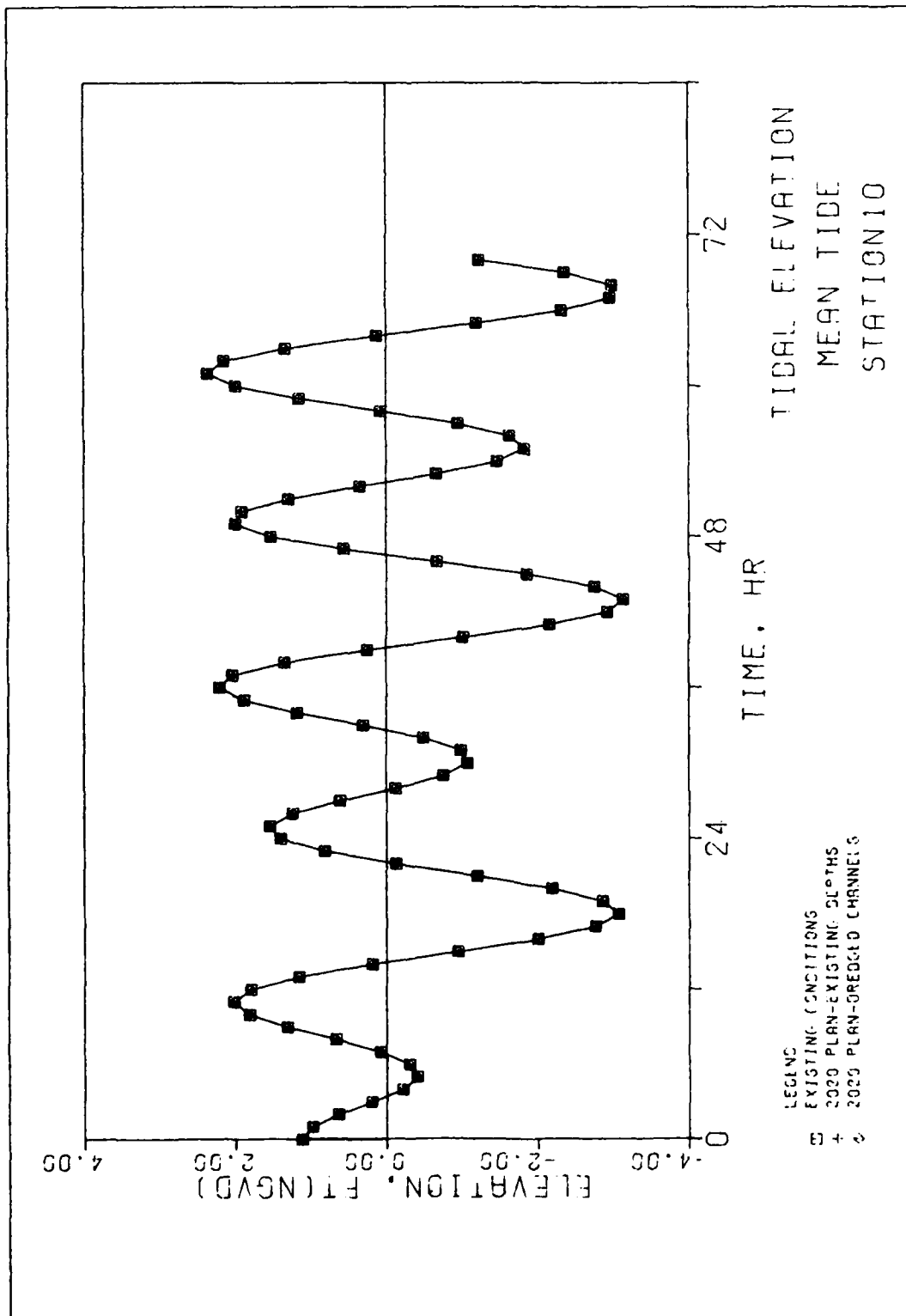


Plate 5

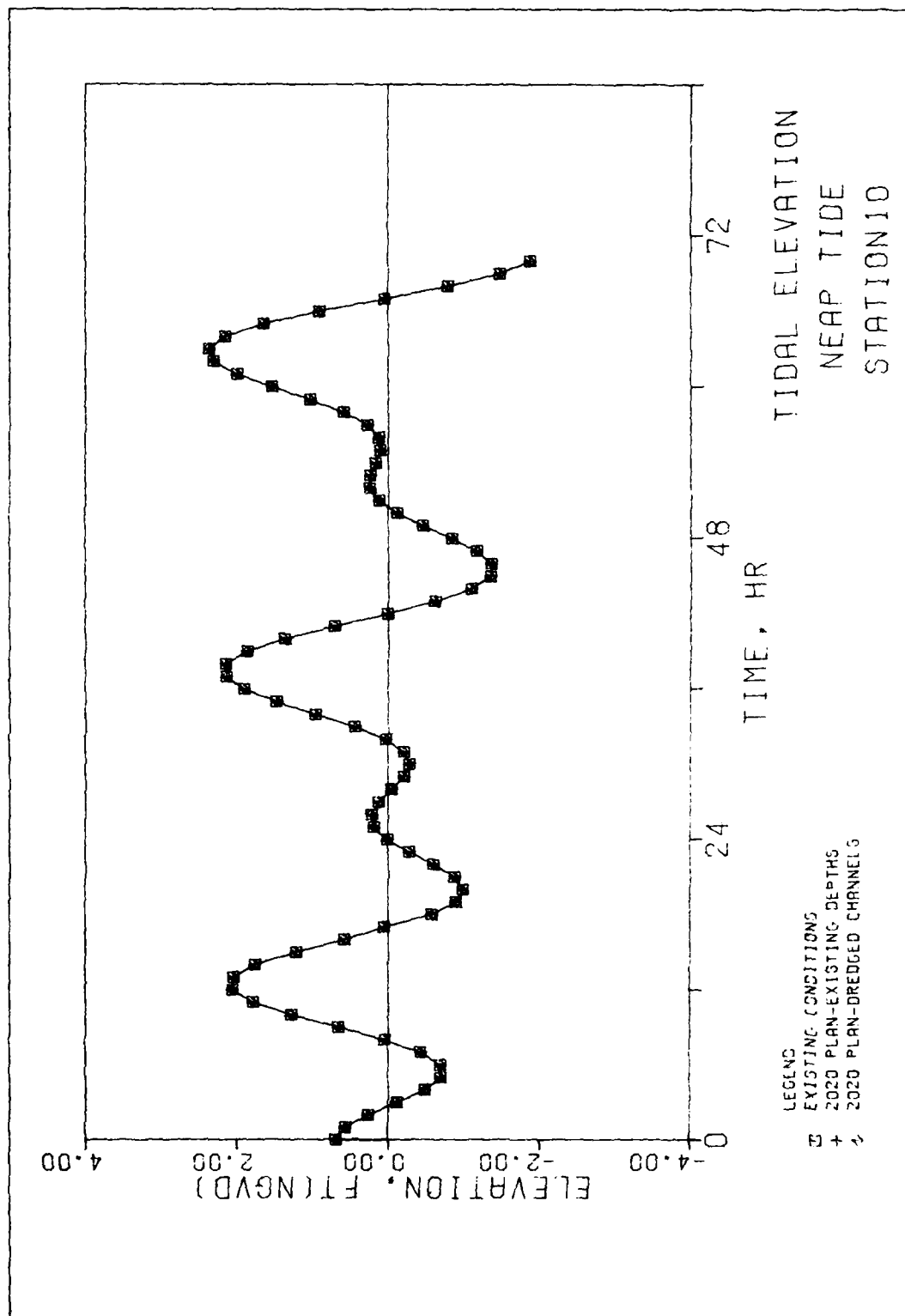


Plate 6

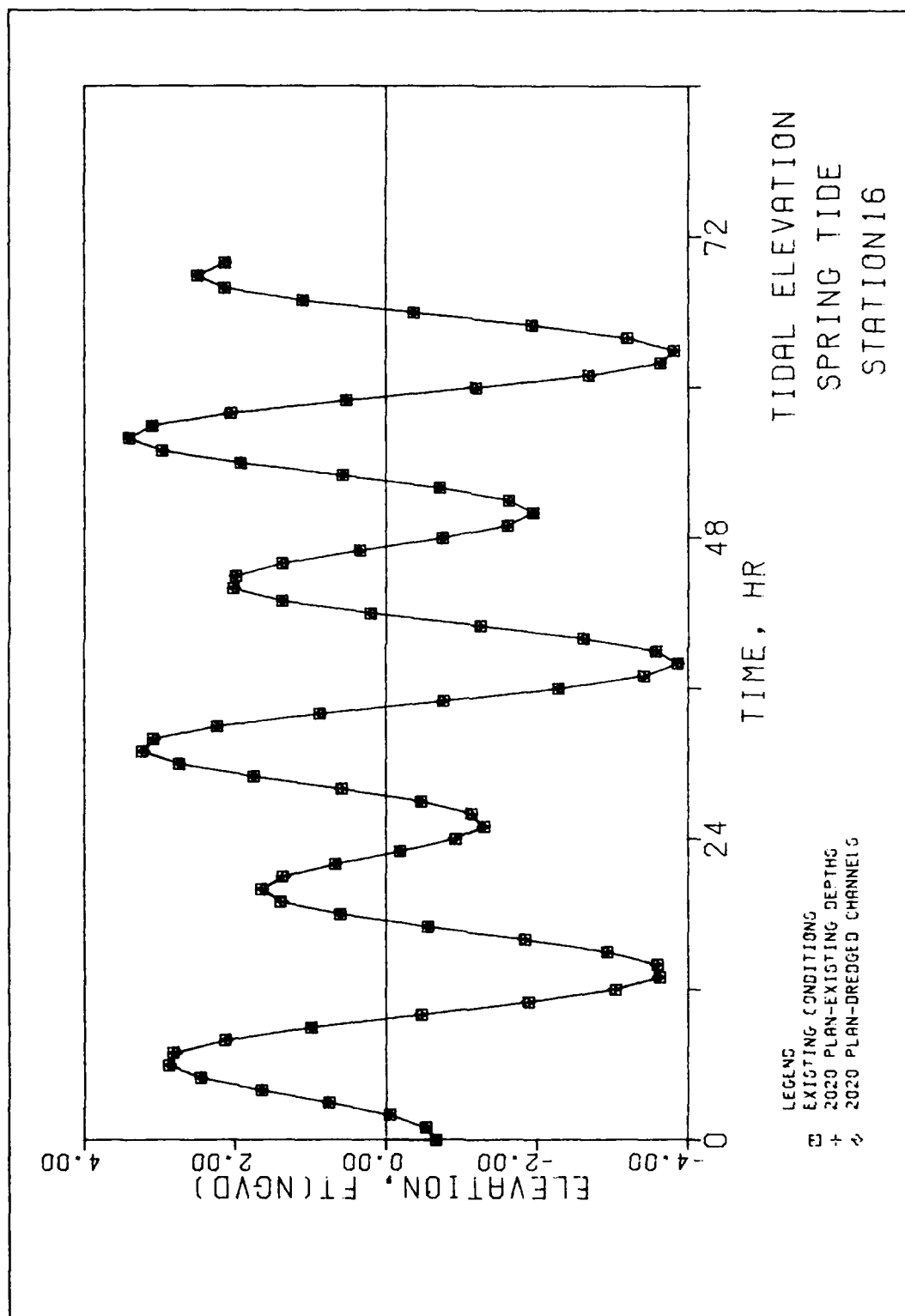


Plate 7

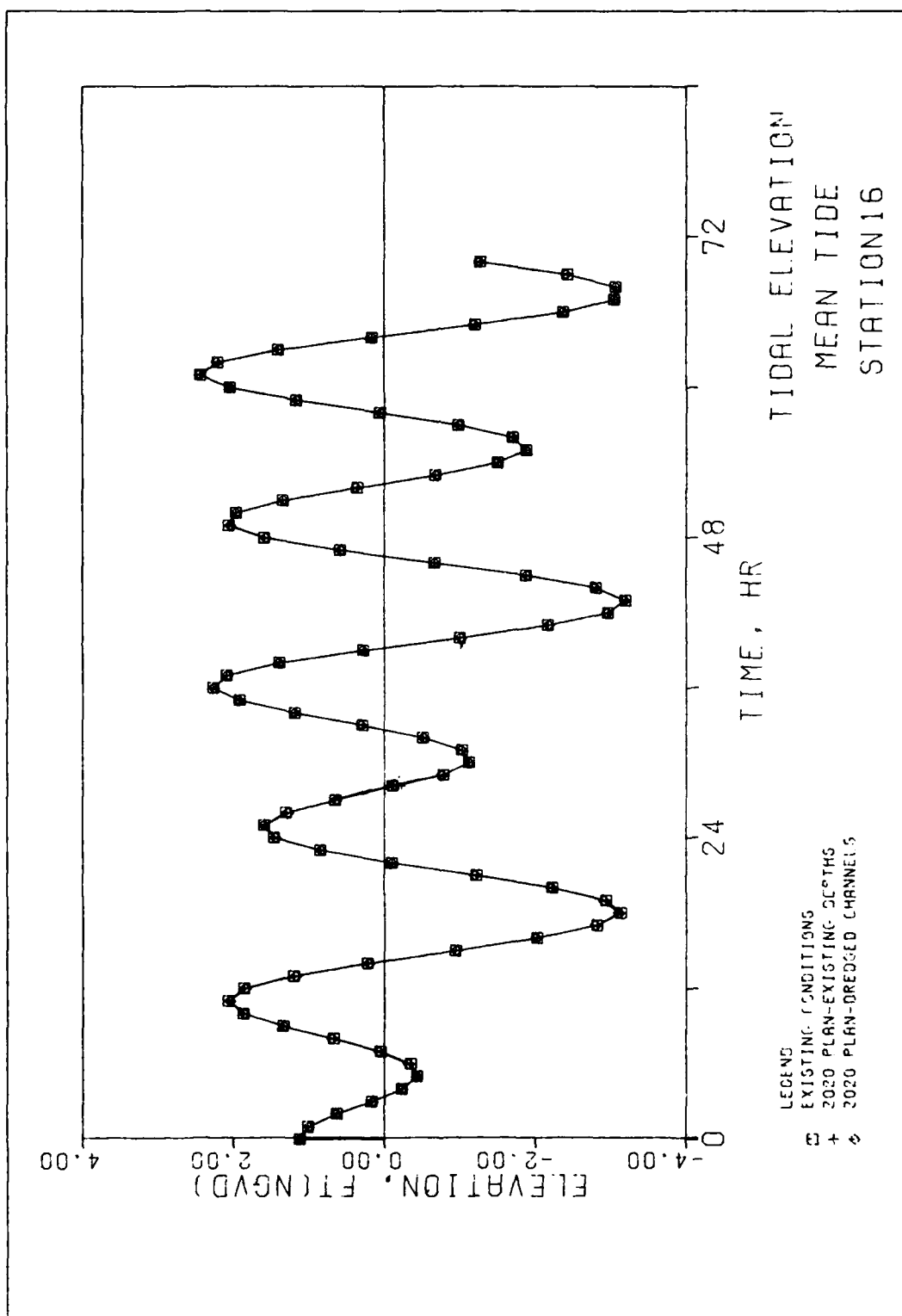


Plate 8

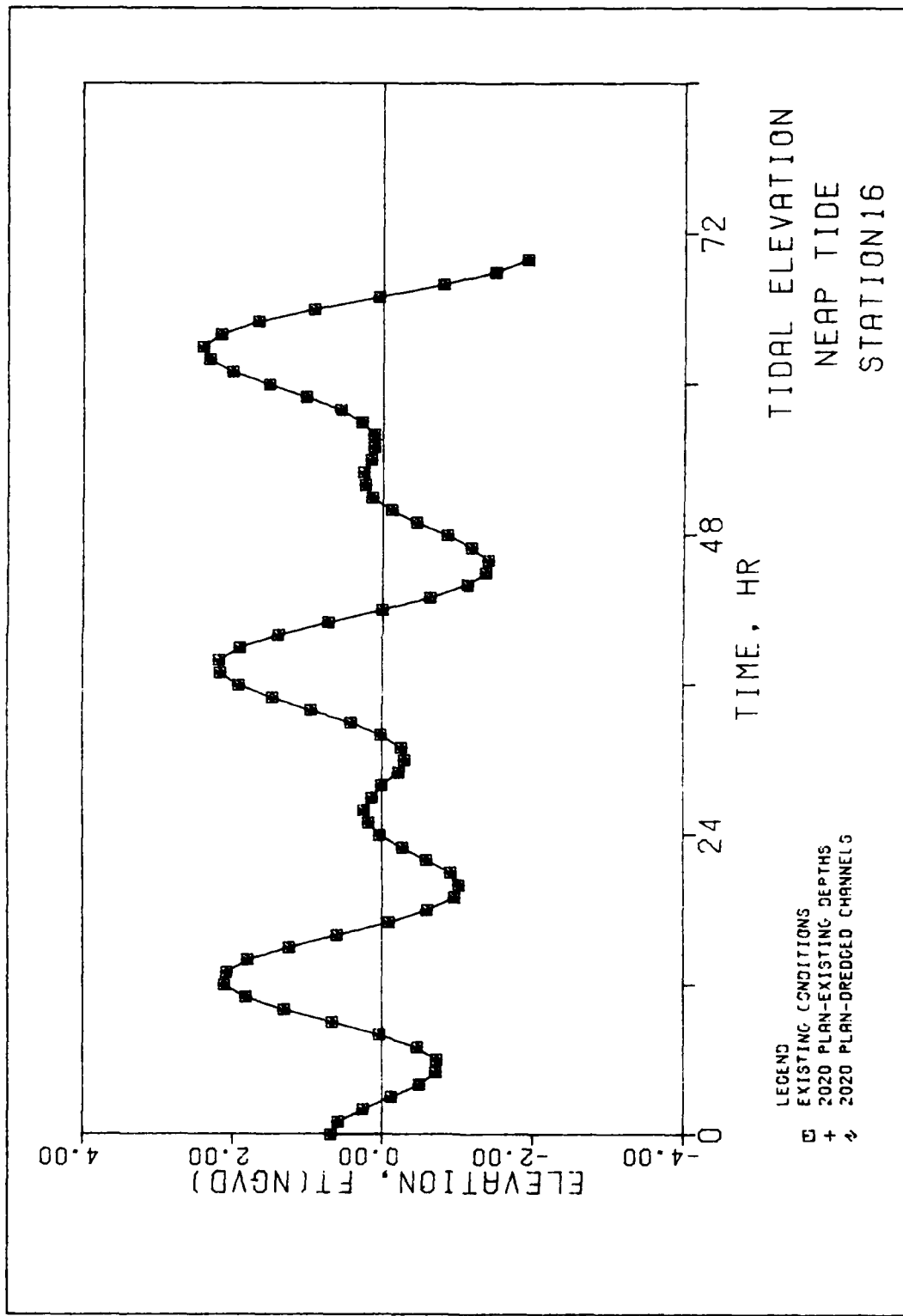


Plate 9

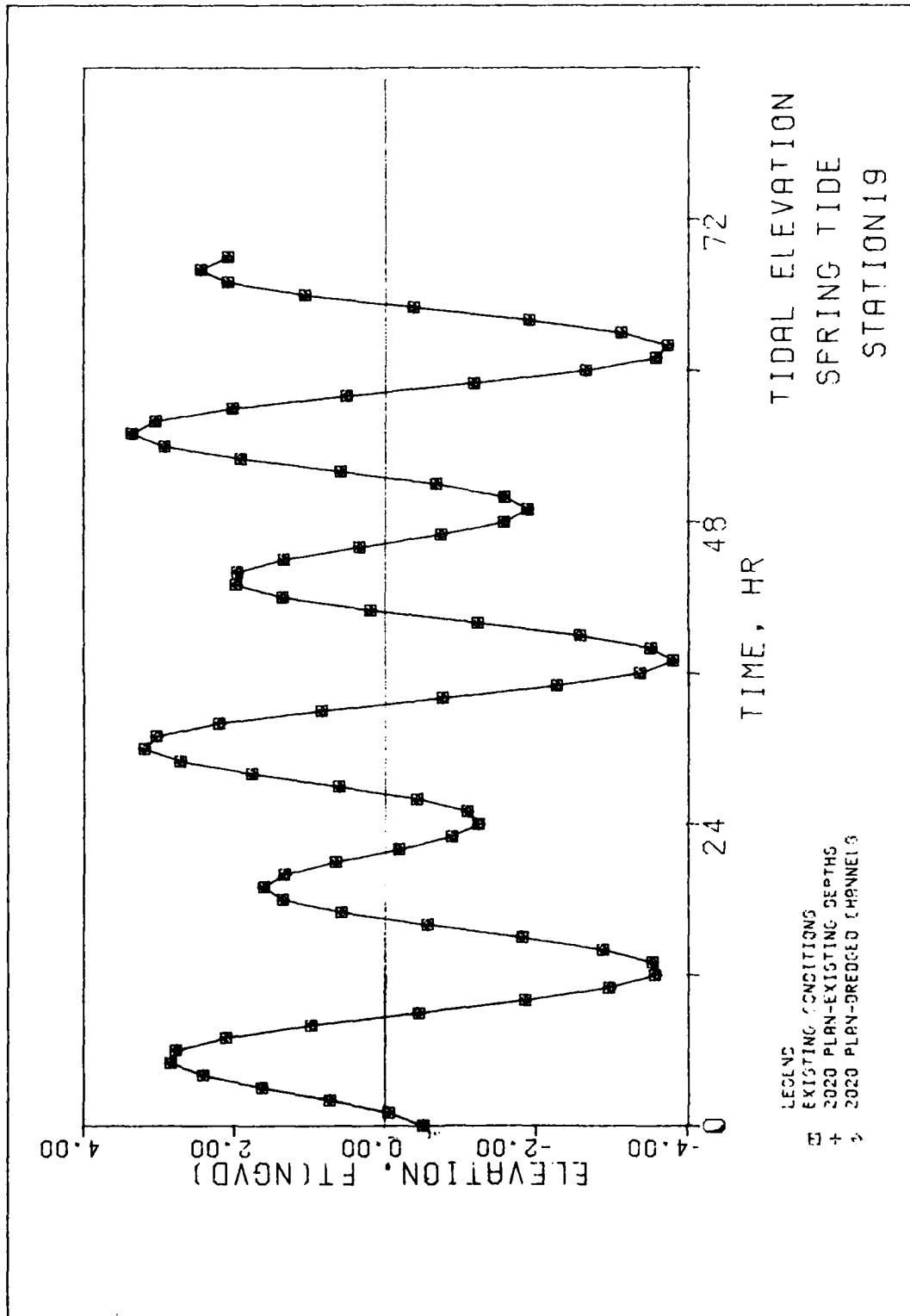


Plate 10

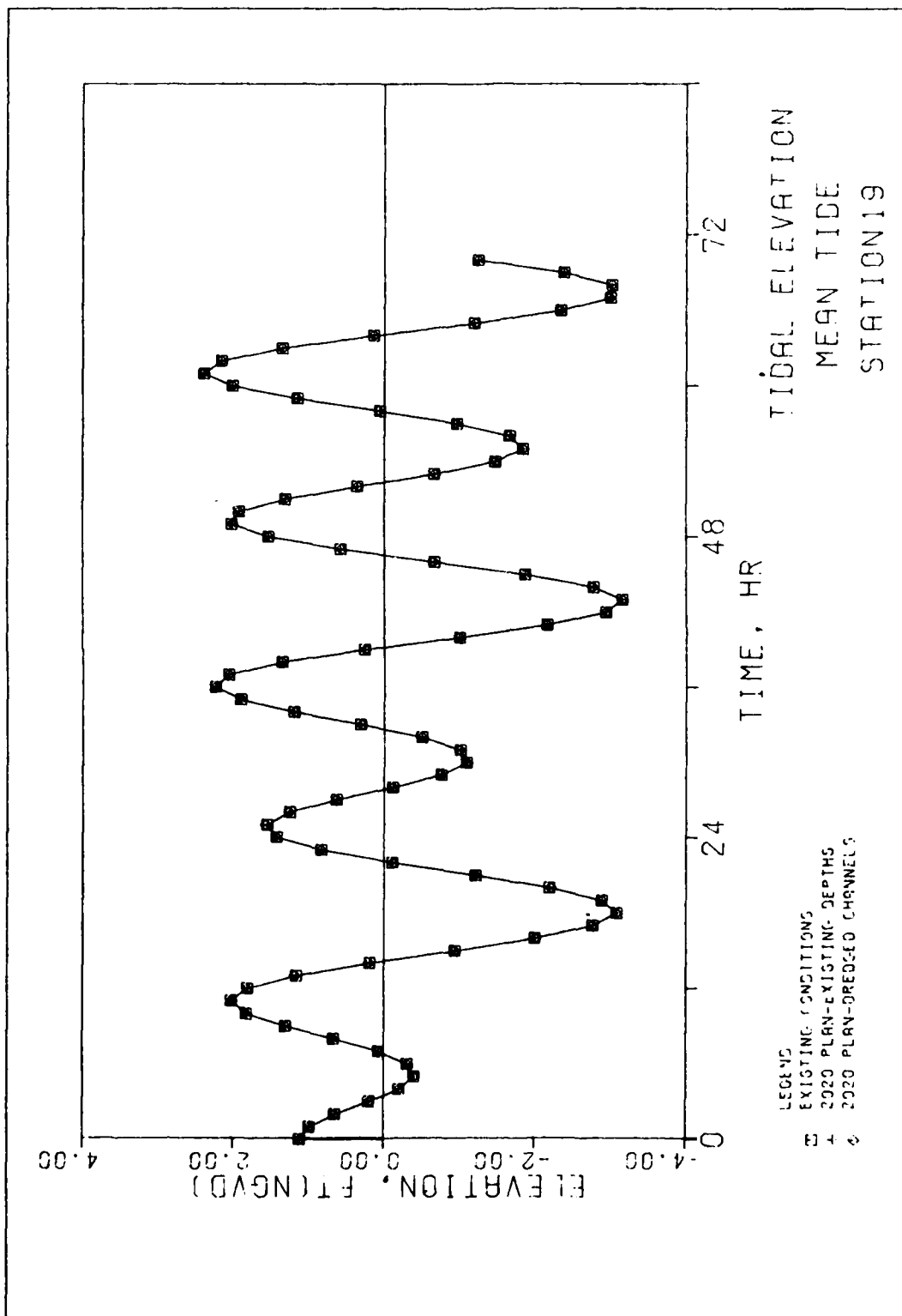


Plate 11

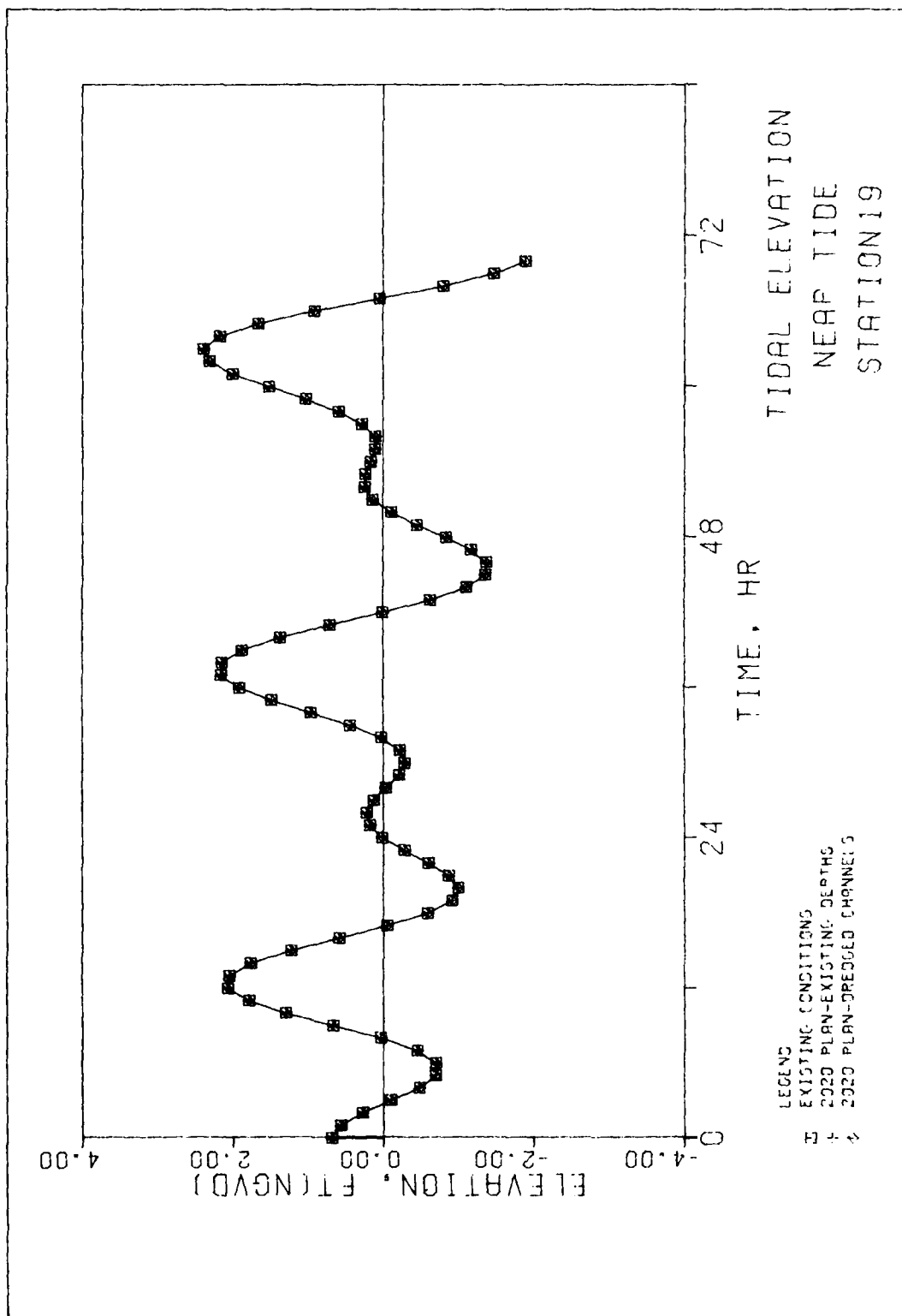


Plate 12

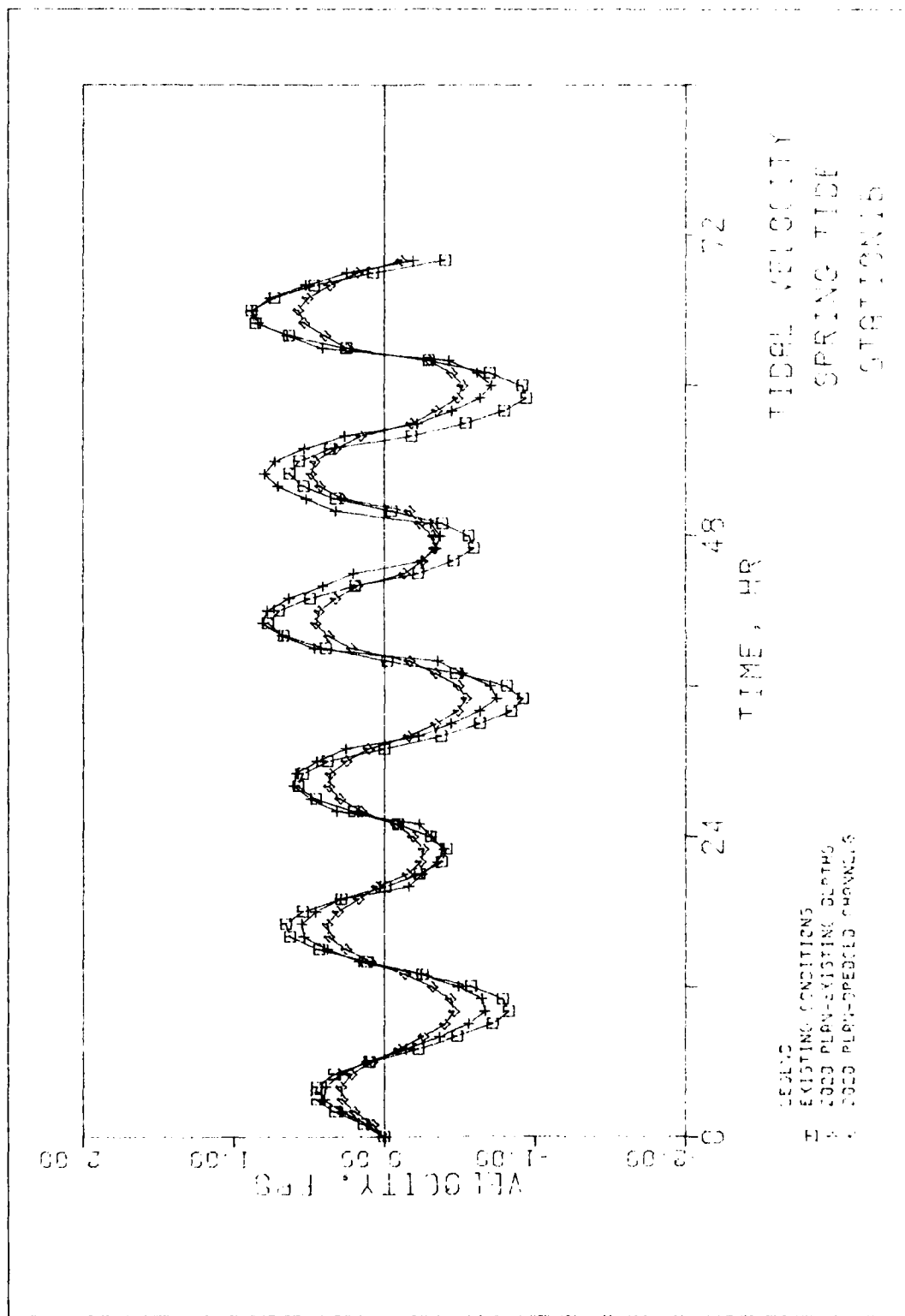


Plate 13

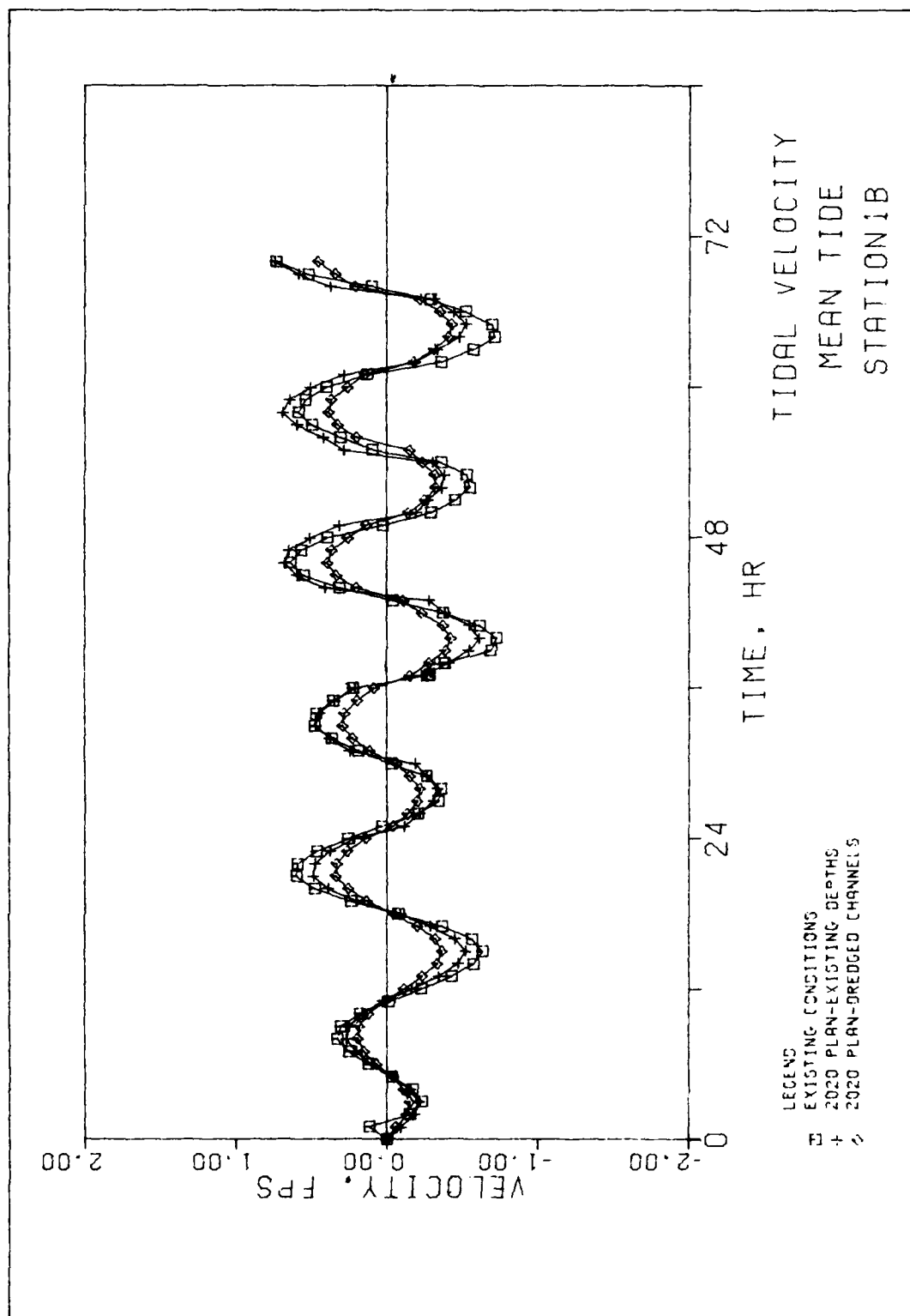


Plate 14

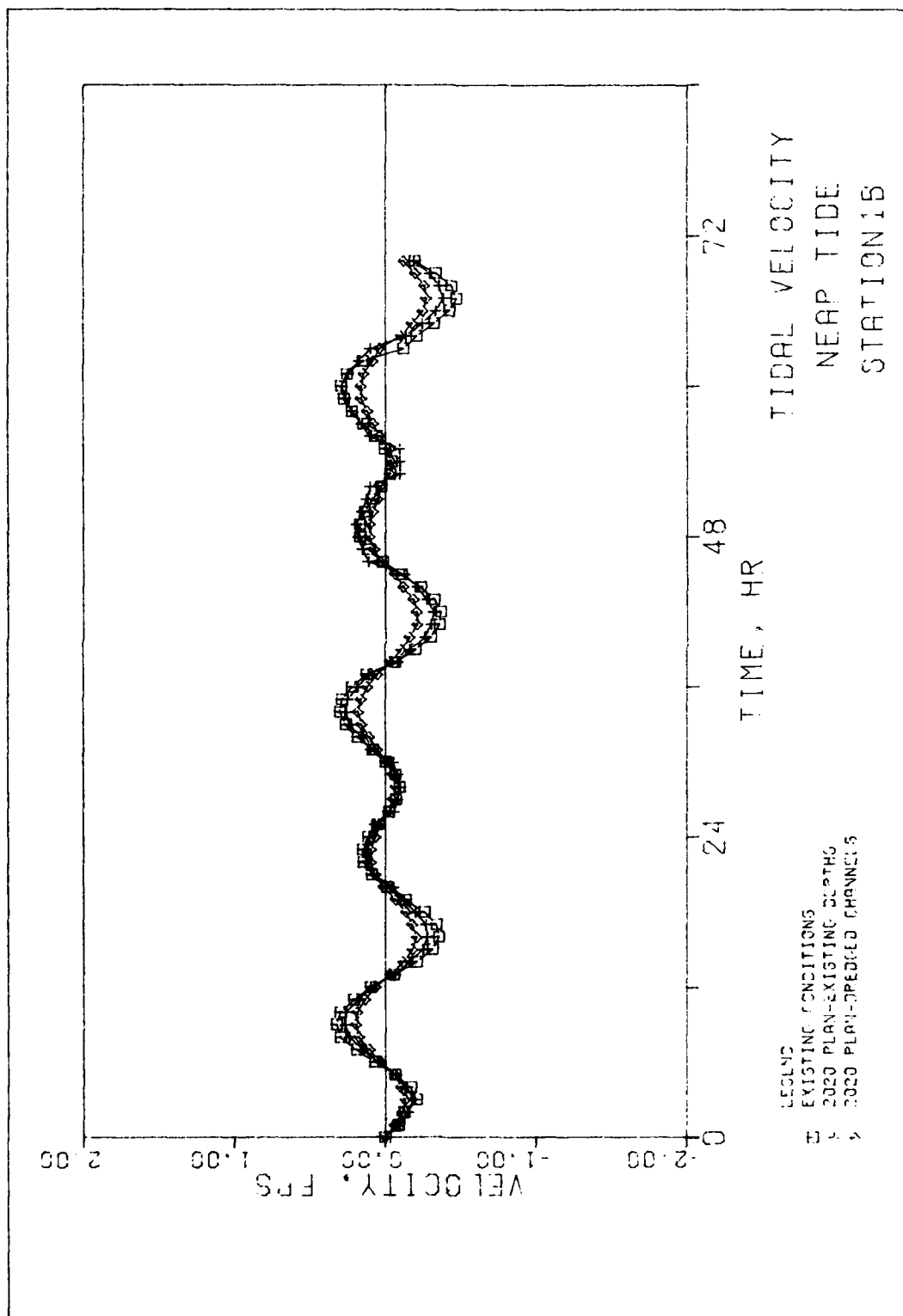


Plate 15

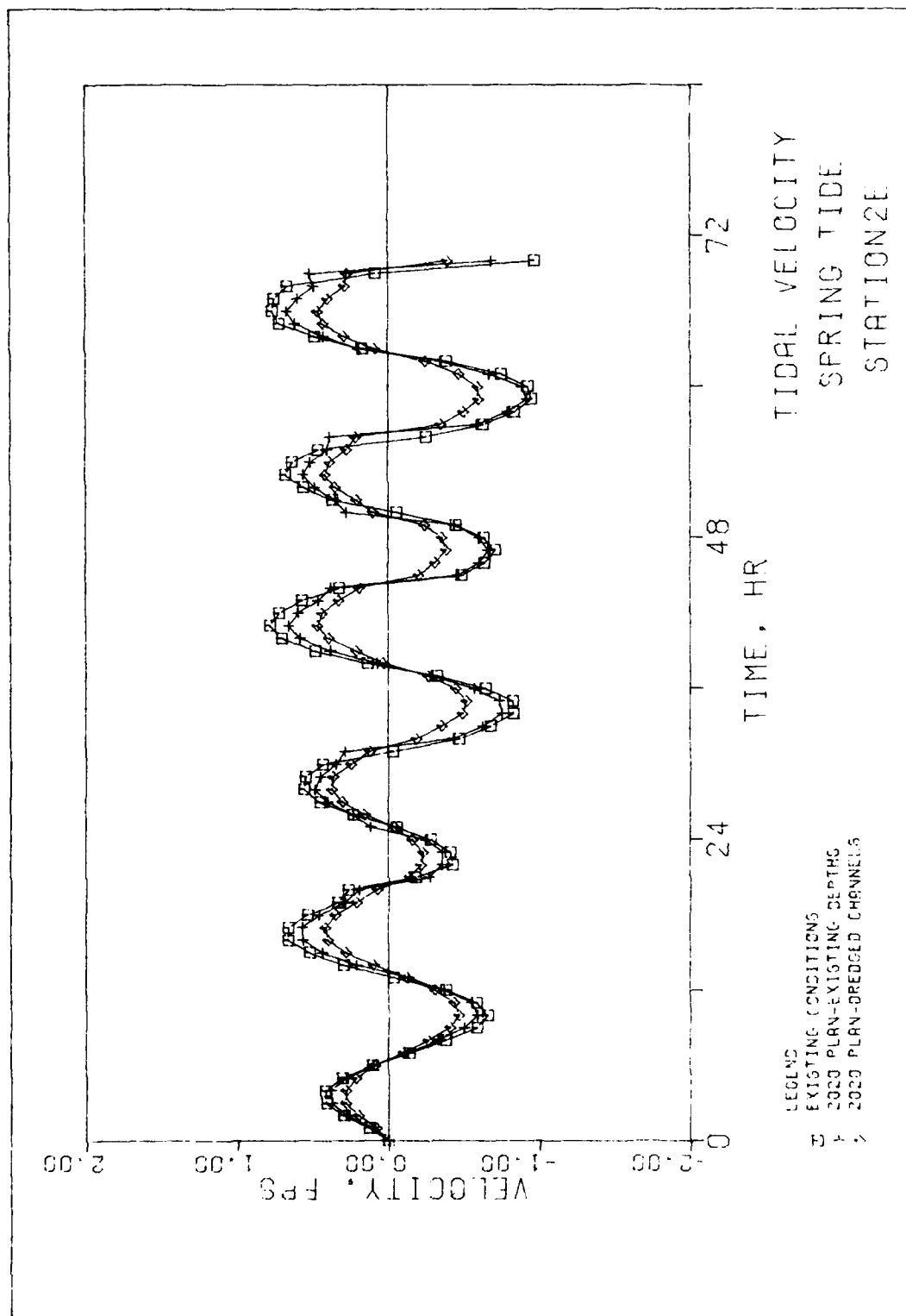


Plate 16

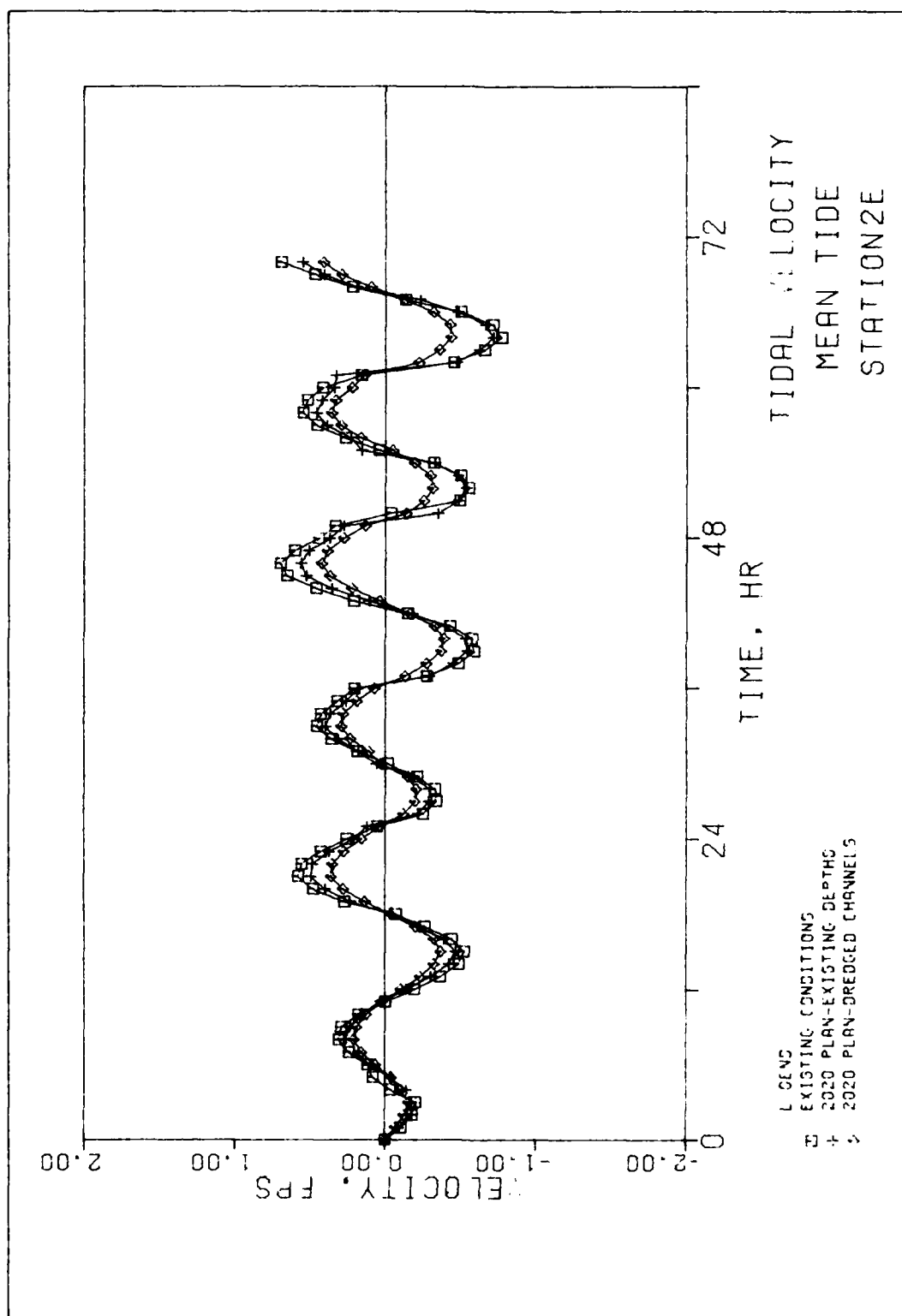


Plate 17

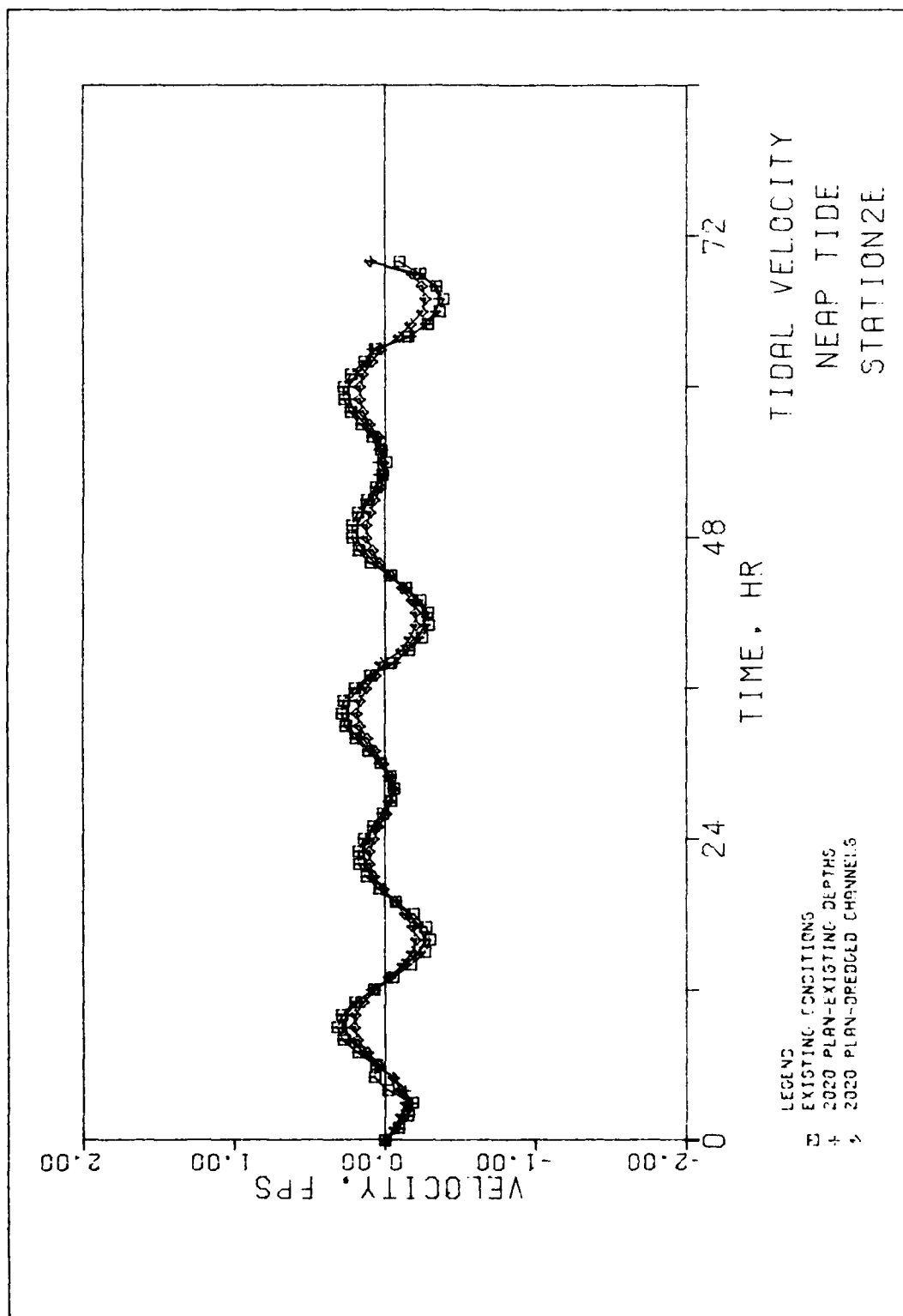


Plate 18

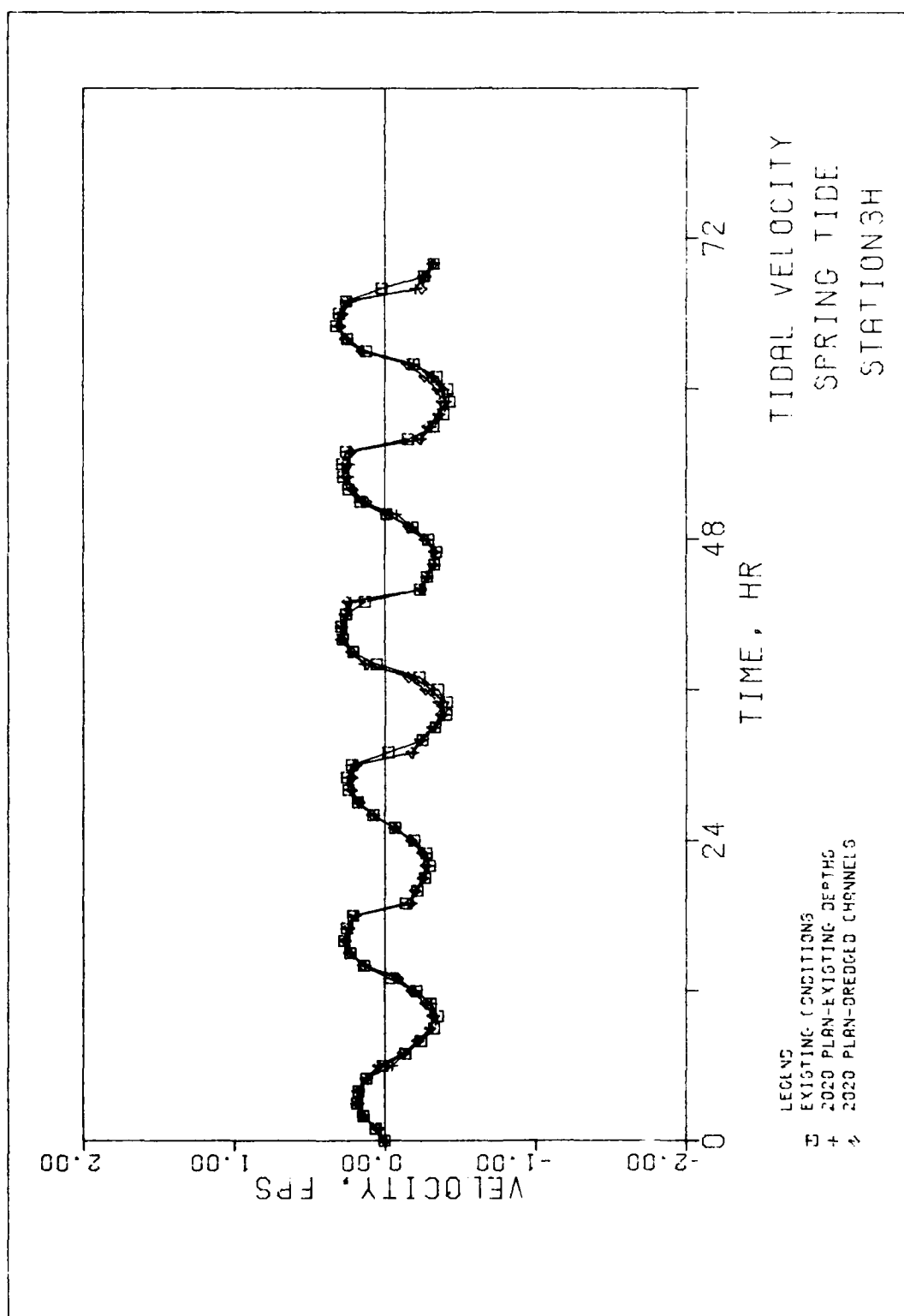


Plate 19

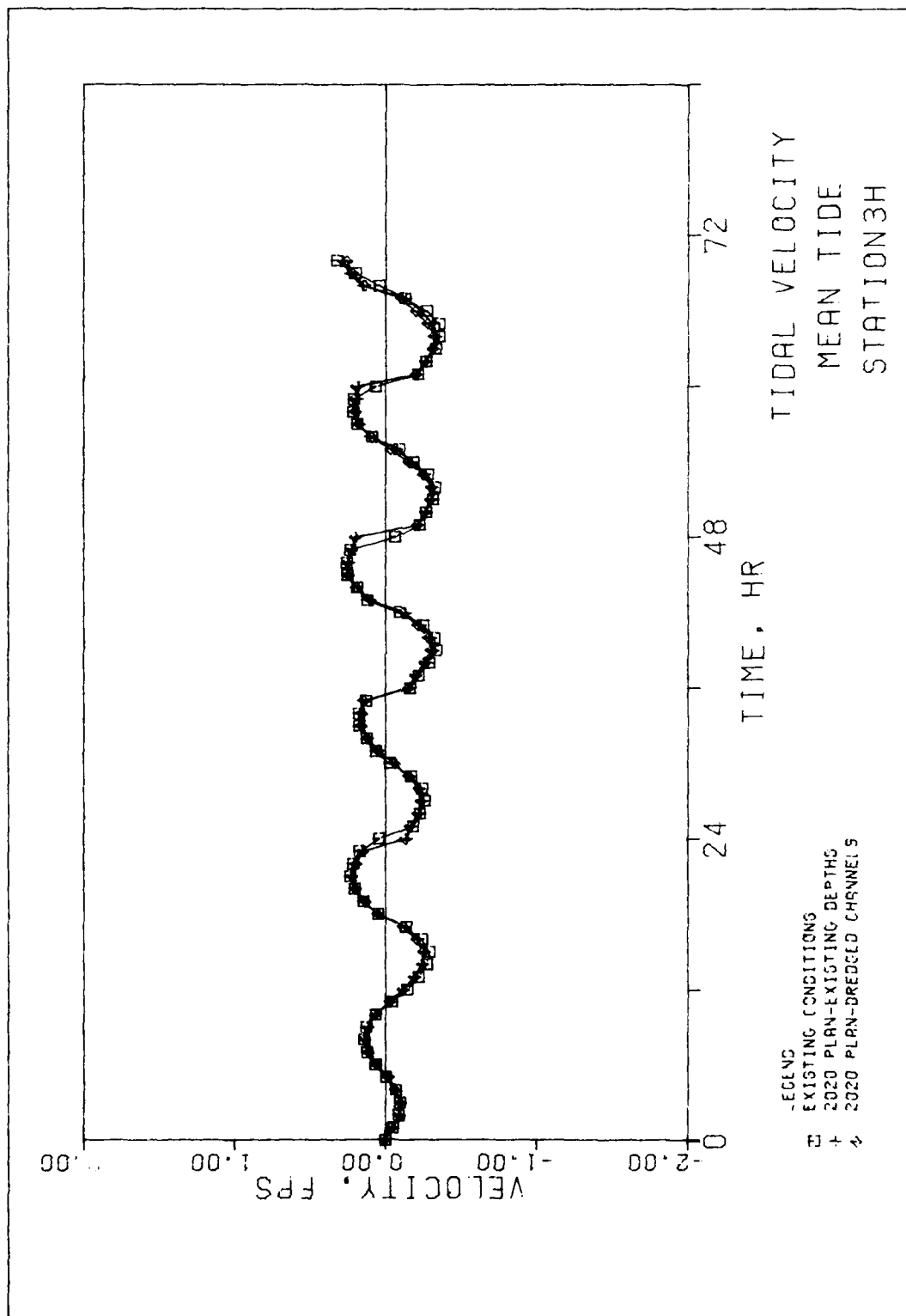


Plate 20

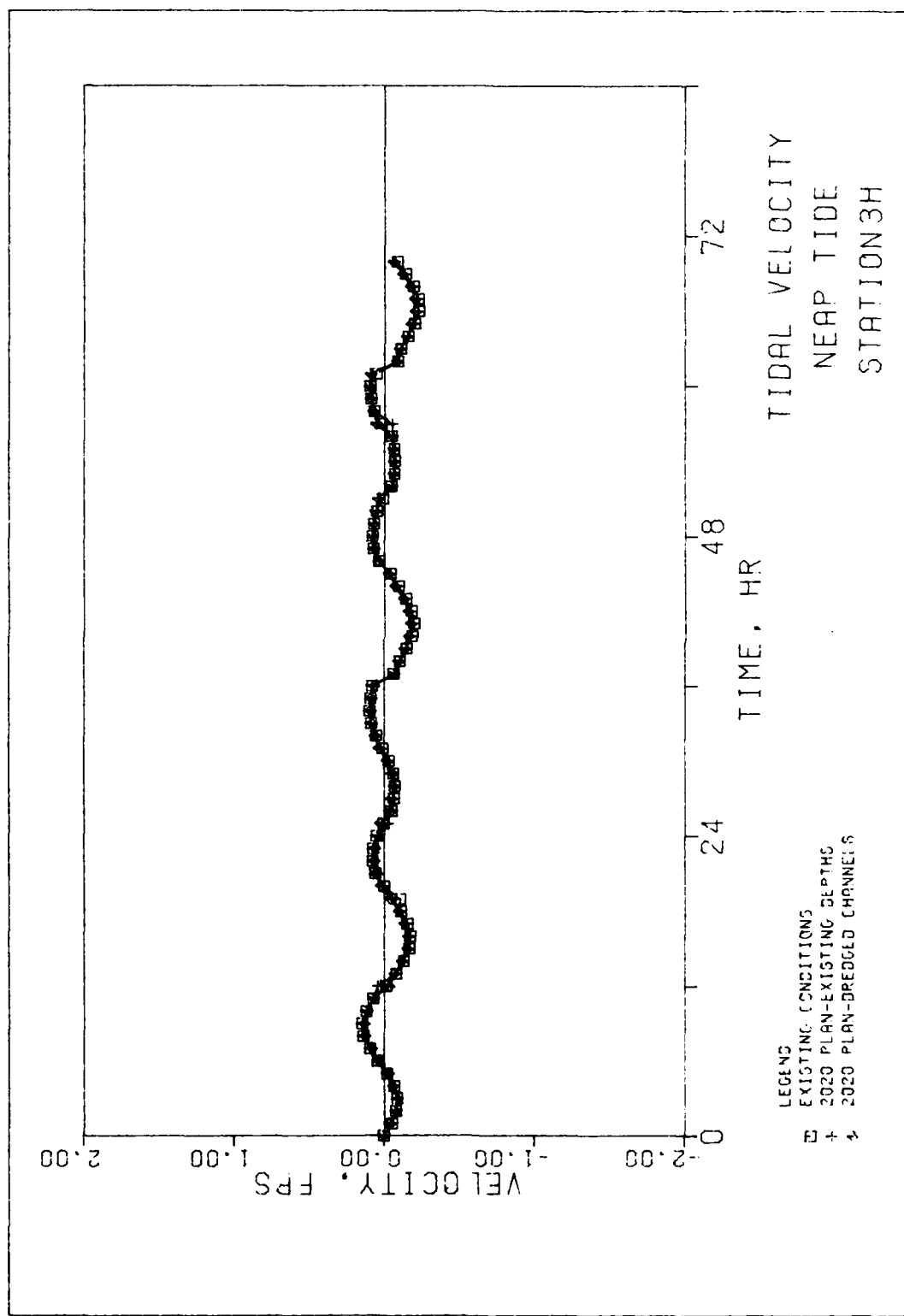


Plate 21

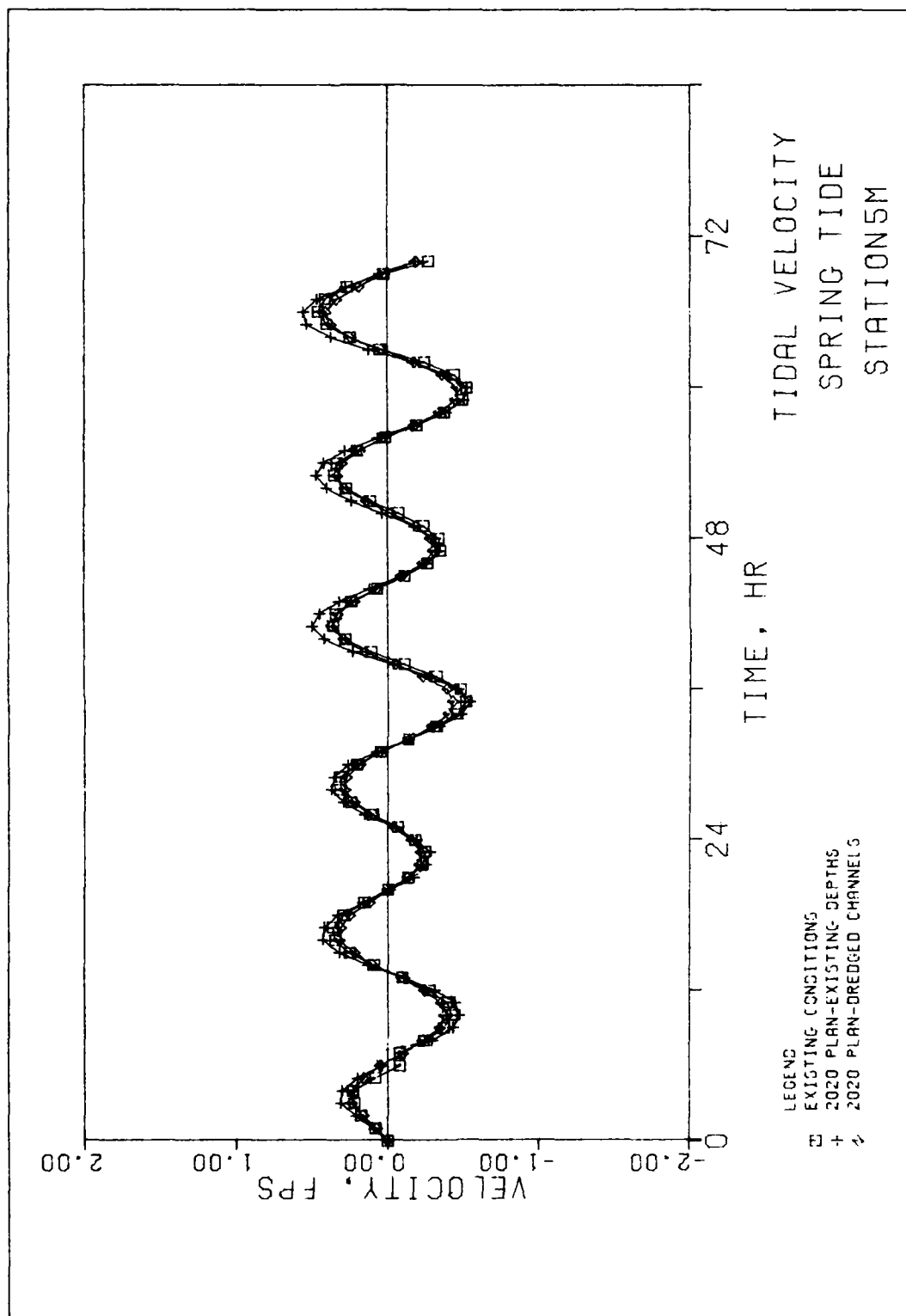


Plate 22

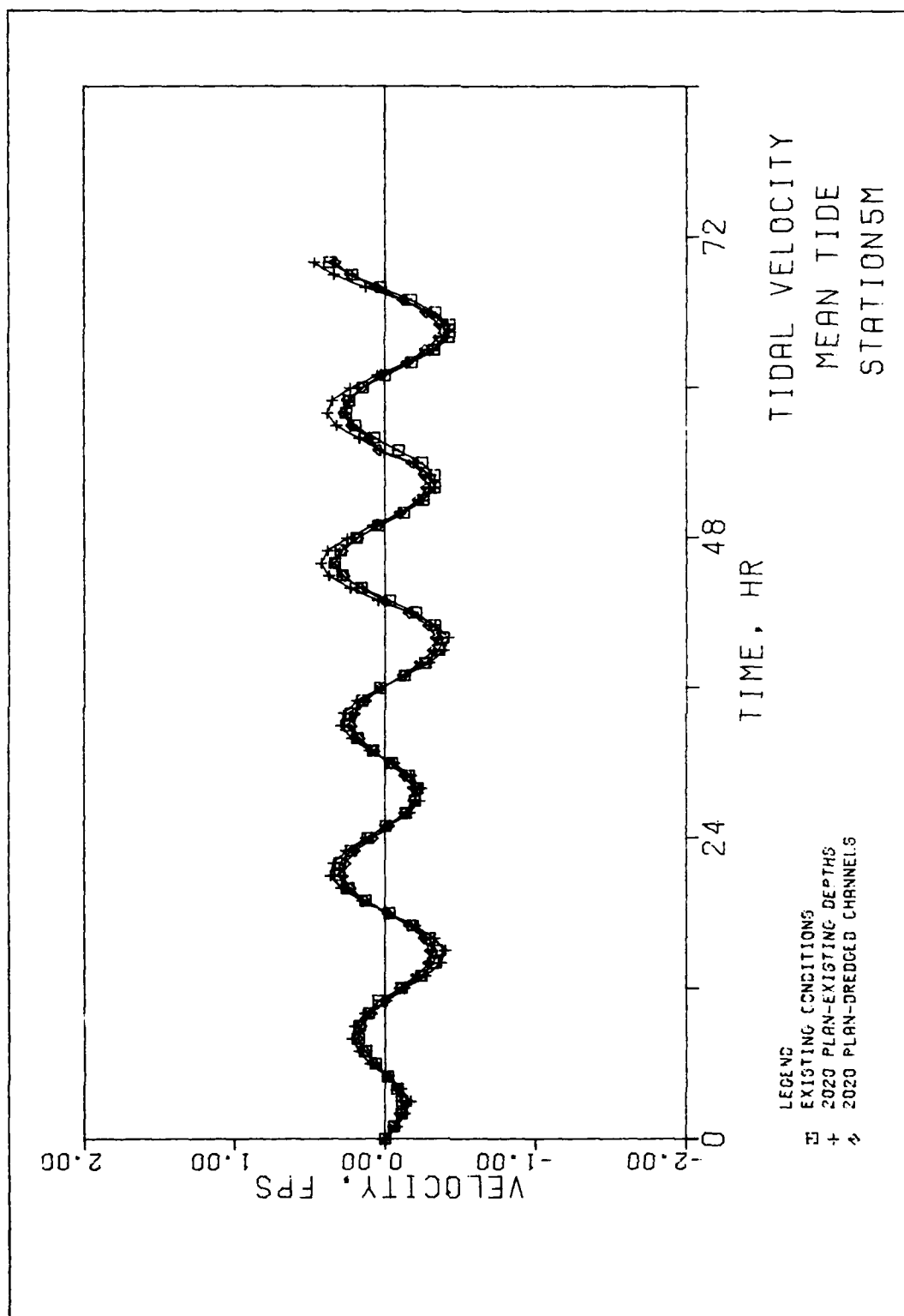


Plate 23

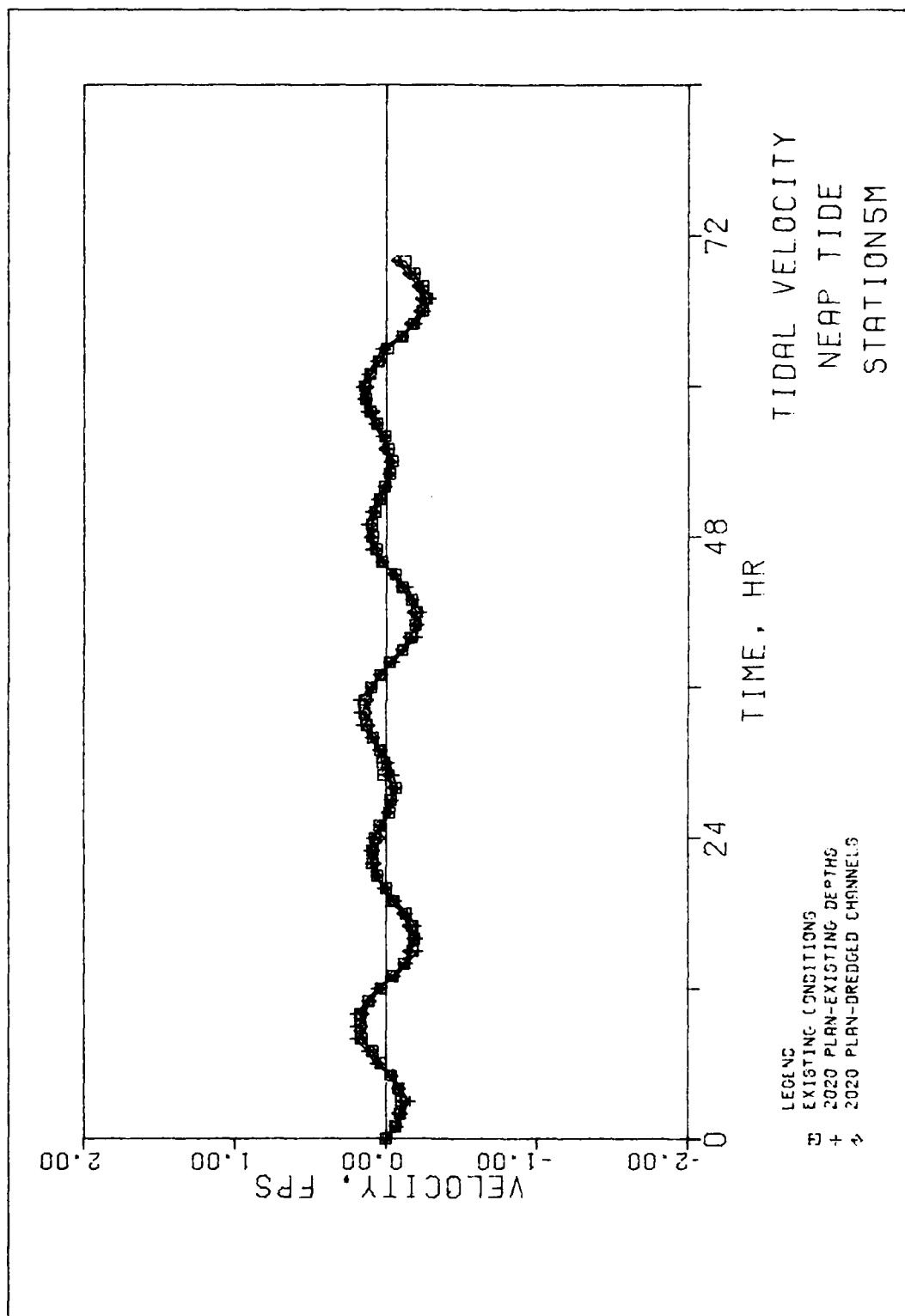


Plate 24

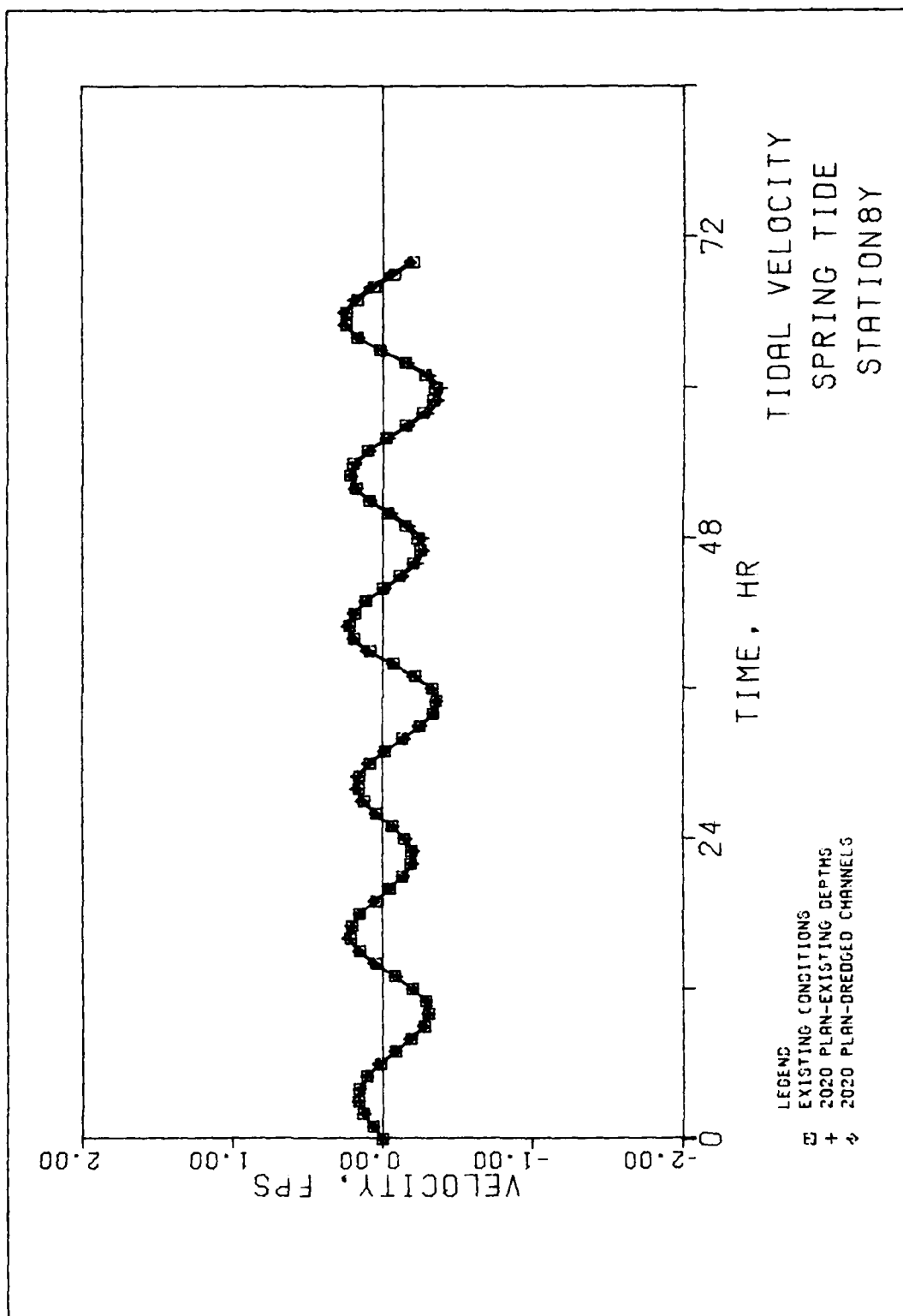


Plate 25

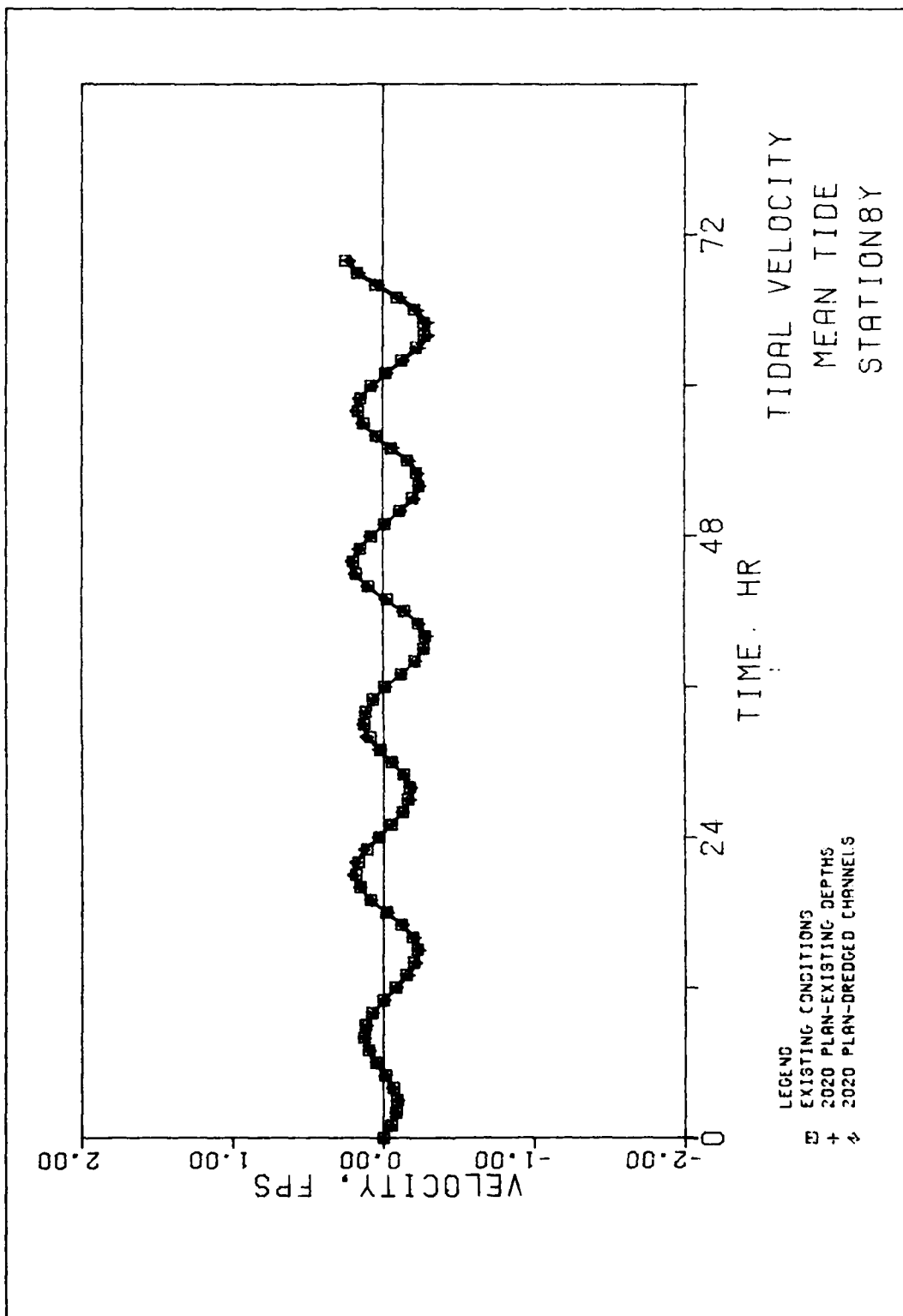


Plate 26

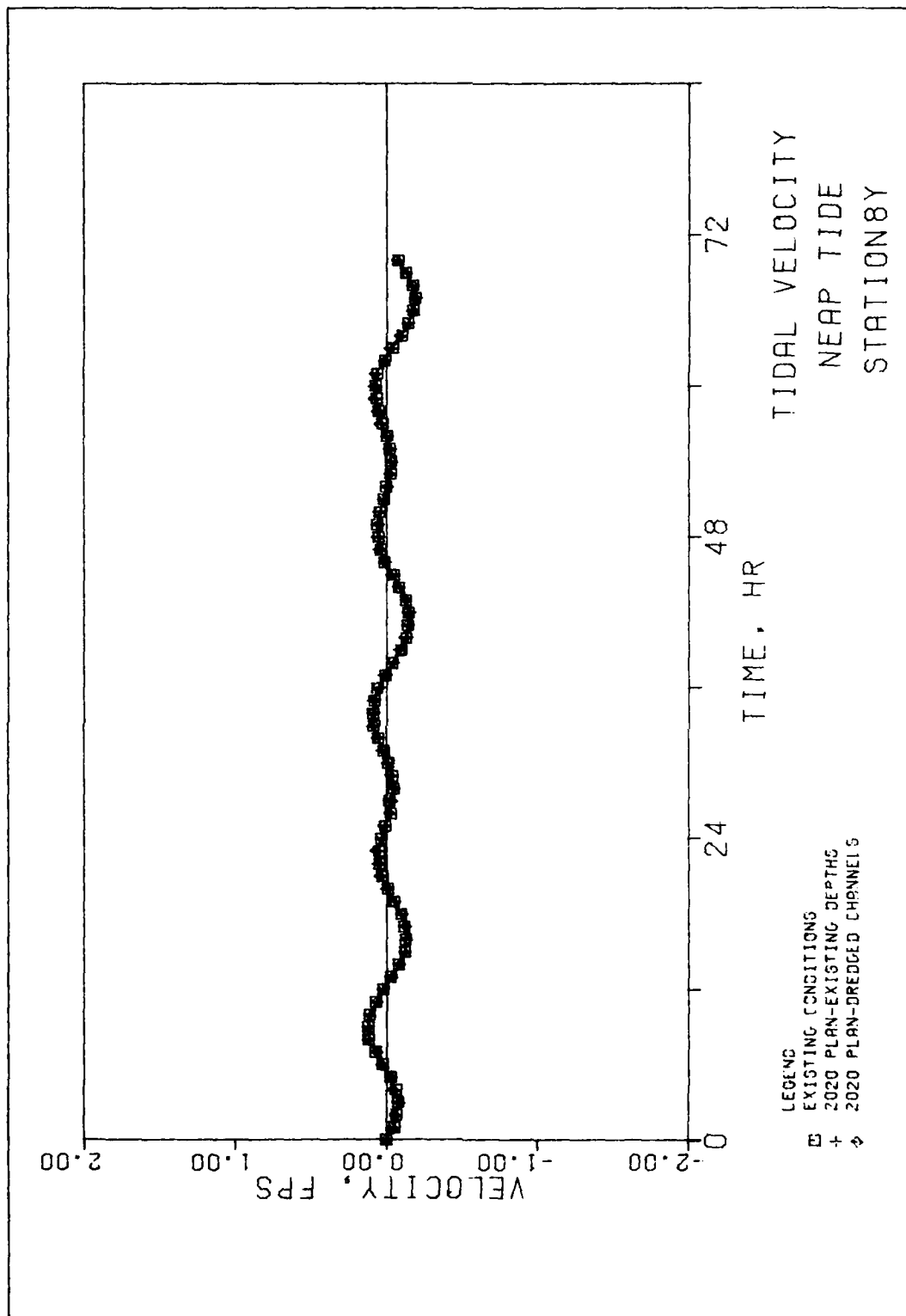


Plate 27

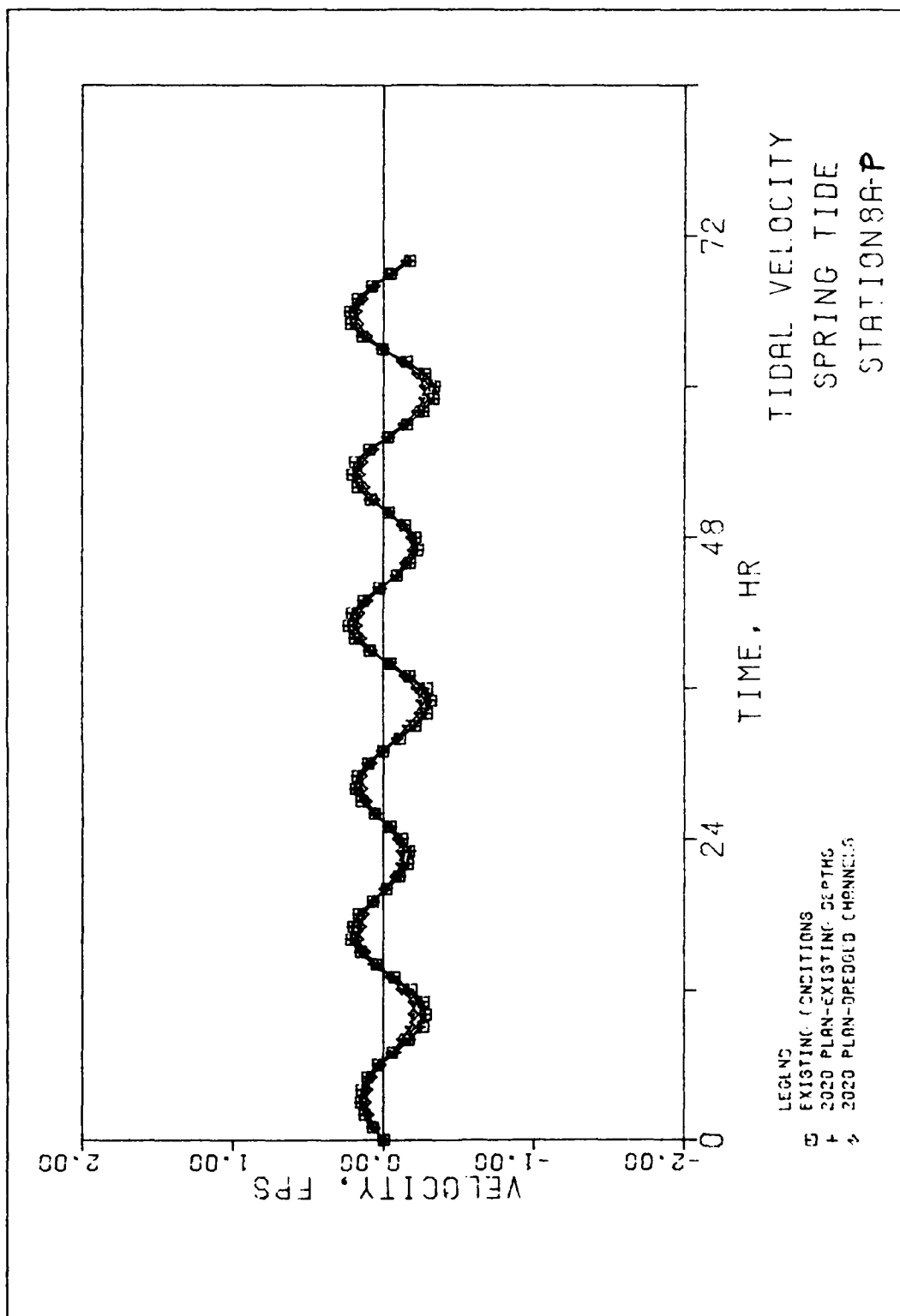


Plate 28

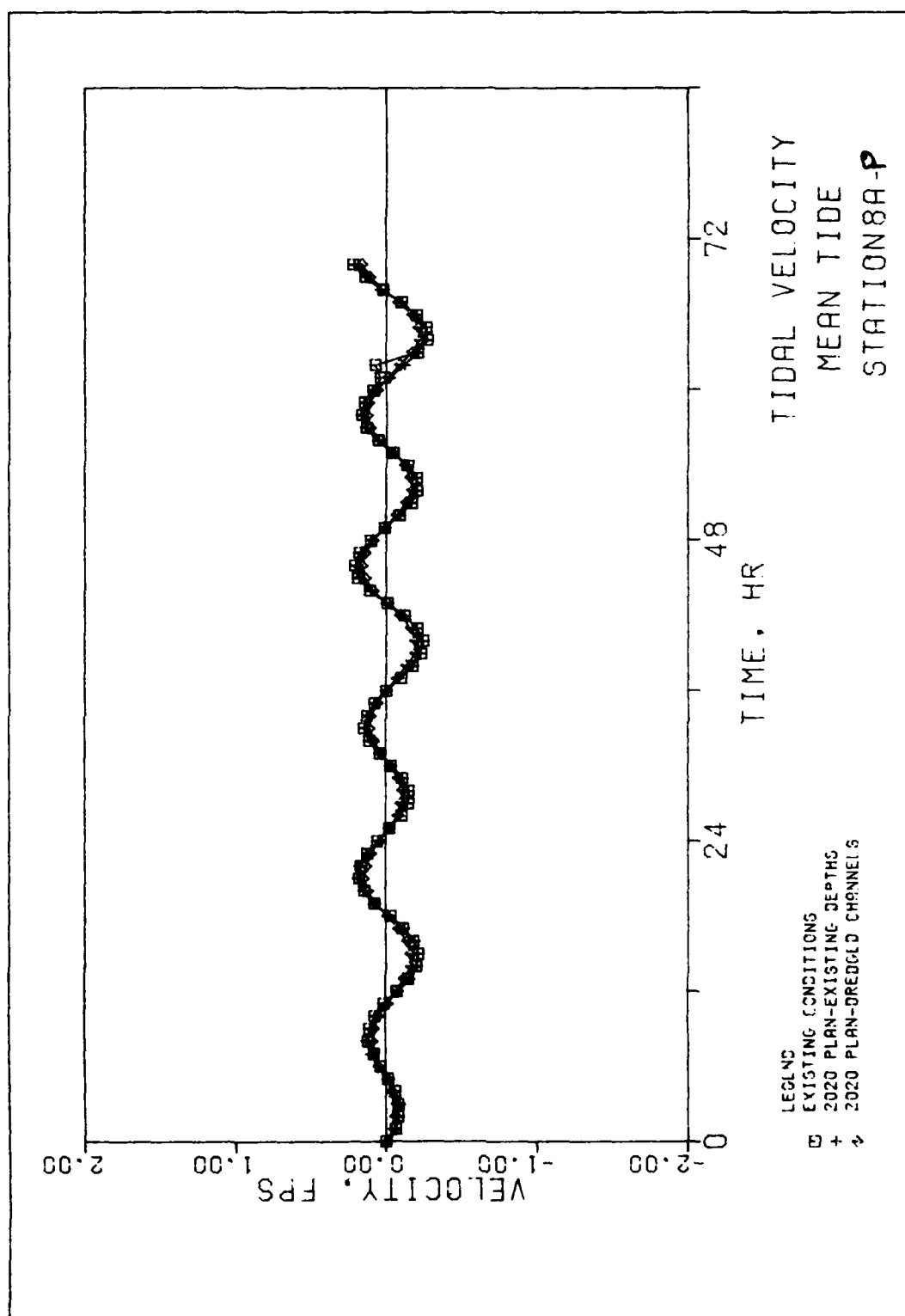


Plate 29

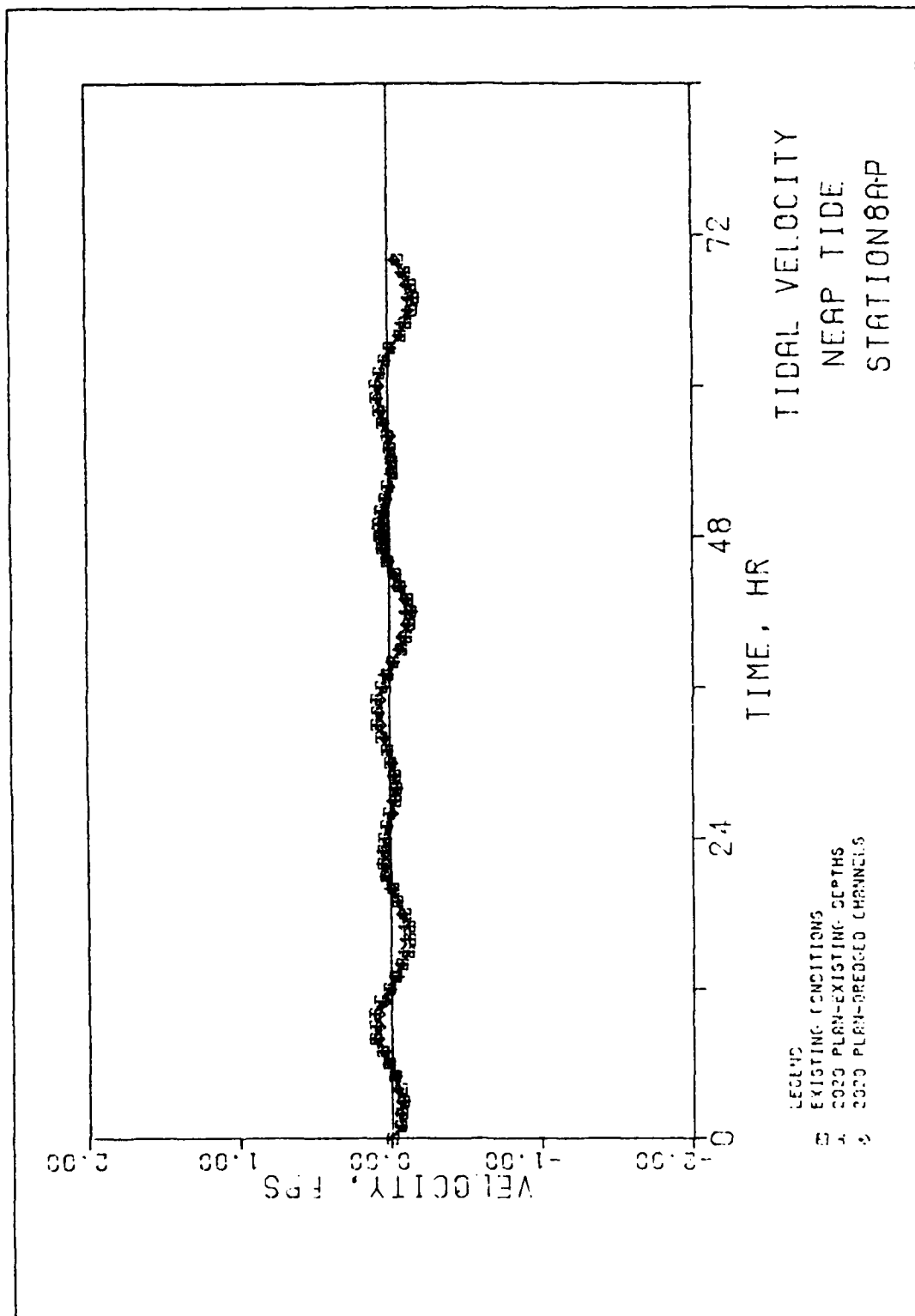


Plate 30

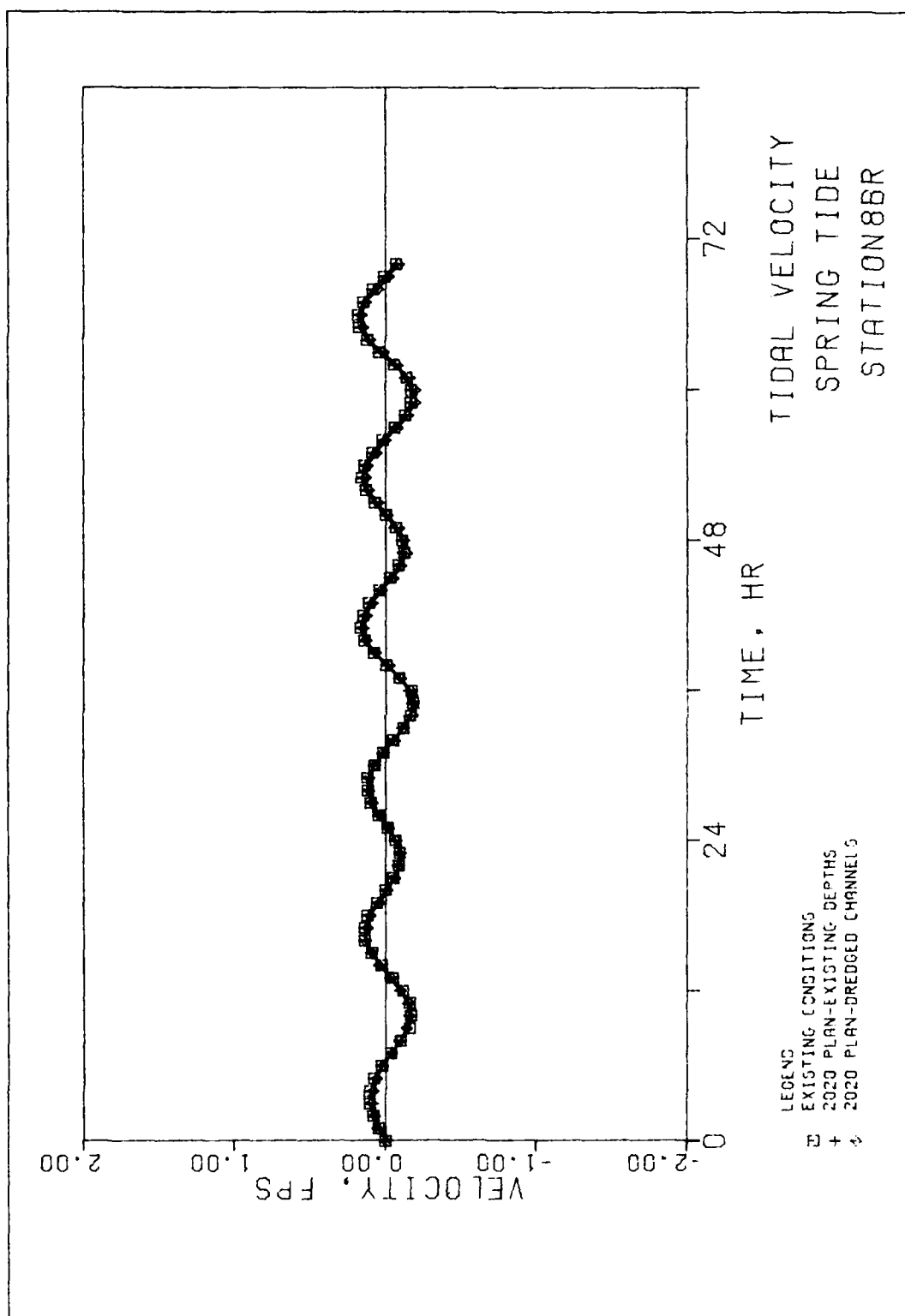


Plate 31

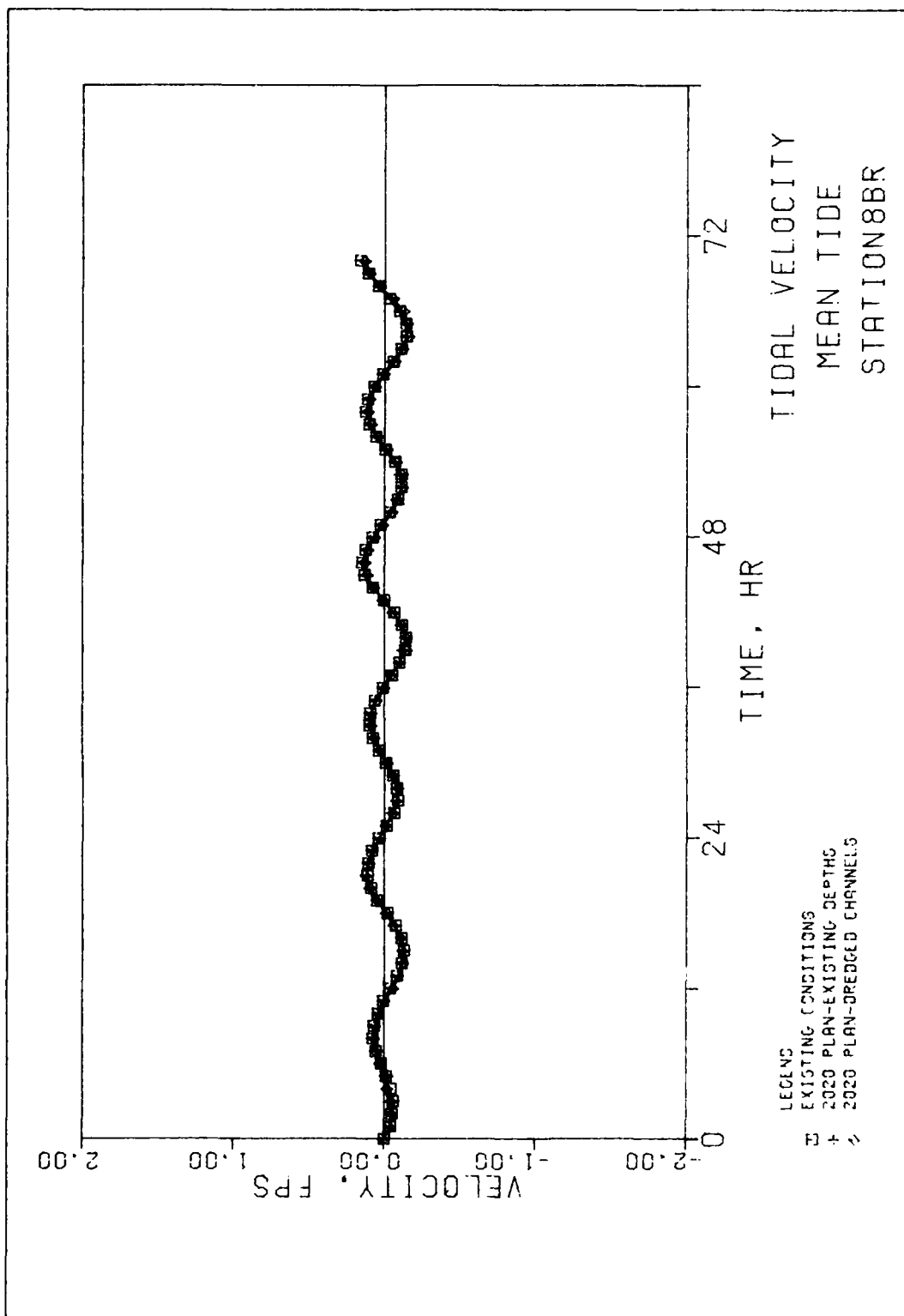


Plate 32

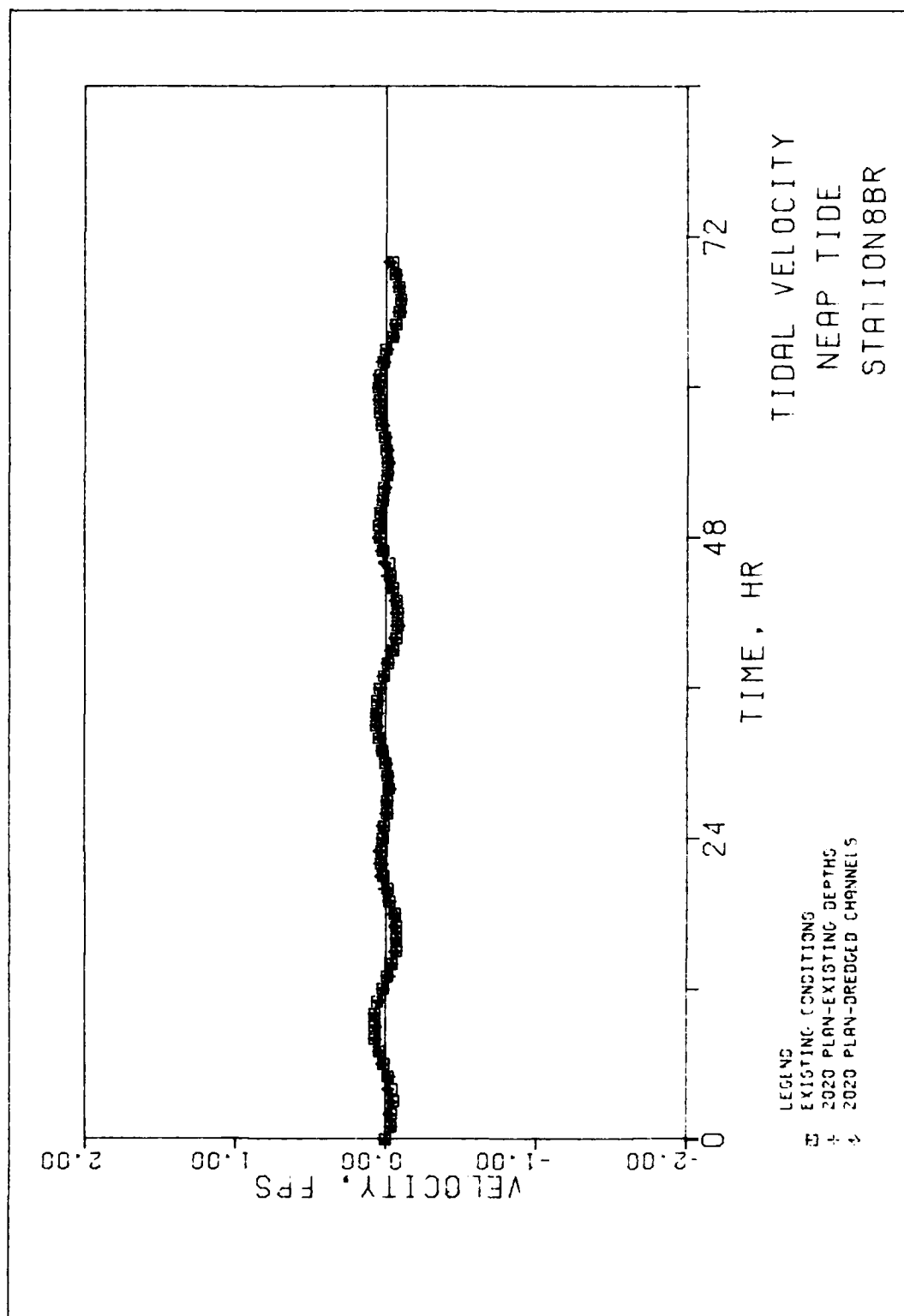


Plate 33

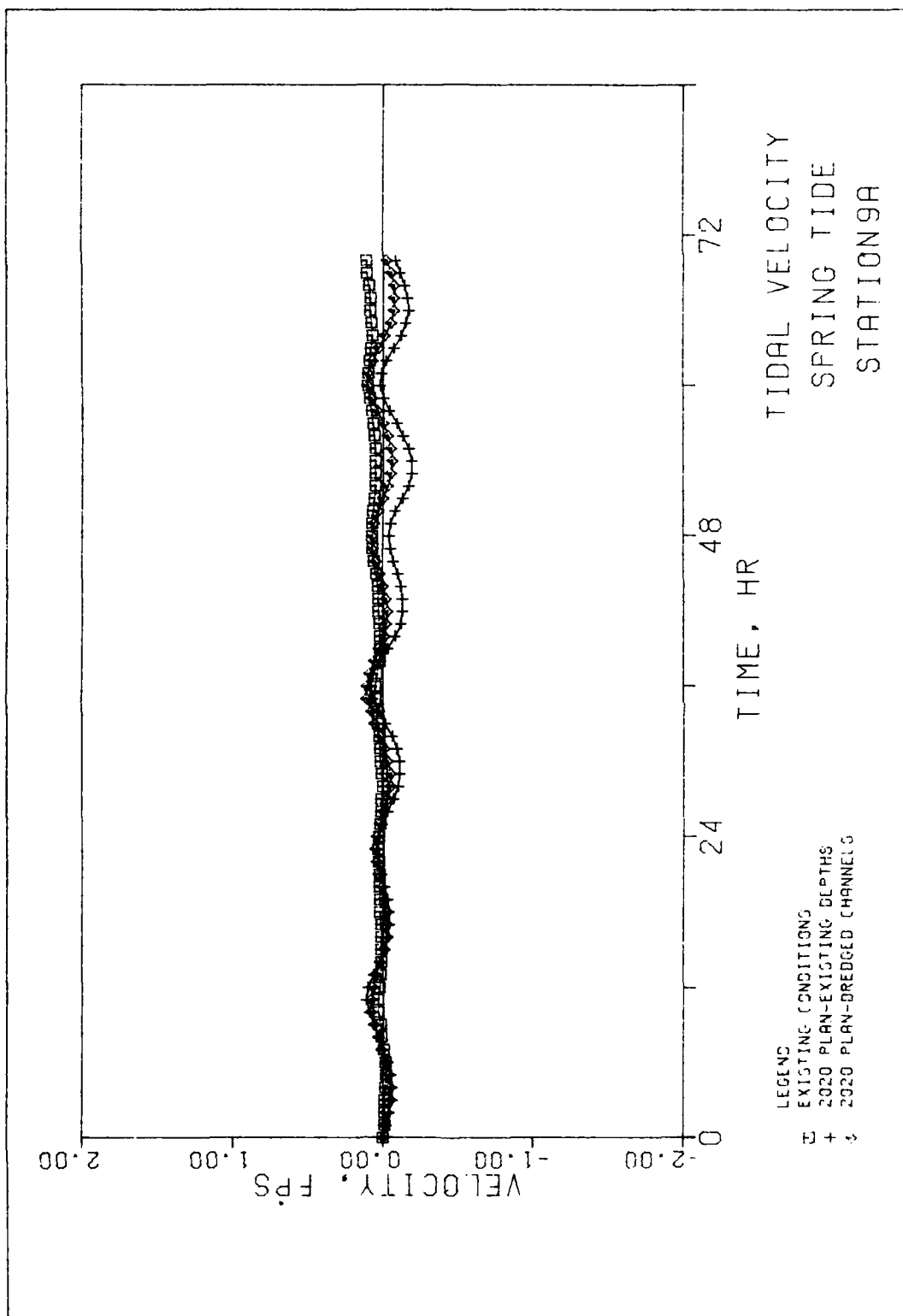


Plate 34

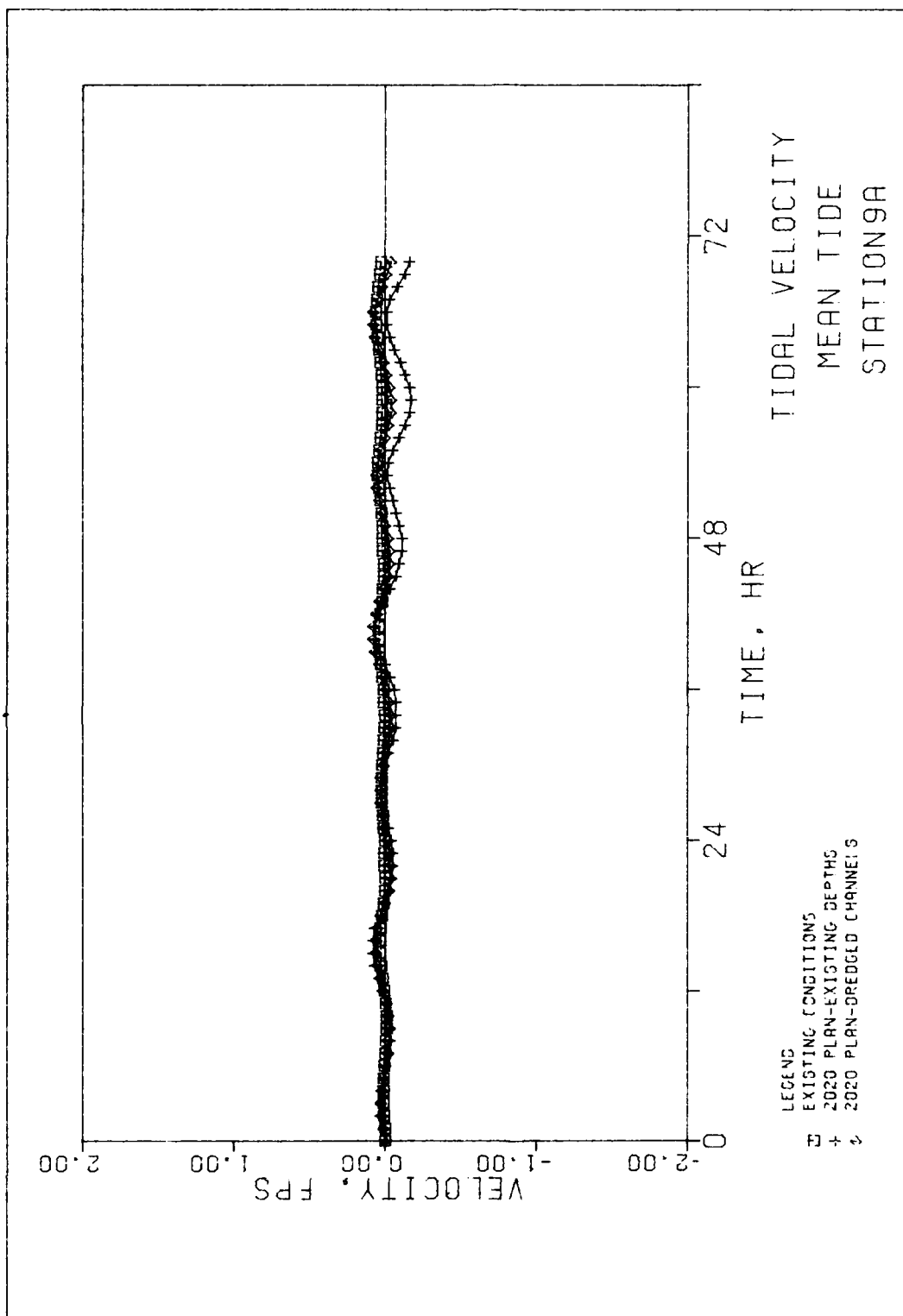


Plate 35

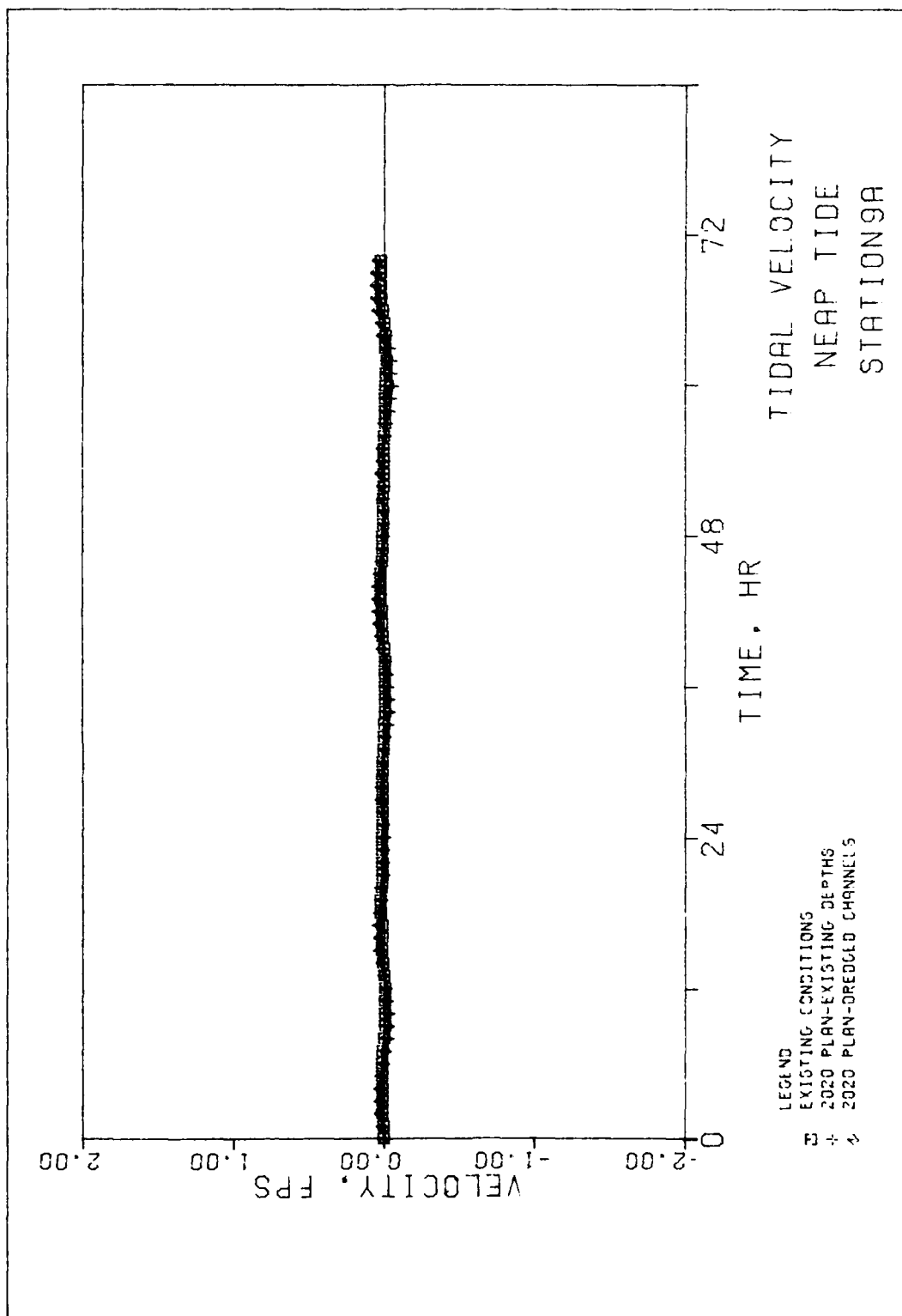


Plate 36

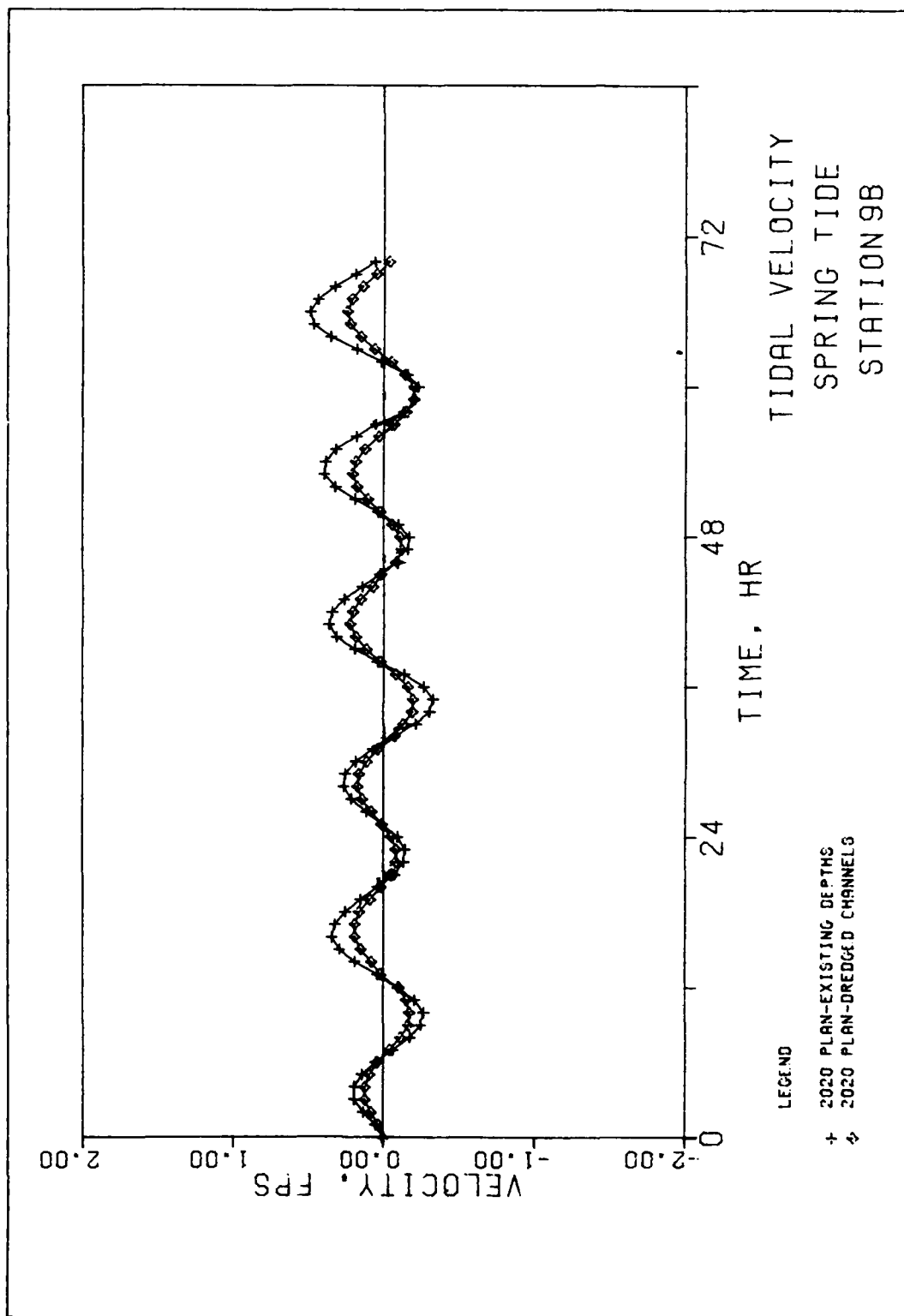


Plate 37

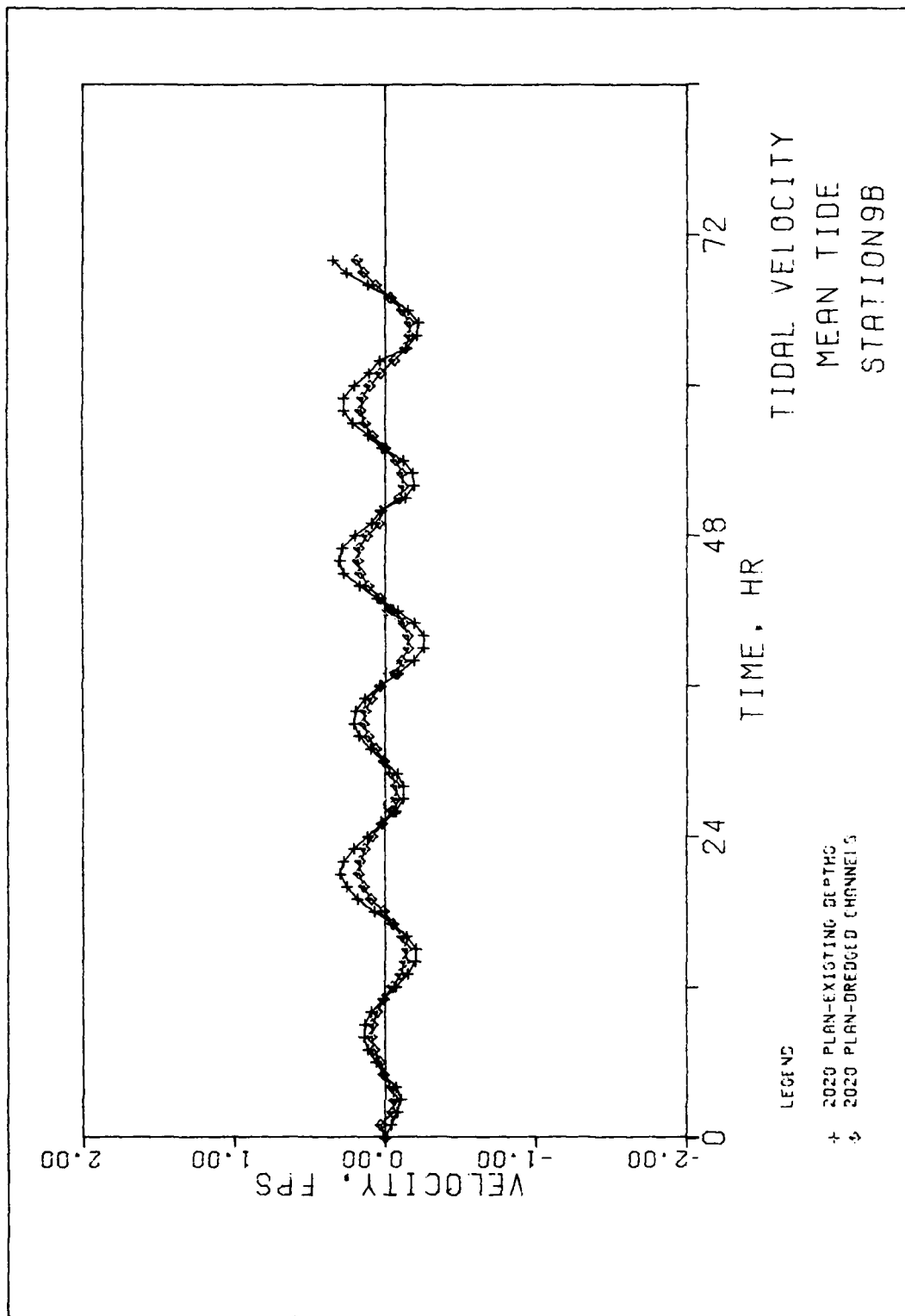


Plate 38

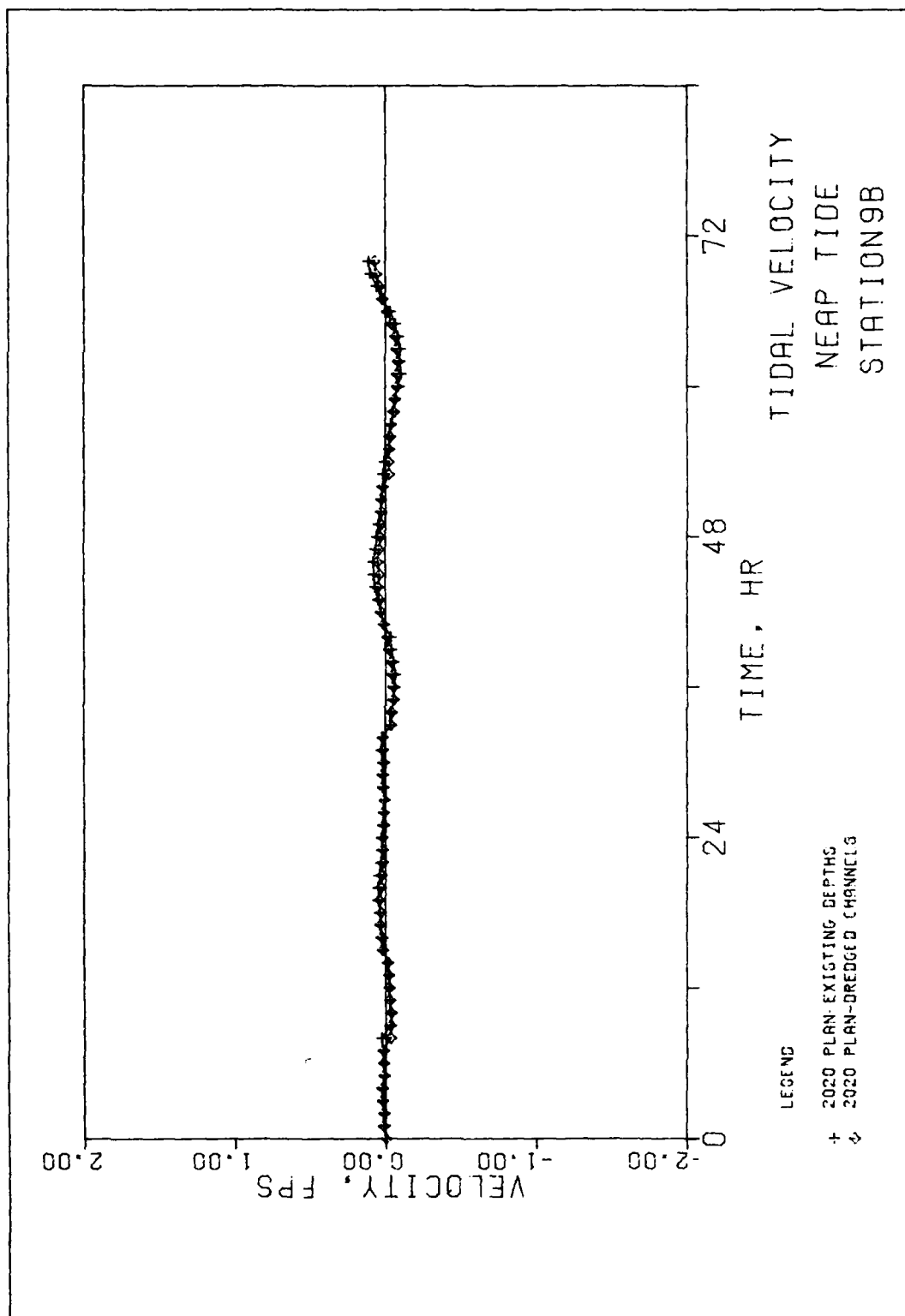


Plate 39

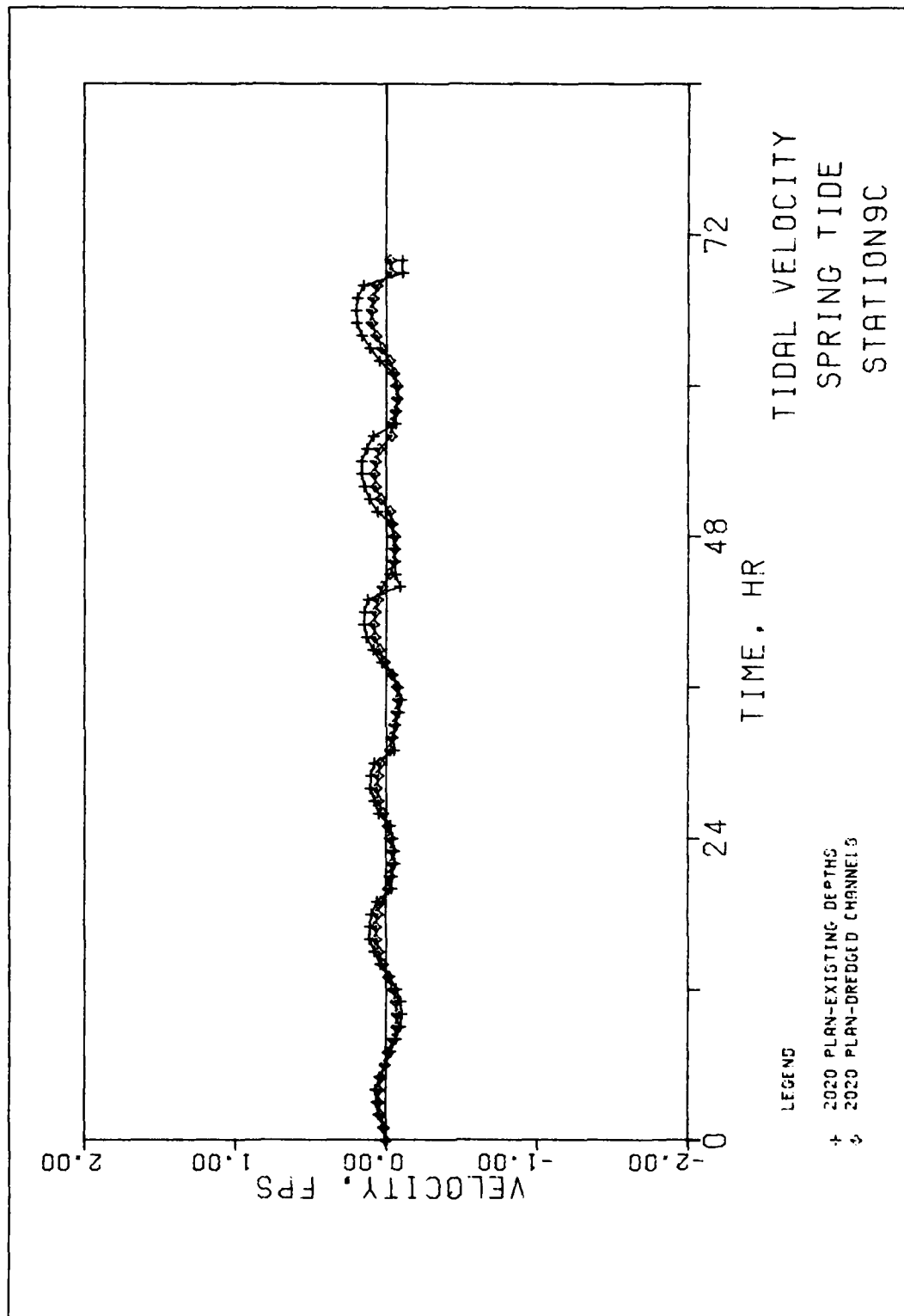


Plate 40

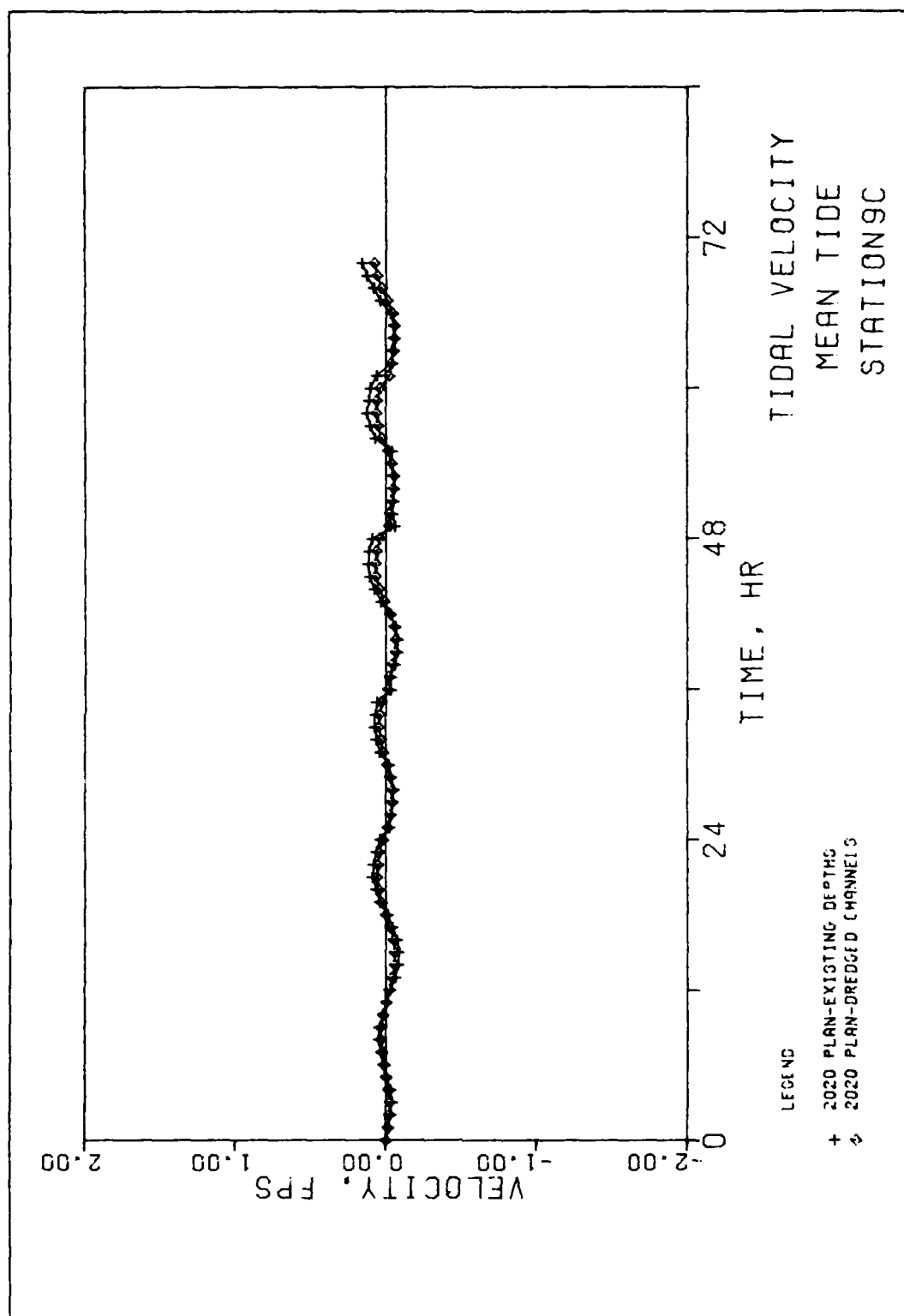


Plate 41

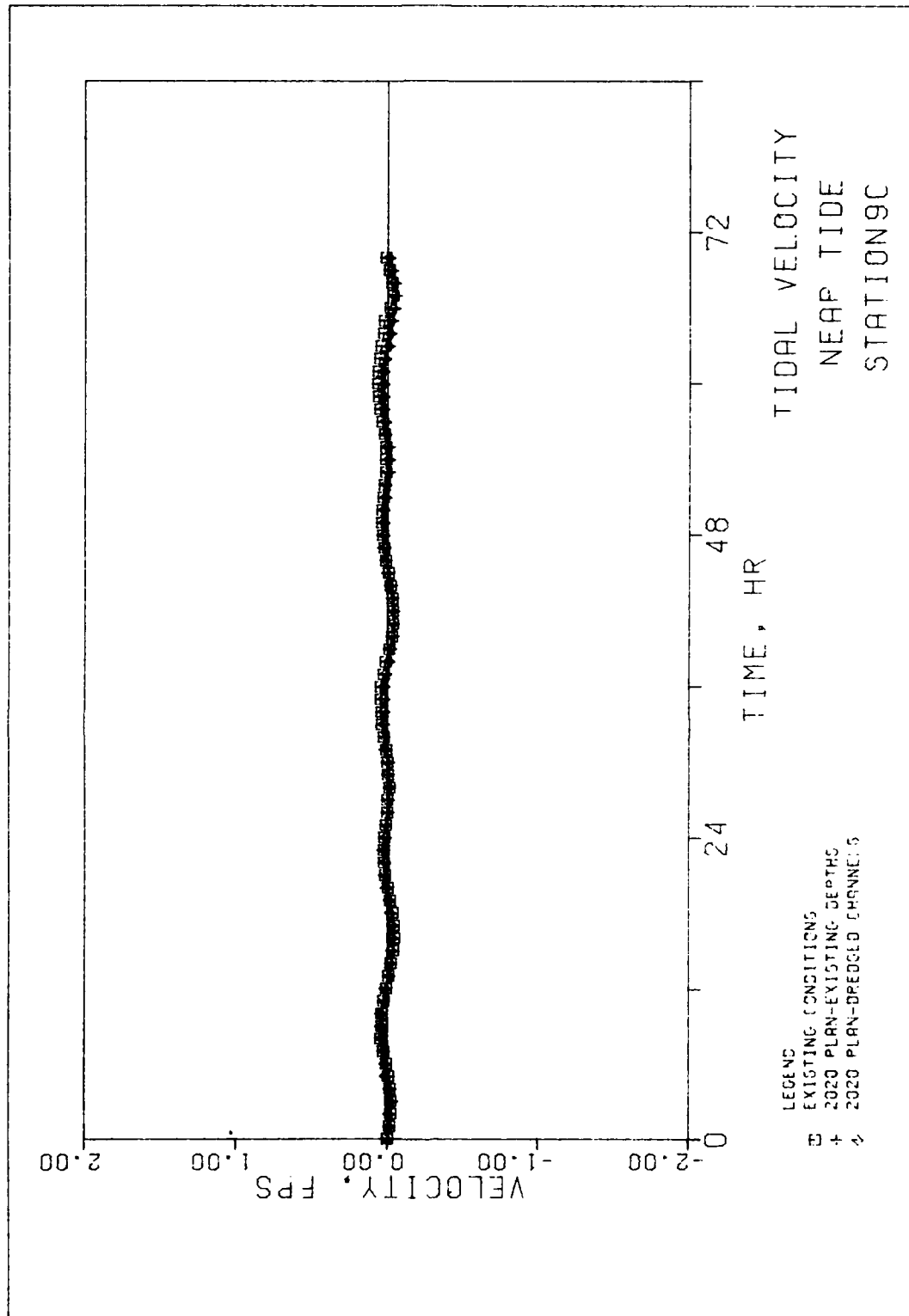


Plate 42

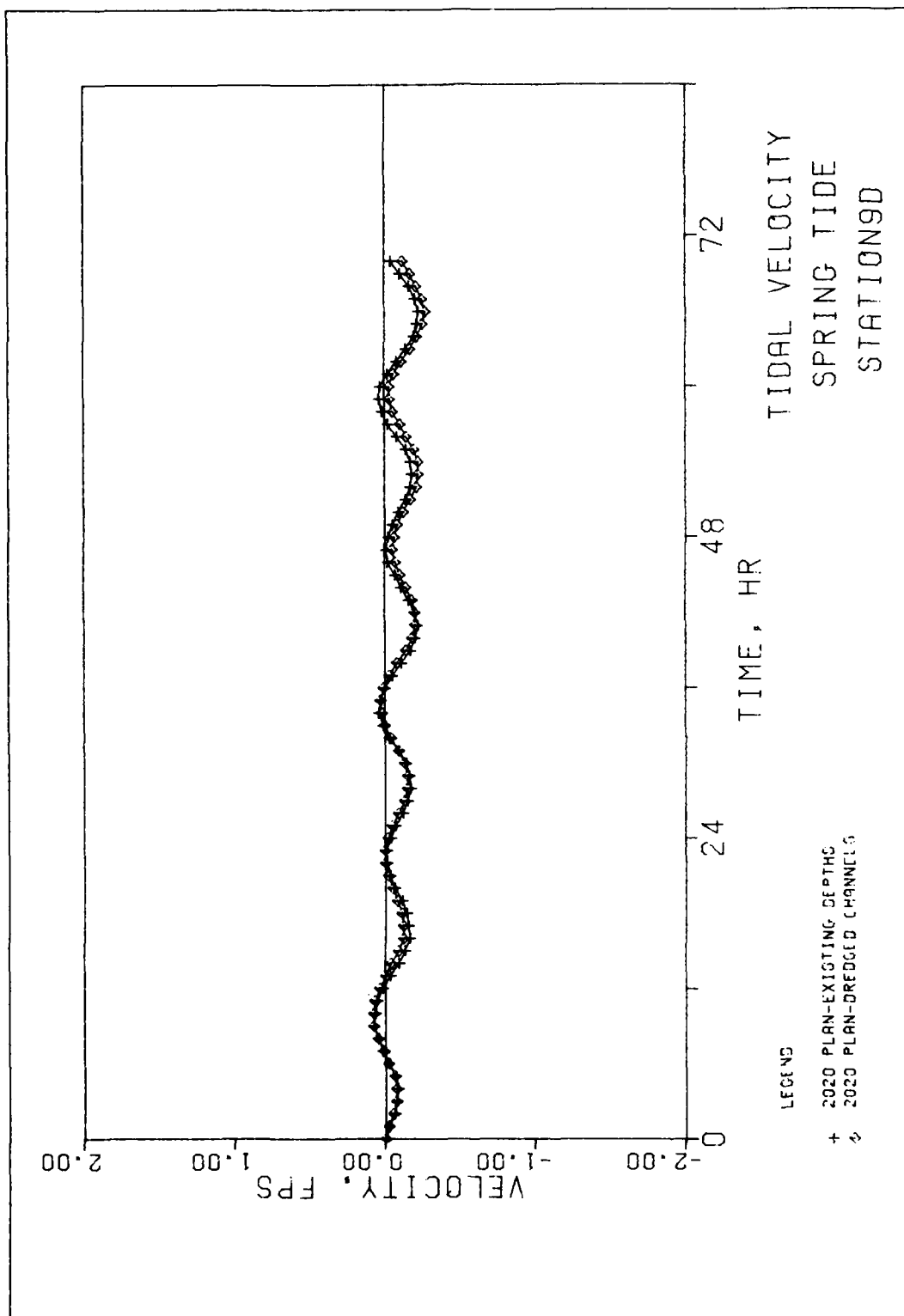


Plate 43

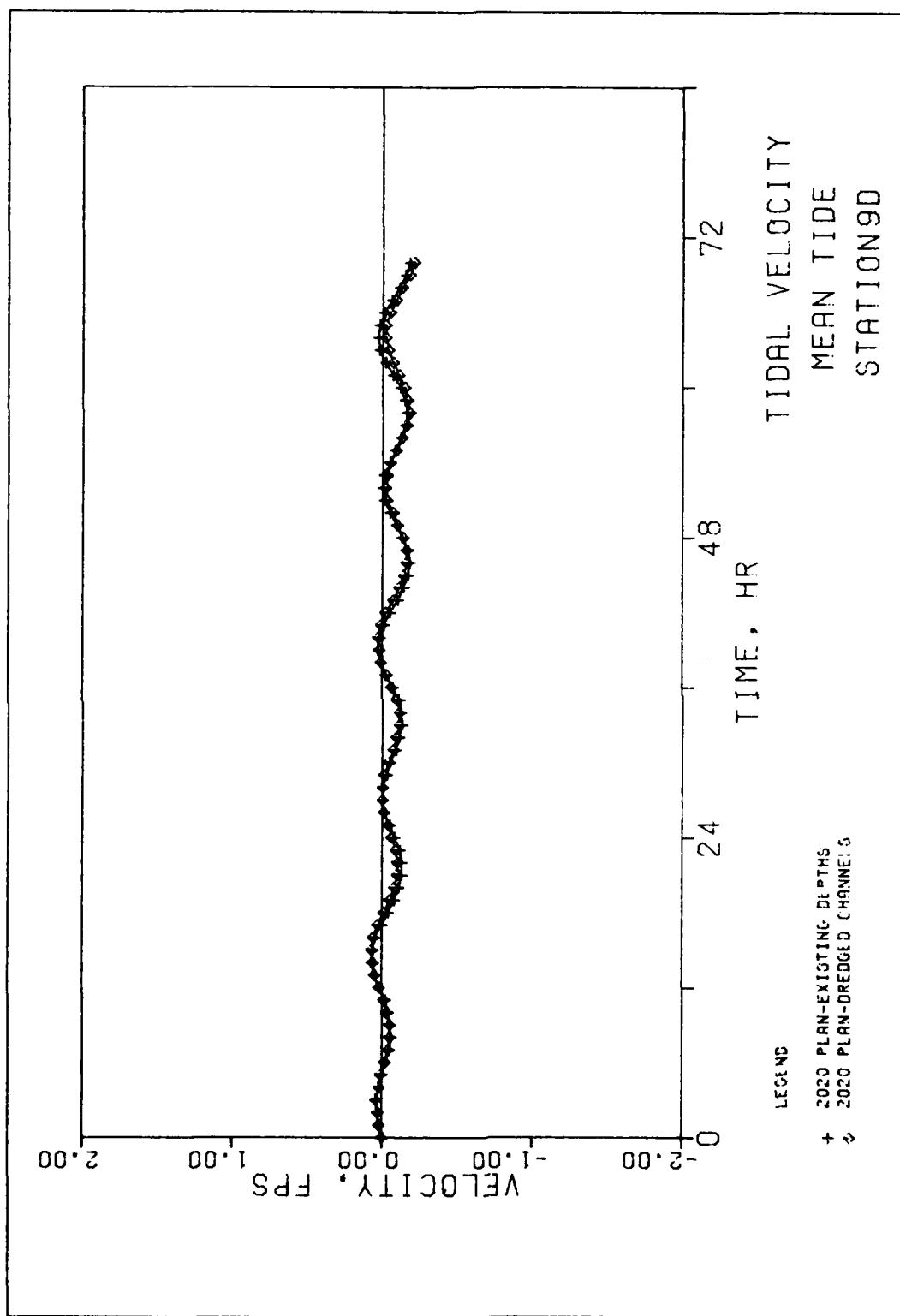


Plate 44

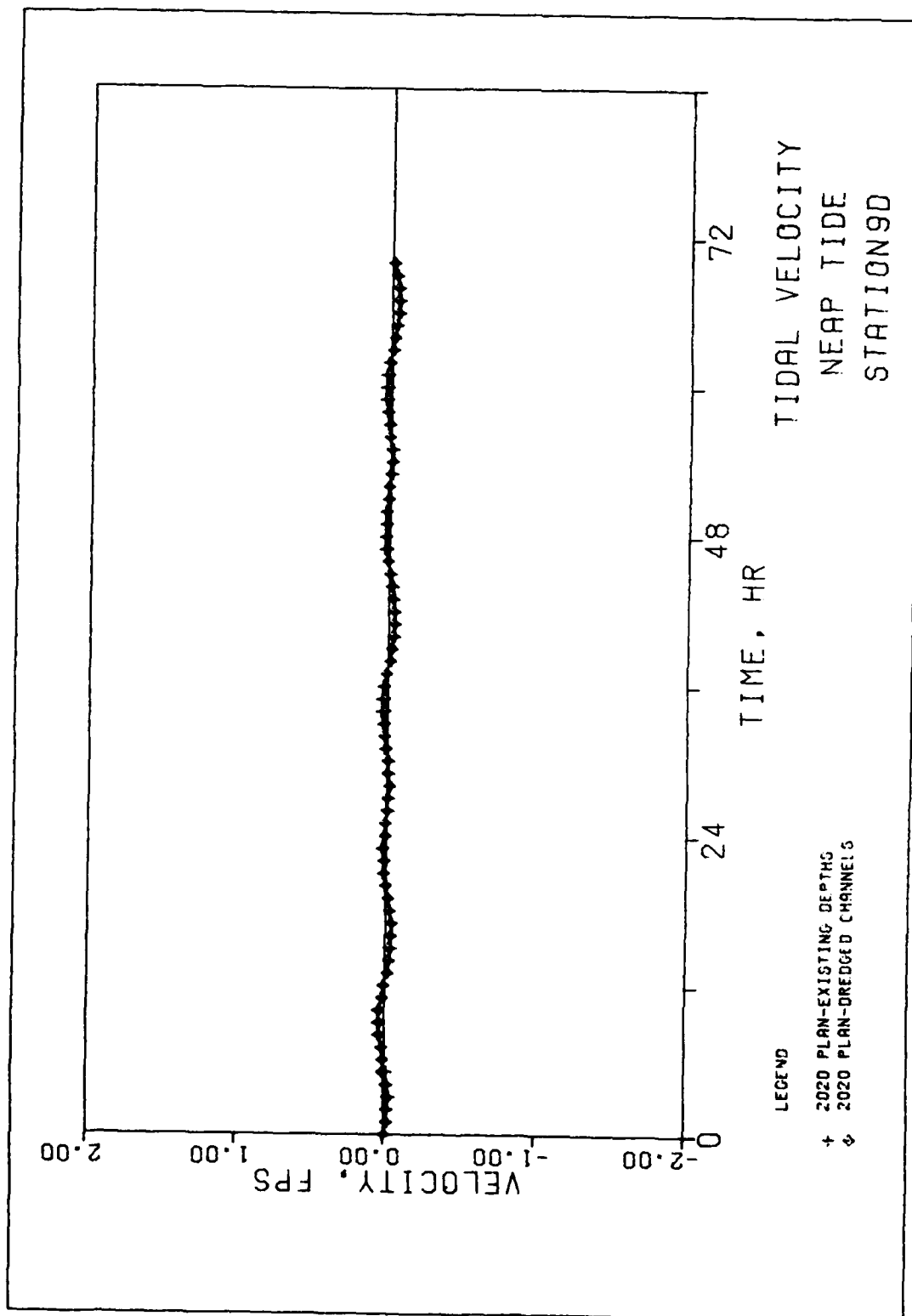


Plate 45

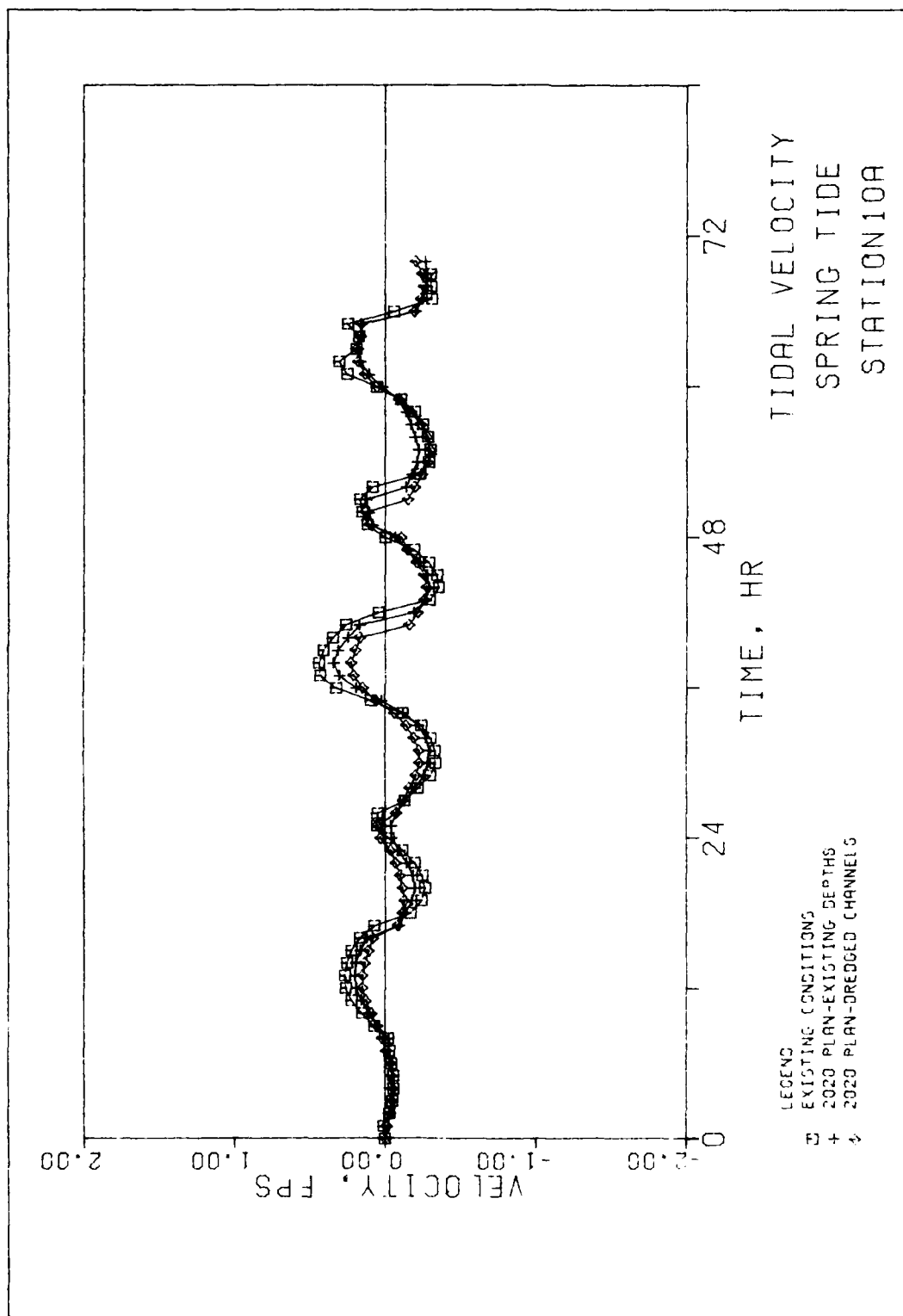


Plate 46

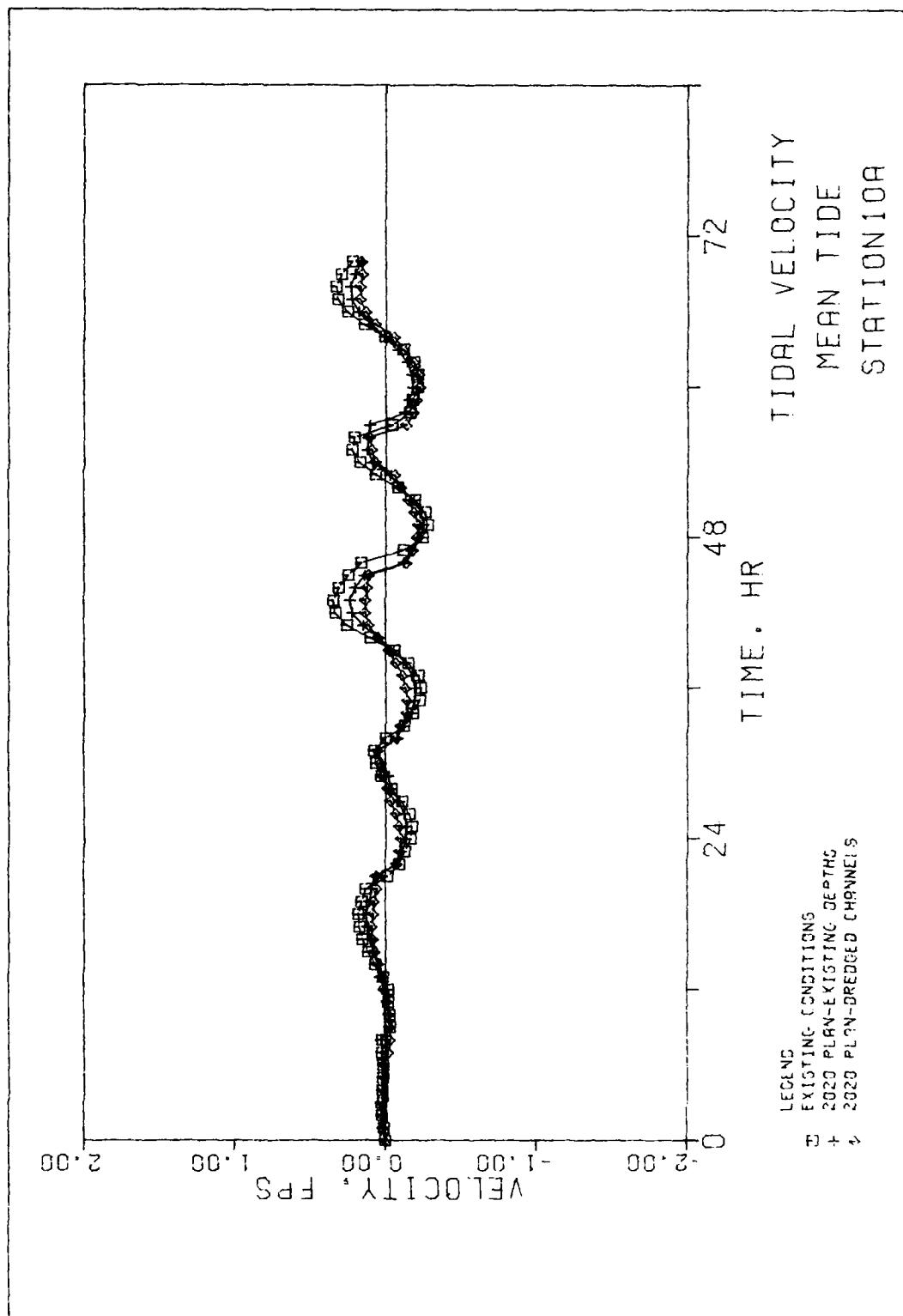


Plate 47

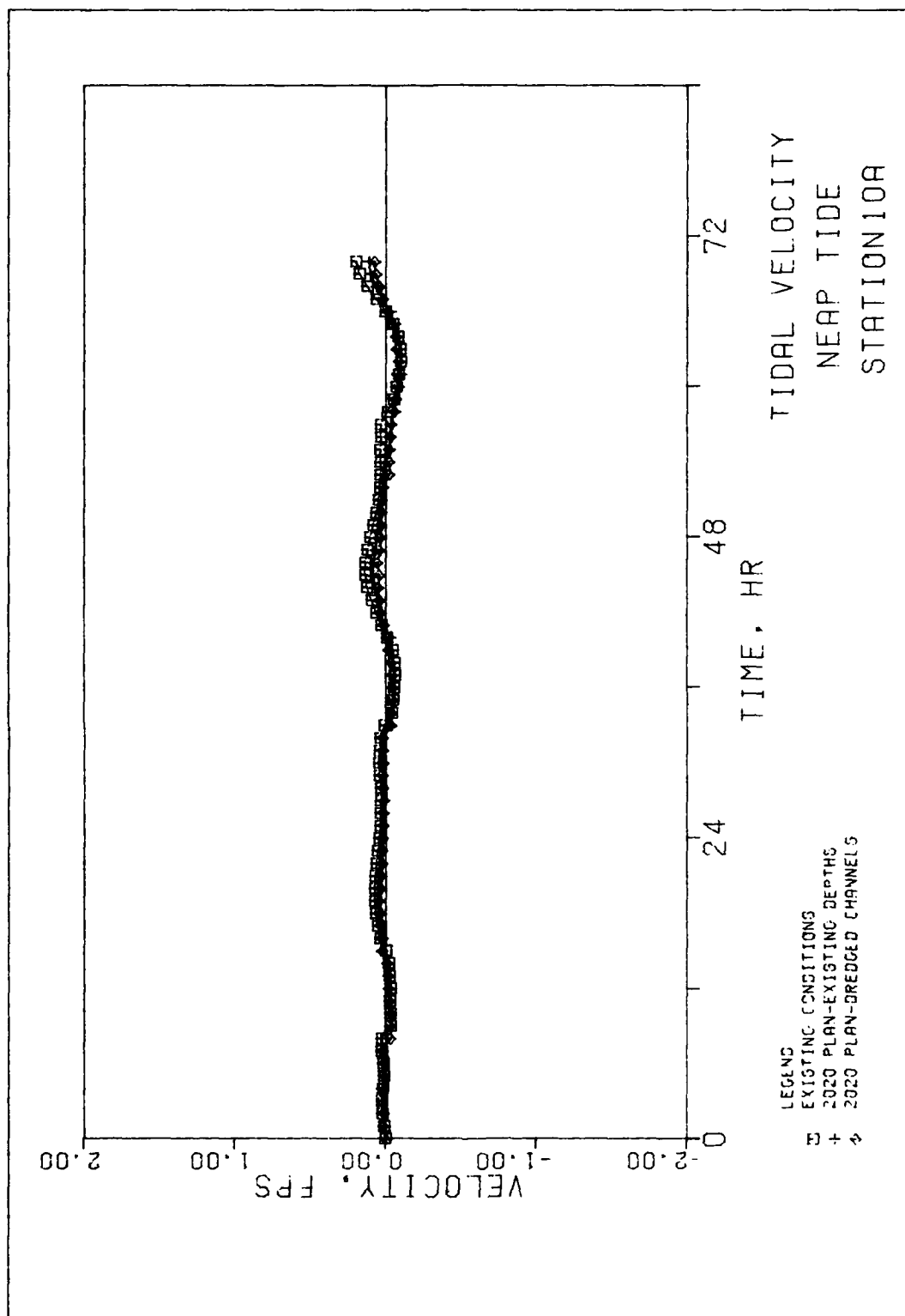


Plate 48

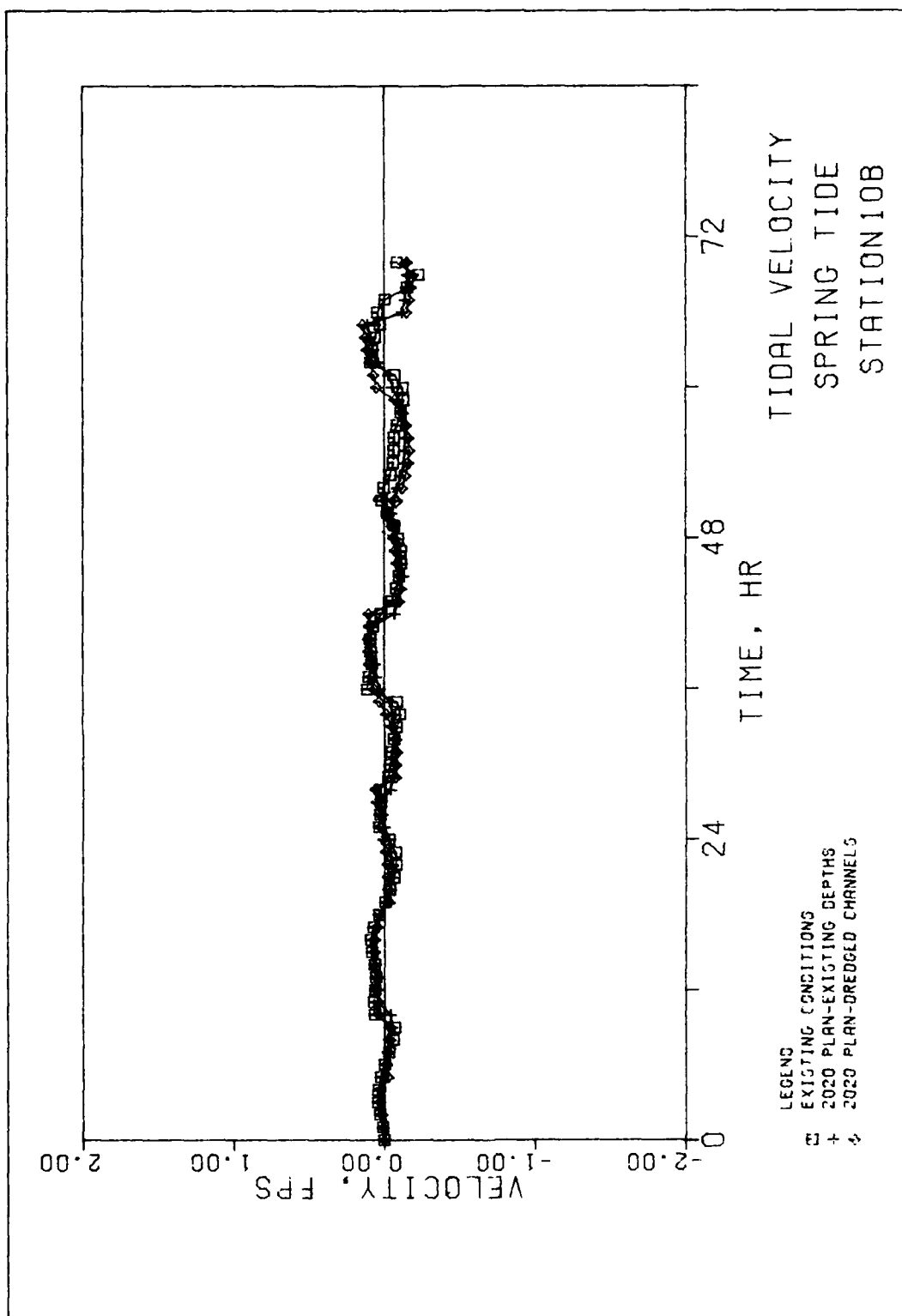


Plate 49

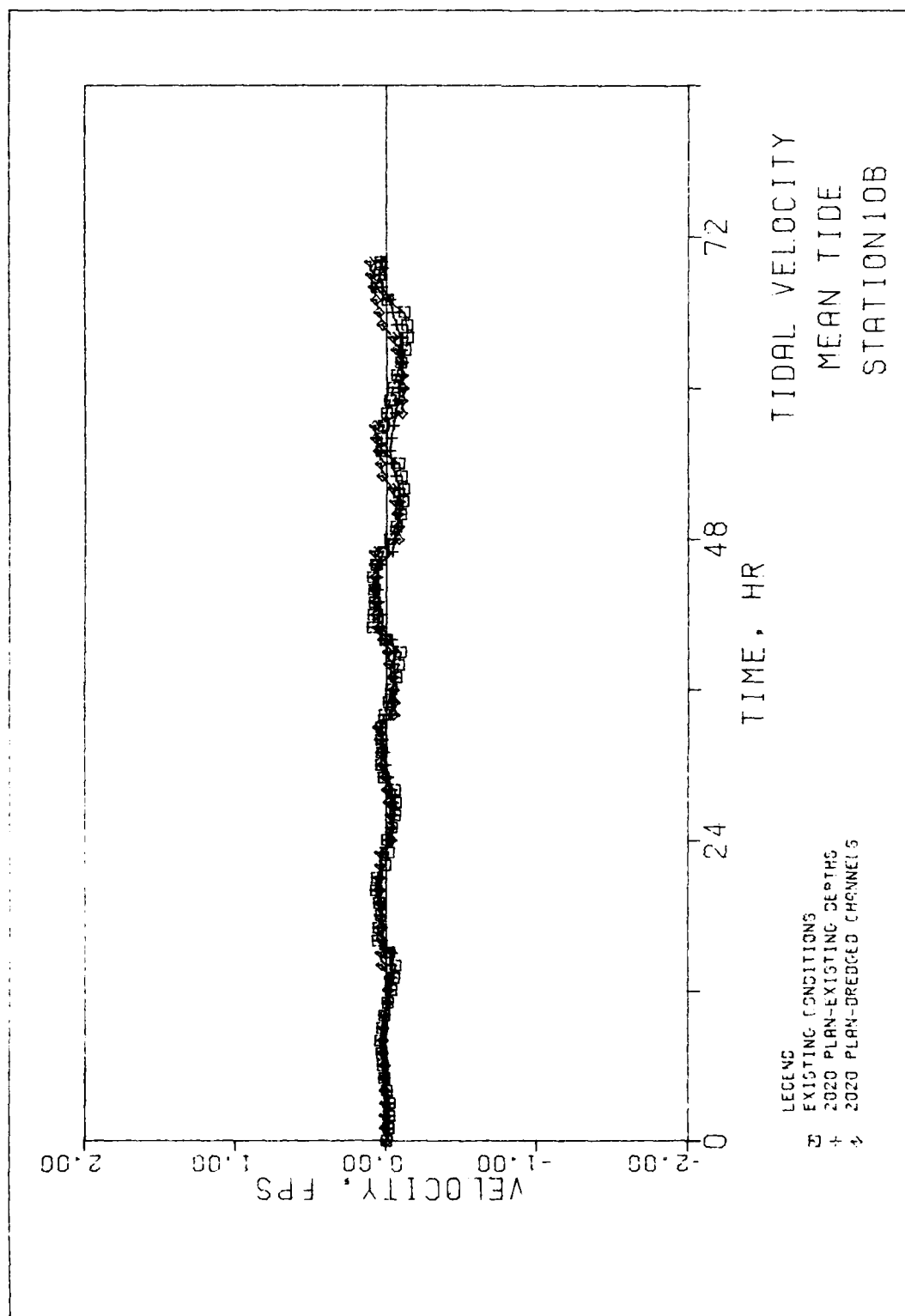


Plate 50

AD-A145 142

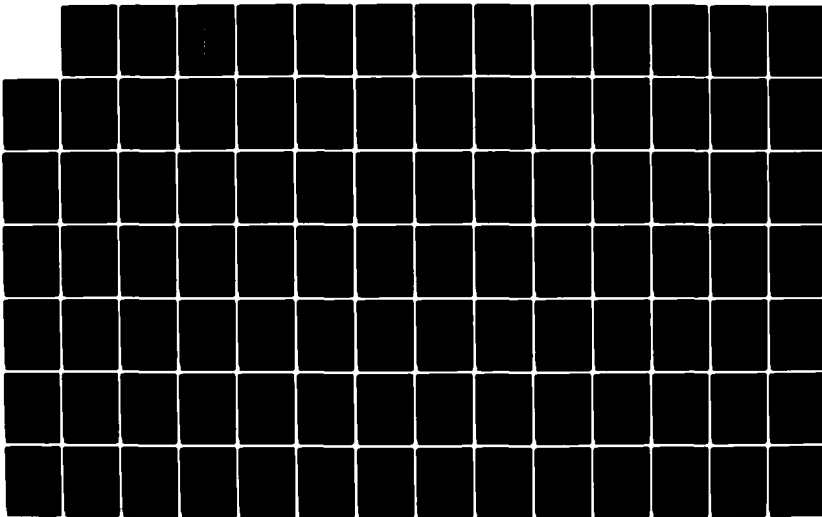
LOS ANGELES AND LONG BEACH HARBORS MODEL STUDY
NUMERICAL ANALYSIS OF TIDA... (U) COASTAL ENGINEERING
RESEARCH CENTER VICKSBURG MS W C SEABERGH ET AL.
JUN 84 CERC-MP-84-5

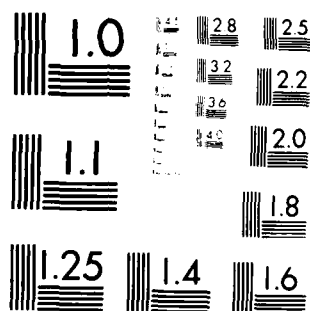
2/3

UNCLASSIFIED

F/G 8/3

NL





MICROCOPY RESOLUTION TEST CHART
NATIONAL BUREAU OF STANDARDS-1963-A

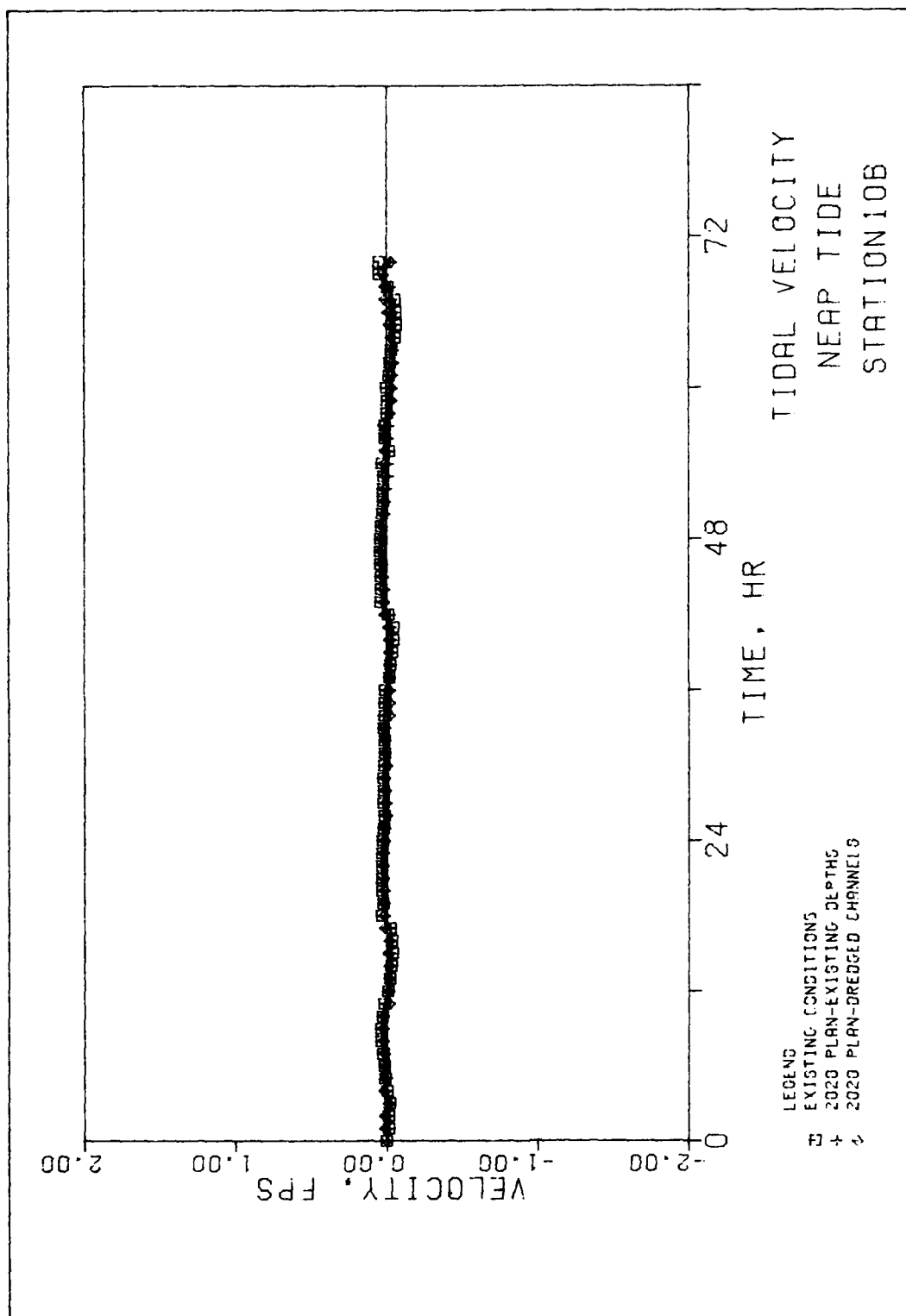


Plate 51

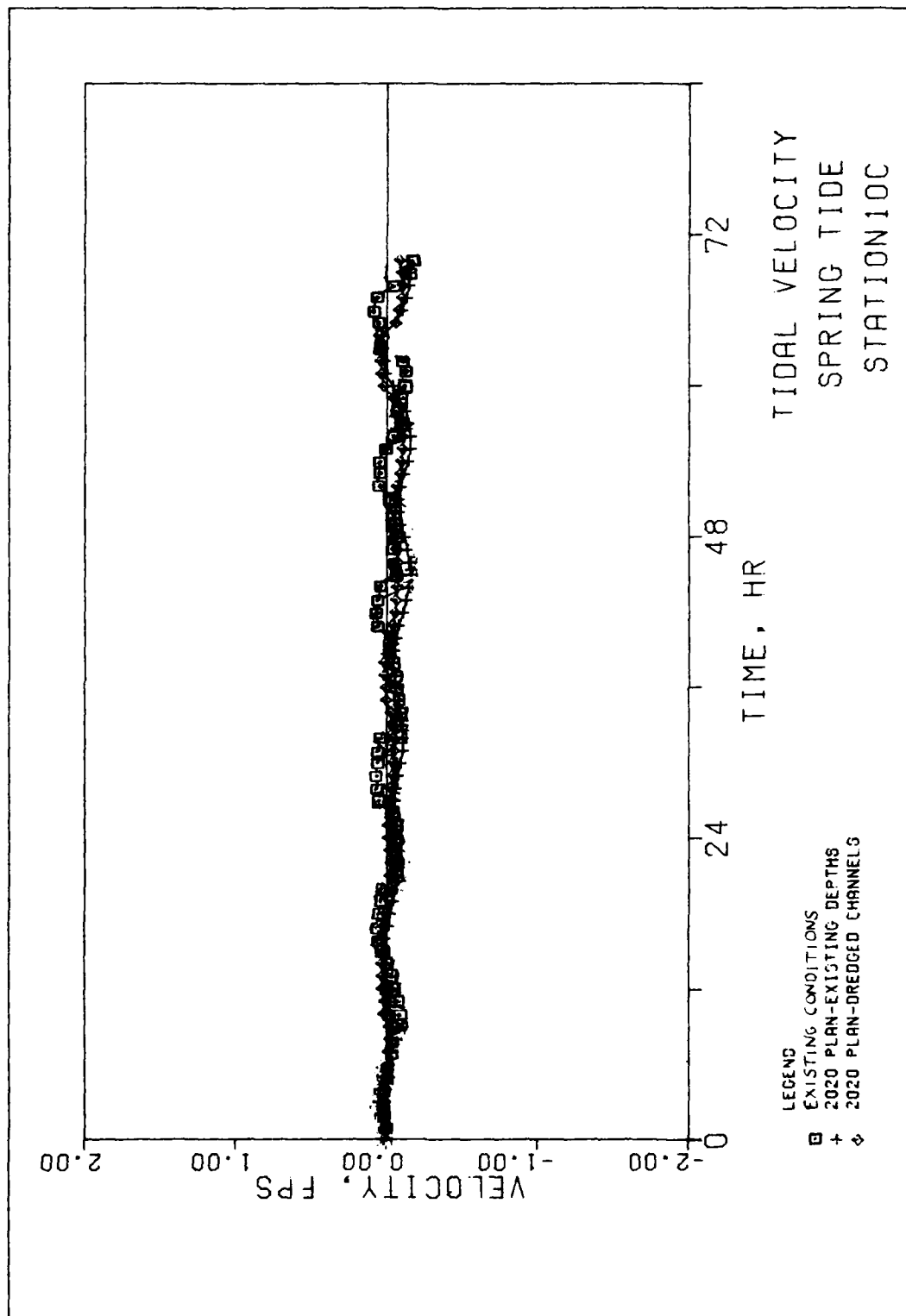


Plate 52

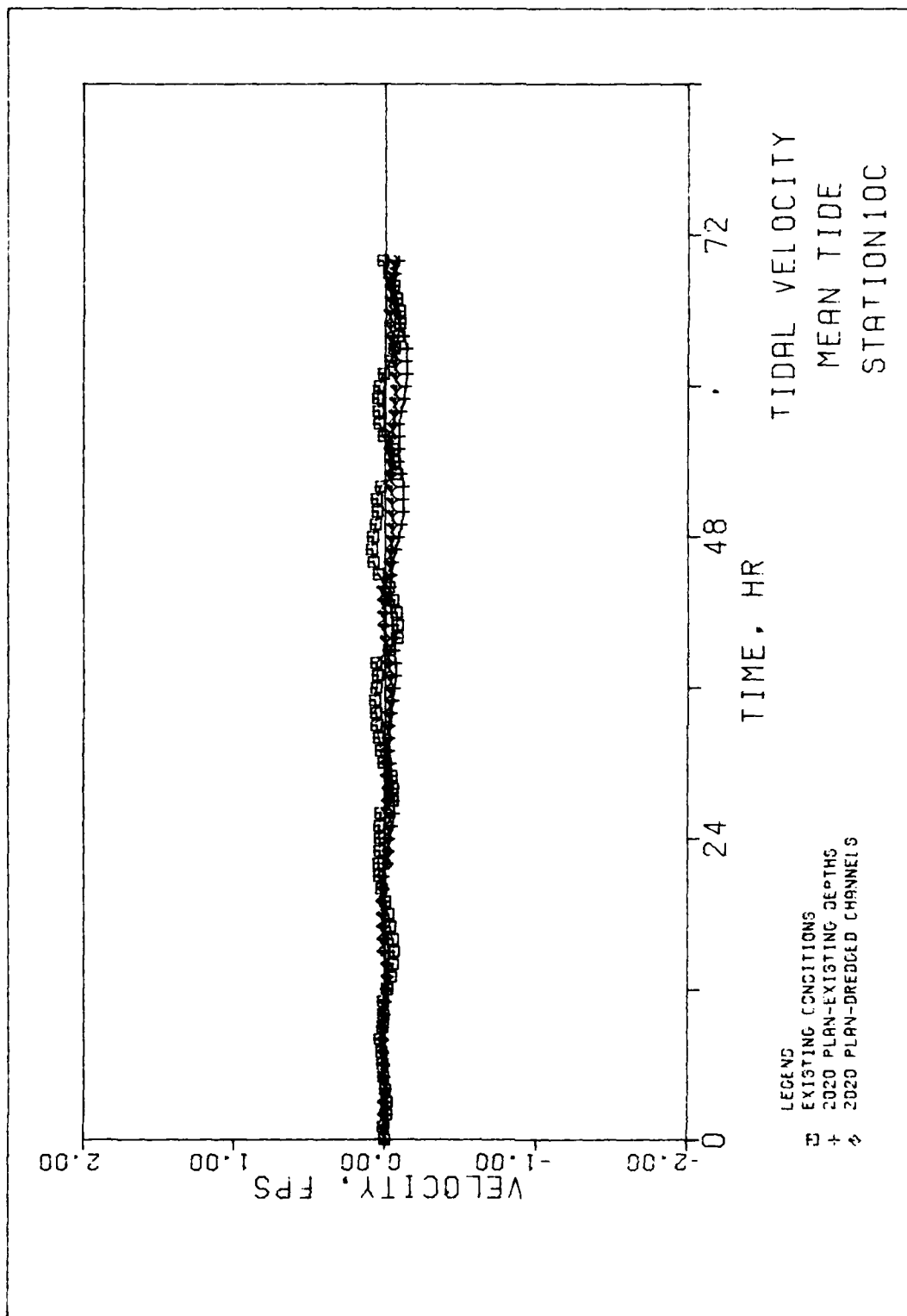


Plate 53

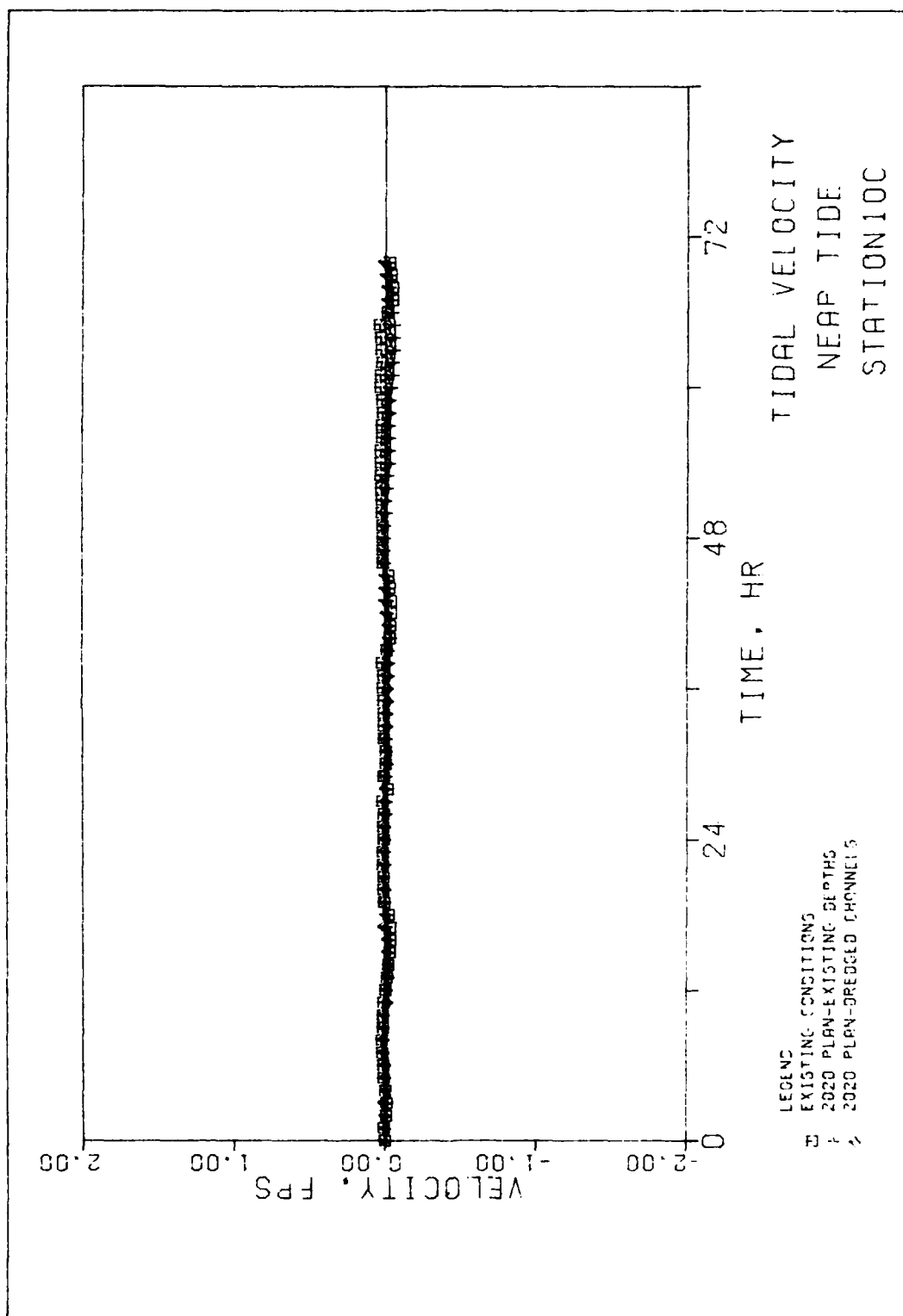


Plate 54

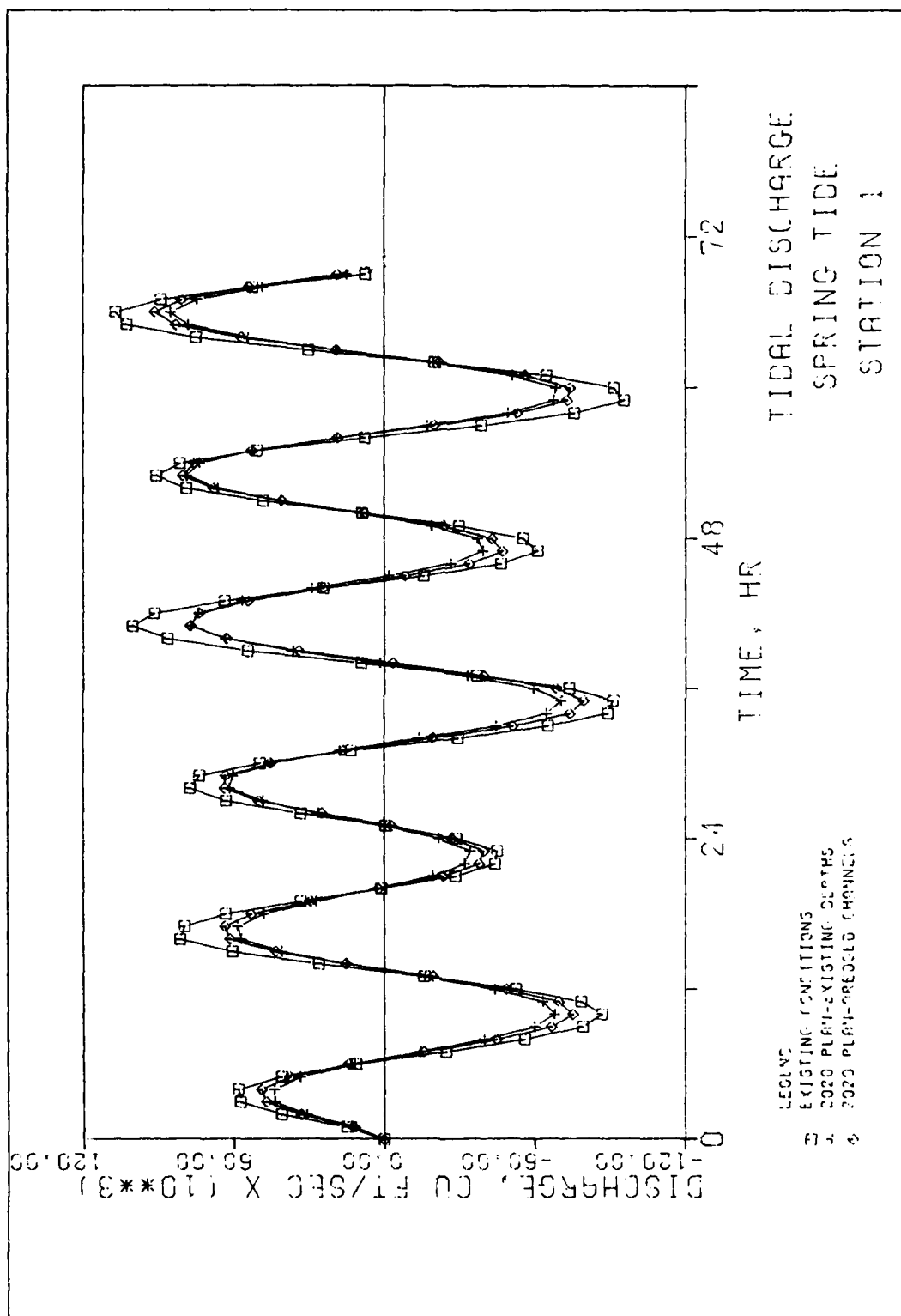


Plate 55

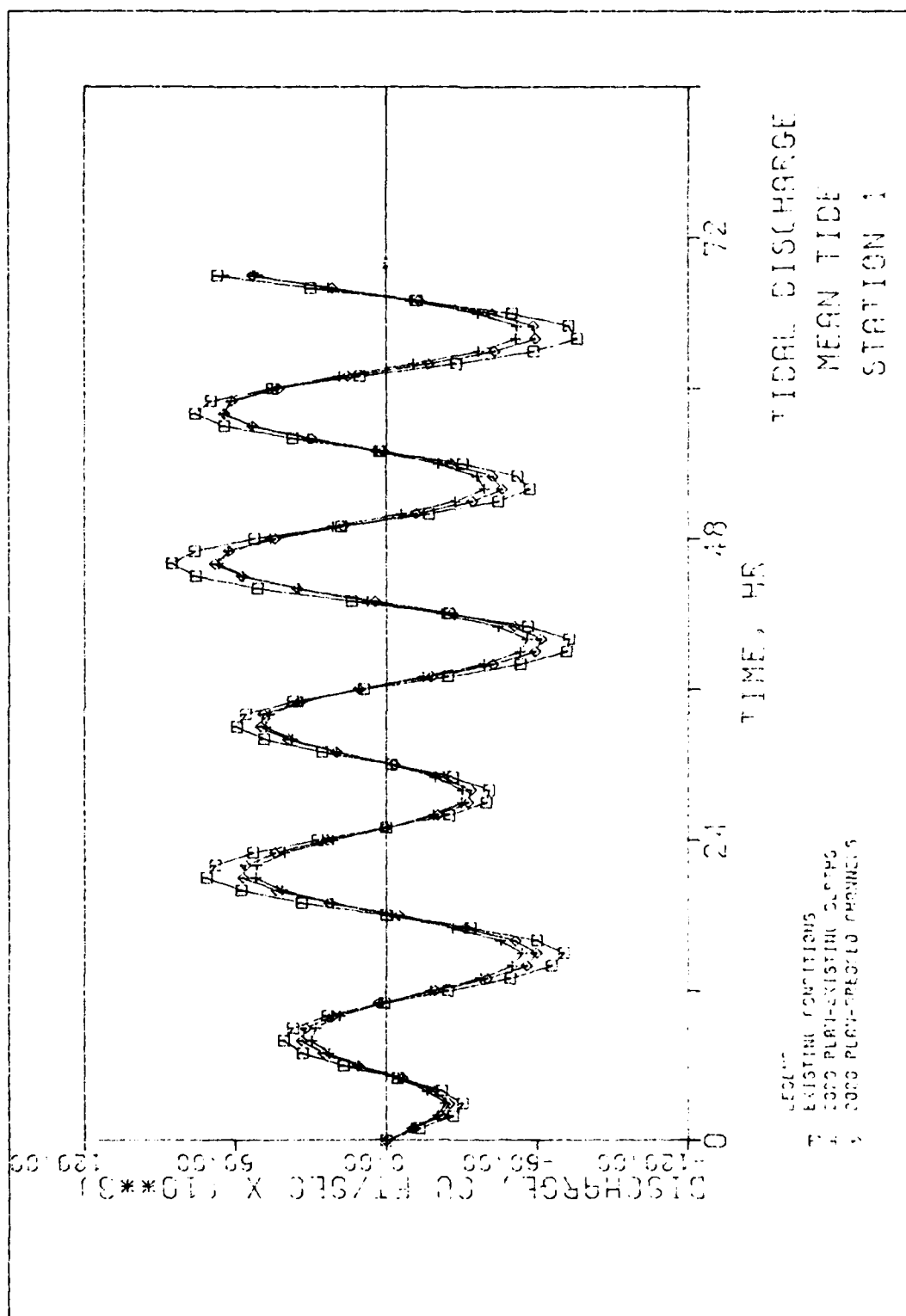


Plate 56

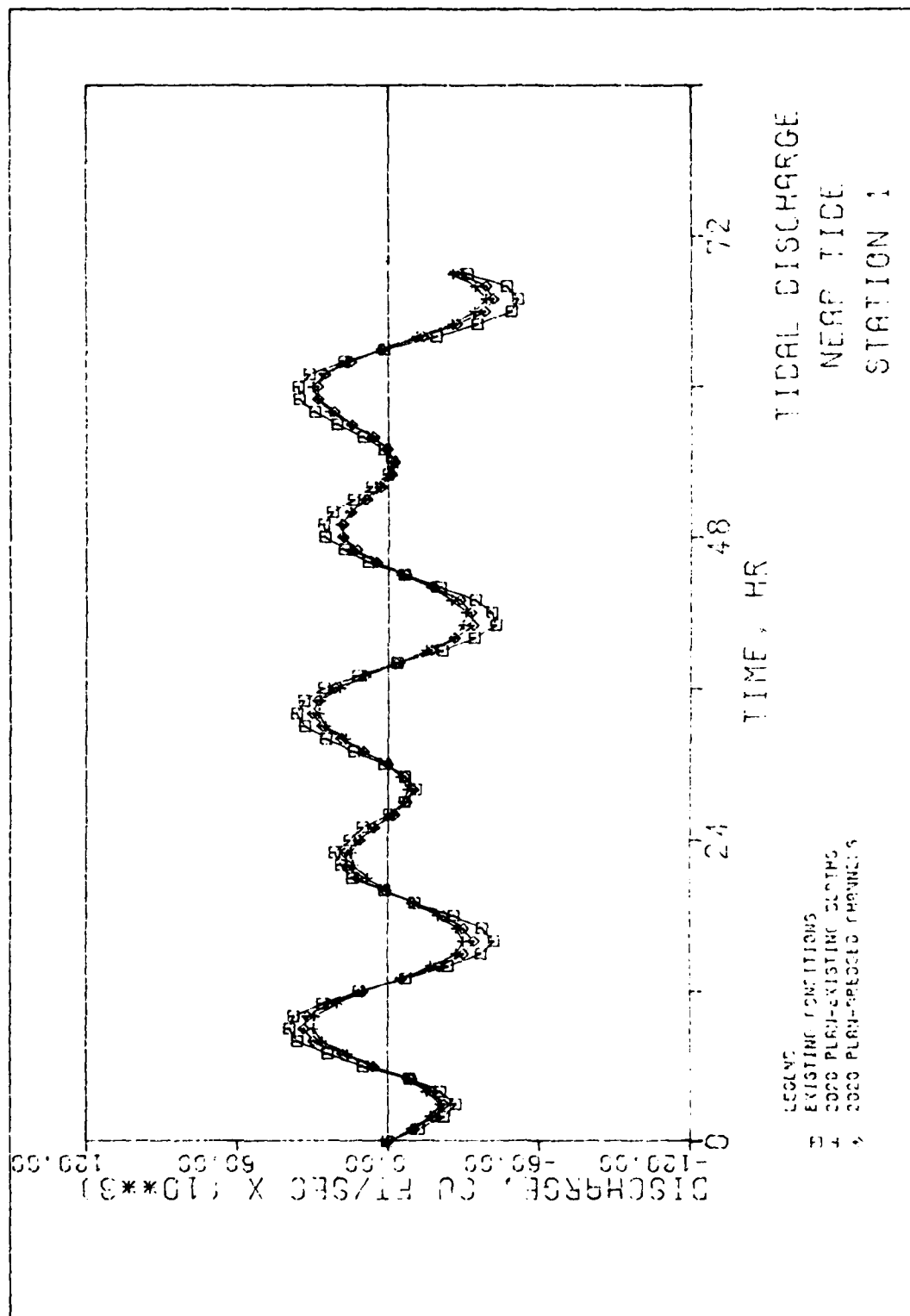


Plate 57

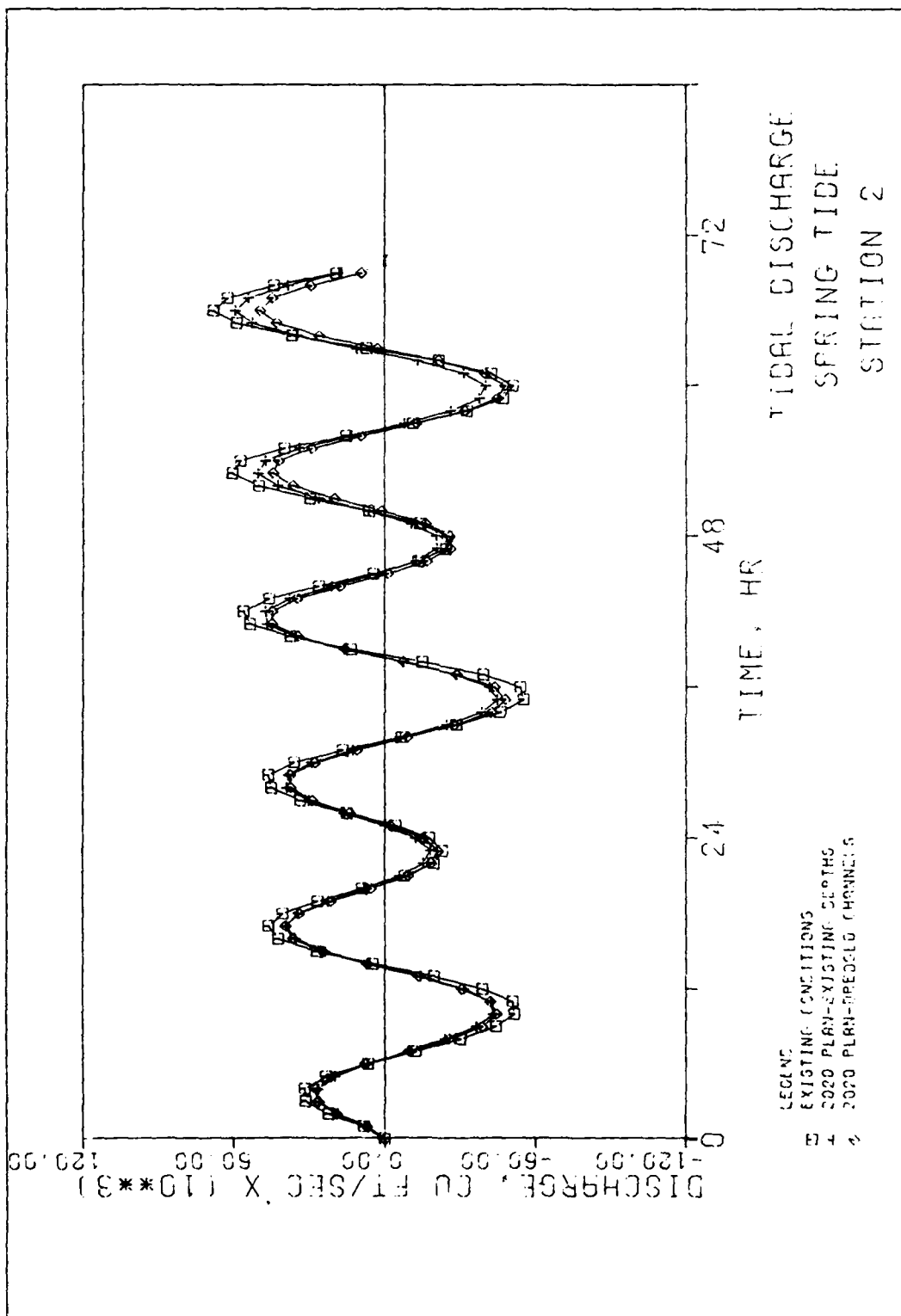
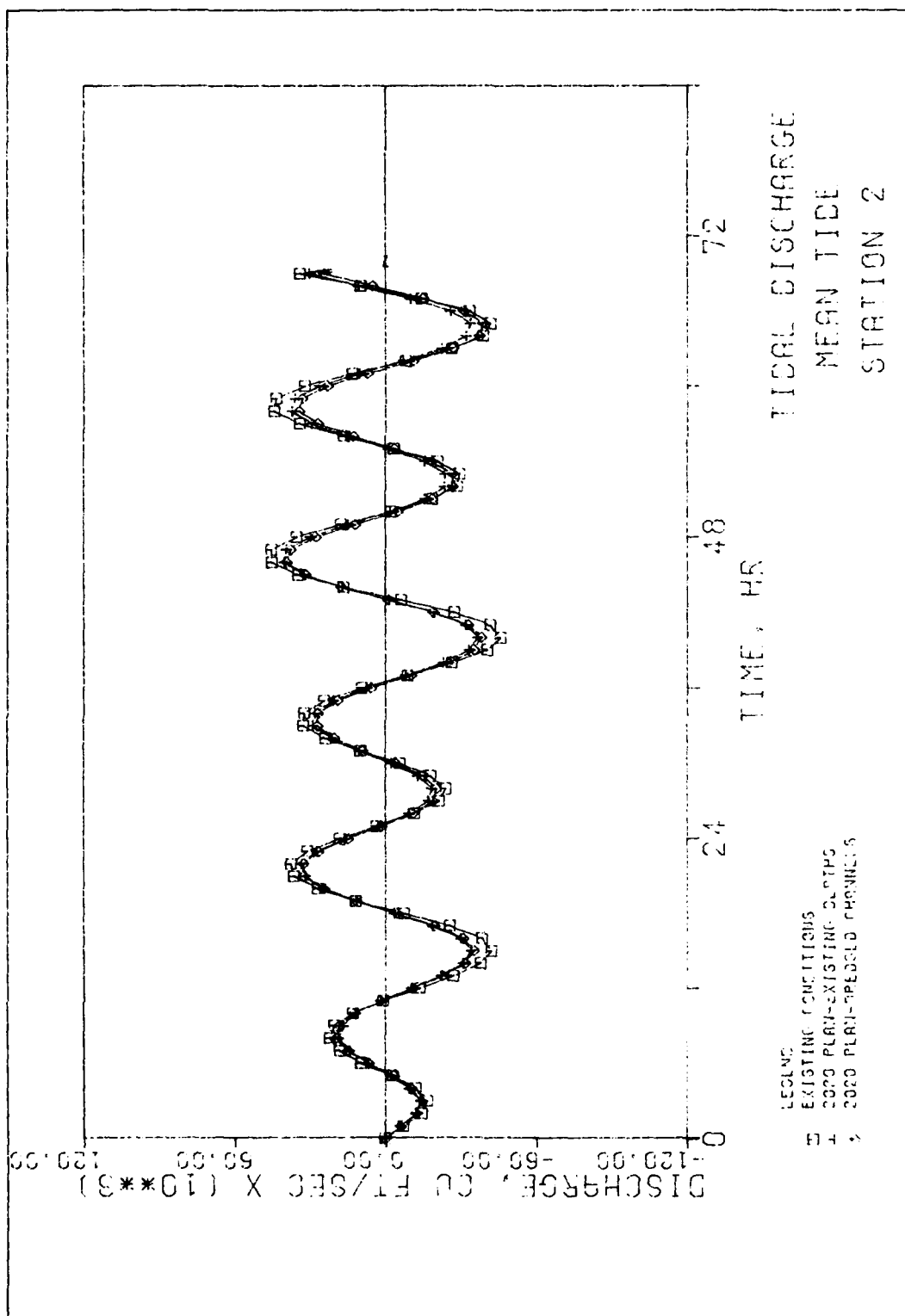


Plate 58



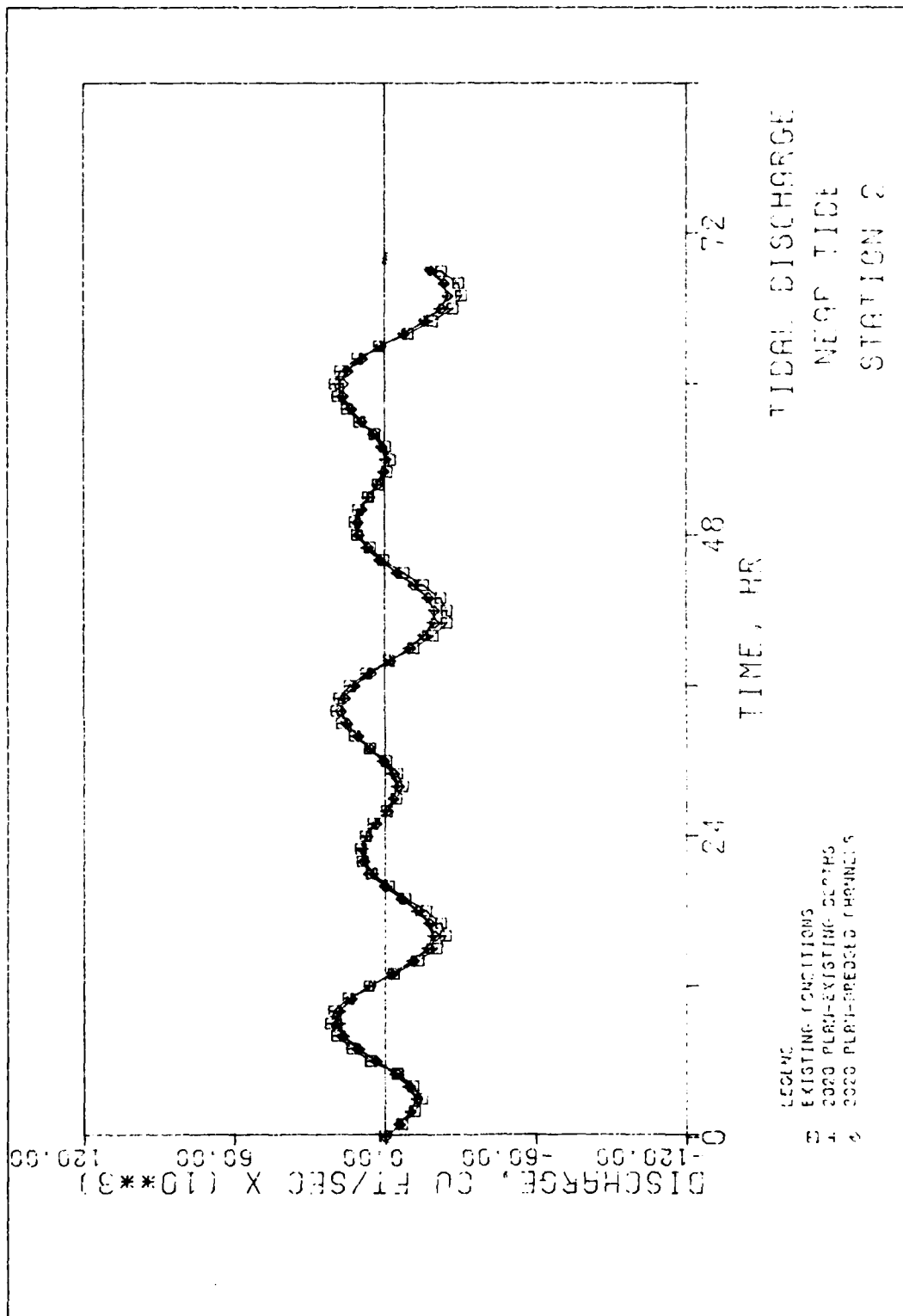


Plate 60

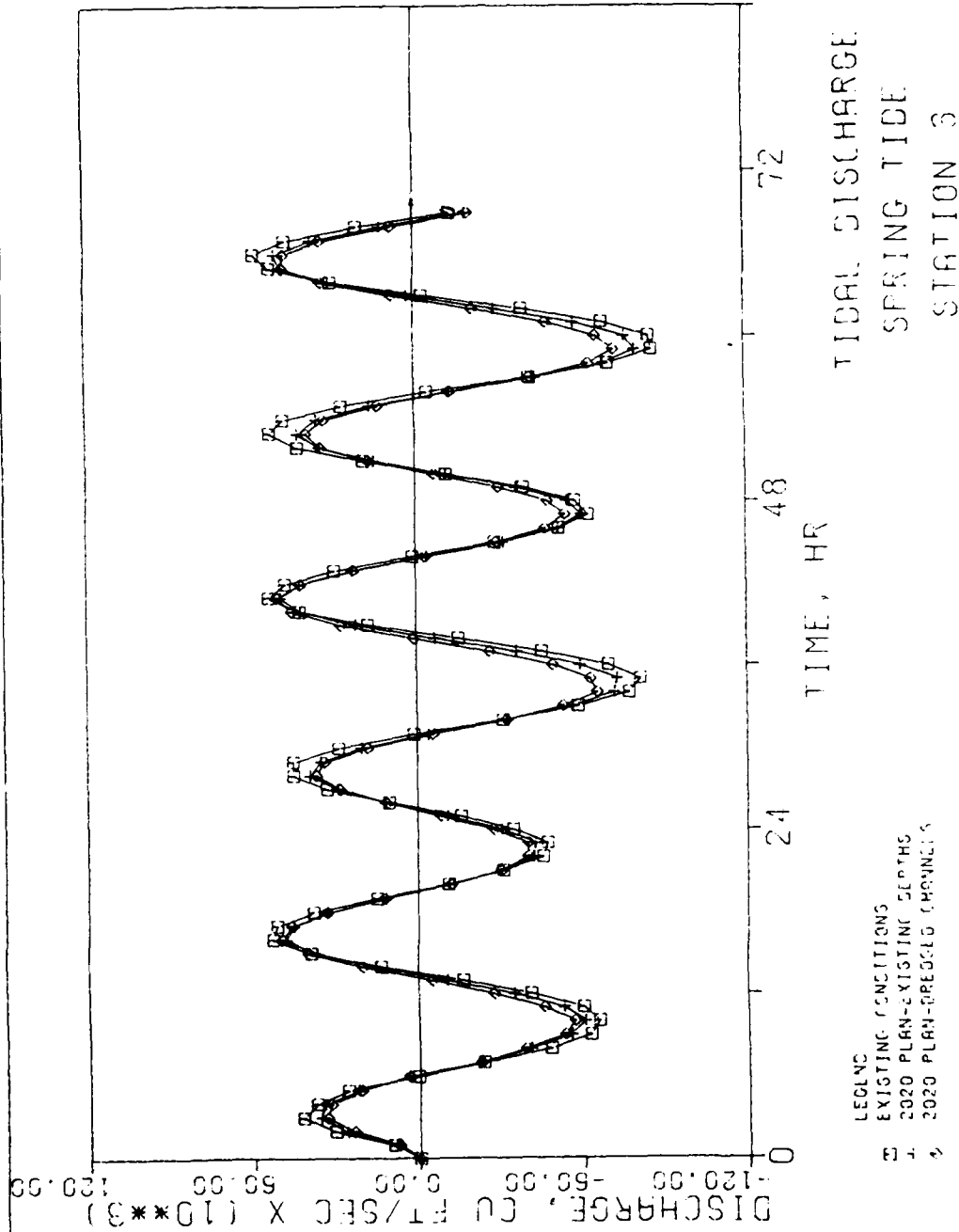


Plate 61

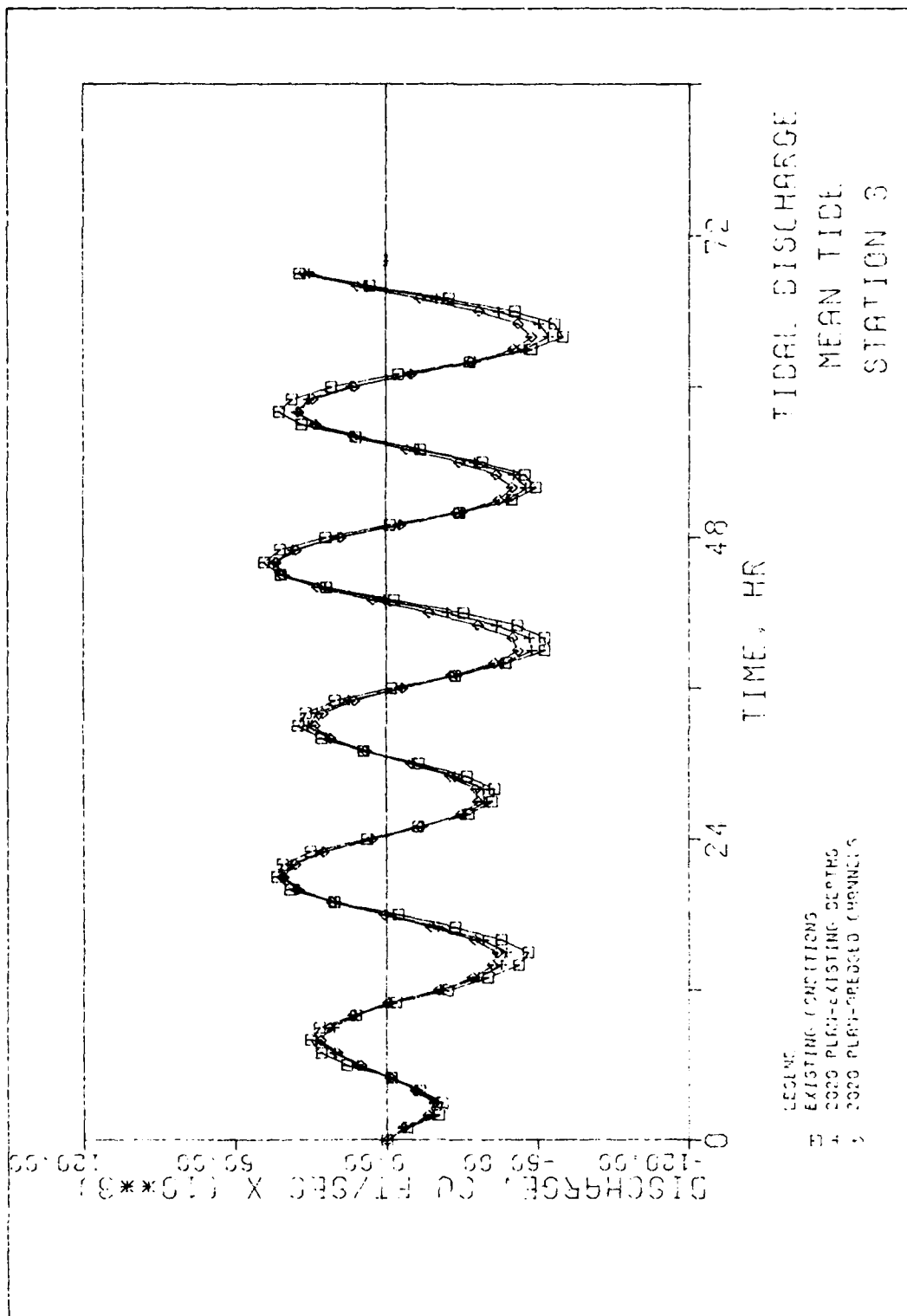


Plate 62

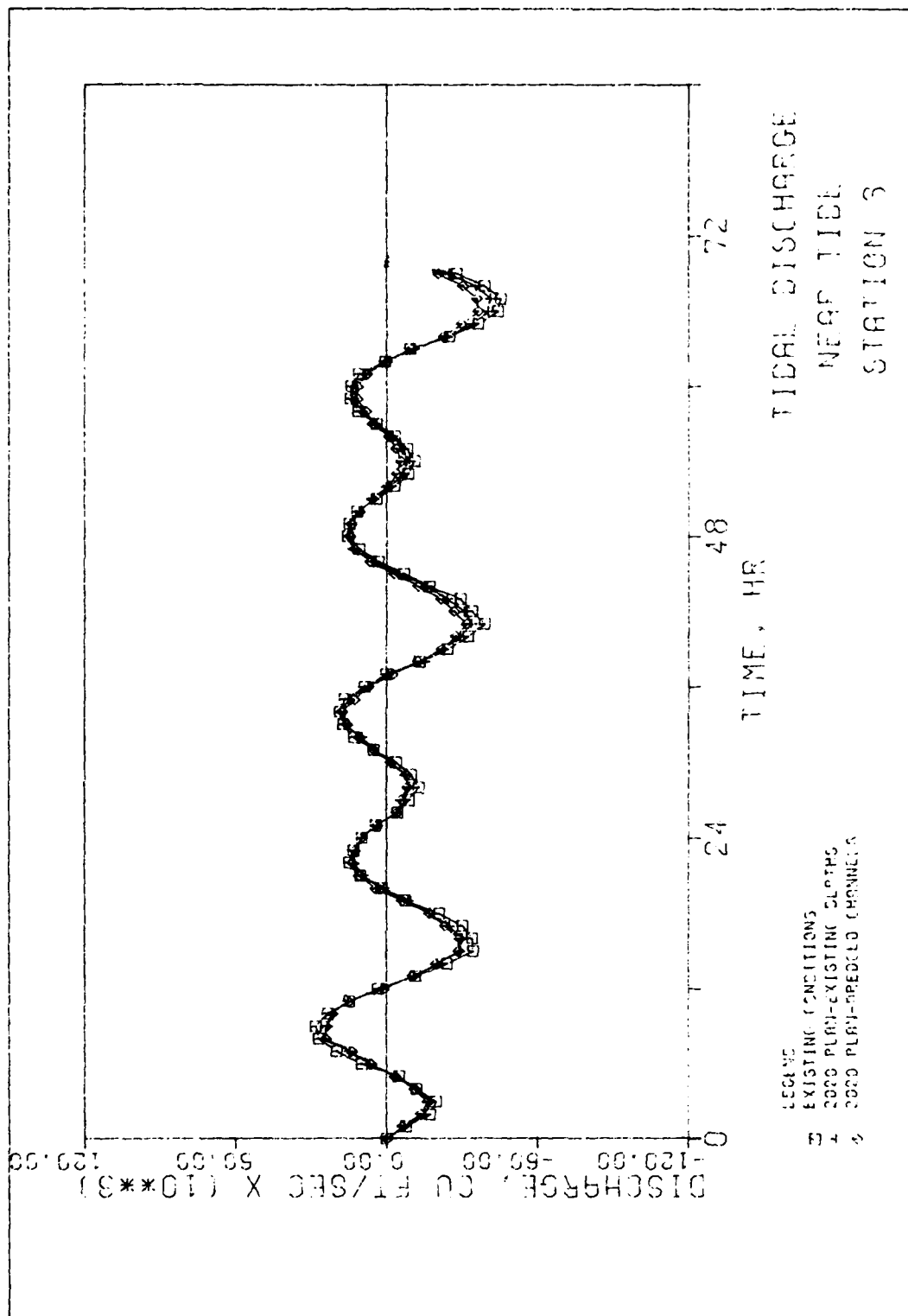


Plate 63

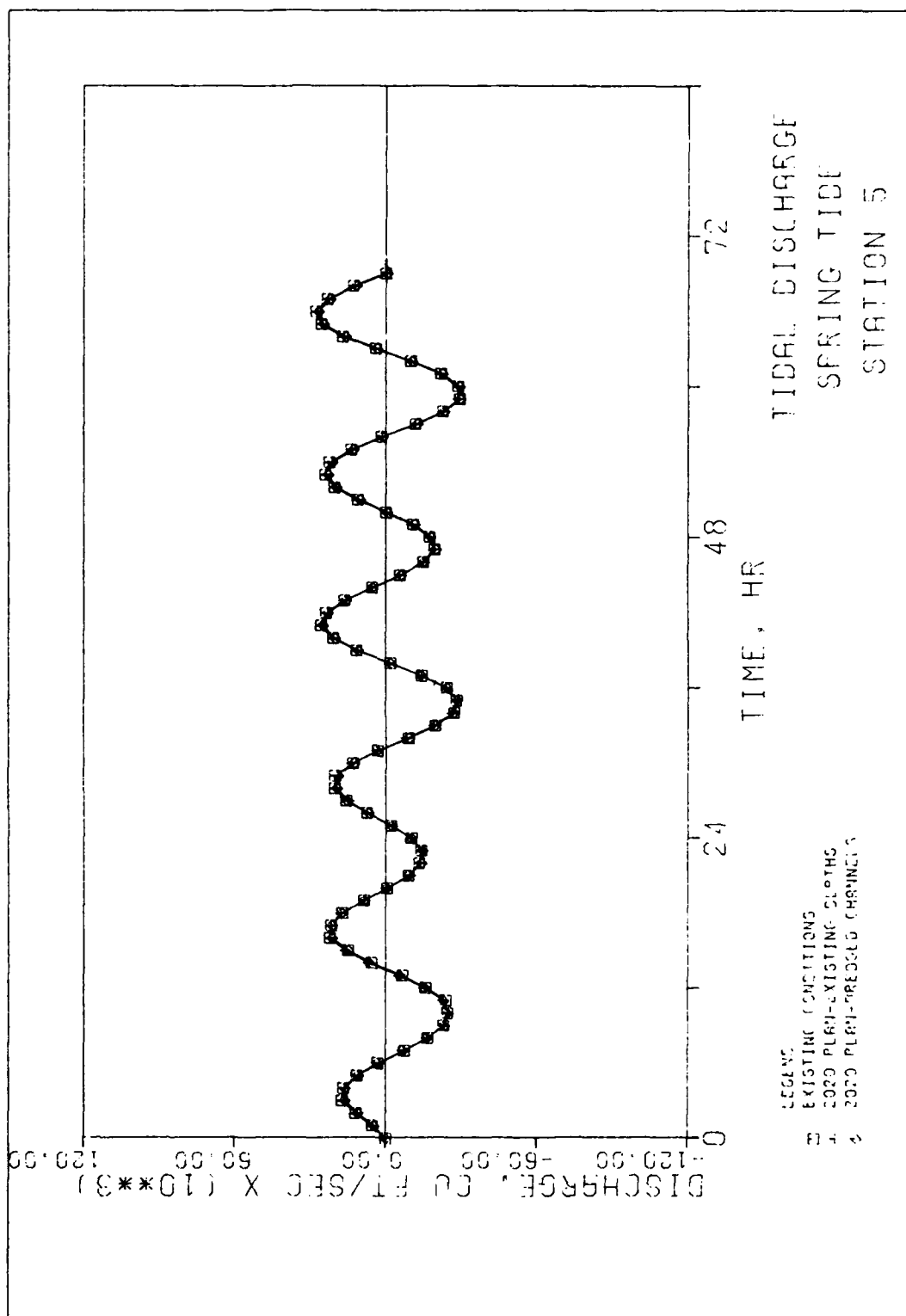


Plate 64

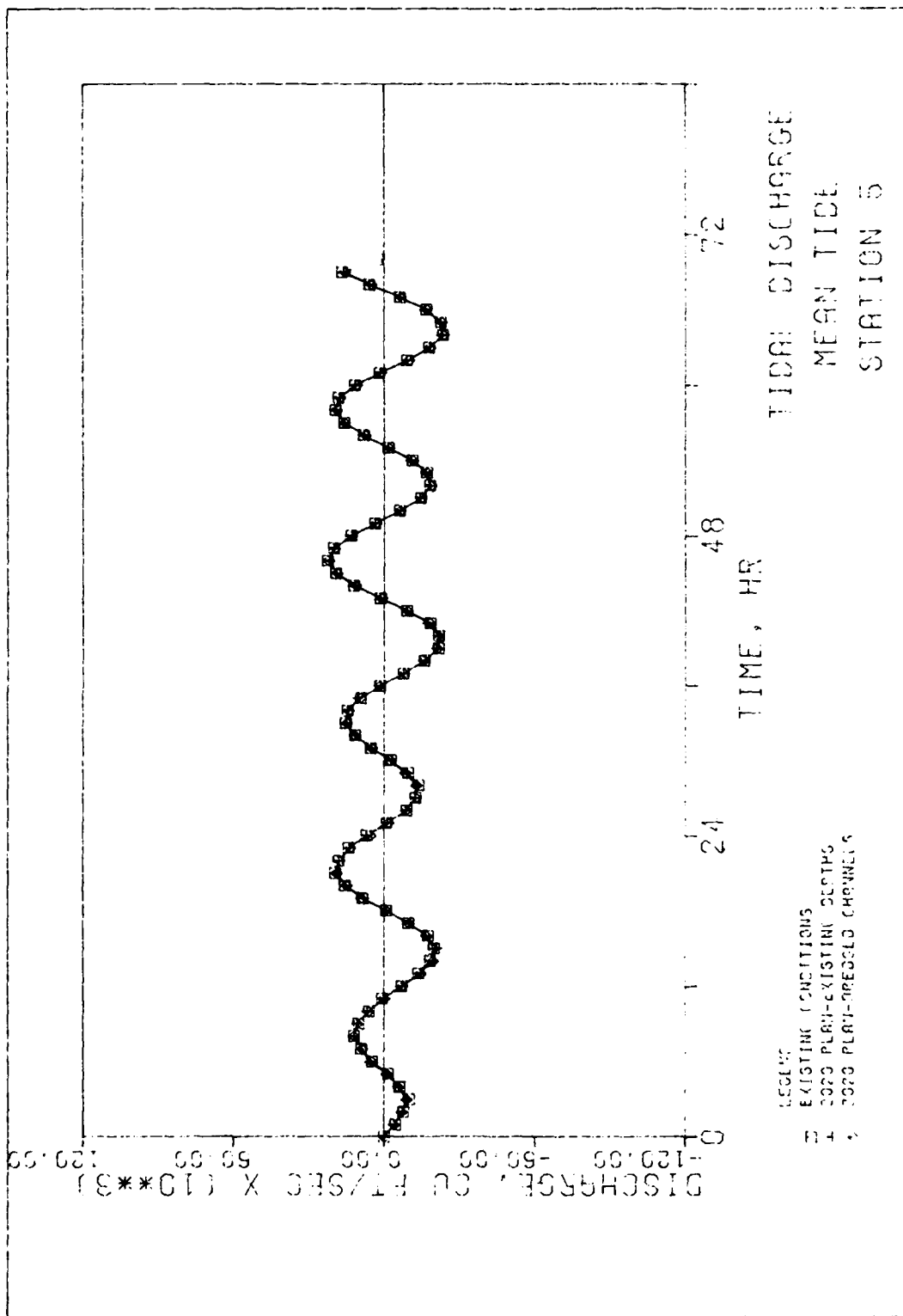


Plate 65

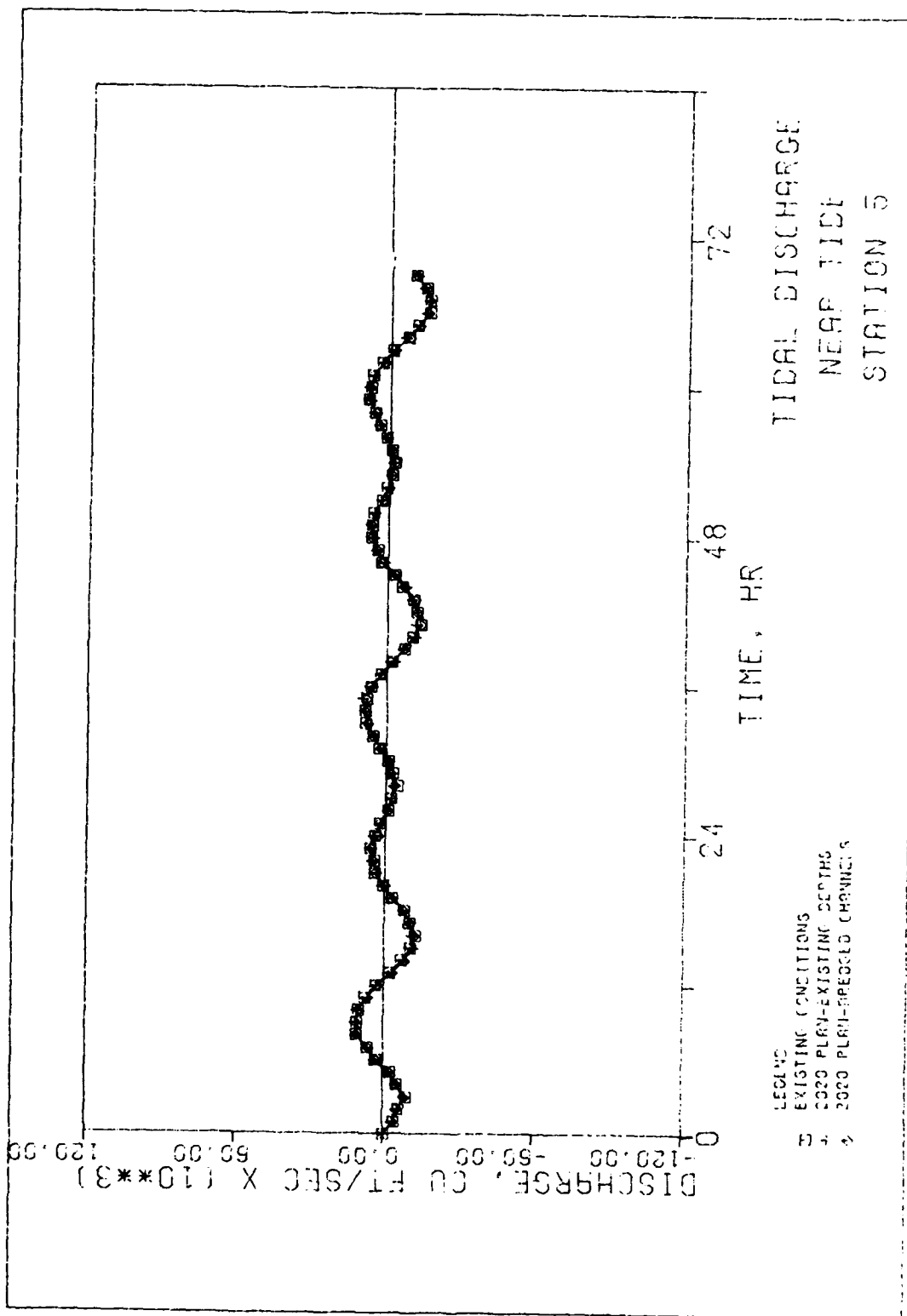


Plate 66

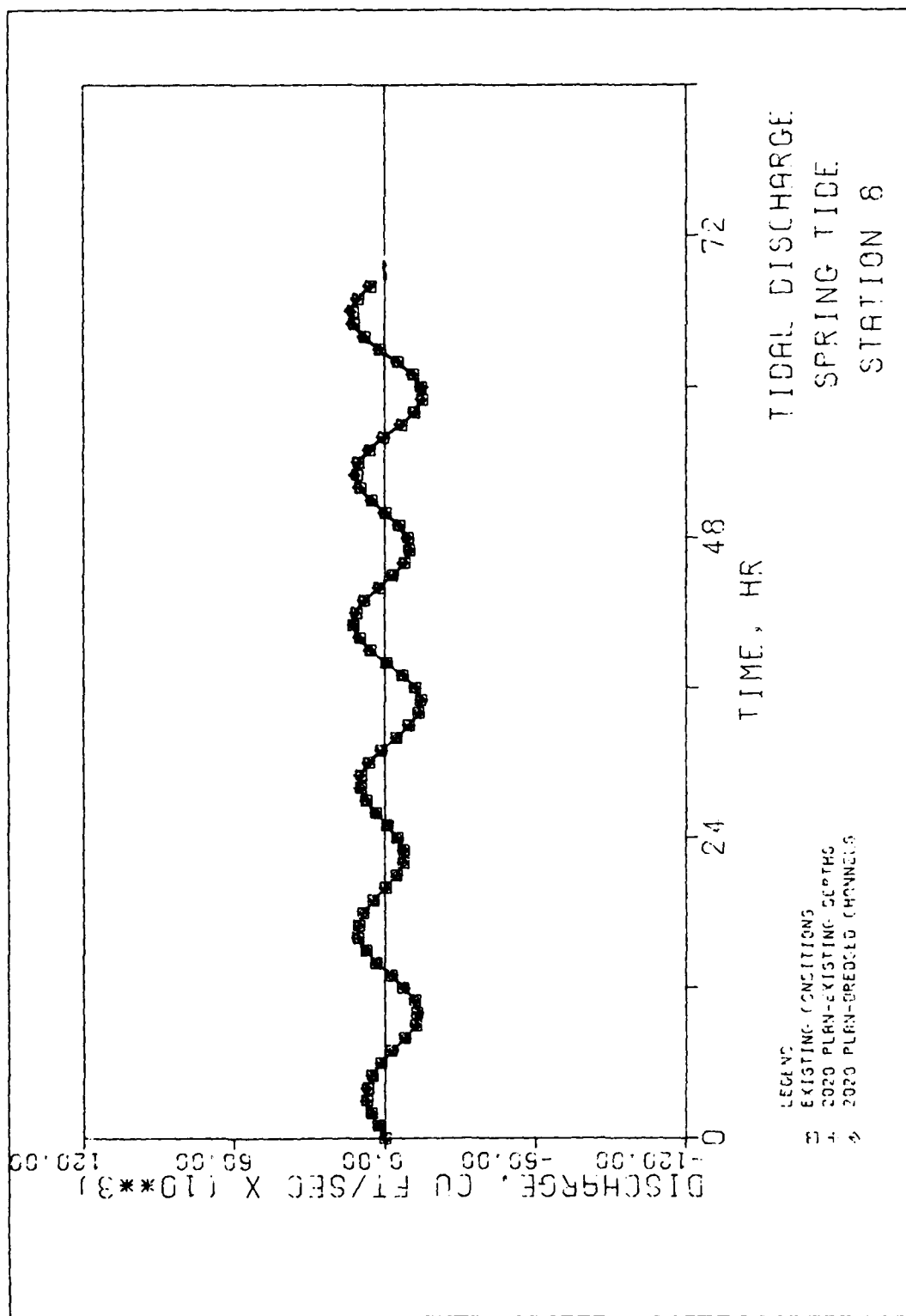


Plate 67

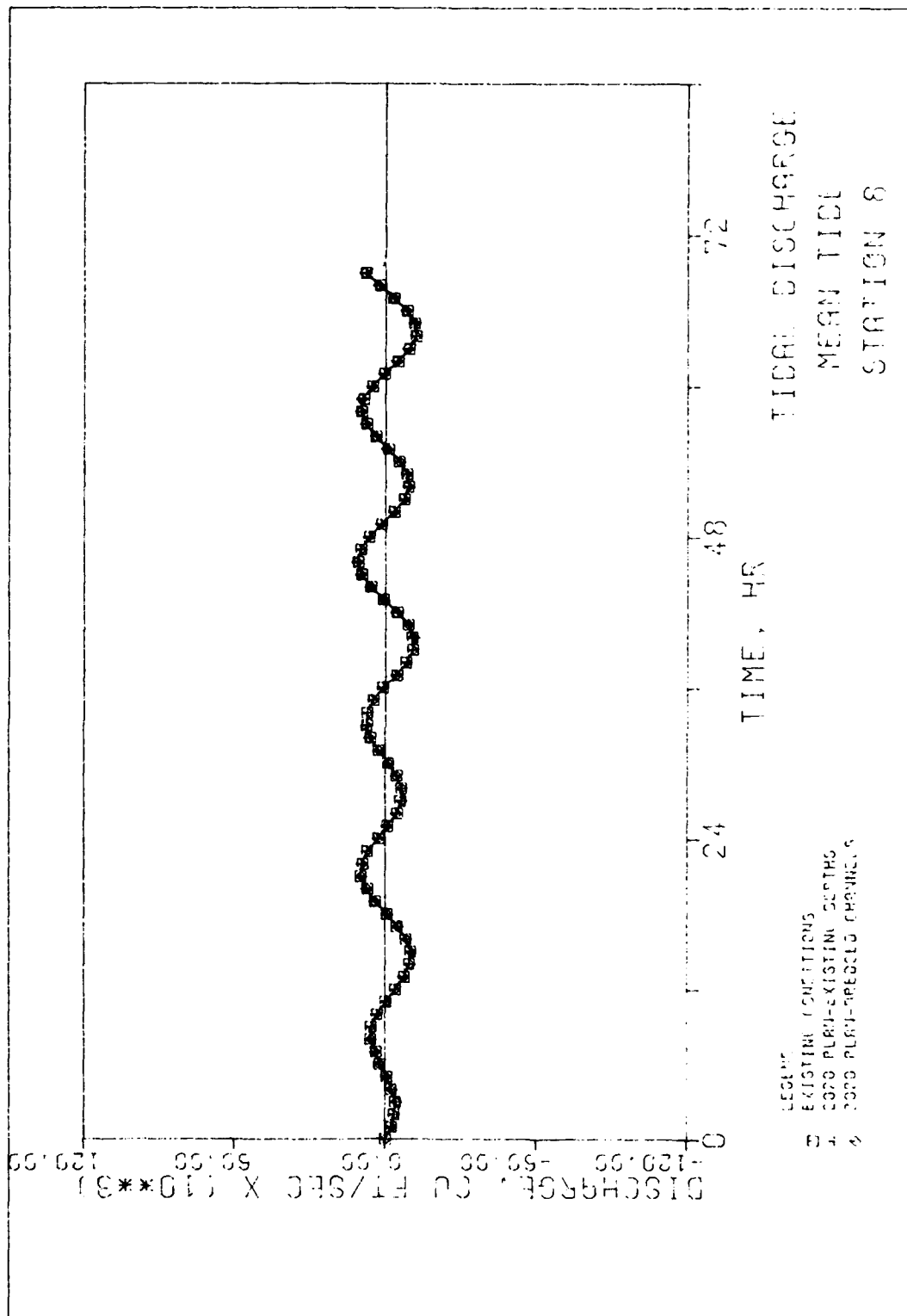


Plate 68

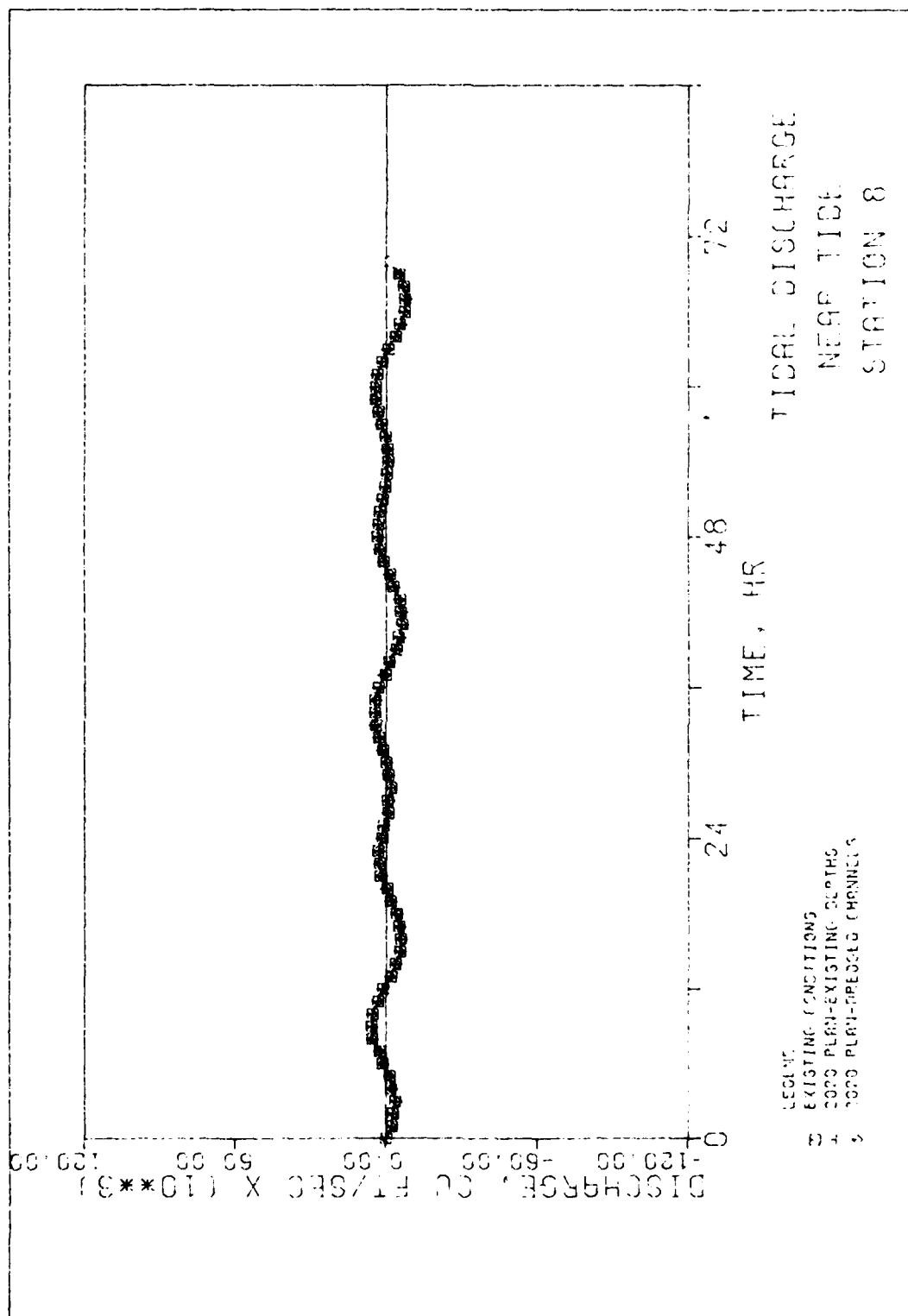


Plate 69

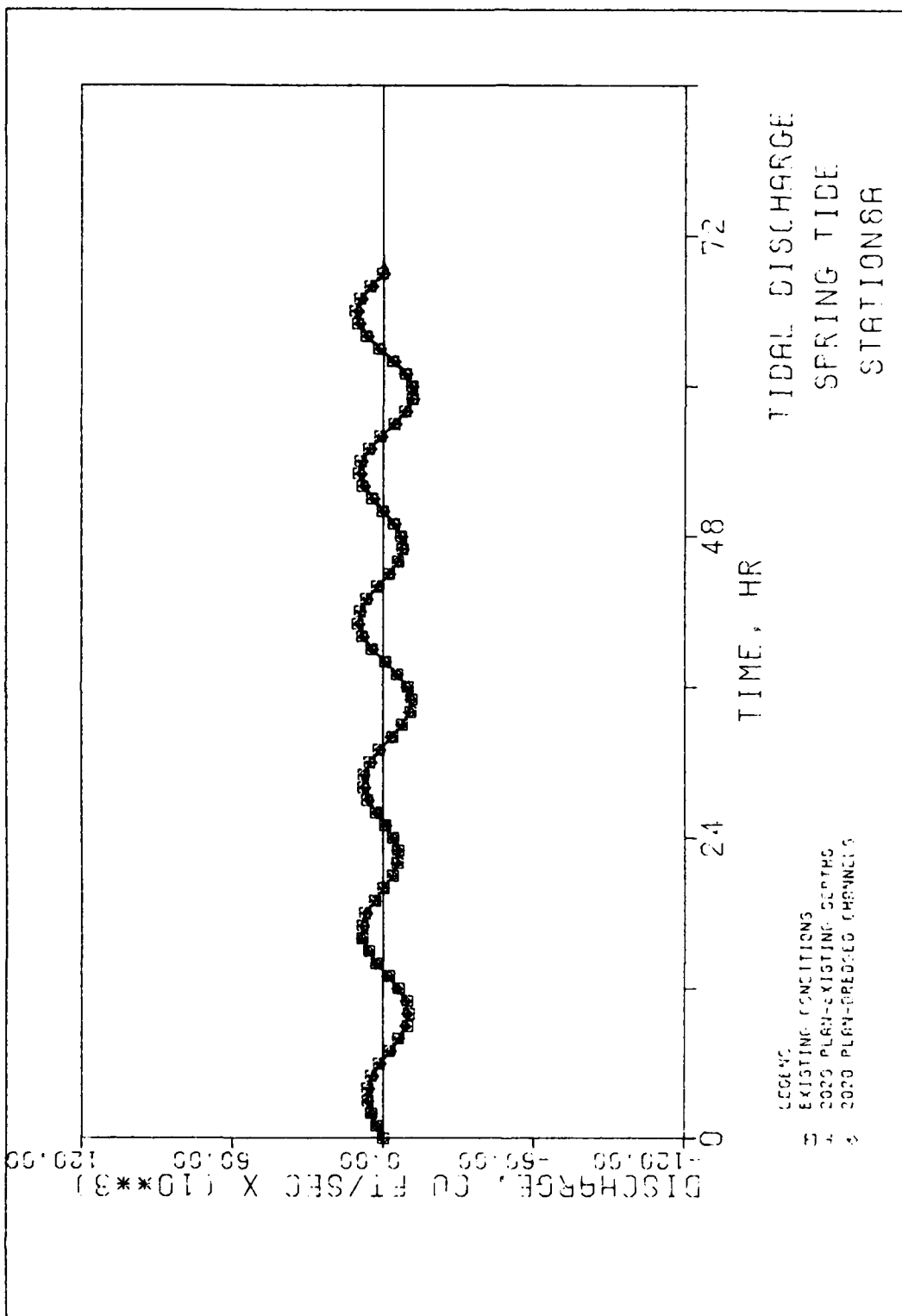


Plate 70

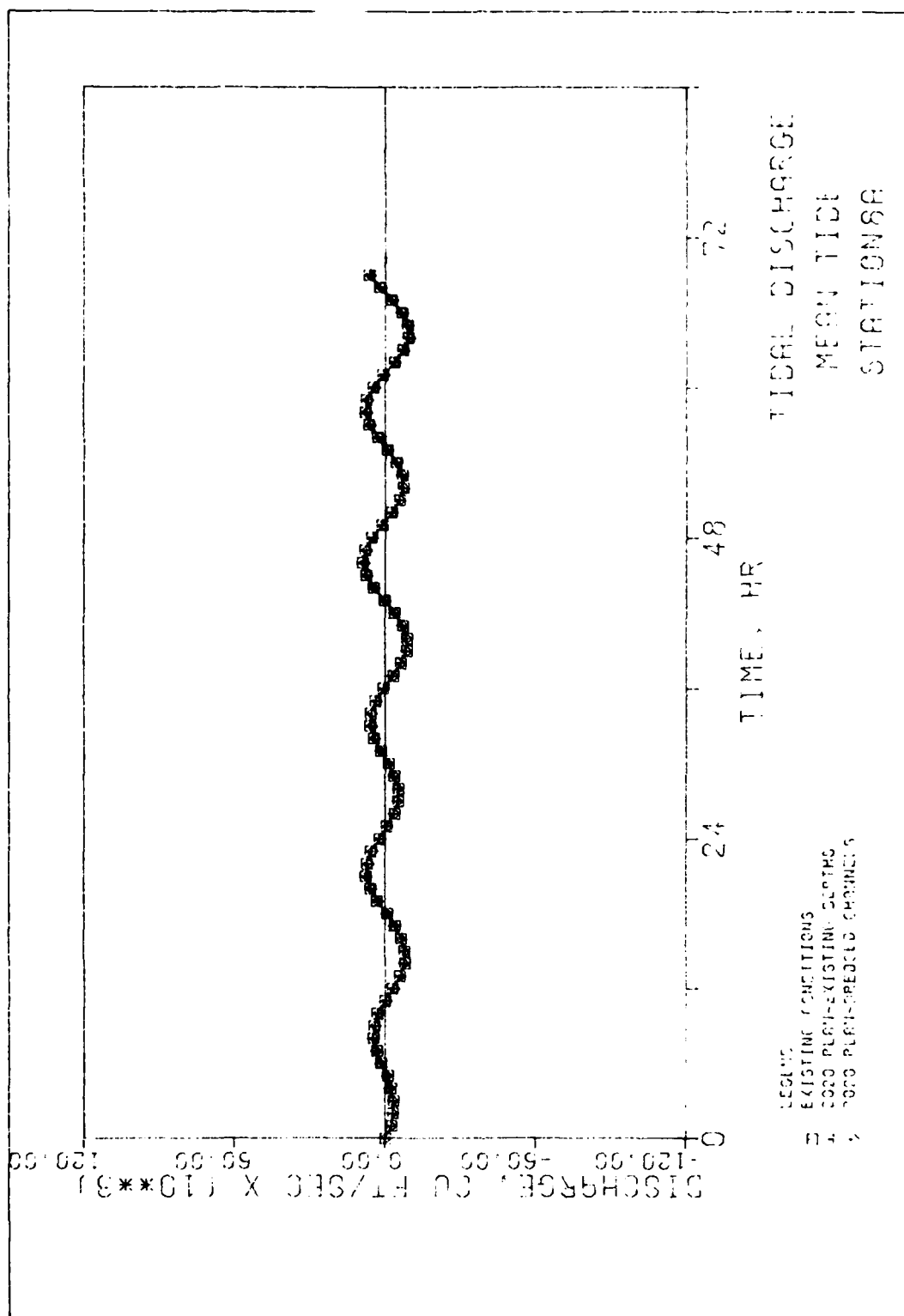


Plate 71

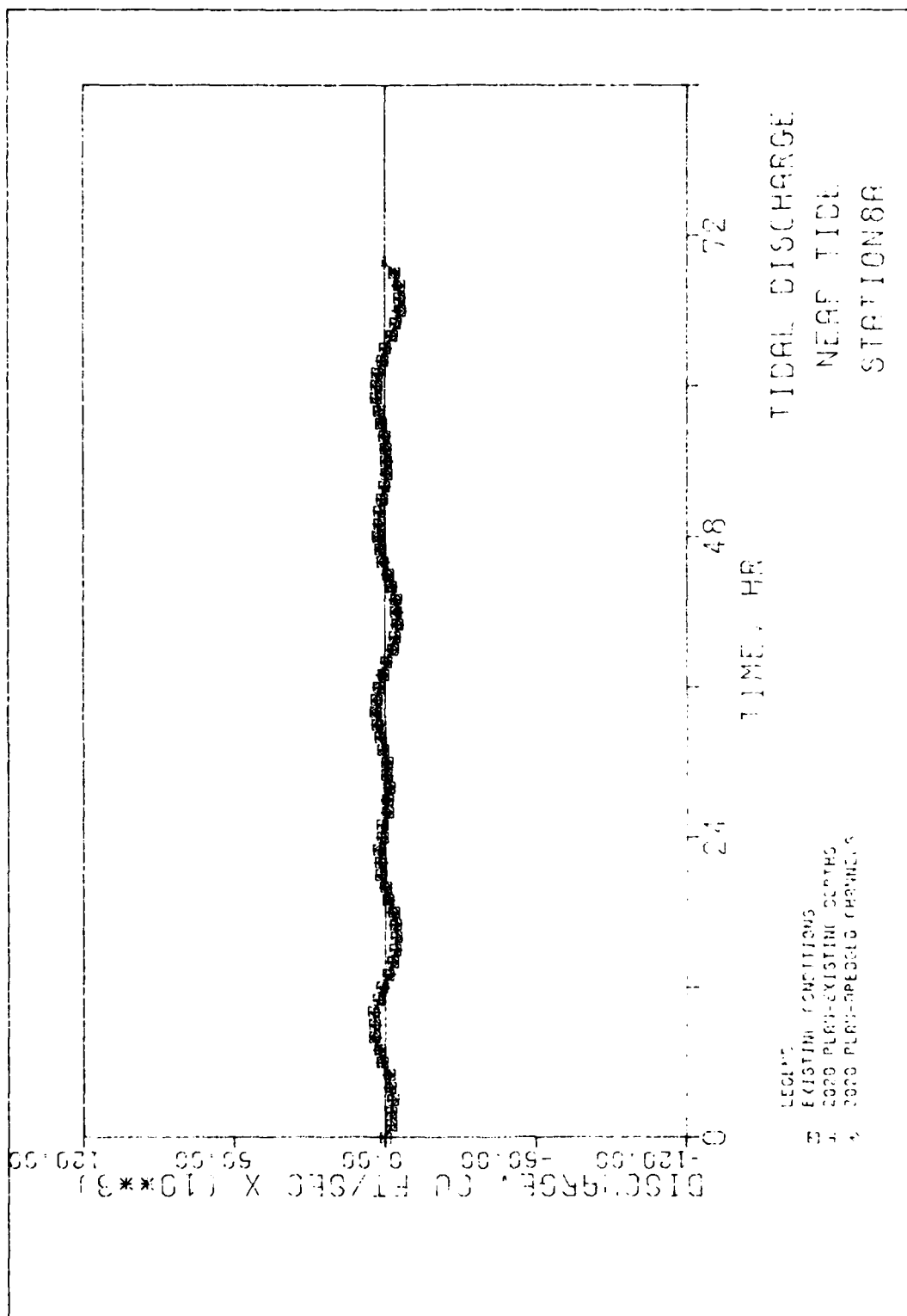


Plate 72

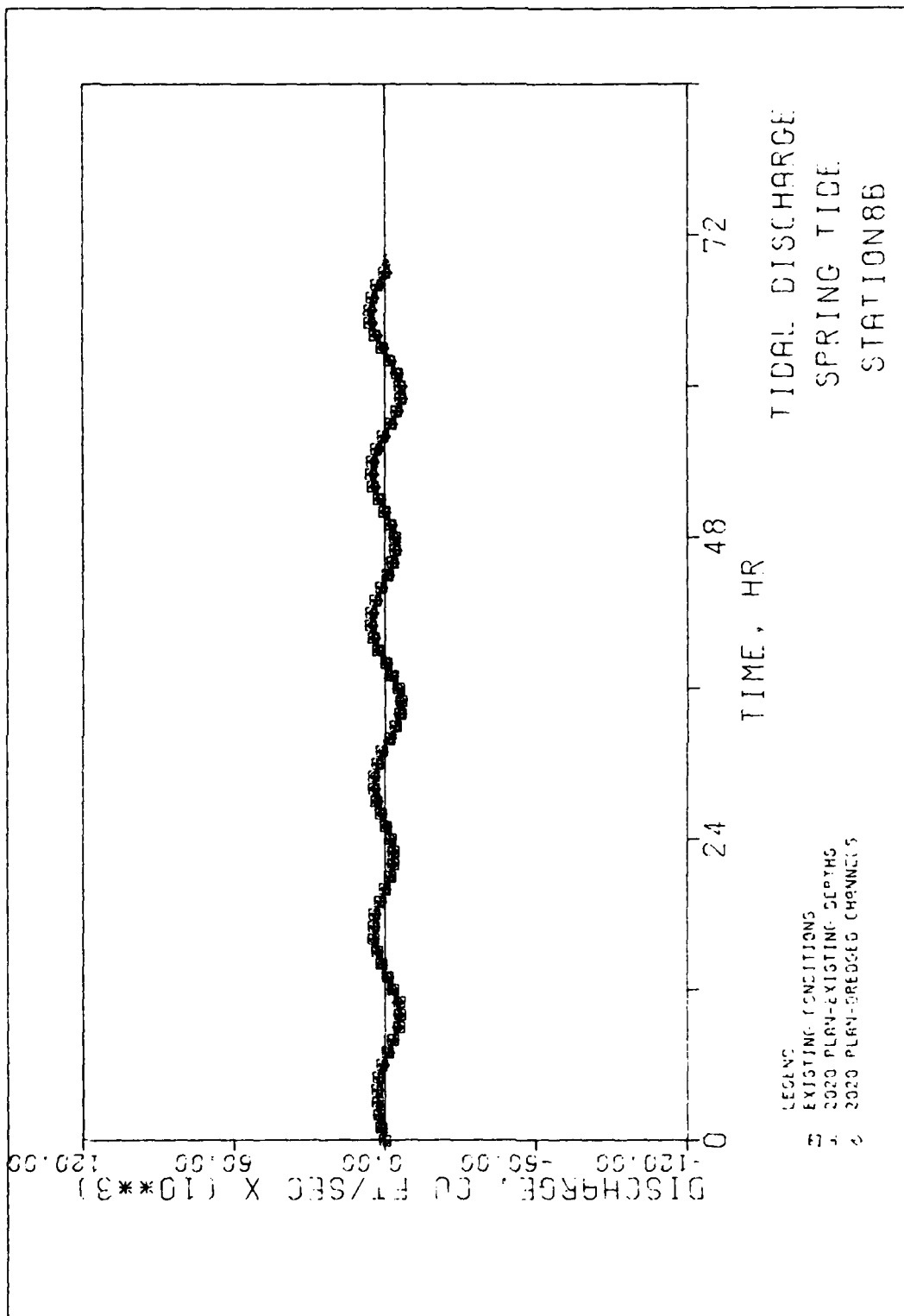


Plate 73

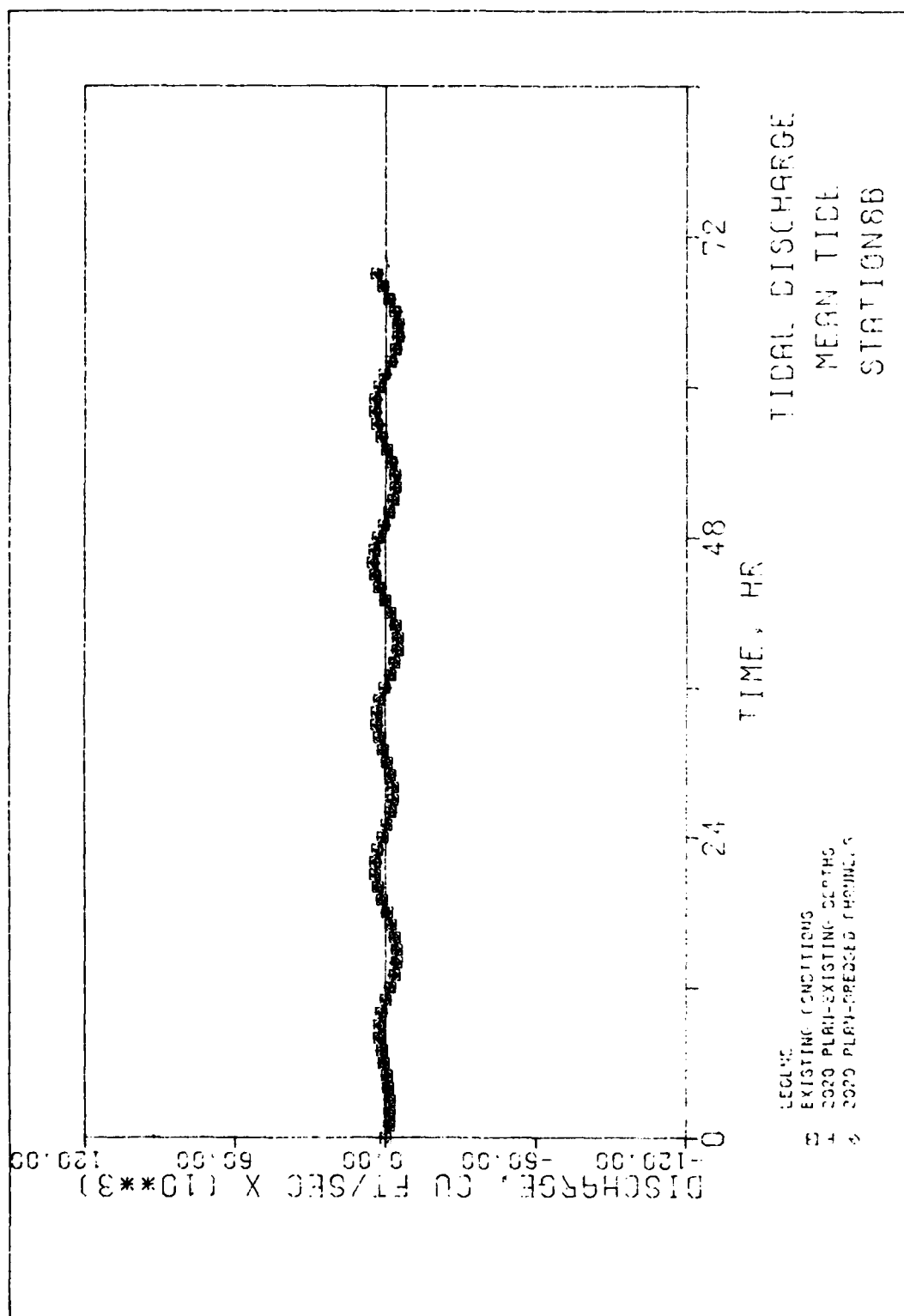


Plate 74

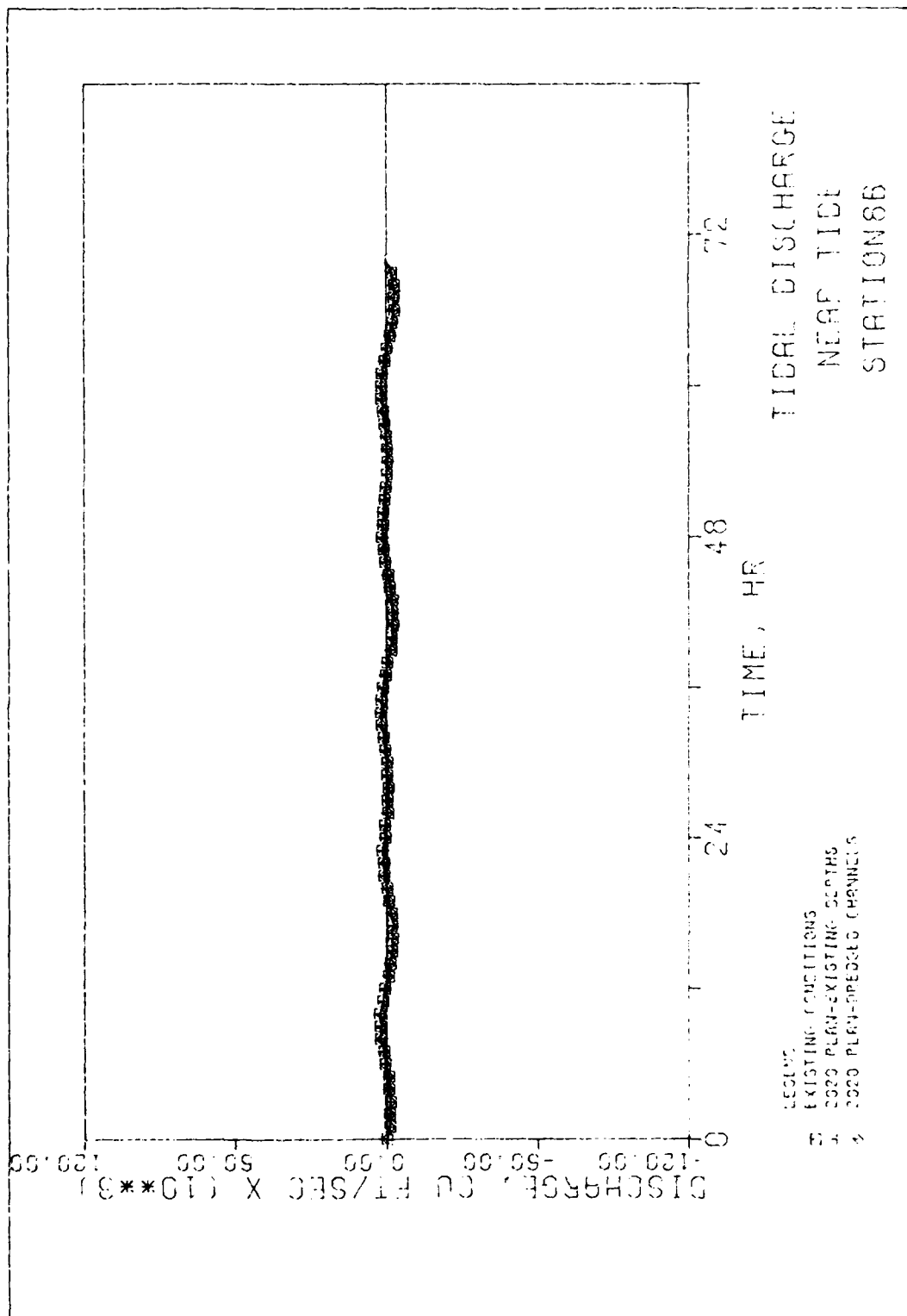


Plate 75

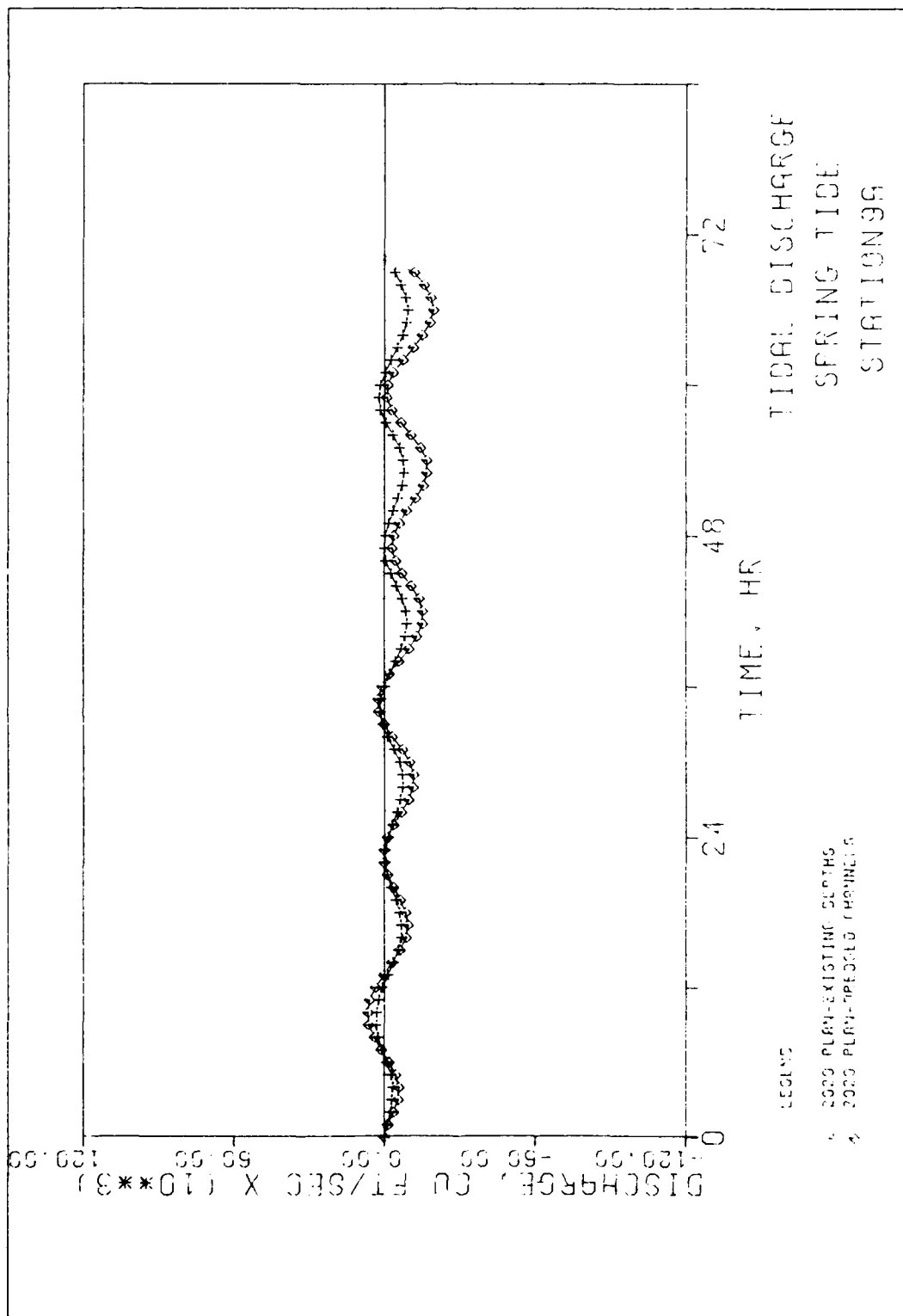


Plate 76

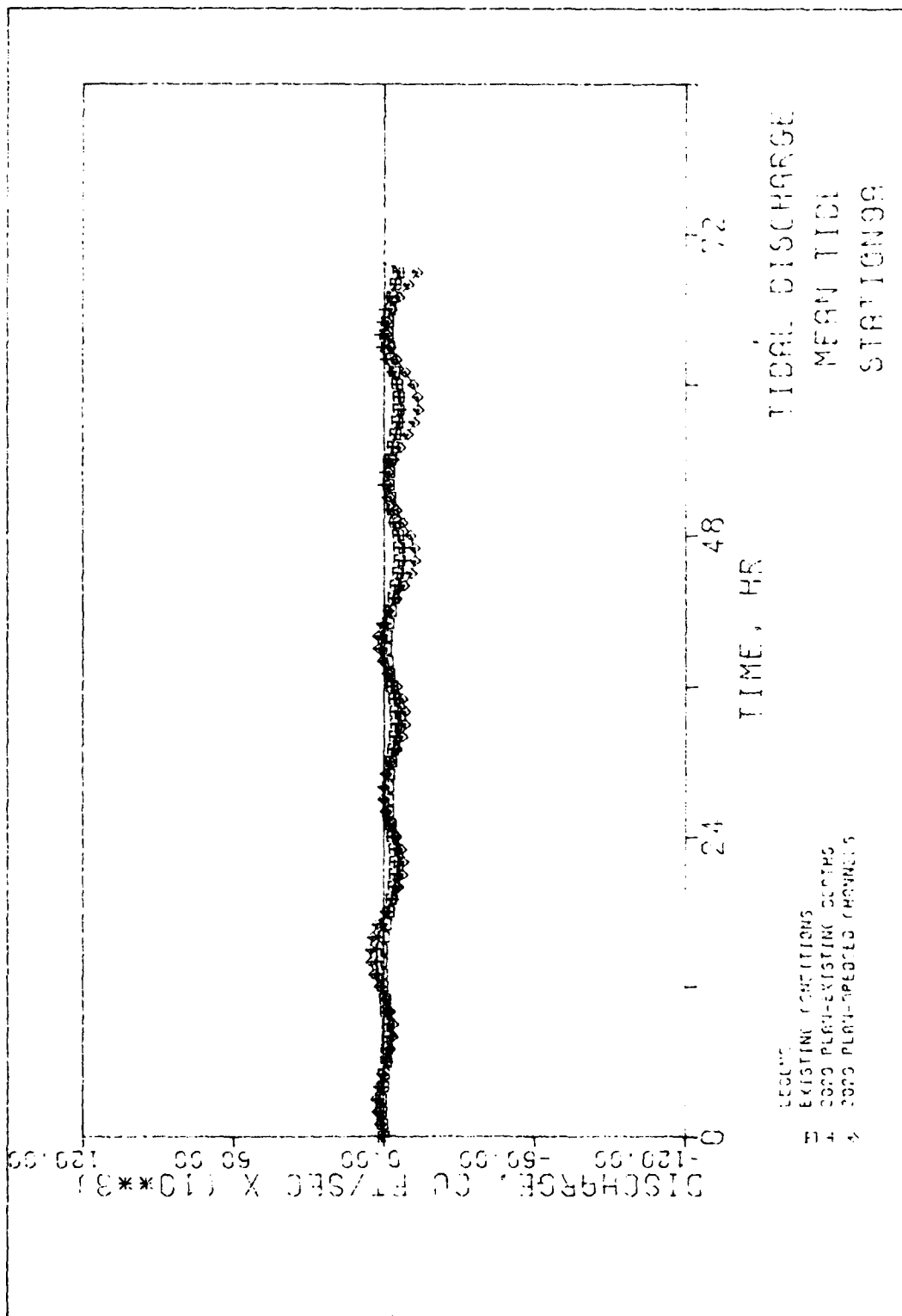


Plate 77

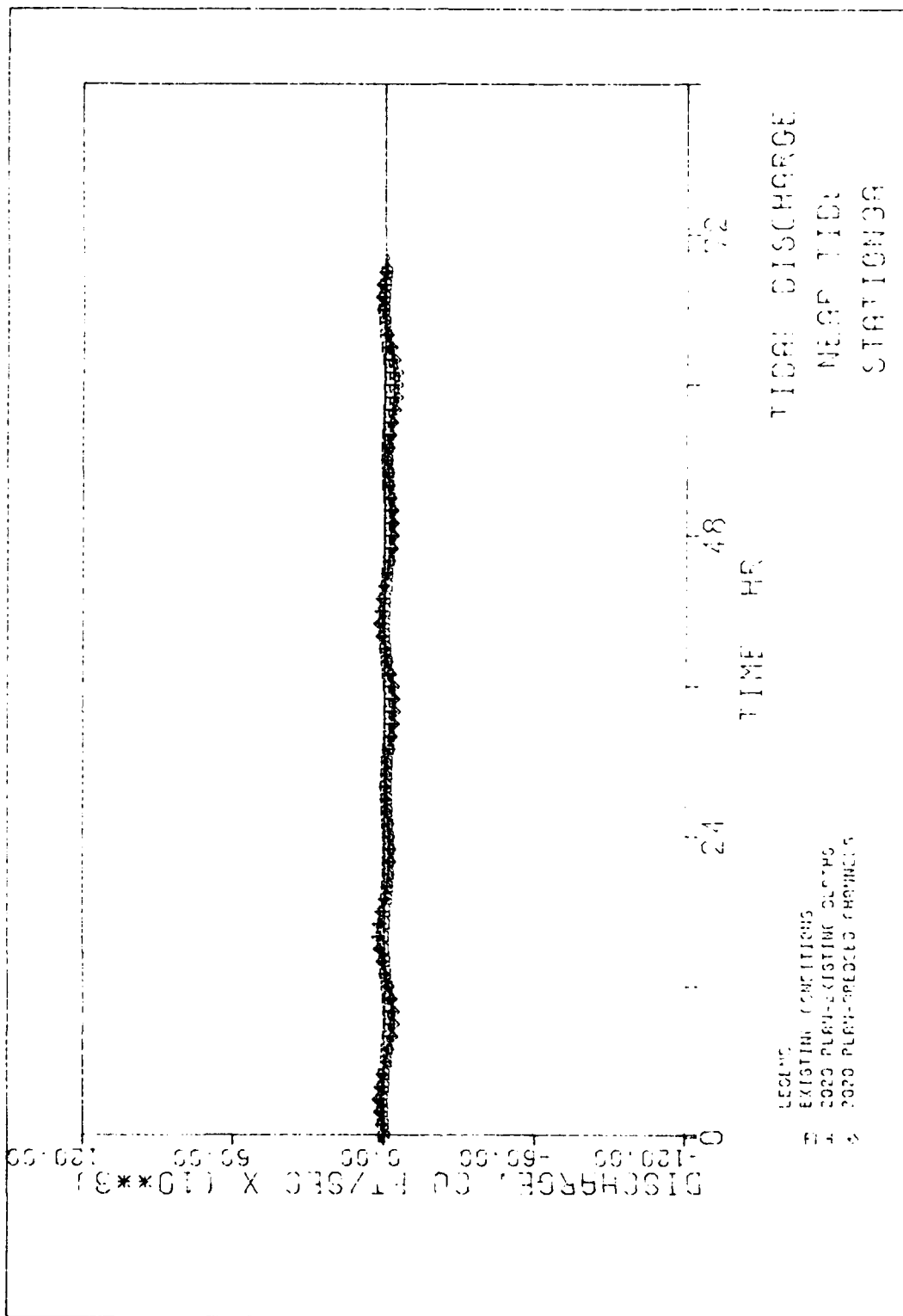


Plate 78

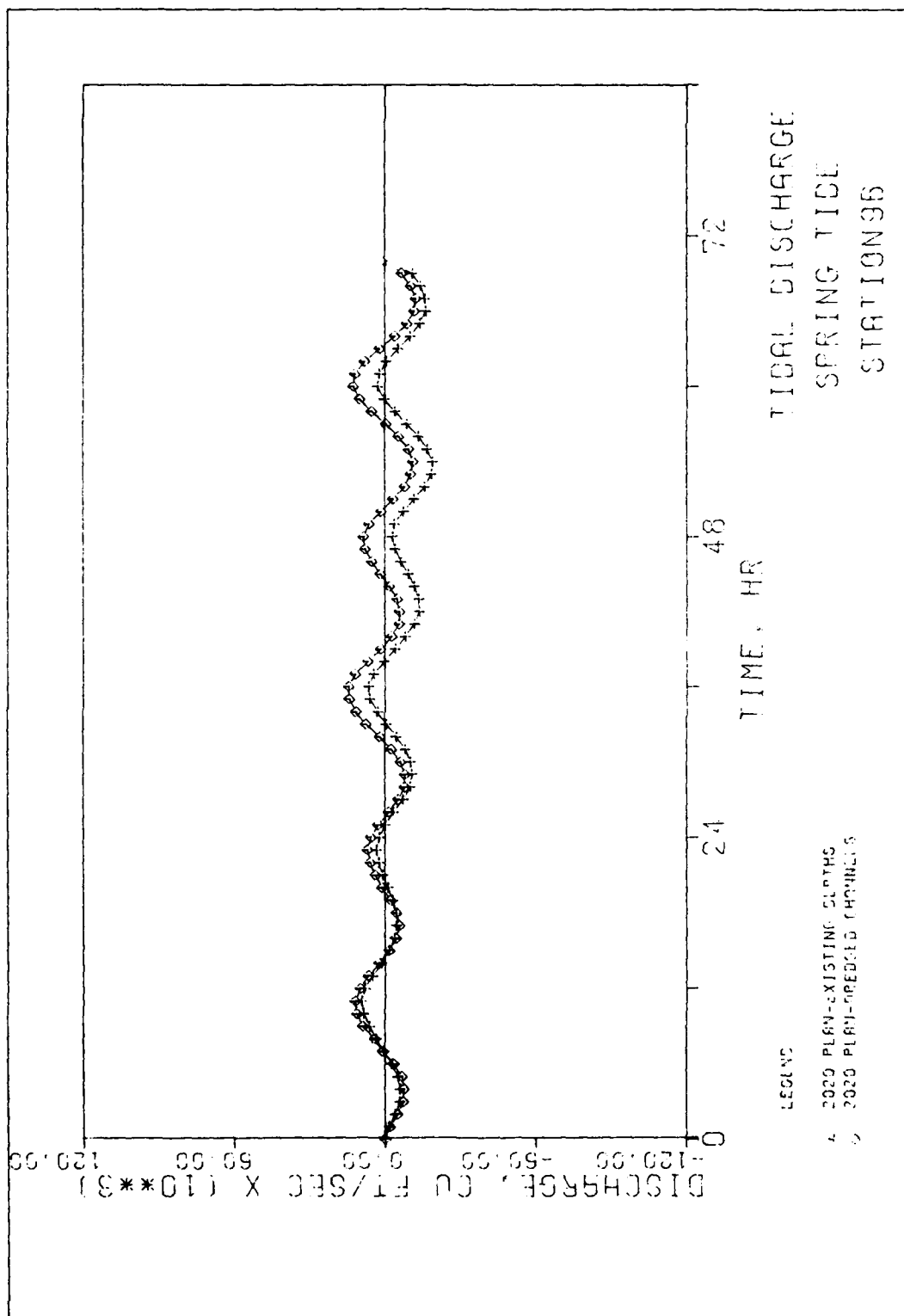


Plate 79

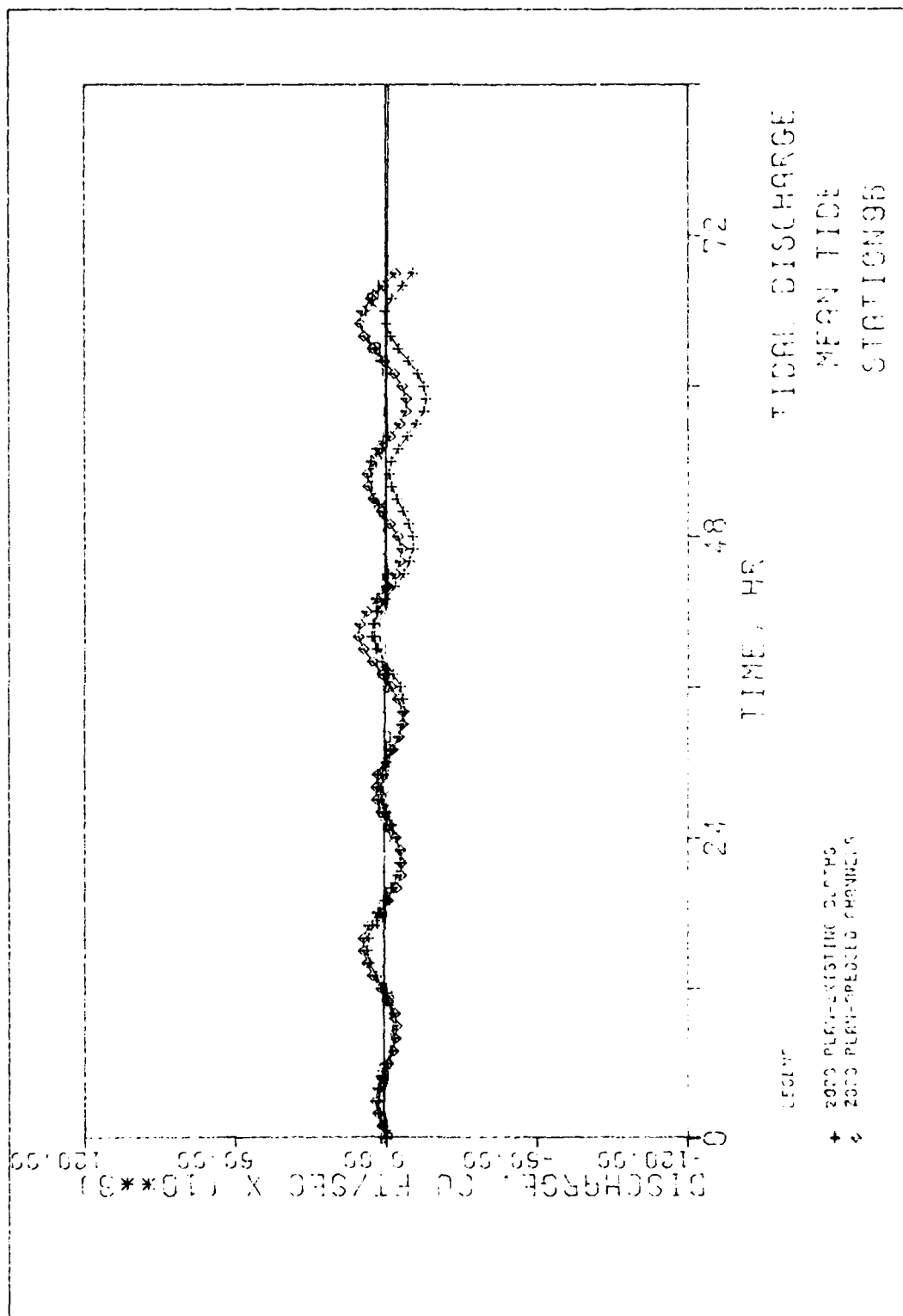


Plate 80

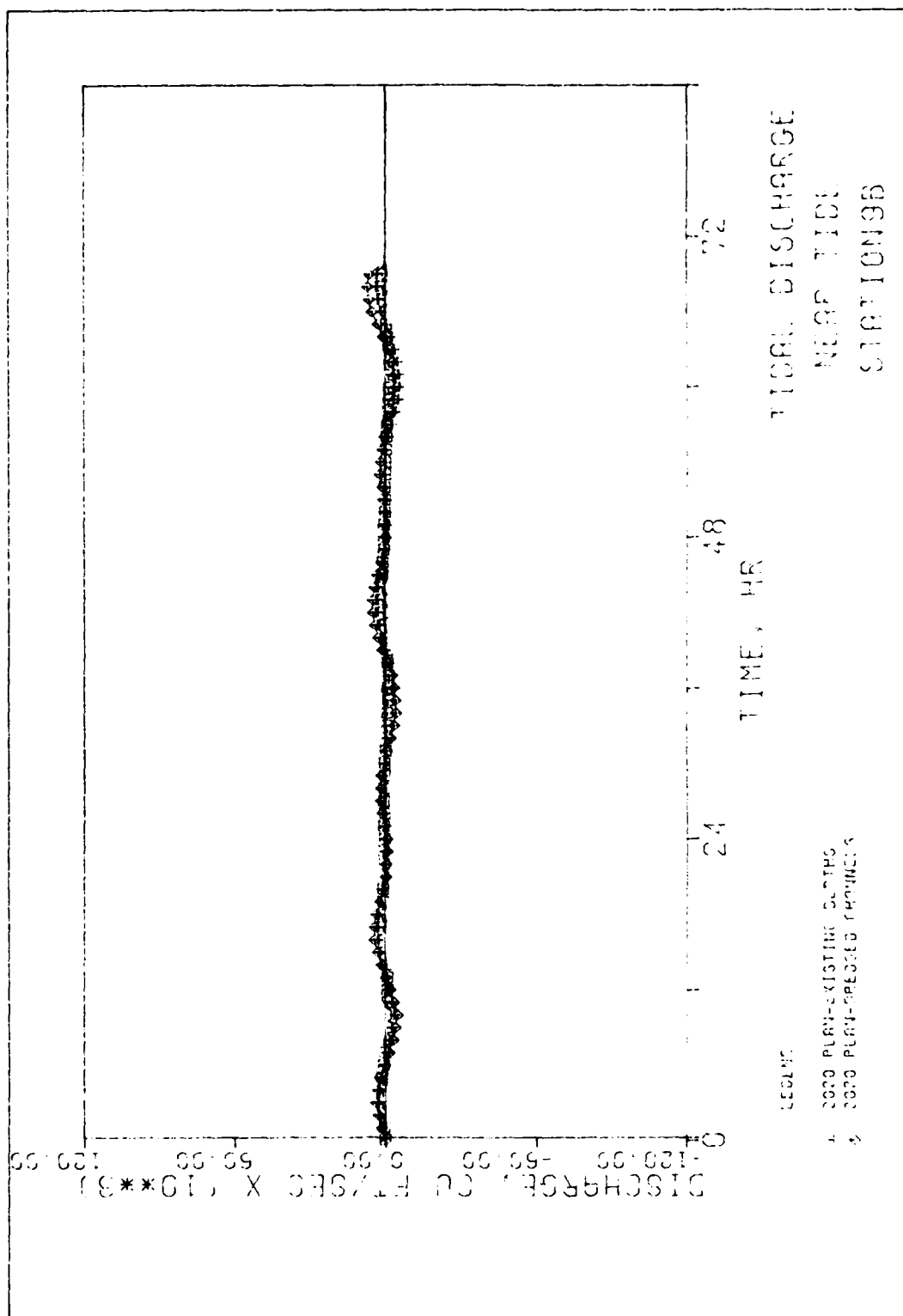
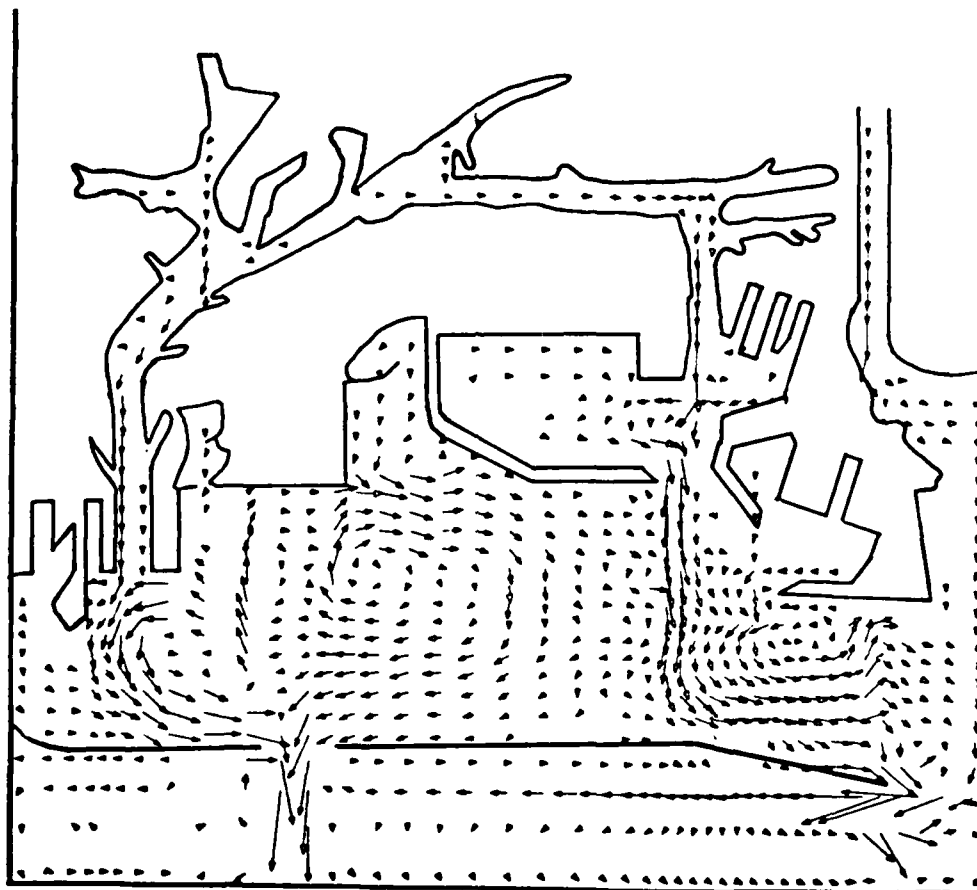
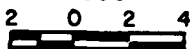


Plate 81



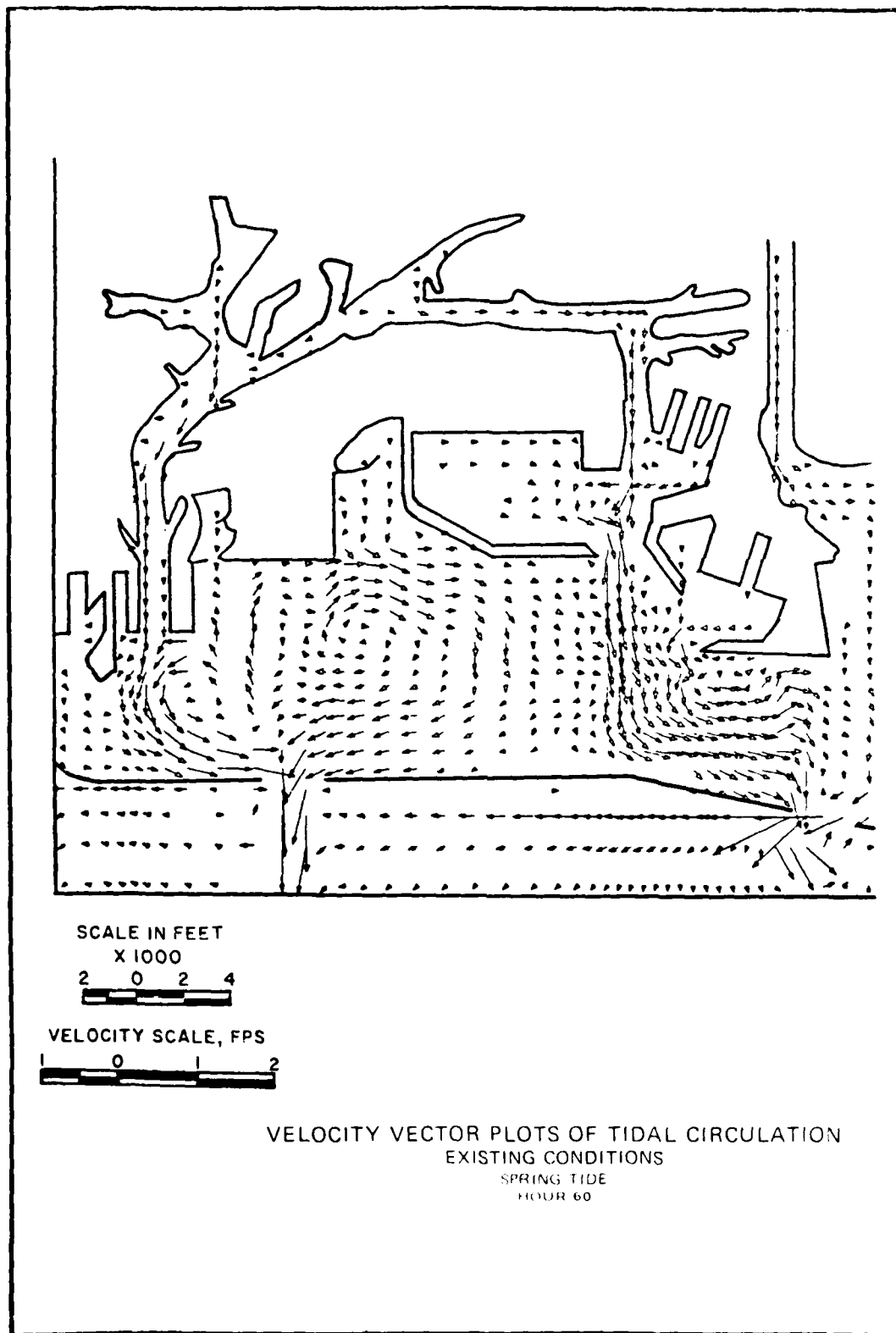
SCALE IN FEET
X 1000

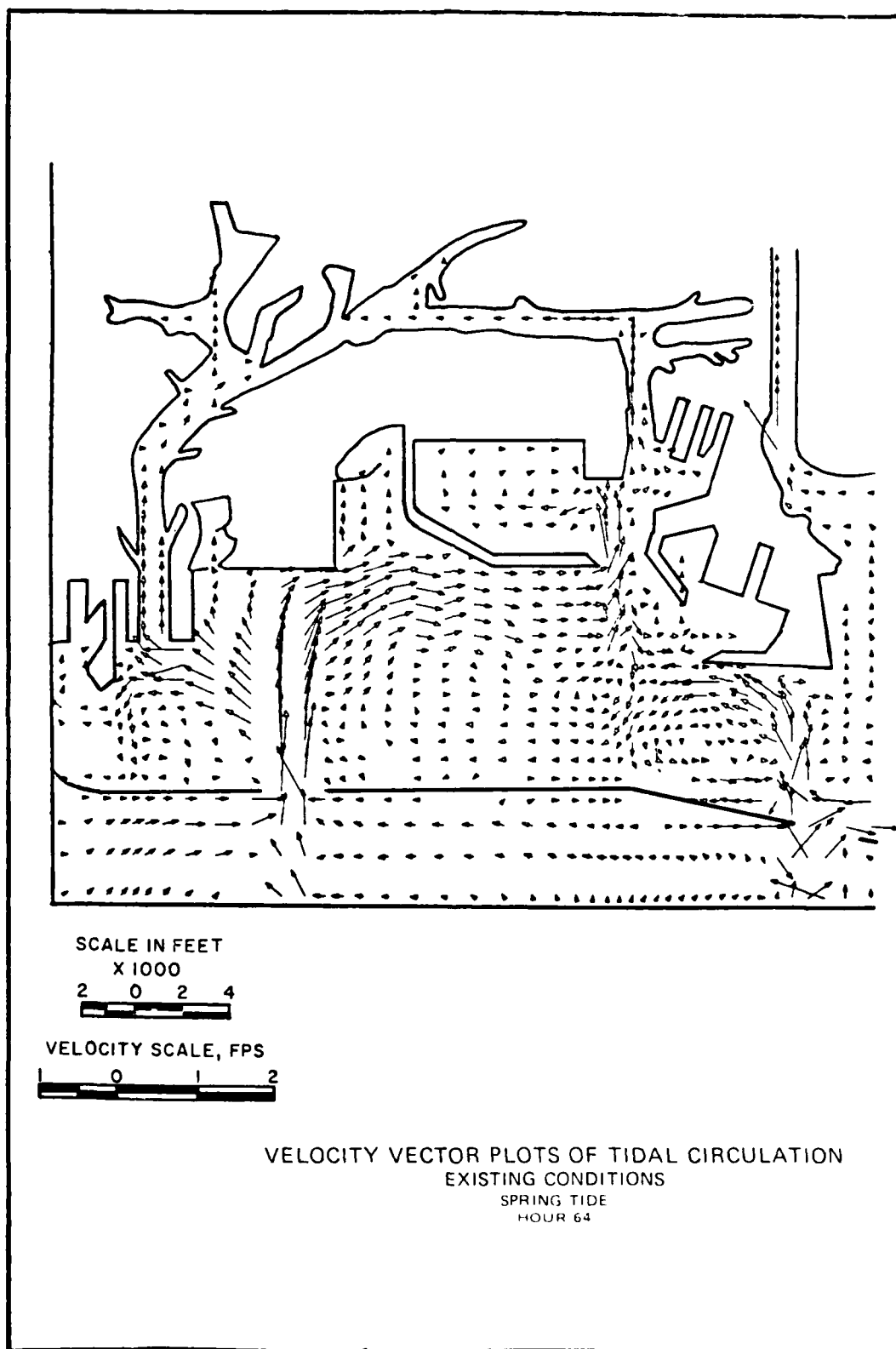


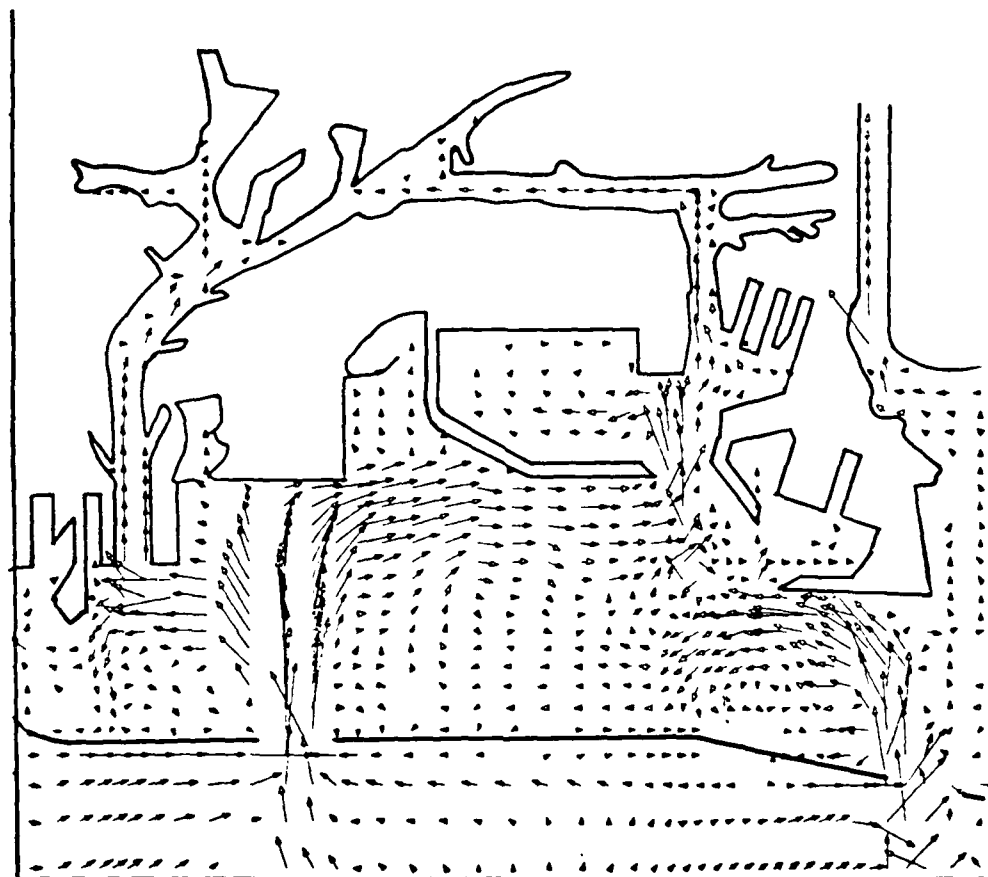
VELOCITY SCALE, FPS



VELOCITY VECTOR PLOTS OF TIDAL CIRCULATION
EXISTING CONDITIONS
SPRING TIDE
HOUR 58







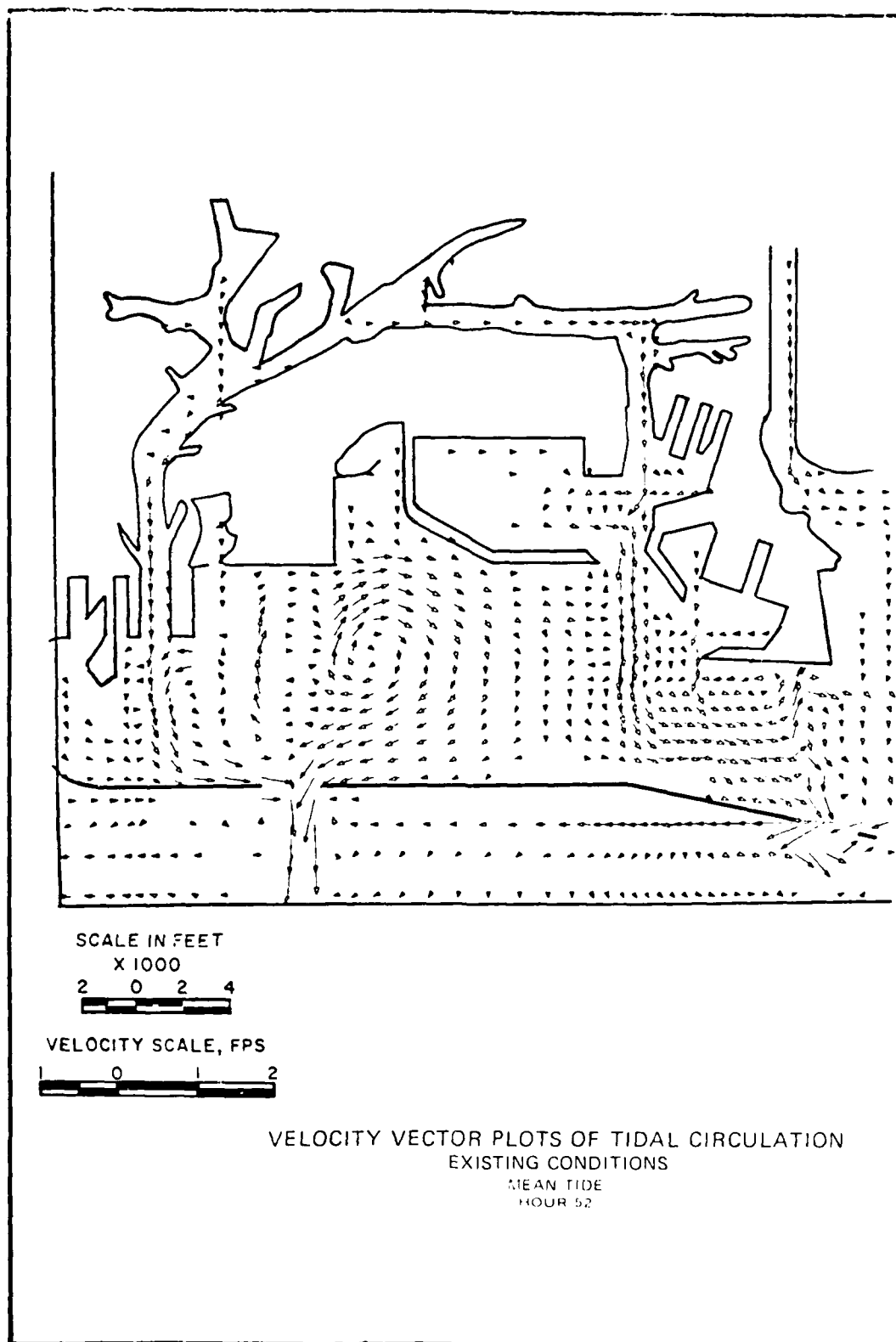
SCALE IN FEET
X 1000

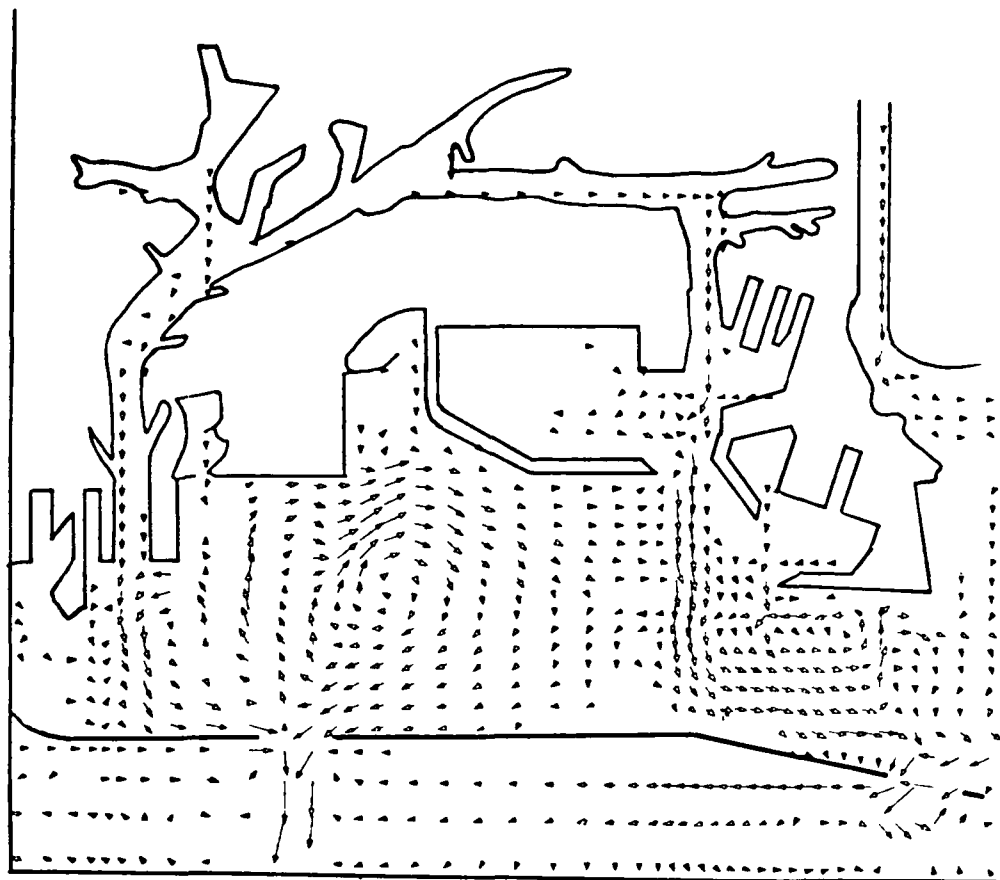


VELOCITY SCALE, FPS

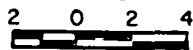


VELOCITY VECTOR PLOTS OF TIDAL CIRCULATION
EXISTING CONDITIONS
SPRING TIDE
HOUR 66





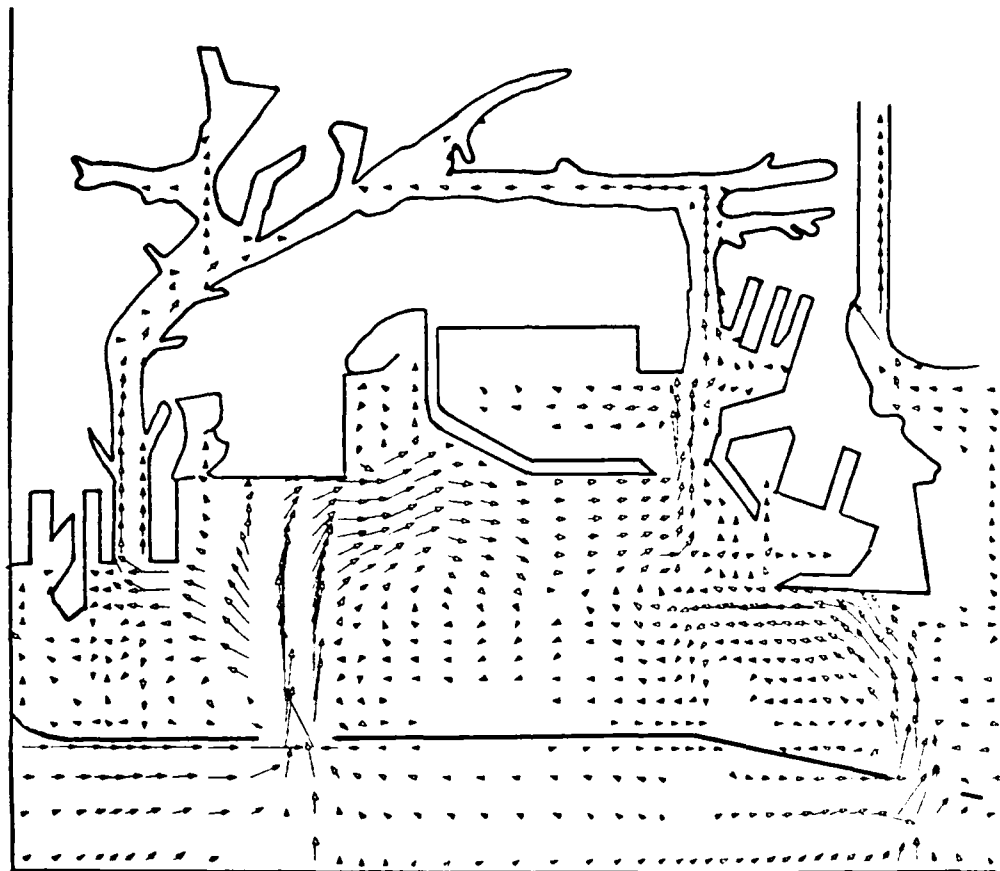
SCALE IN FEET
X 1000



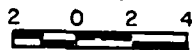
VELOCITY SCALE, FPS



VELOCITY VECTOR PLOTS OF TIDAL CIRCULATION
EXISTING CONDITIONS
MEAN TIDE
HOUR 54



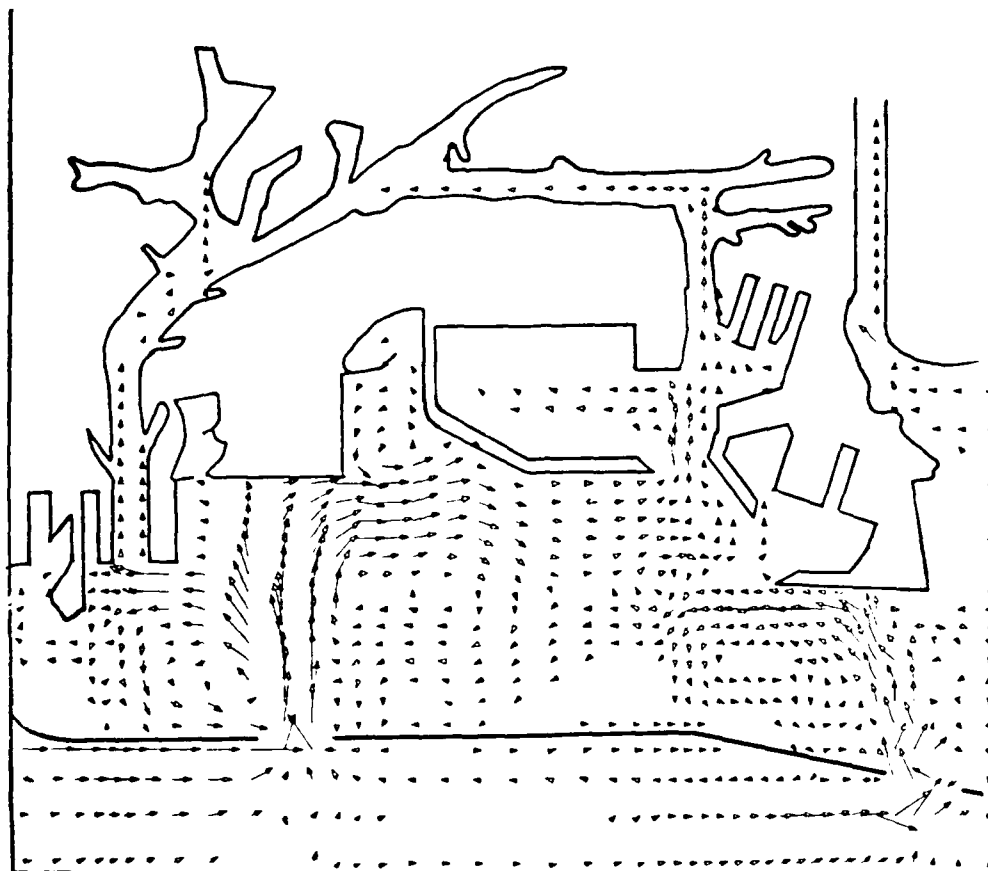
SCALE IN FEET
X 1000



VELOCITY SCALE, FPS



VELOCITY VECTOR PLOTS OF TIDAL CIRCULATION
EXISTING CONDITIONS
MEAN TIDE
NOVEMBER 1964



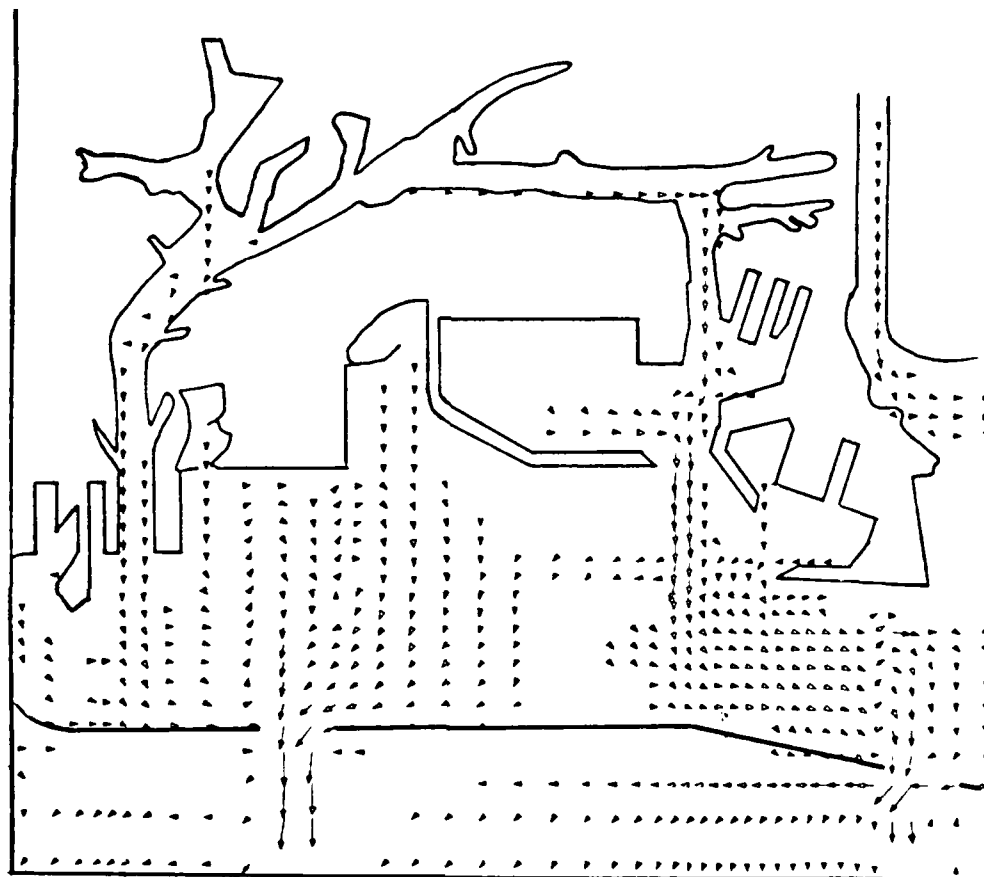
SCALE IN FEET
X 1000



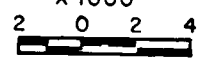
VELOCITY SCALE, FPS



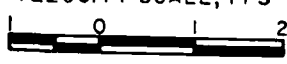
VELOCITY VECTOR PLOTS OF TIDAL CIRCULATION
EXISTING CONDITIONS
MEAN TIDE
HOUR 60



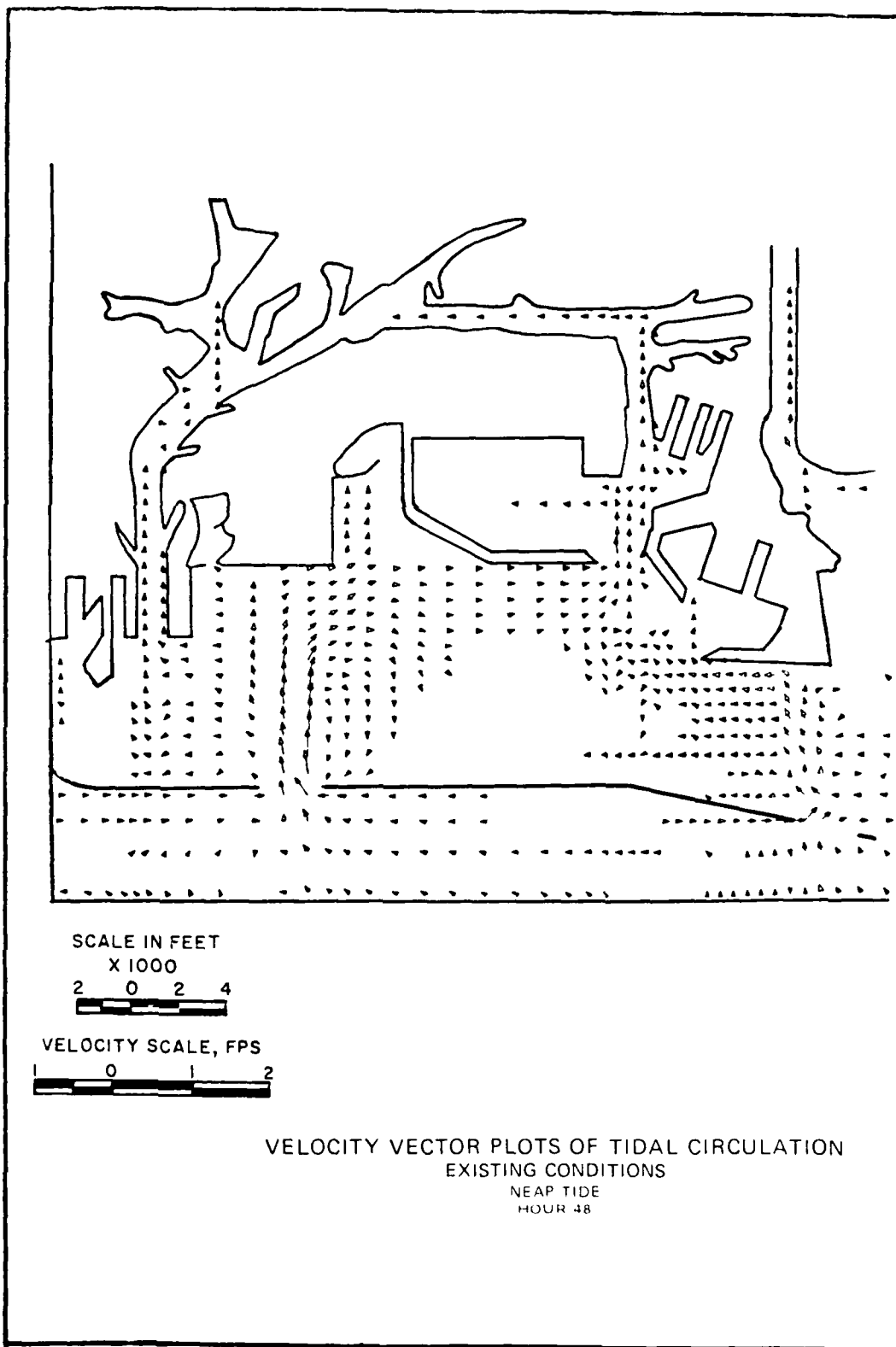
SCALE IN FEET
X 1000

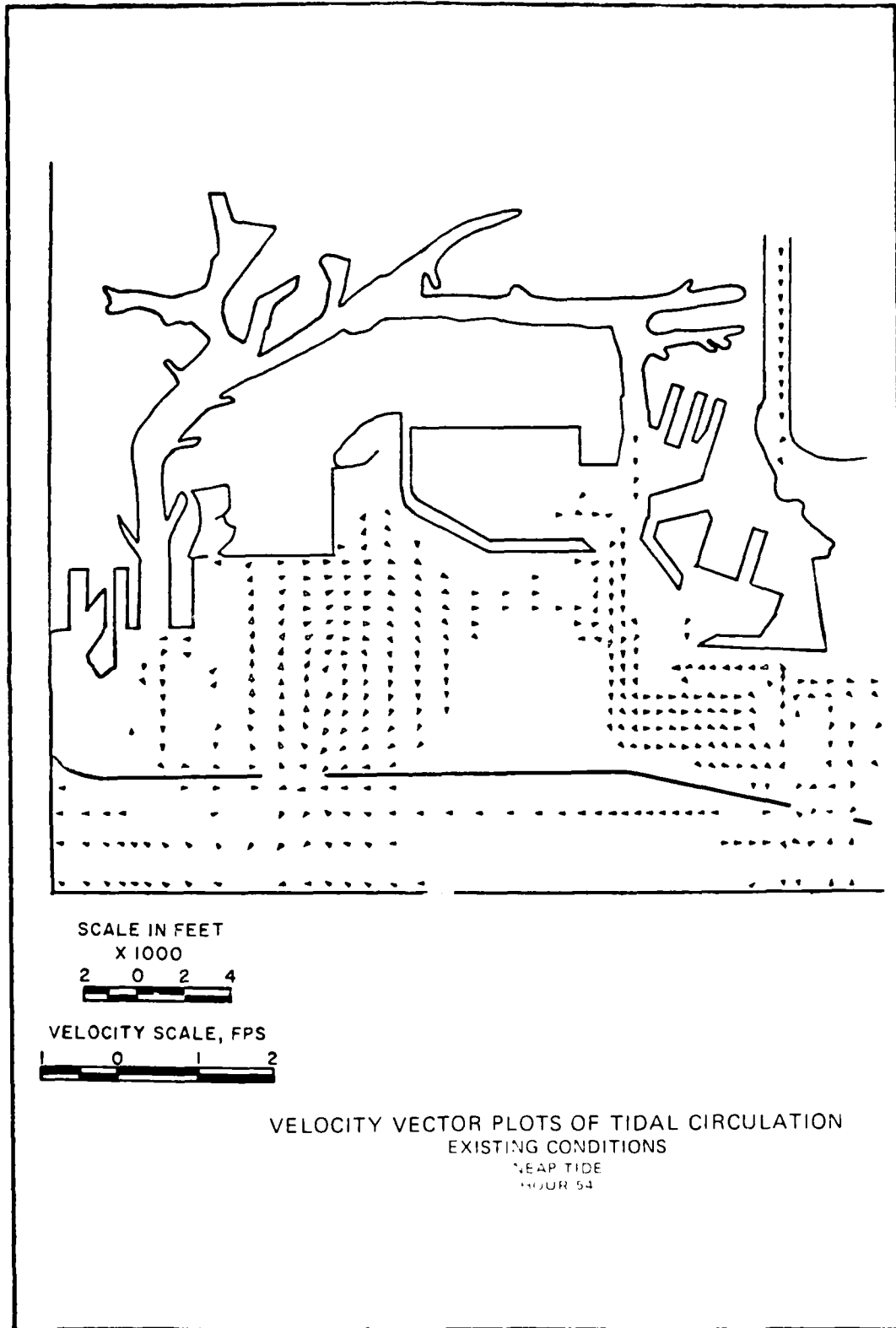


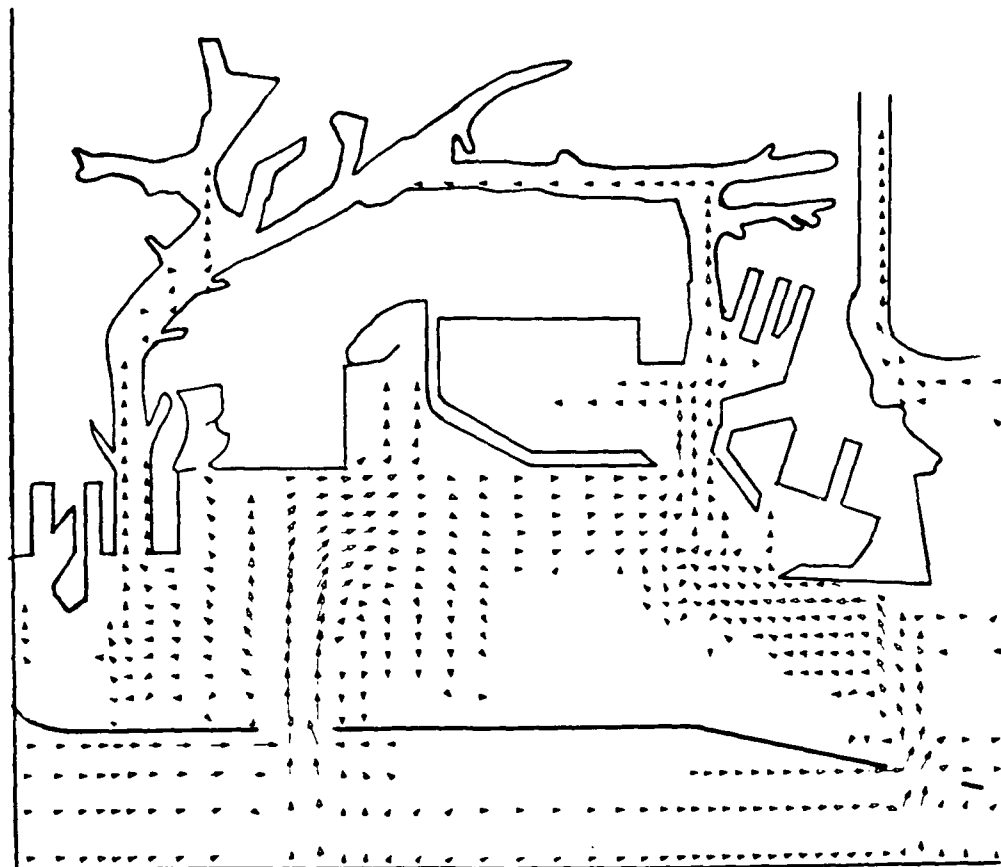
VELOCITY SCALE, FPS



VELOCITY VECTOR PLOTS OF TIDAL CIRCULATION
EXISTING CONDITIONS
NEAP TIDE
HOUR 42







SCALE IN FEET
X 1000

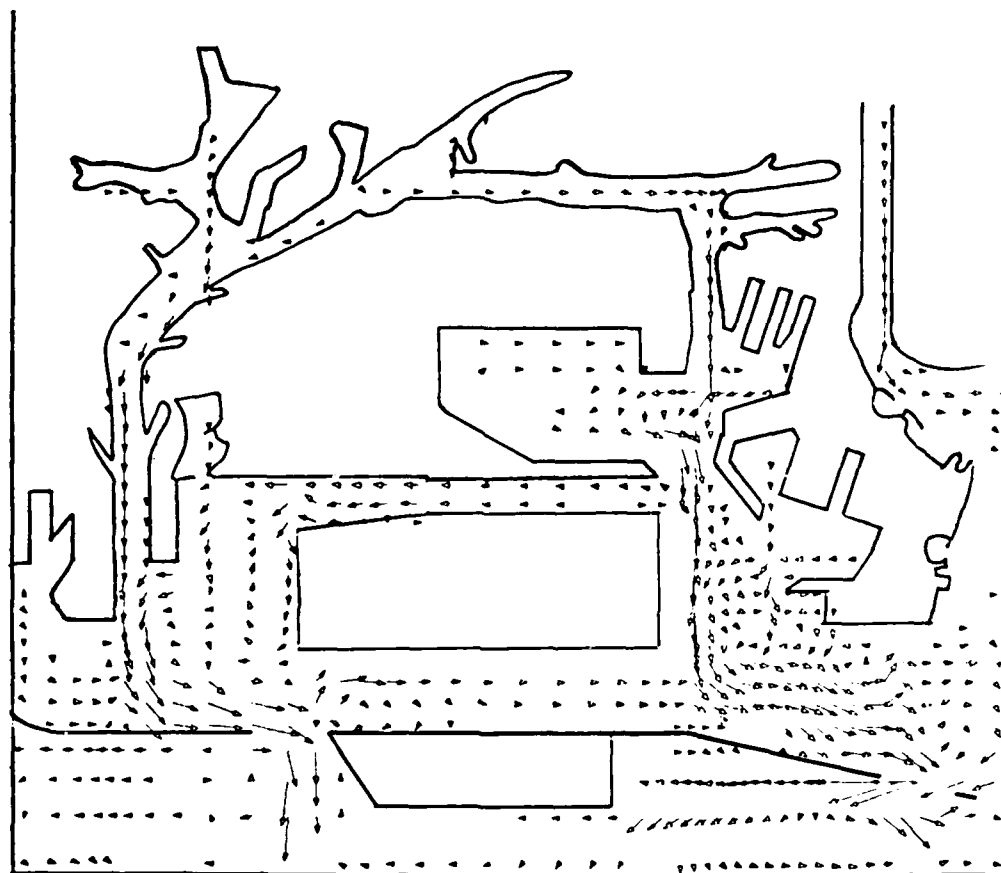
2 0 2 4

VELOCITY SCALE, FPS

1 0 1 2

VELOCITY VECTOR PLOTS OF TIDAL CIRCULATION
EXISTING CONDITIONS

NEAP TIDE
FLOWING



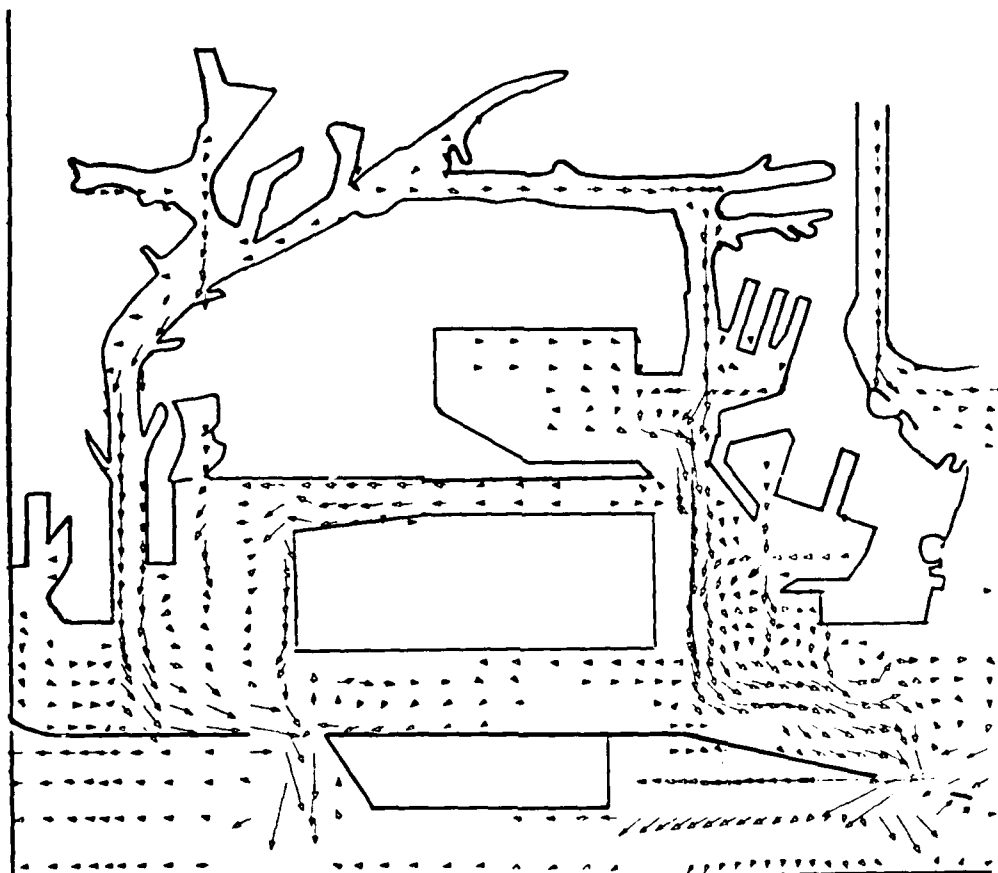
SCALE IN FEET
X 1000



VELOCITY SCALE, FPS



VELOCITY VECTOR PLOTS OF TIDAL CIRCULATION
2020 MASTER PLAN
EXISTING CHANNELS
SPRING TIDE
HOUR 58



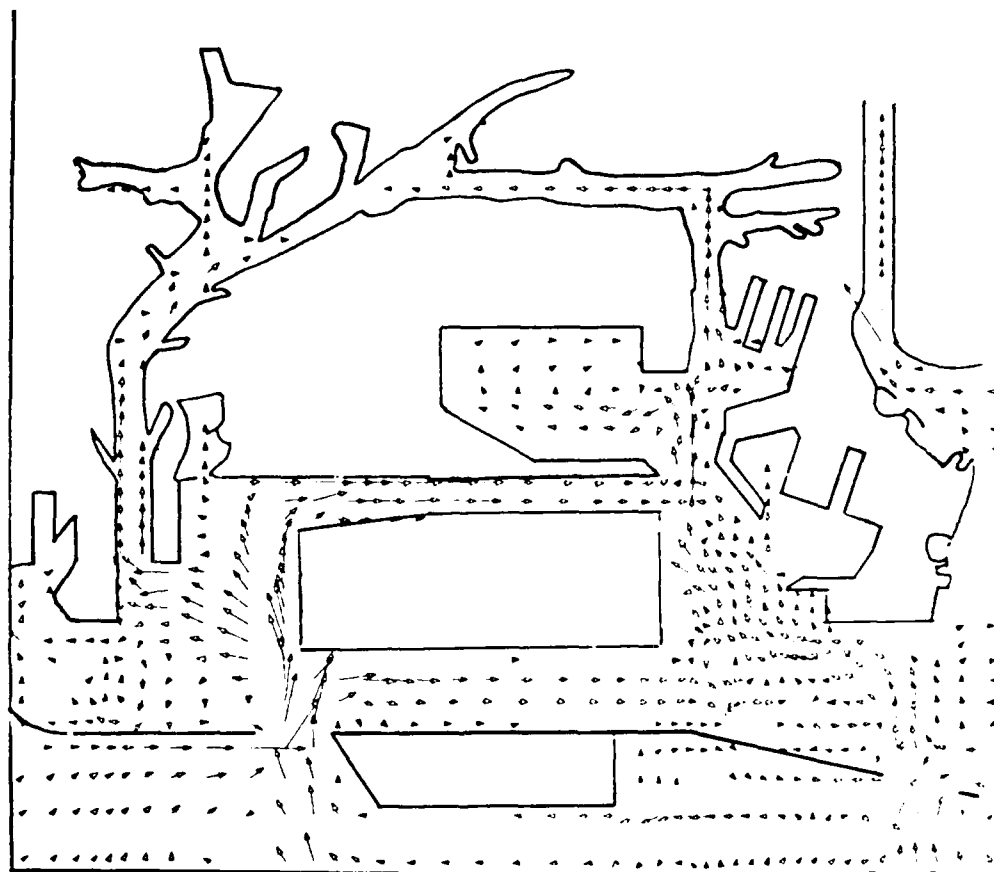
SCALE IN FEET
X 1000



VELOCITY SCALE, FPS



VELOCITY VECTOR PLOTS OF TIDAL CIRCULATION
2020 MASTER PLAN
EXISTING CHANNELS
SPRING TIDE
HOUR 60



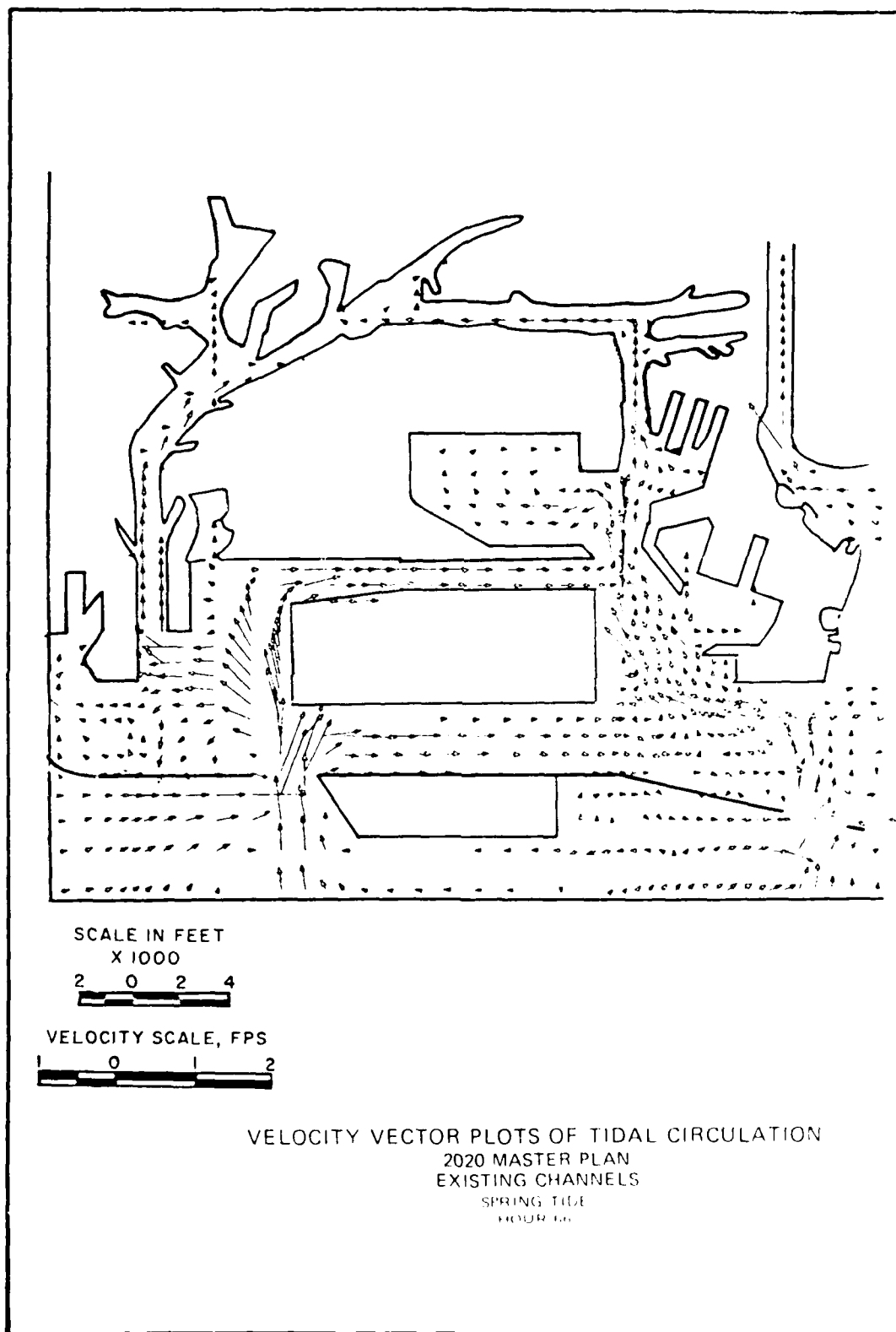
SCALE IN FEET
X 1000

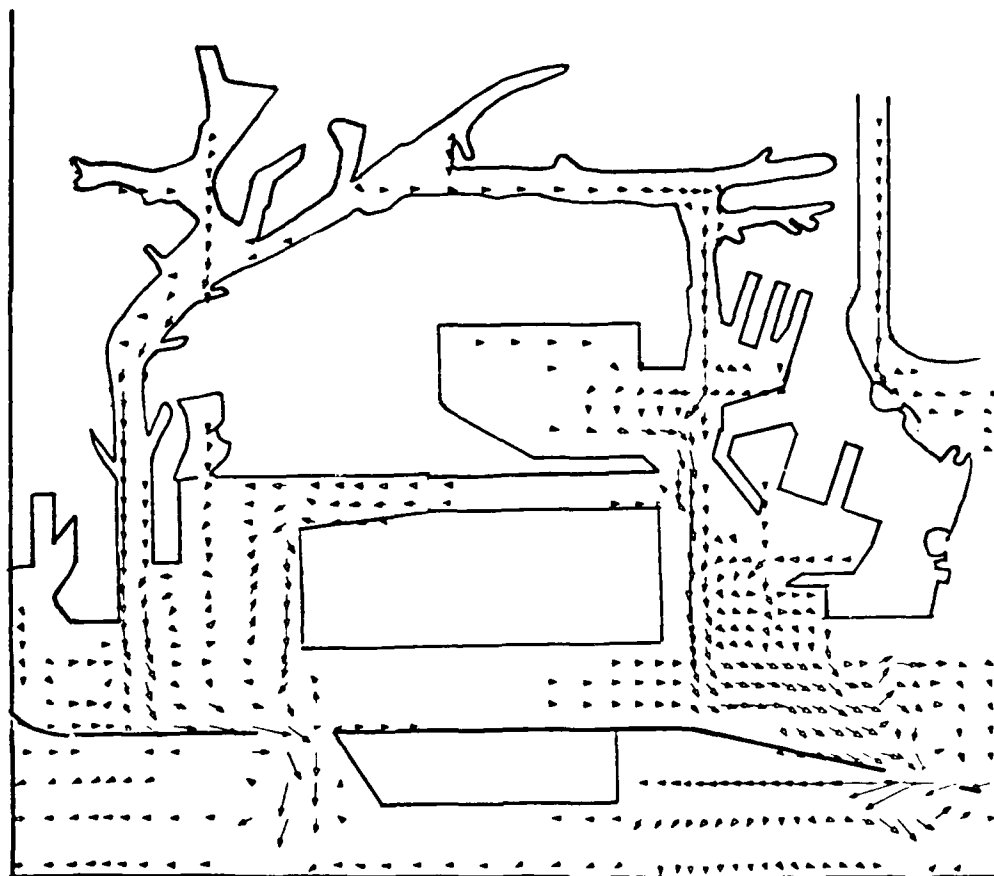
2 0 2 4

VELOCITY SCALE, FPS

1 0 1 2

VELOCITY VECTOR PLOTS OF TIDAL CIRCULATION
2020 MASTER PLAN
EXISTING CHANNELS
SPRING TIDE
HOOR 64





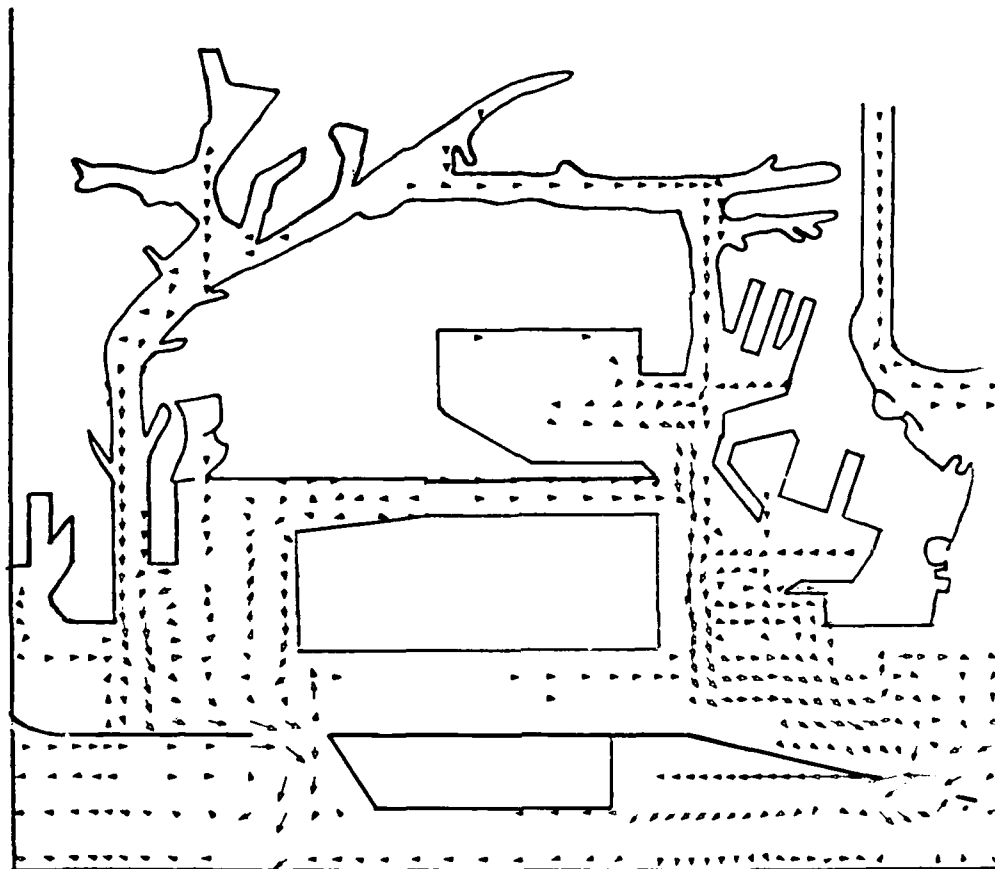
SCALE IN FEET
X 1000



VELOCITY SCALE, FPS



VELOCITY VECTOR PLOTS OF TIDAL CIRCULATION
2020 MASTER PLAN
EXISTING CHANNELS
MEAN TIDE
HOUR 52



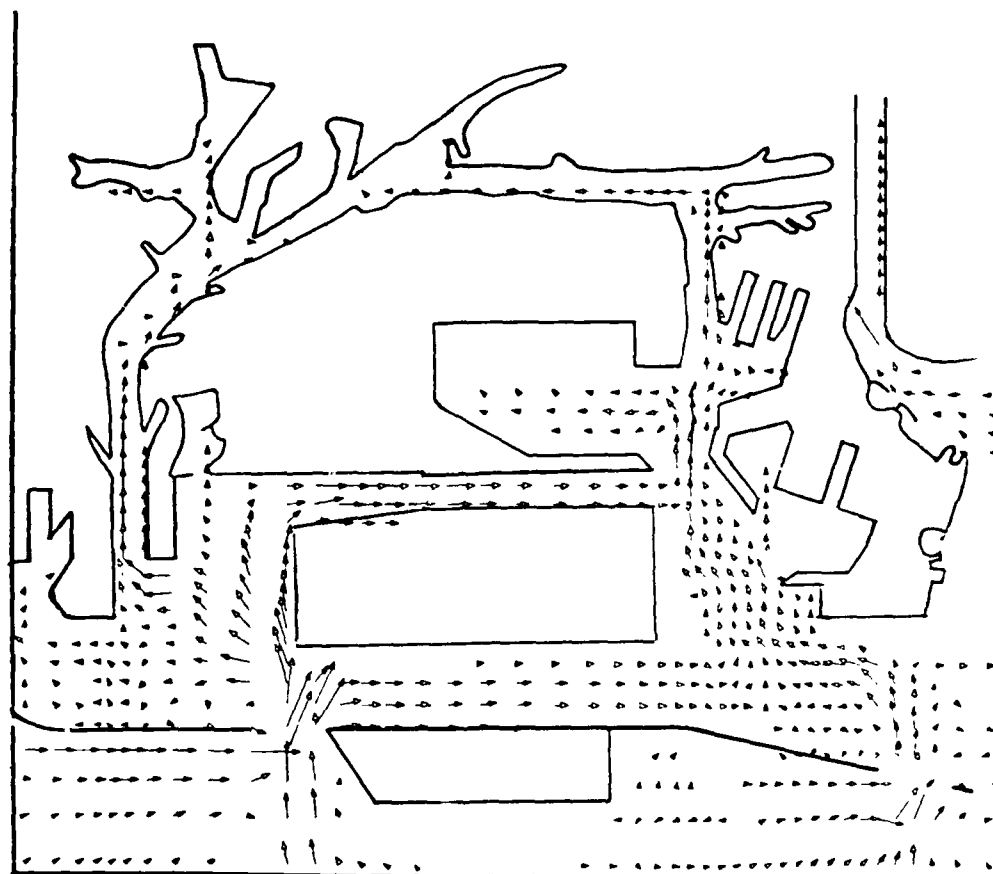
SCALE IN FEET
X 1000



VELOCITY SCALE, FPS



VELOCITY VECTOR PLOTS OF TIDAL CIRCULATION
2020 MASTER PLAN
EXISTING CHANNELS
MEAN TIDE
HOUR 54



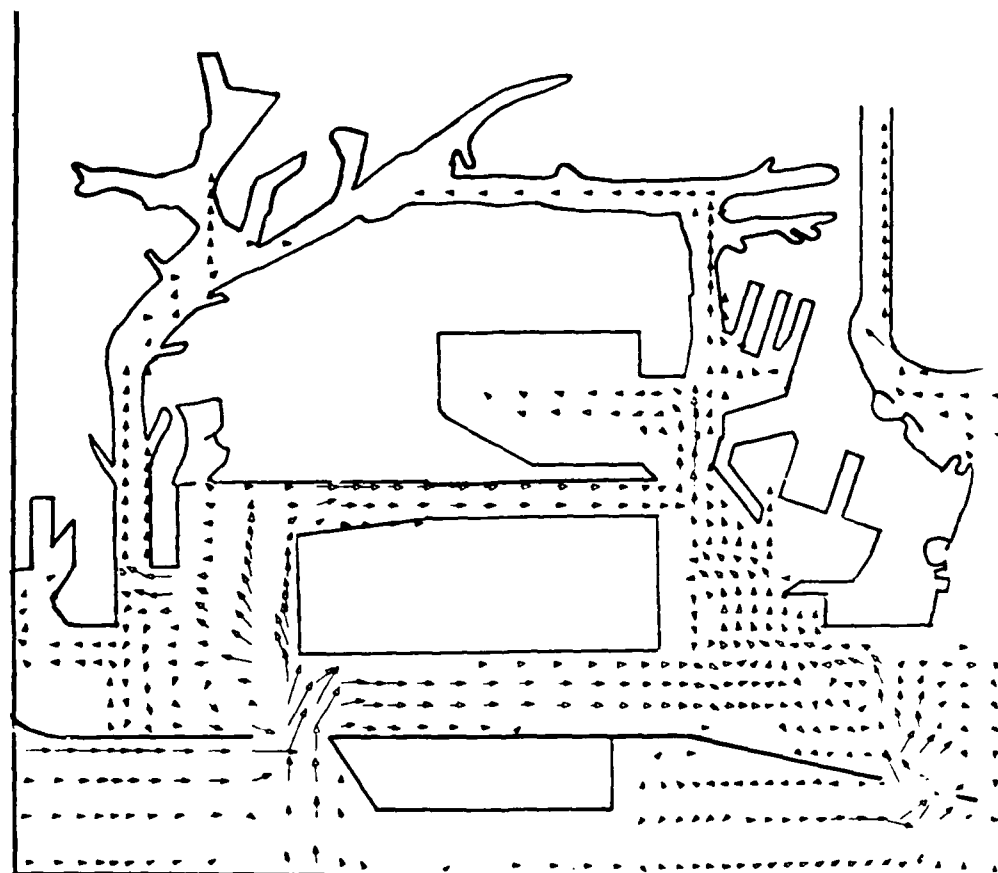
SCALE IN FEET
X 1000



VELOCITY SCALE, FPS



VELOCITY VECTOR PLOTS OF TIDAL CIRCULATION
2020 MASTER PLAN
EXISTING CHANNELS
MEAN TIDE
FOUR 58



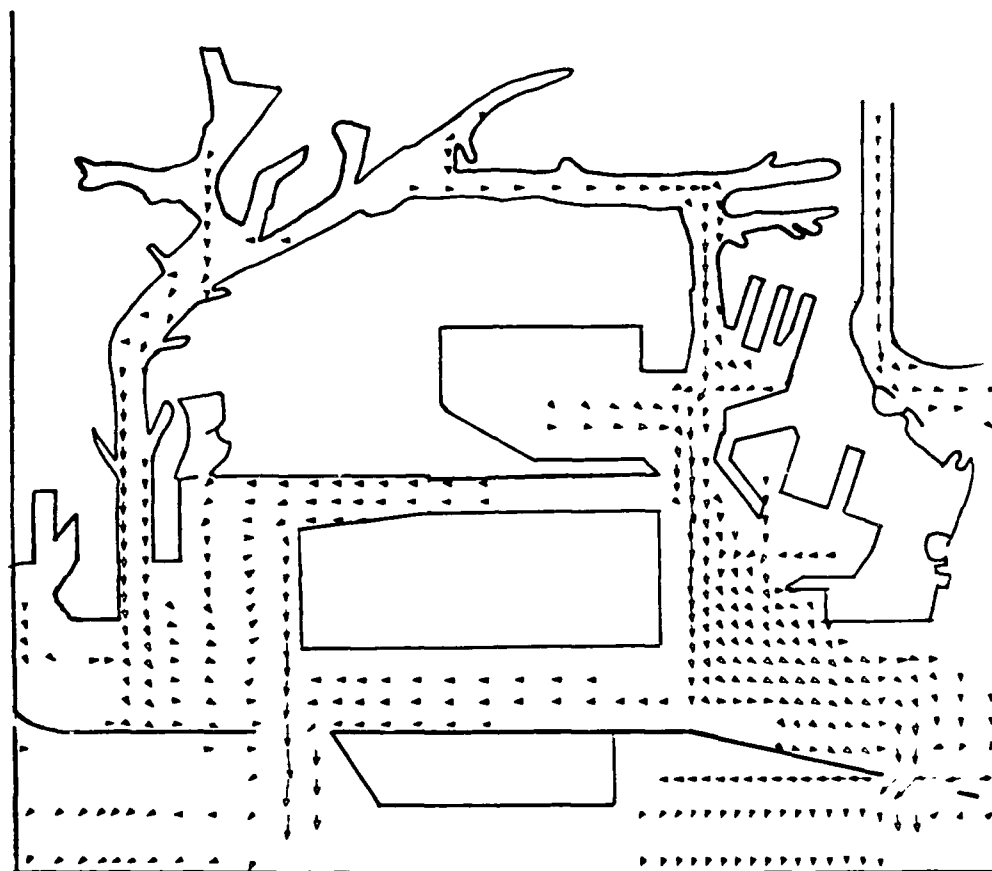
SCALE IN FEET
X 1000

2 0 2 4

VELOCITY SCALE, FPS

1 0 1 2

VELOCITY VECTOR PLOTS OF TIDAL CIRCULATION
2020 MASTER PLAN
EXISTING CHANNELS
MEAN TIDE
HOUR 60



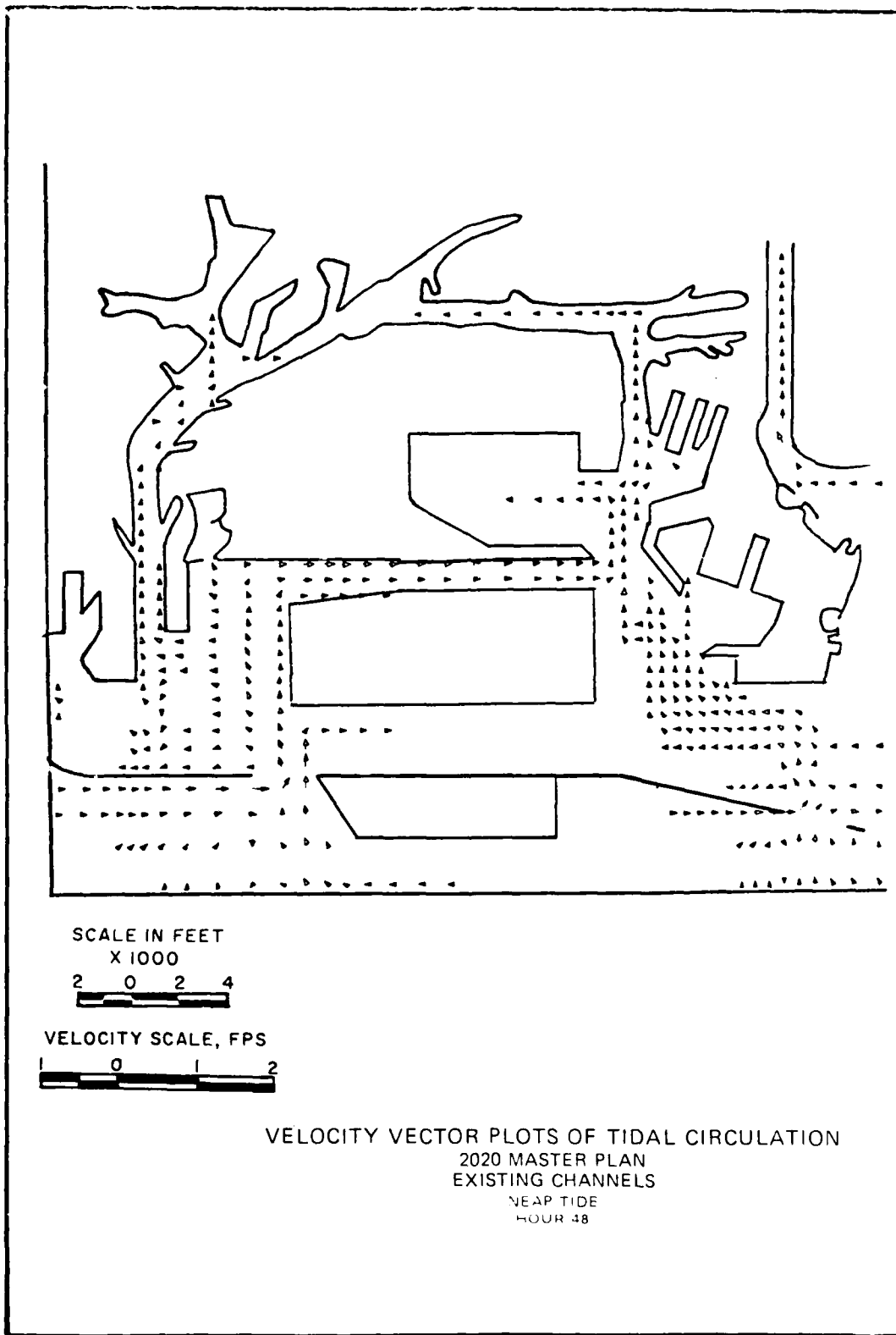
SCALE IN FEET
X 1000

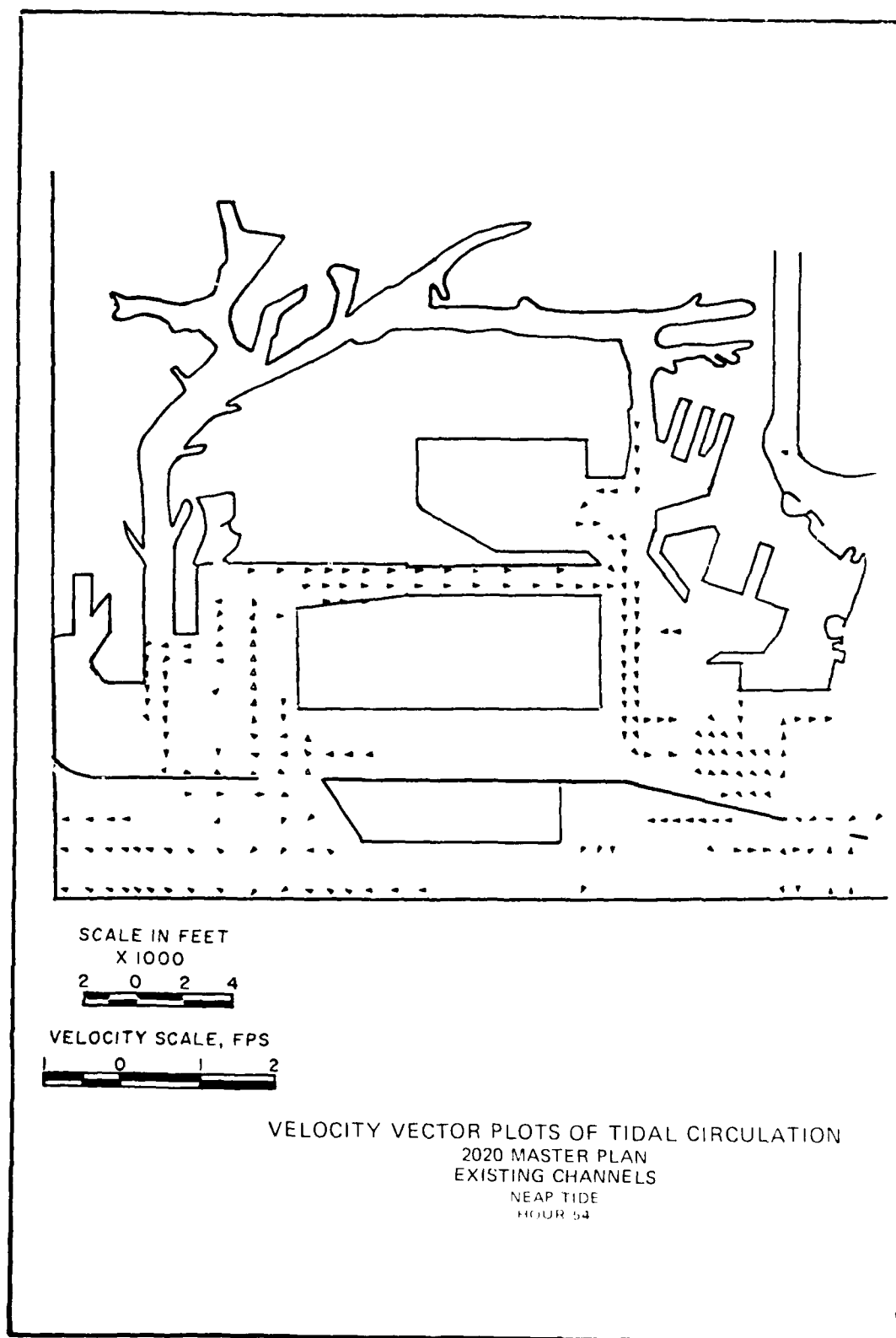


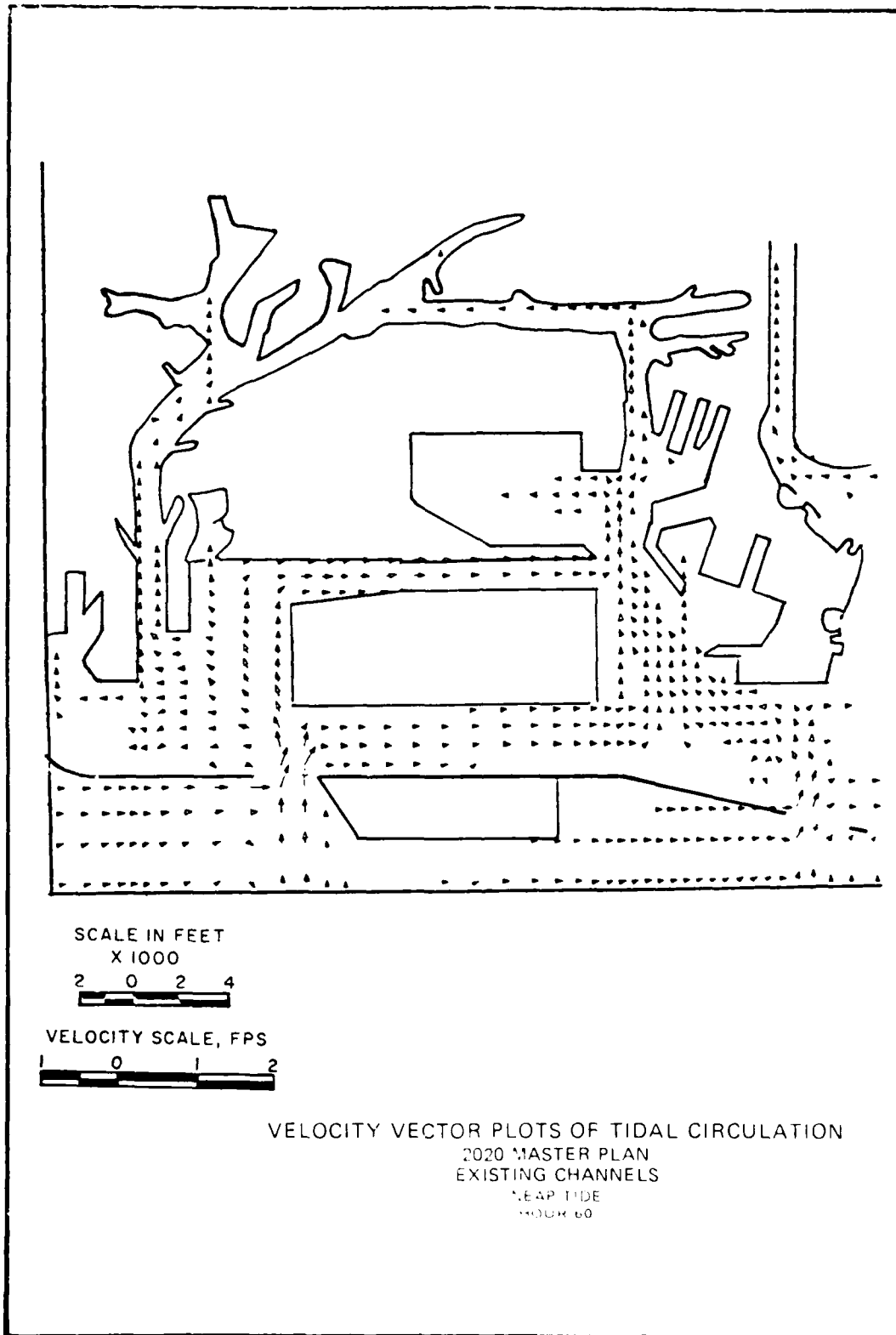
VELOCITY SCALE, FPS

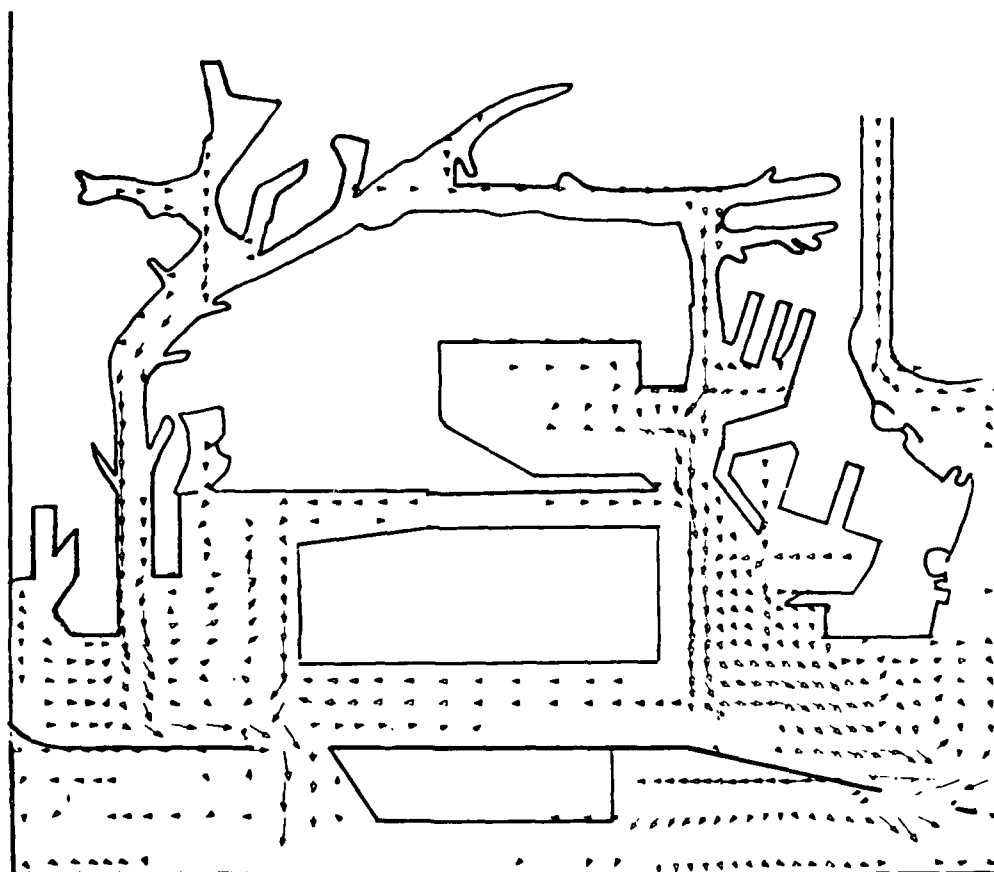


VELOCITY VECTOR PLOTS OF TIDAL CIRCULATION
2020 MASTER PLAN
EXISTING CHANNELS
NEAP TIDE
HOUR 42

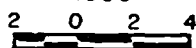








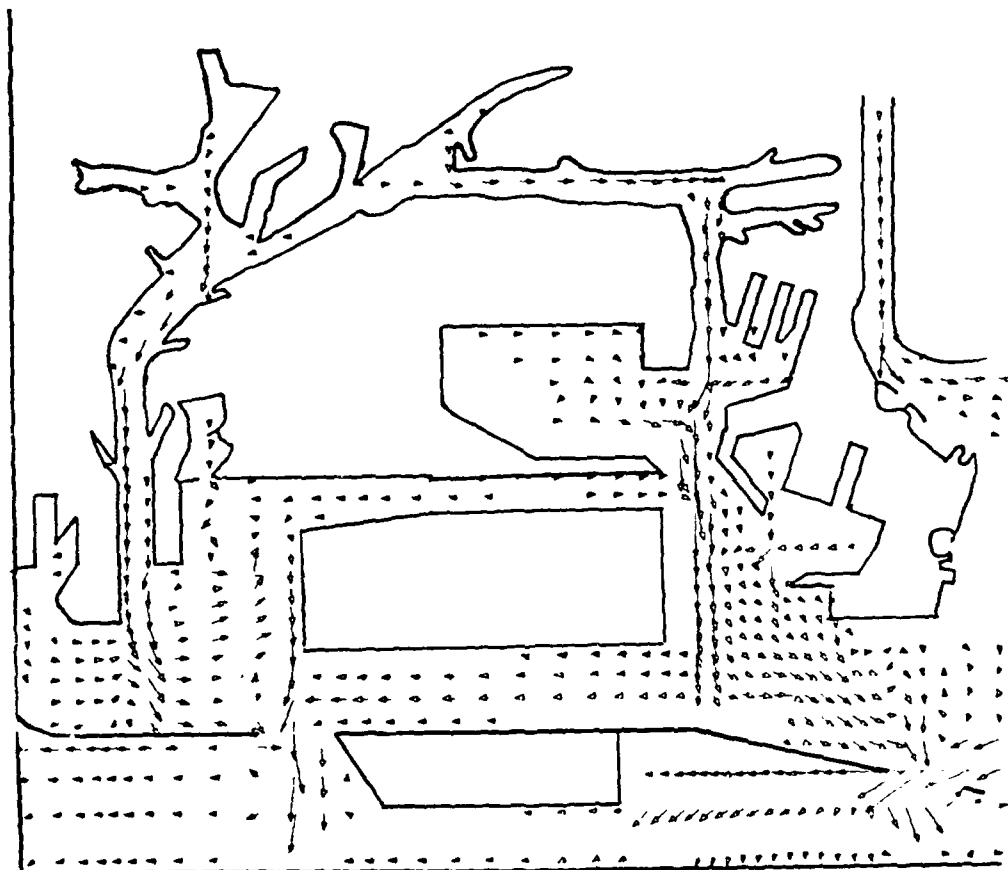
SCALE IN FEET
X 1000



VELOCITY SCALE, FPS



VELOCITY VECTOR PLOTS OF TIDAL CIRCULATION
2020 MASTER PLAN
DREDGED CHANNELS
SPRING TIDE
HOUR 58



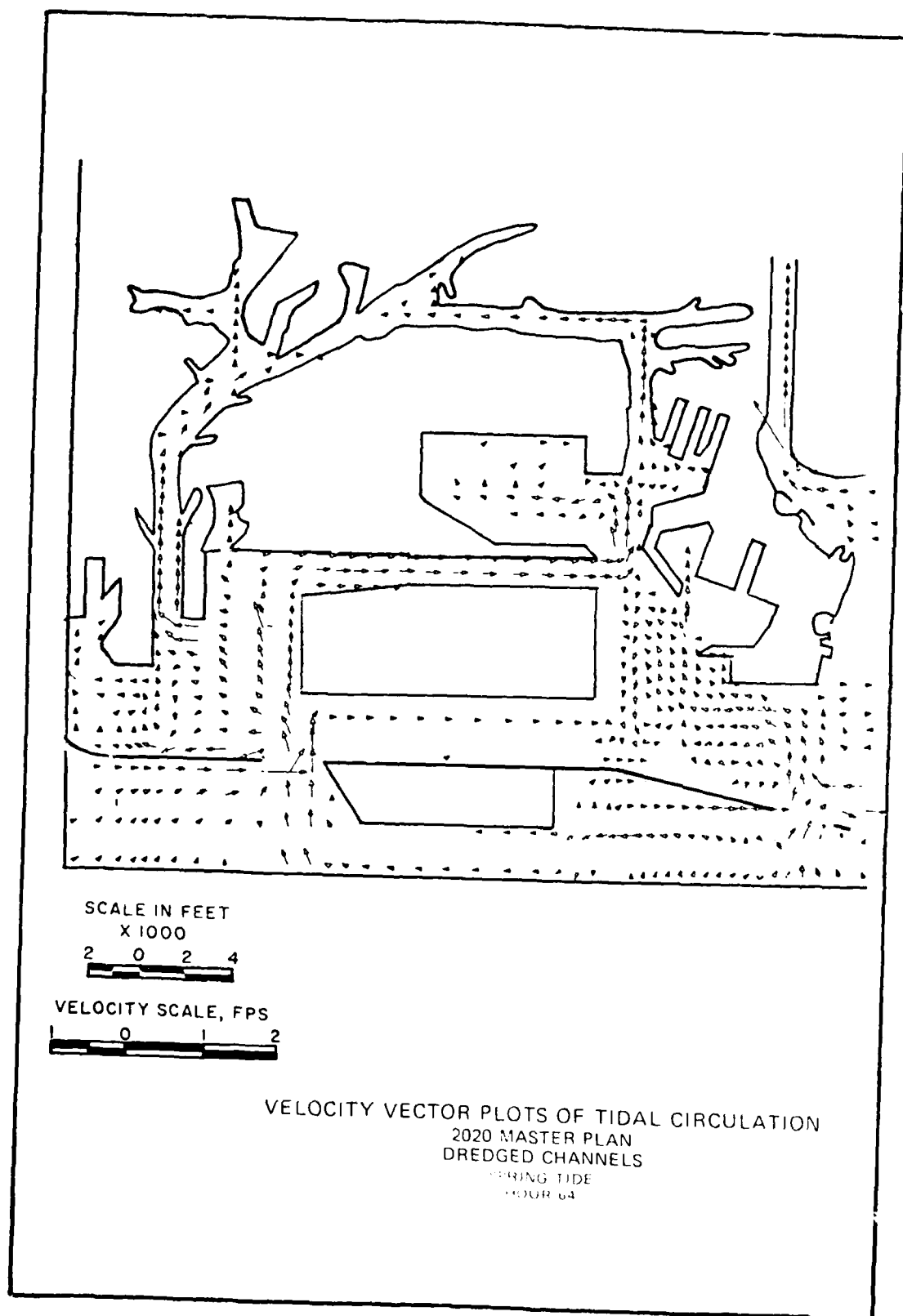
SCALE IN FEET
X 1000

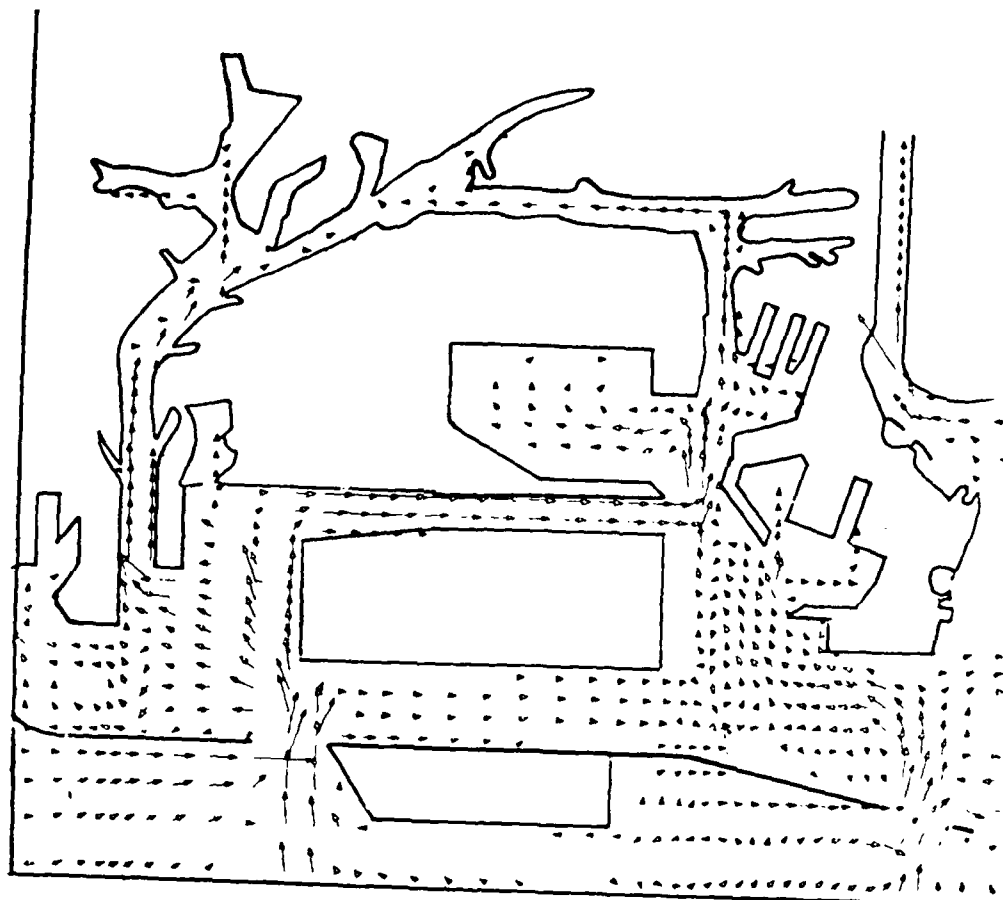


VELOCITY SCALE, FPS



VELOCITY VECTOR PLOTS OF TIDAL CIRCULATION
2020 MASTER PLAN
DREDGED CHANNELS
SPRING TIDE
HOUR 60





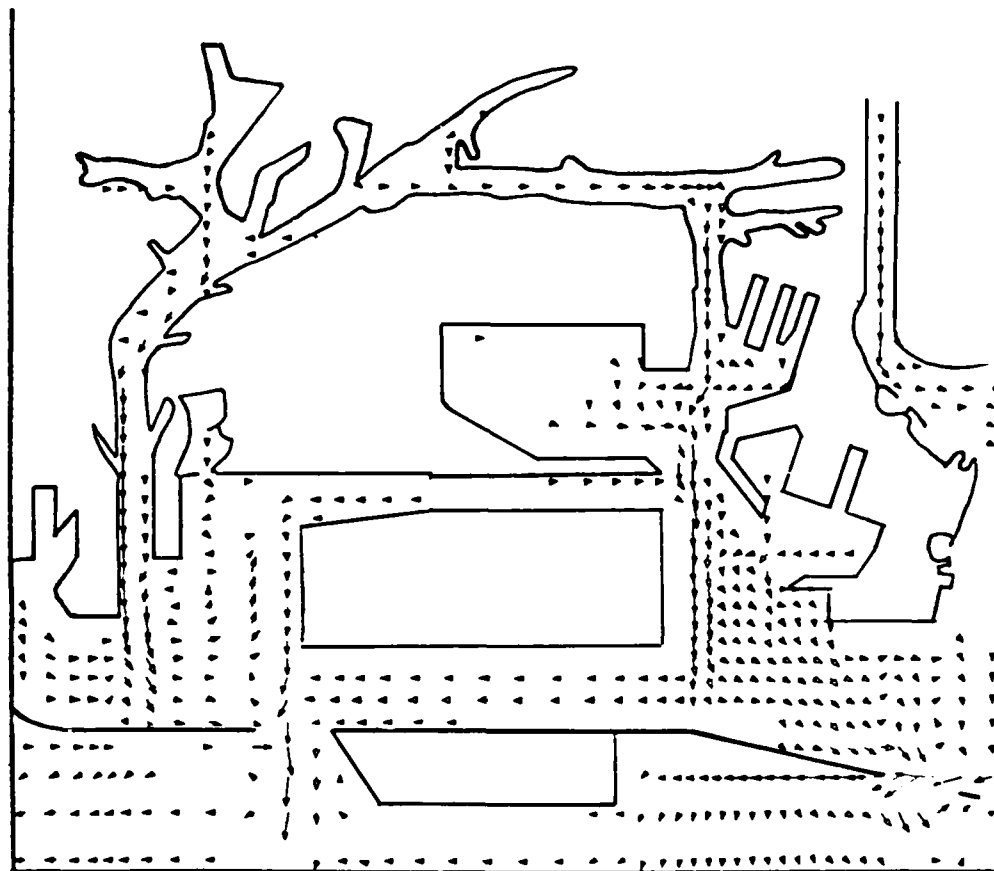
SCALE IN FEET
X 1000



VELOCITY SCALE, FPS



VELOCITY VECTOR PLOTS OF TIDAL CIRCULATION
2020 MASTER PLAN
DREDGED CHANNELS
SPRING TIDE
FOUR 66



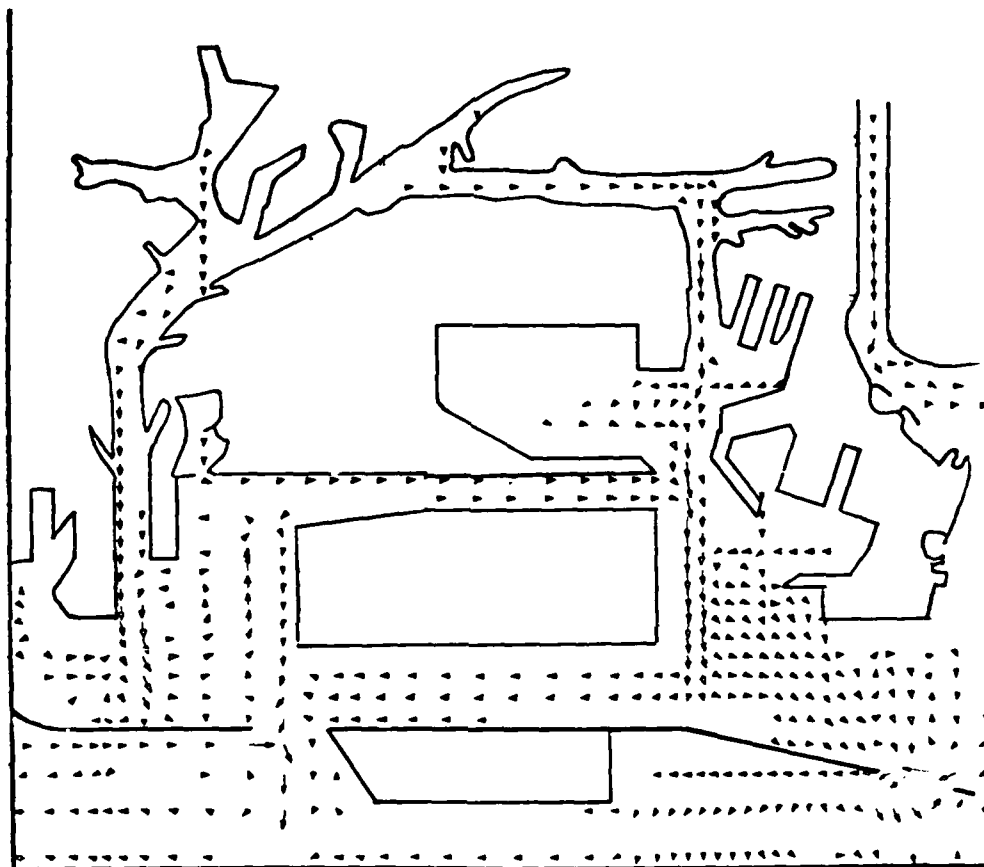
SCALE IN FEET
X 1000



VELOCITY SCALE, FPS



VELOCITY VECTOR PLOTS OF TIDAL CIRCULATION
2020 MASTER PLAN
DREDGED CHANNELS
MEAN TIDE
HOUR 52



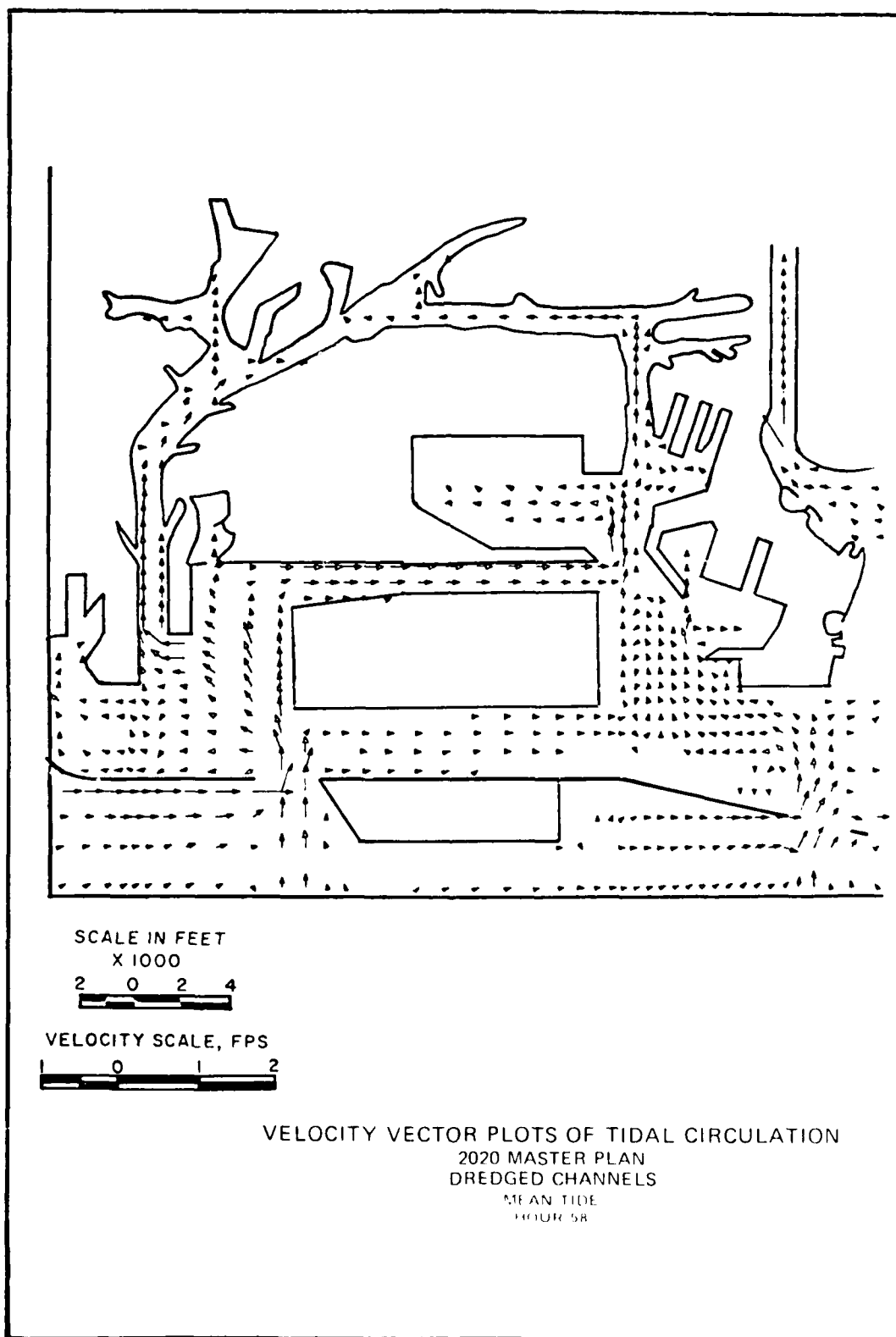
SCALE IN FEET
X 1000

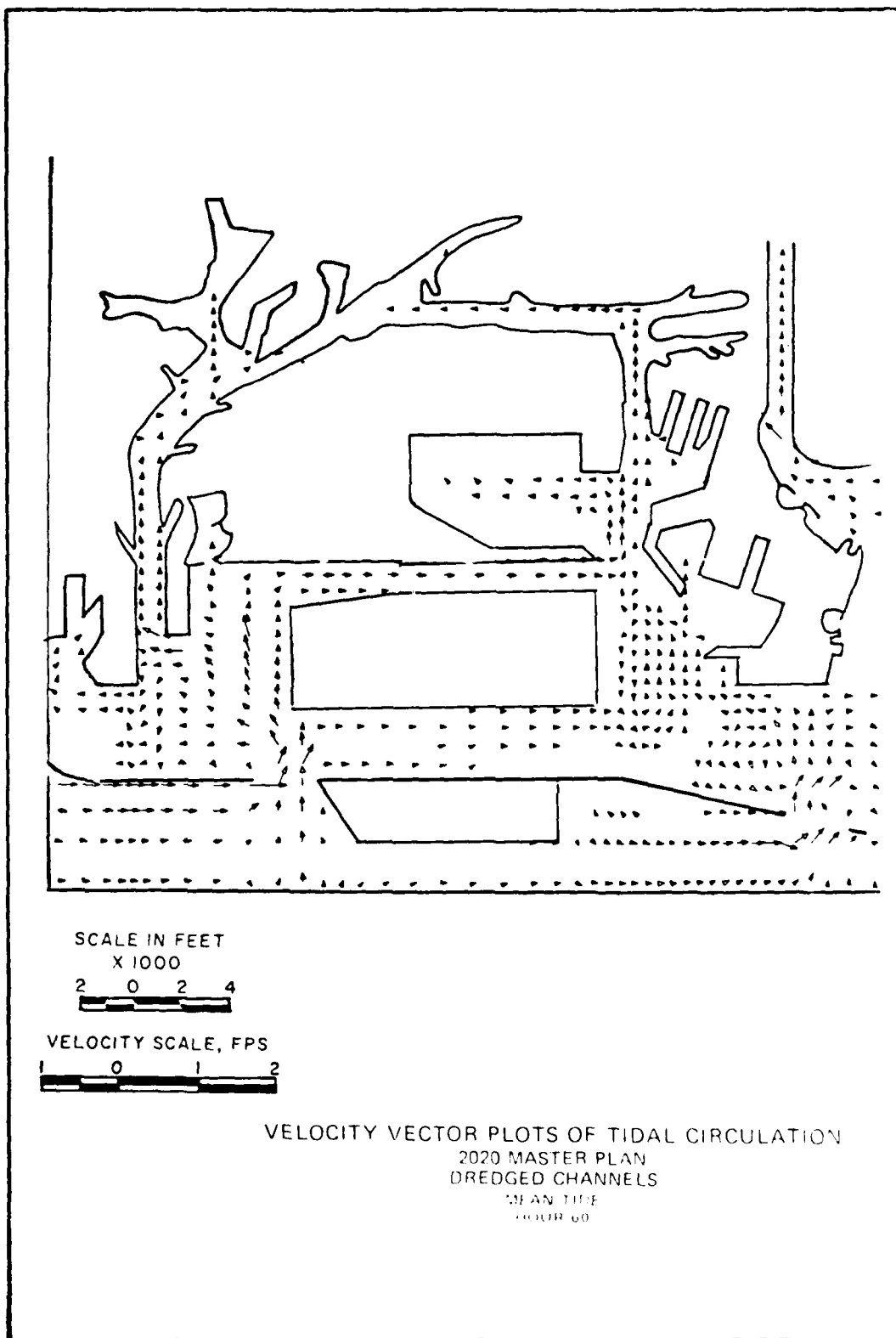


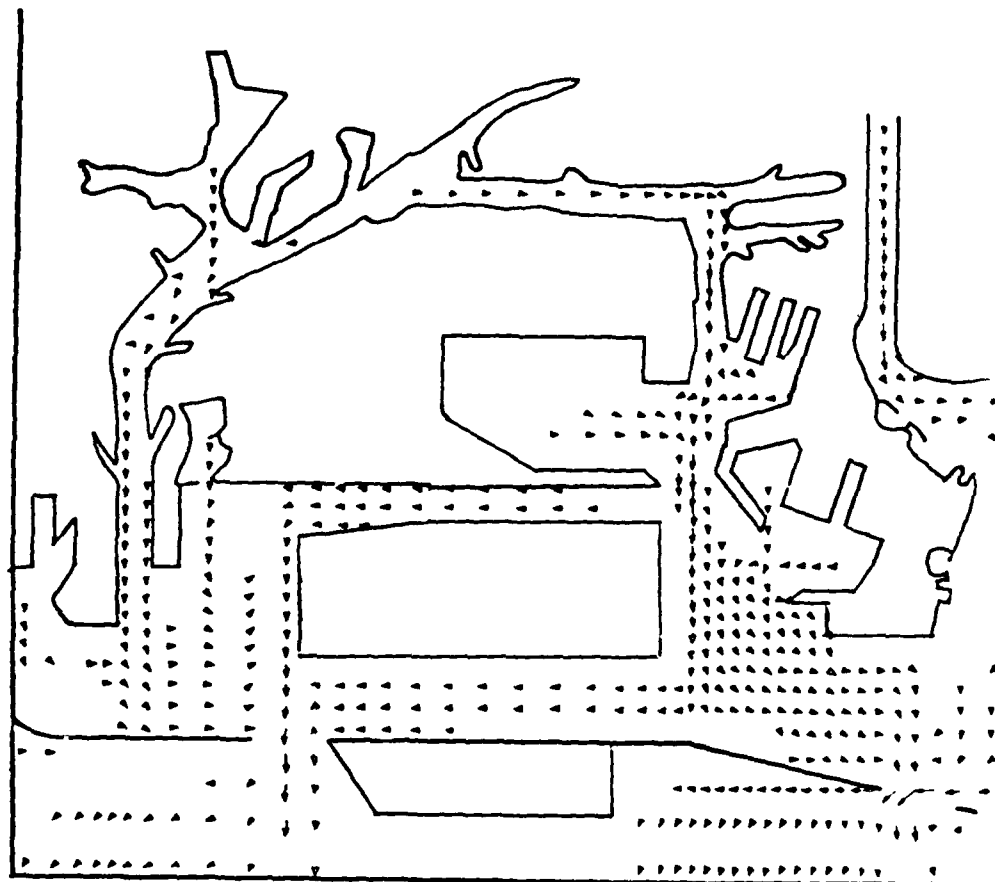
VELOCITY SCALE, FPS



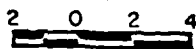
VELOCITY VECTOR PLOTS OF TIDAL CIRCULATION
2020 MASTER PLAN
DREDGED CHANNELS
MEAN TIDE
HOUR 54







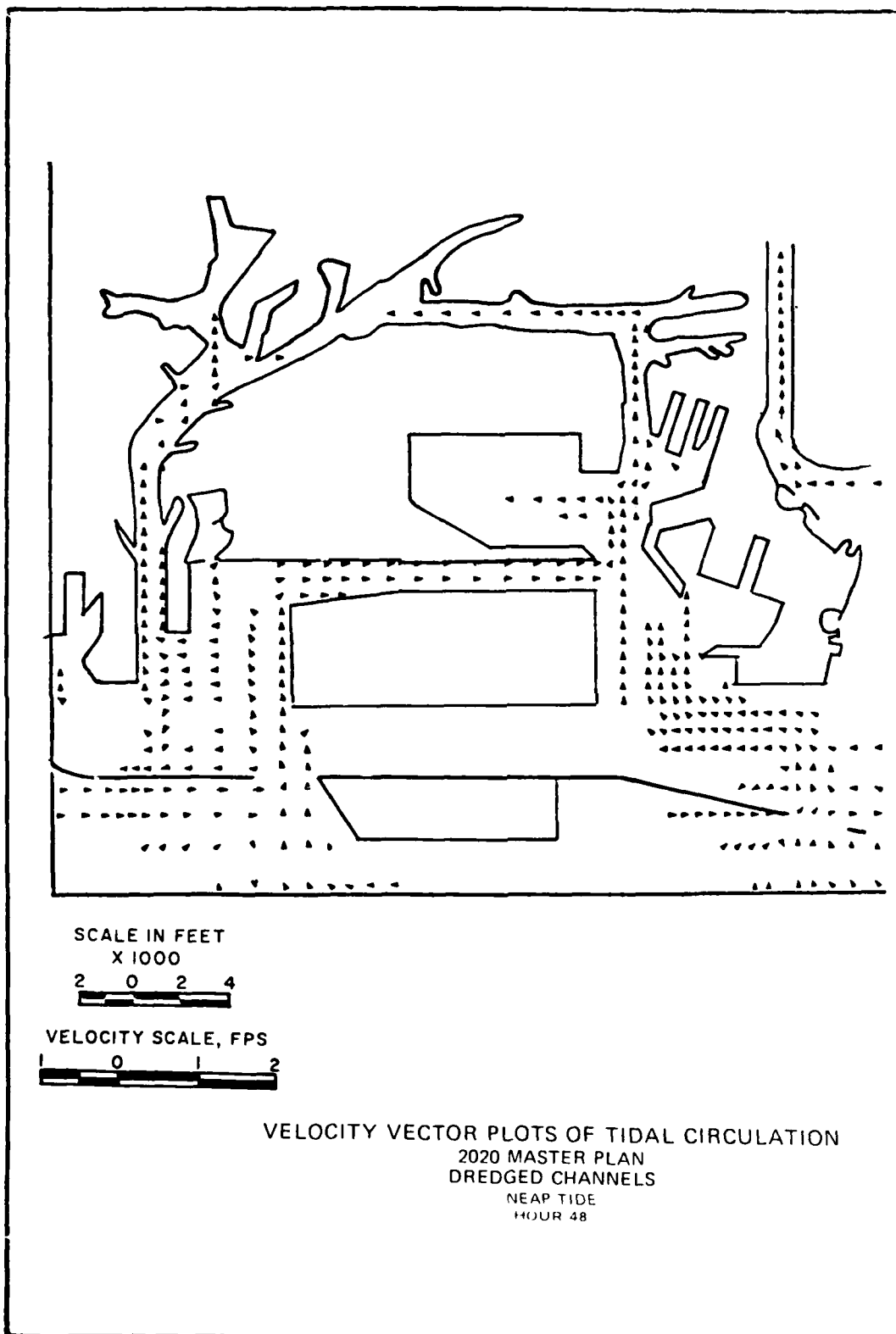
SCALE IN FEET
X 1000



VELOCITY SCALE, FPS



VELOCITY VECTOR PLOTS OF TIDAL CIRCULATION
2020 MASTER PLAN
DREDGED CHANNELS
NEAP TIDE
HOUR 42



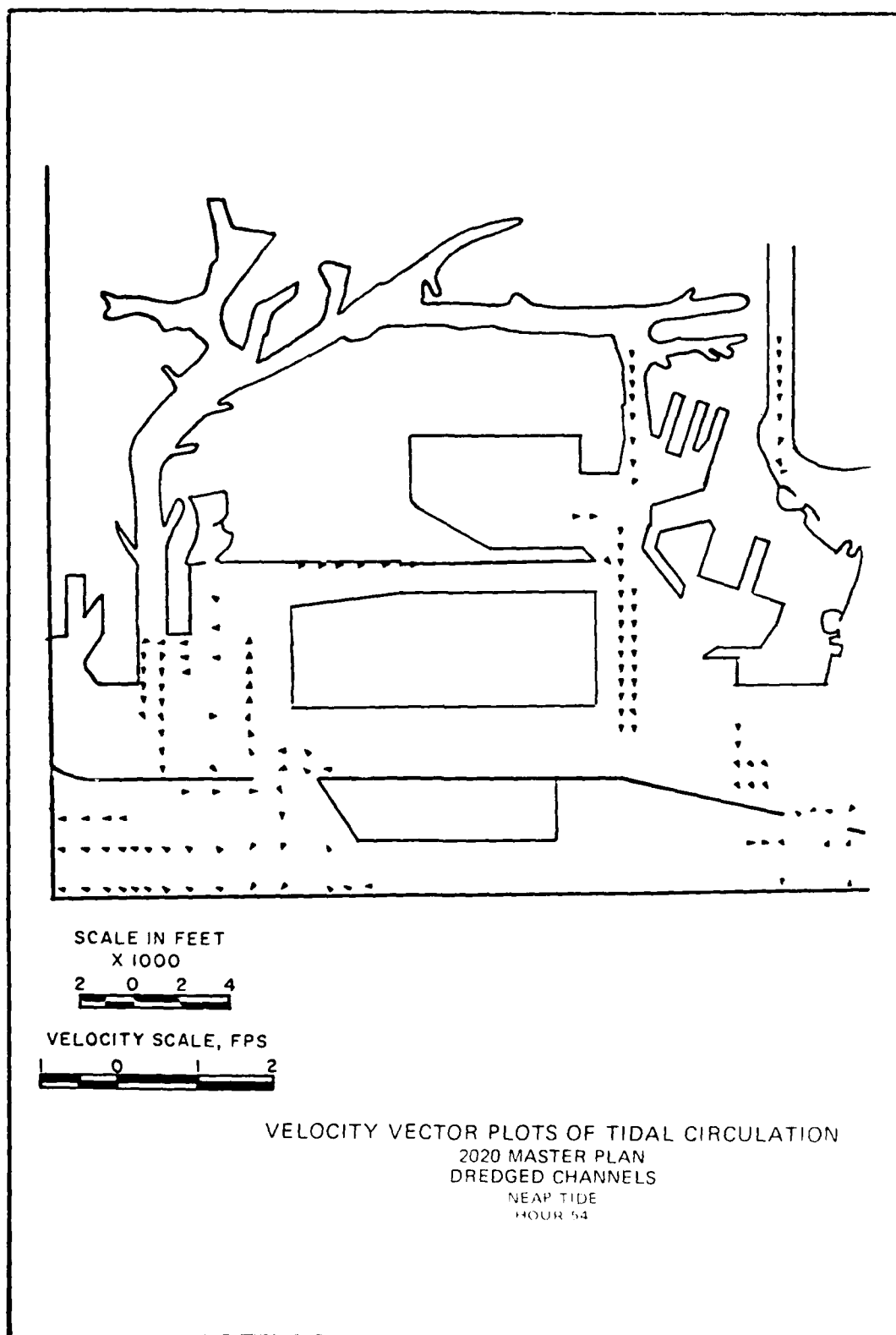
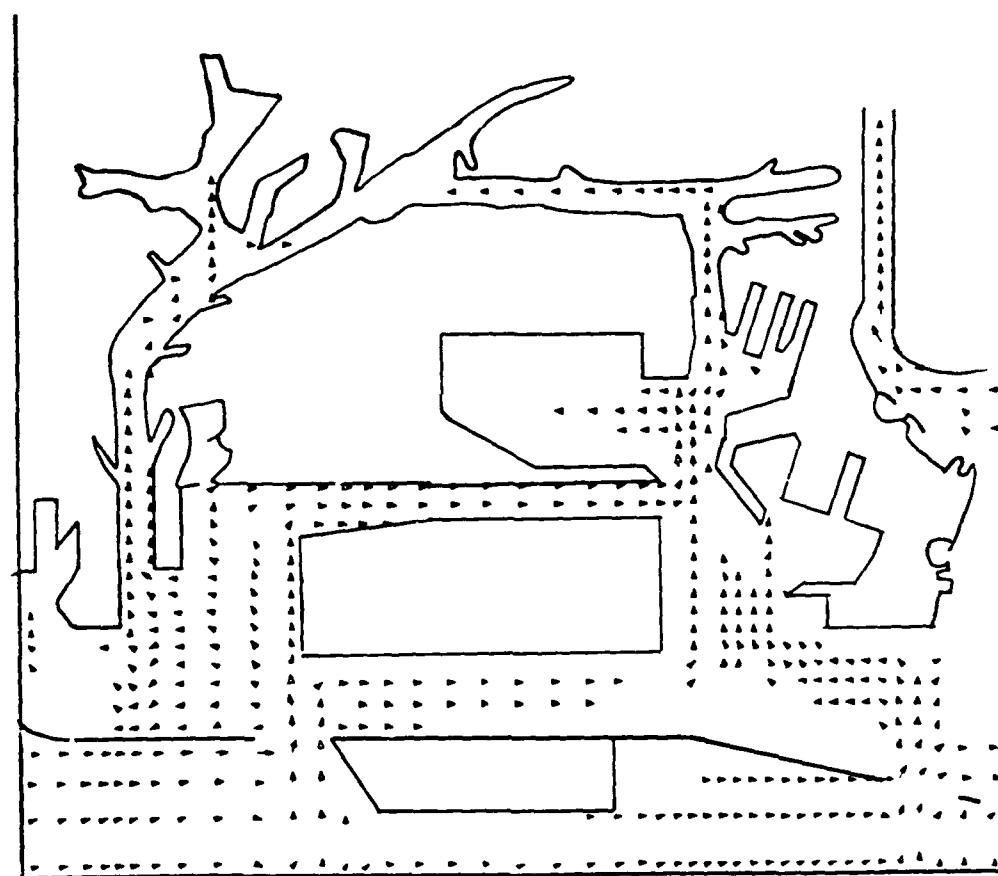


Plate 116



SCALE IN FEET
X 1000



VELOCITY SCALE, FPS



VELOCITY VECTOR PLOTS OF TIDAL CIRCULATION
2020 MASTER PLAN
DREDGED CHANNELS
NEAP TIDE
HOUR 60

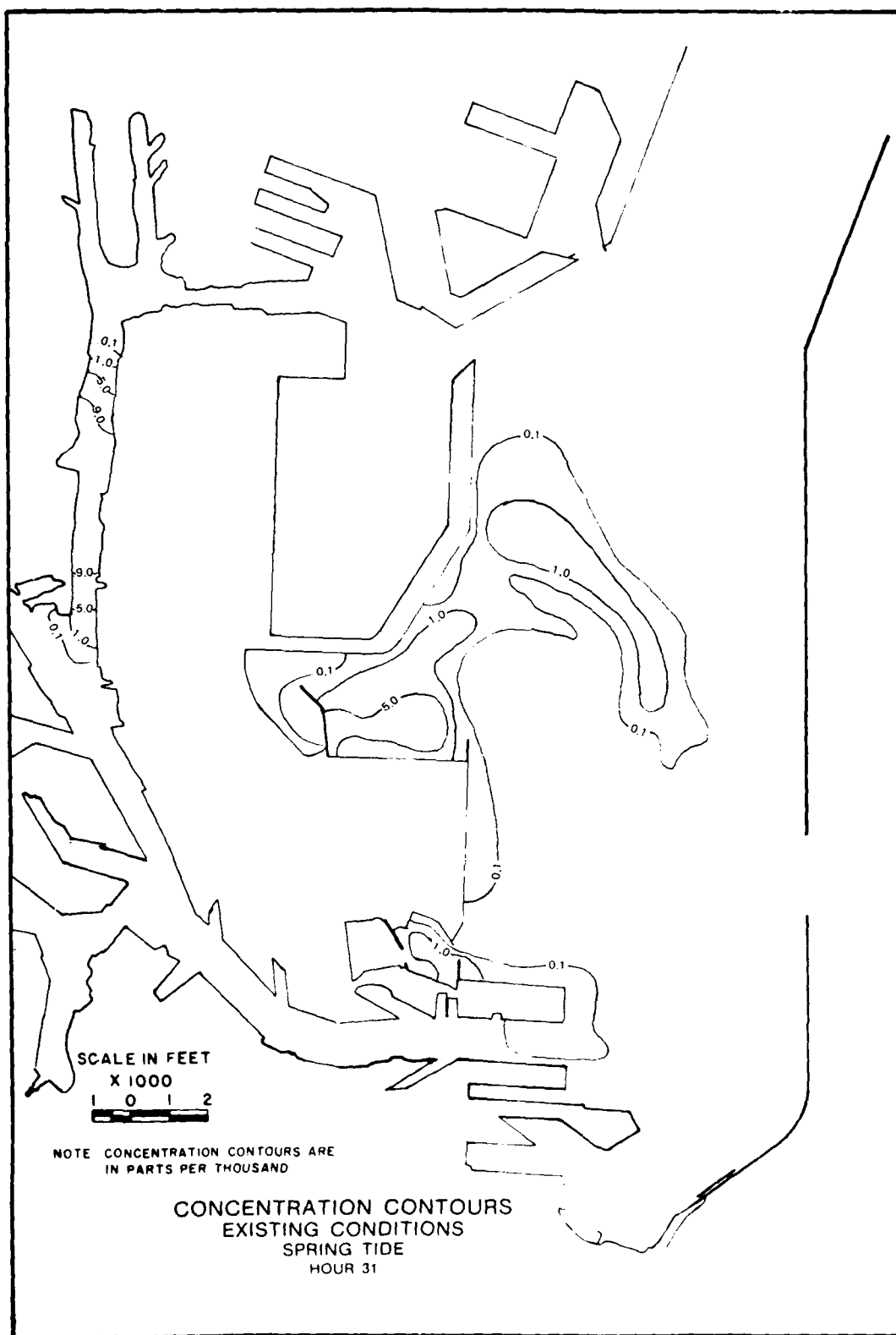
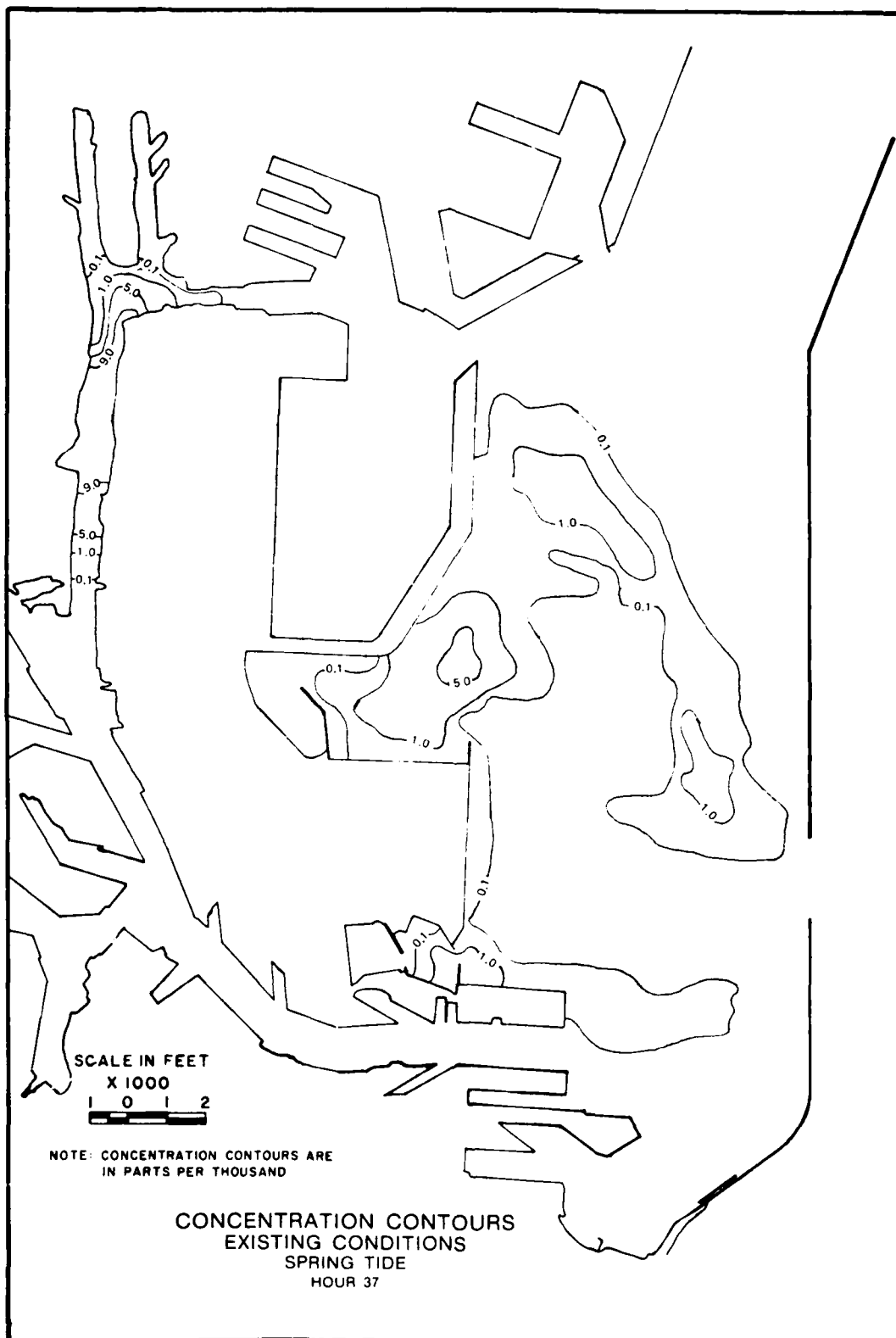


Plate 118



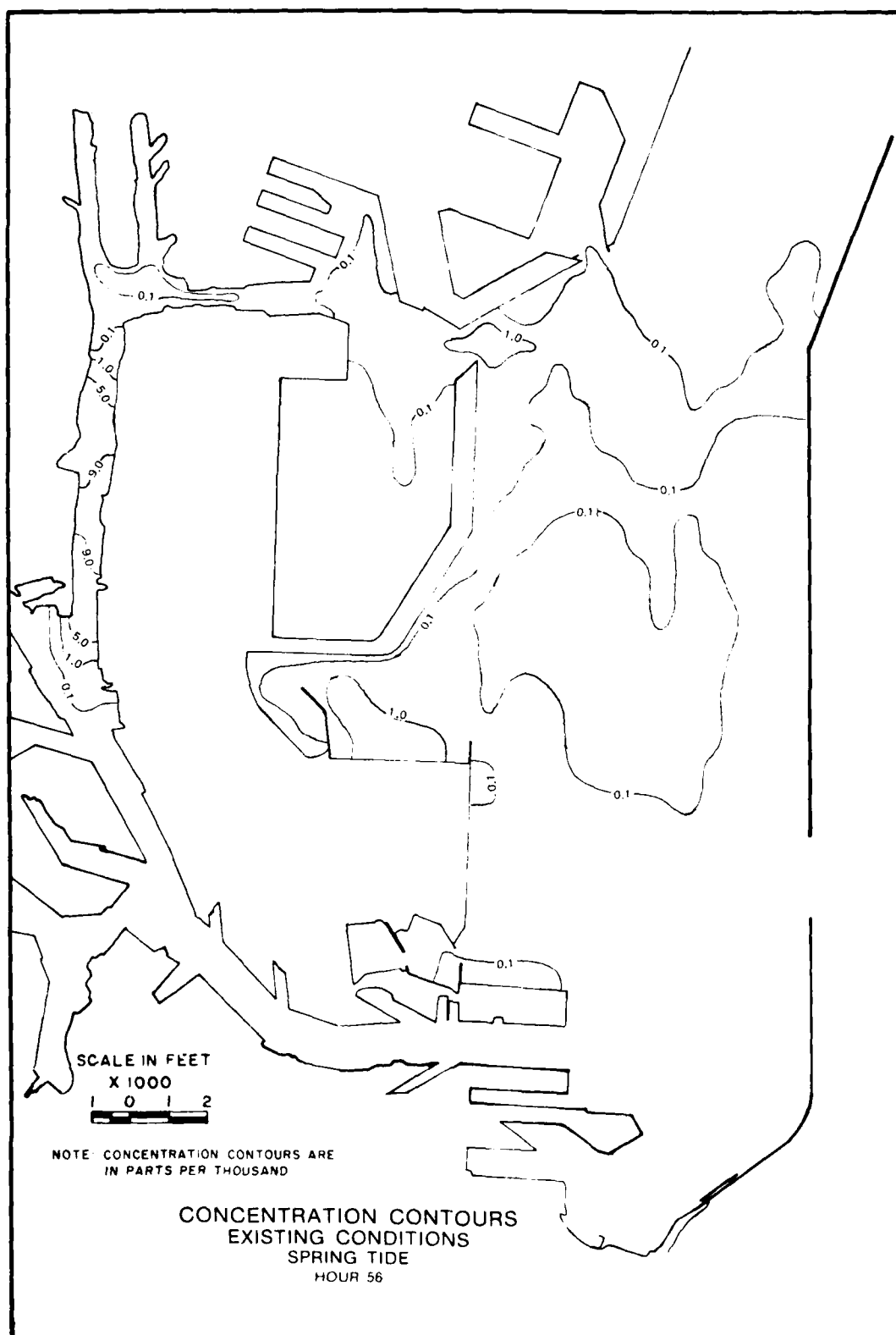


Plate 120

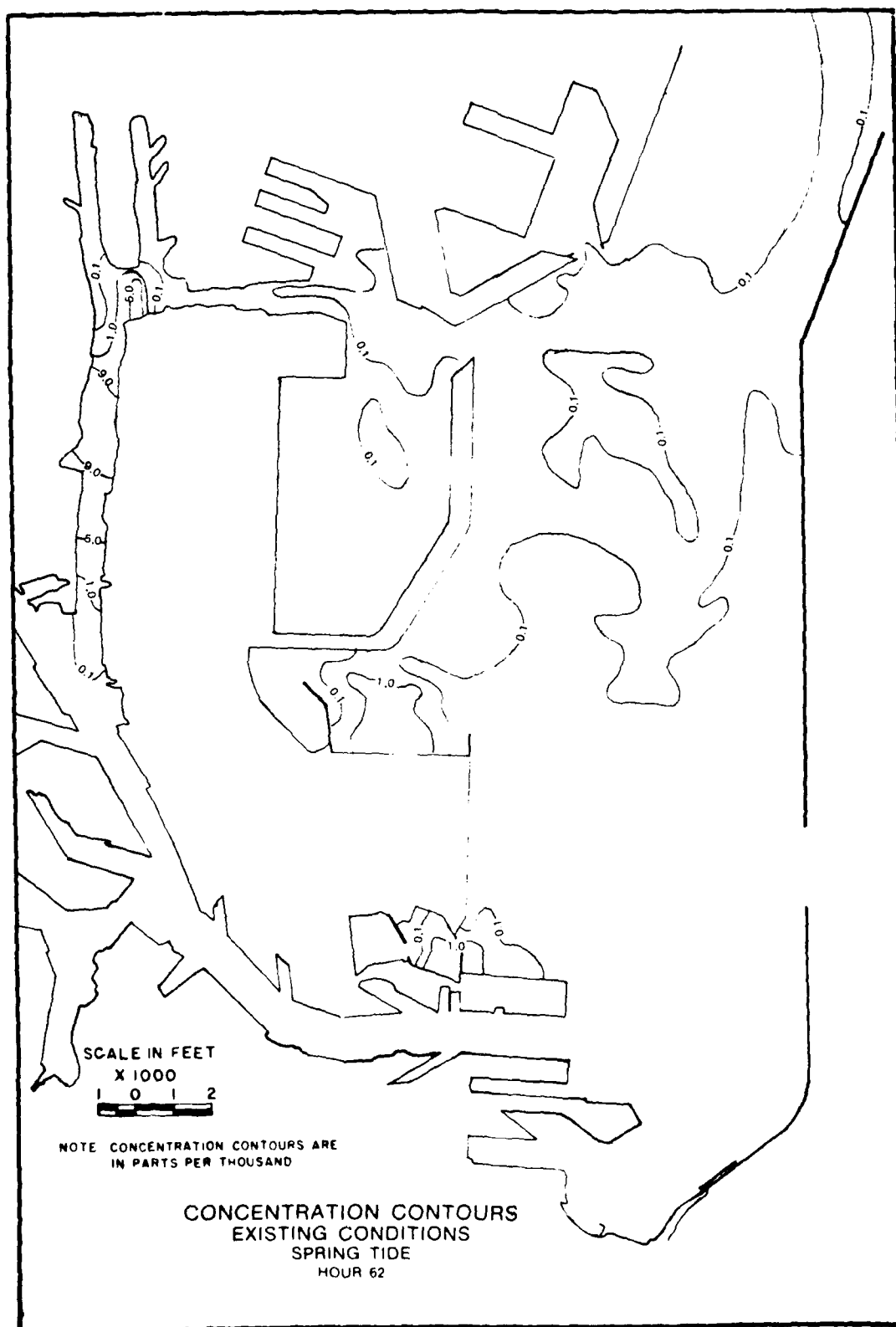


Plate 121

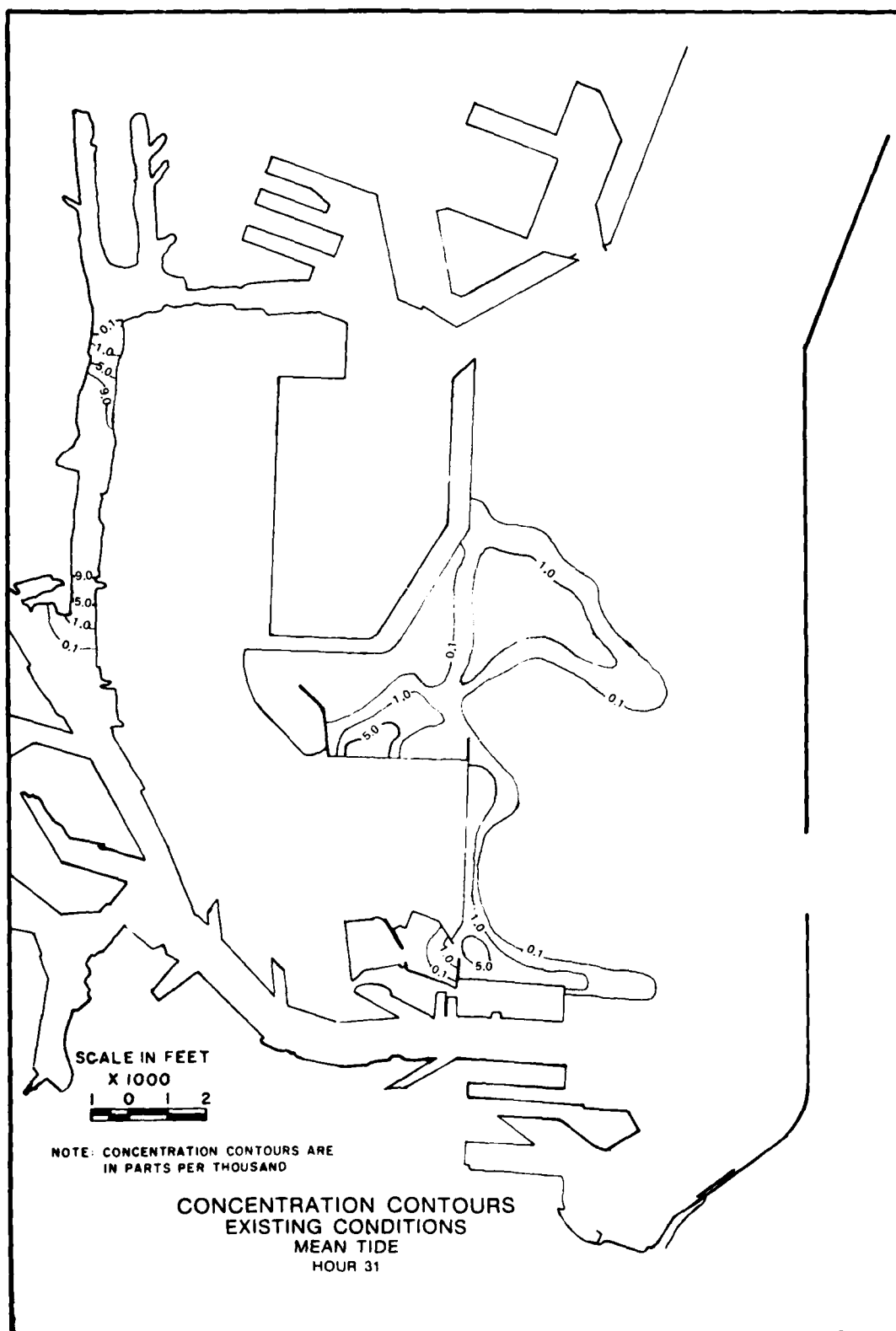
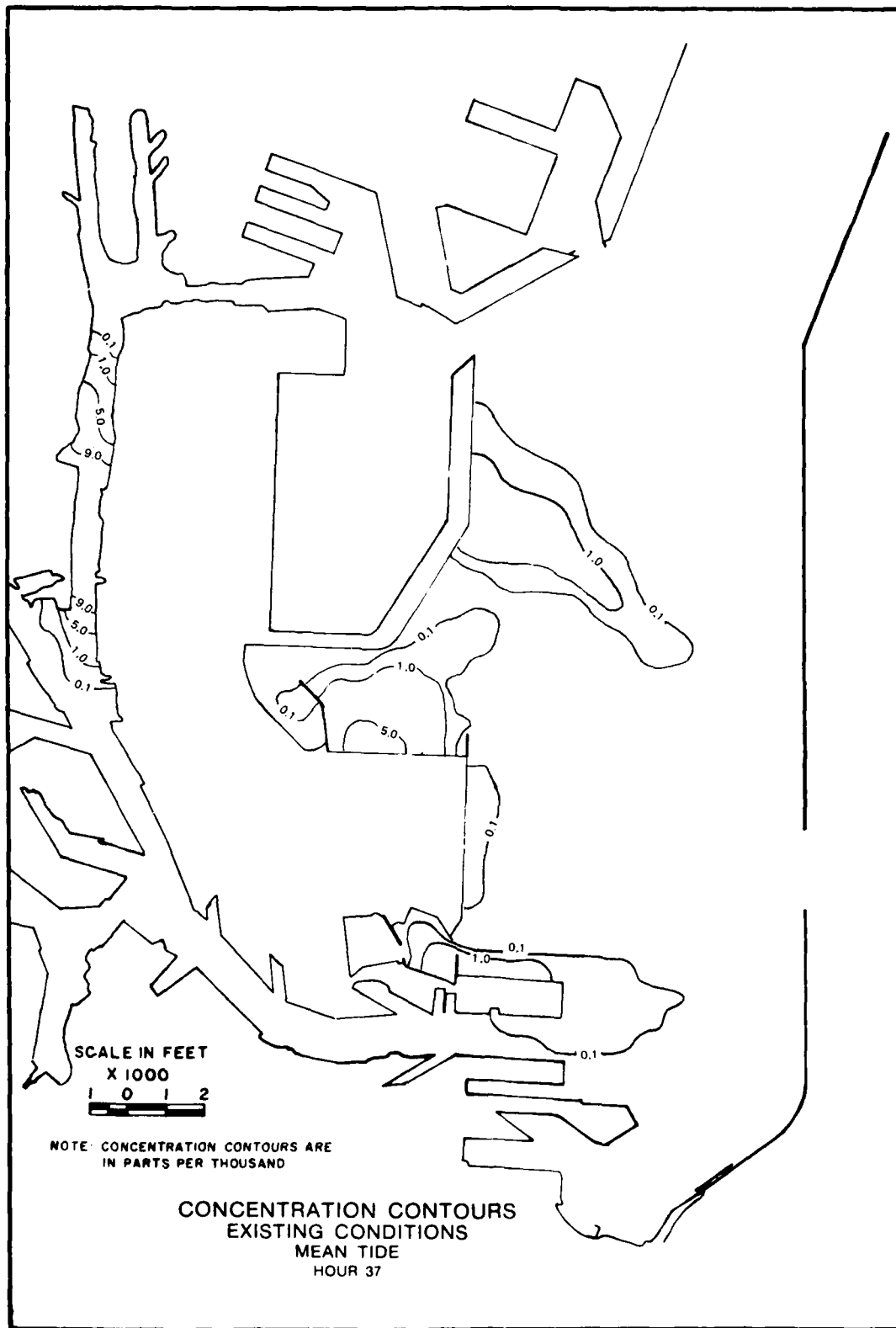


Plate 122



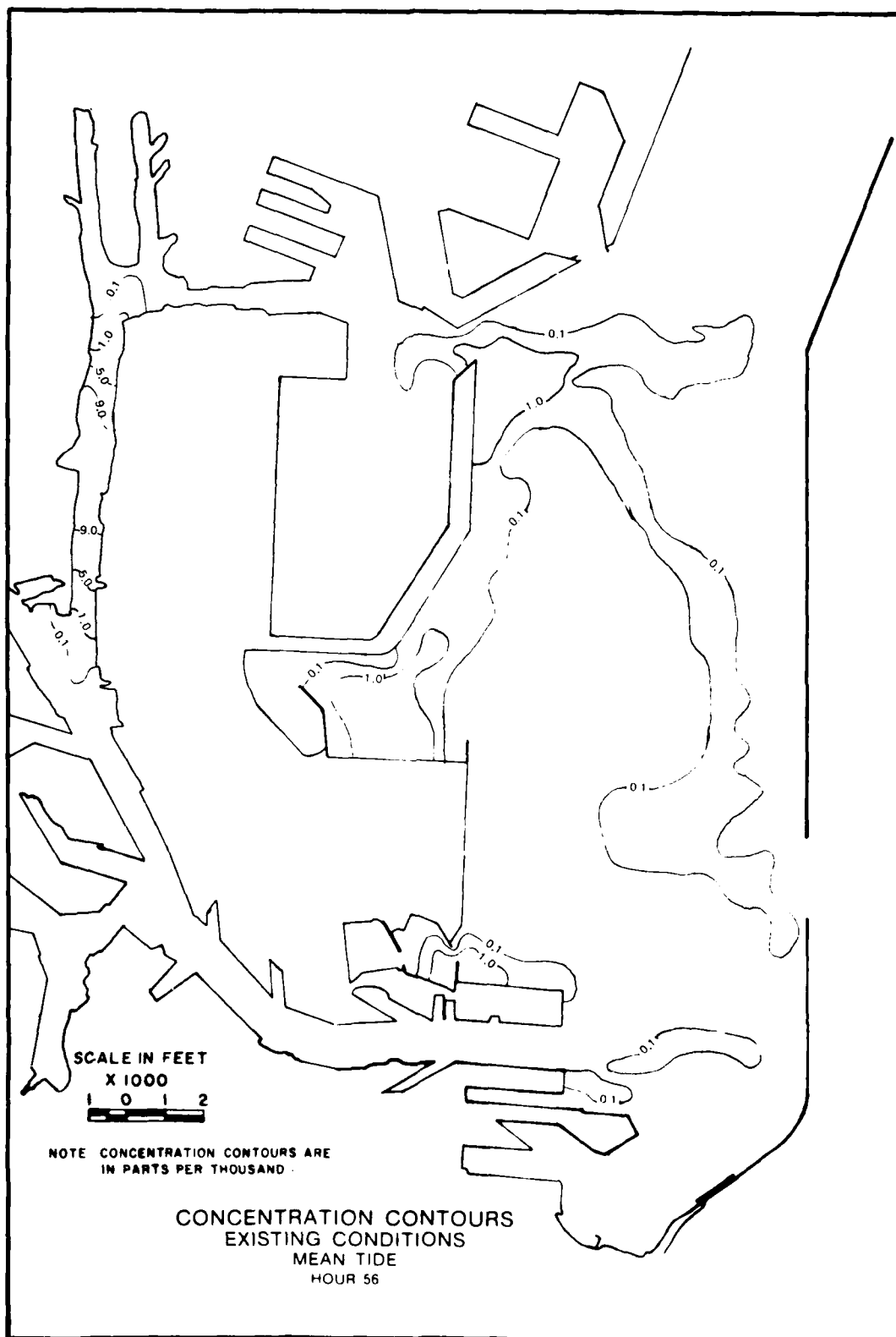
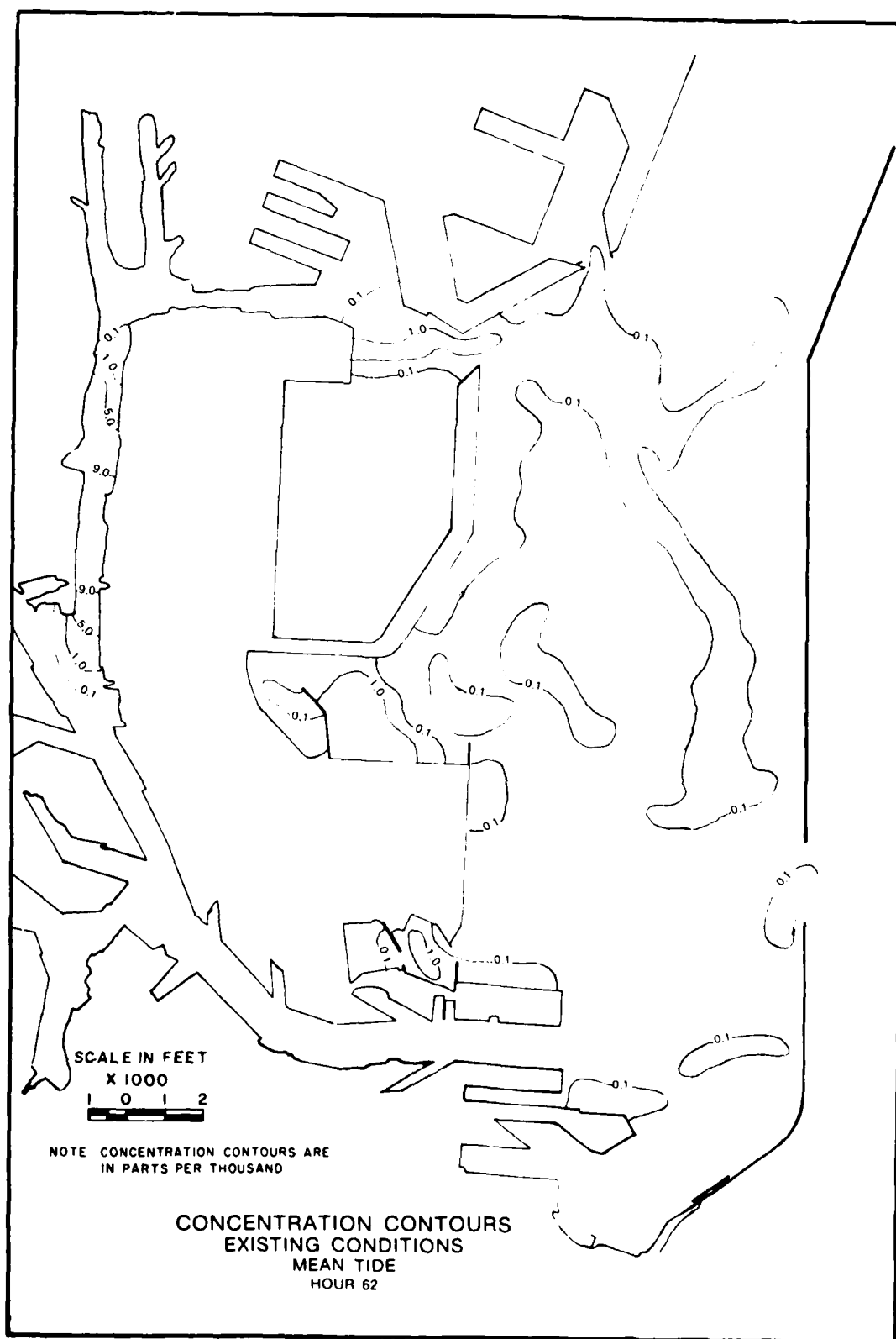
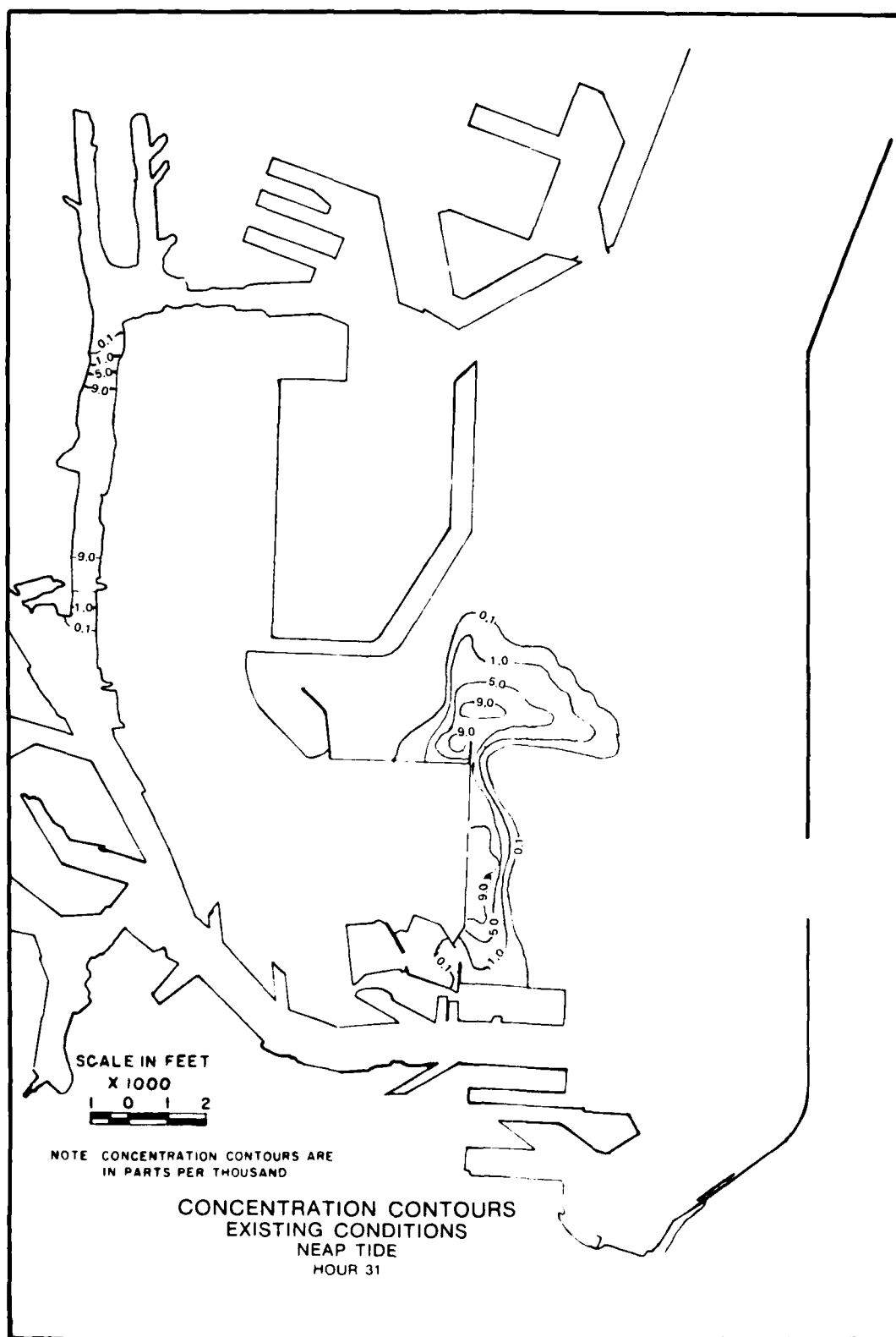
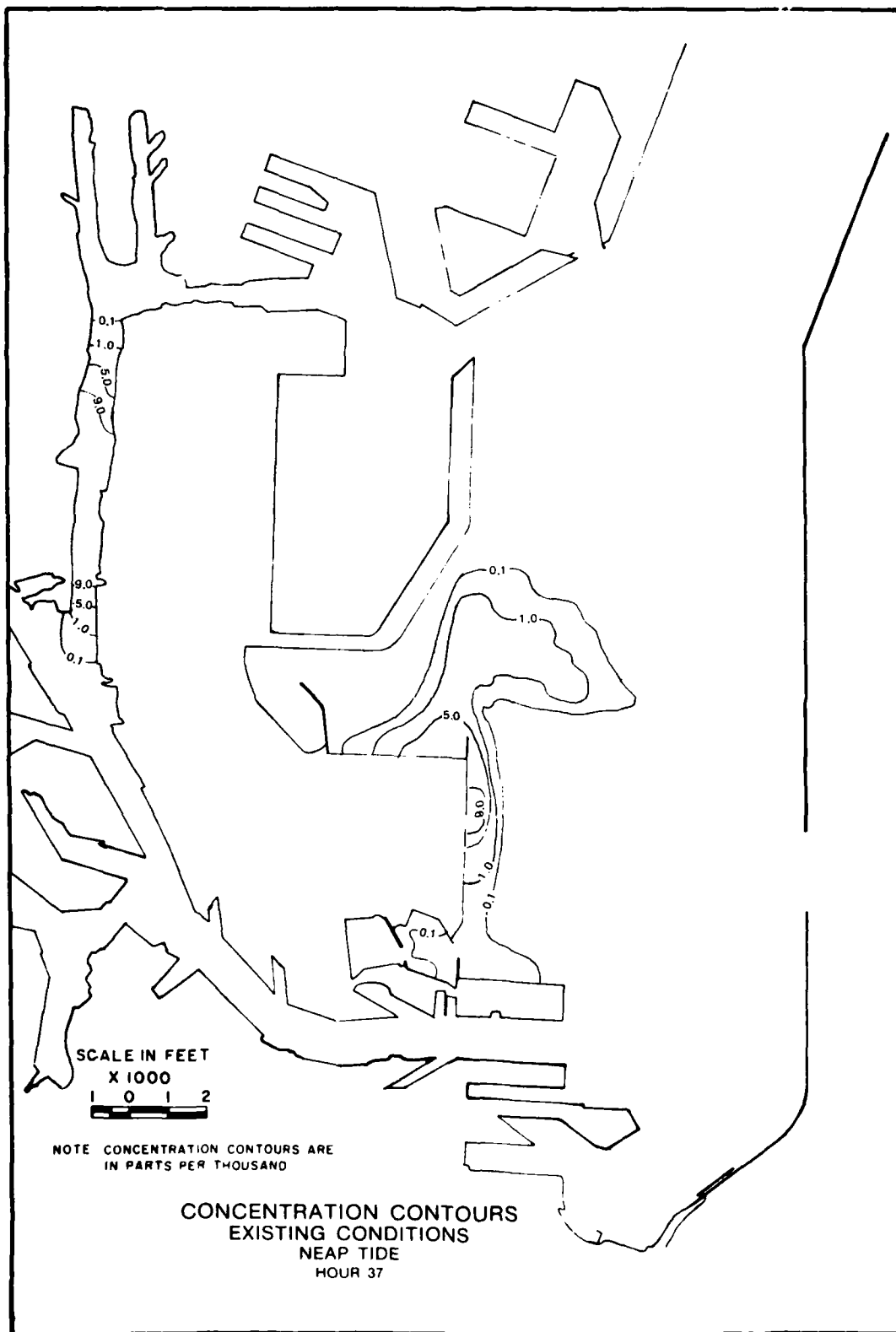


Plate 124







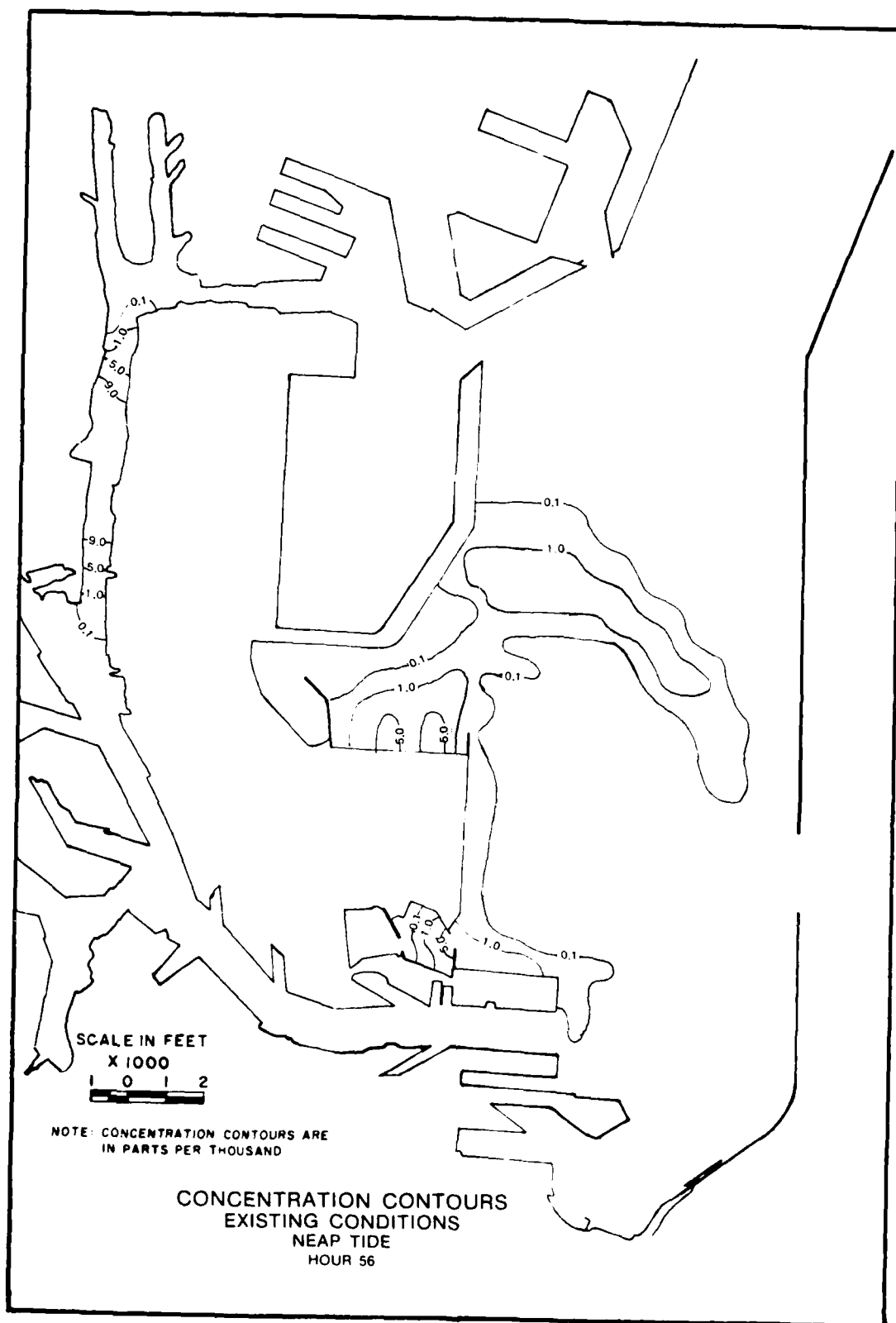
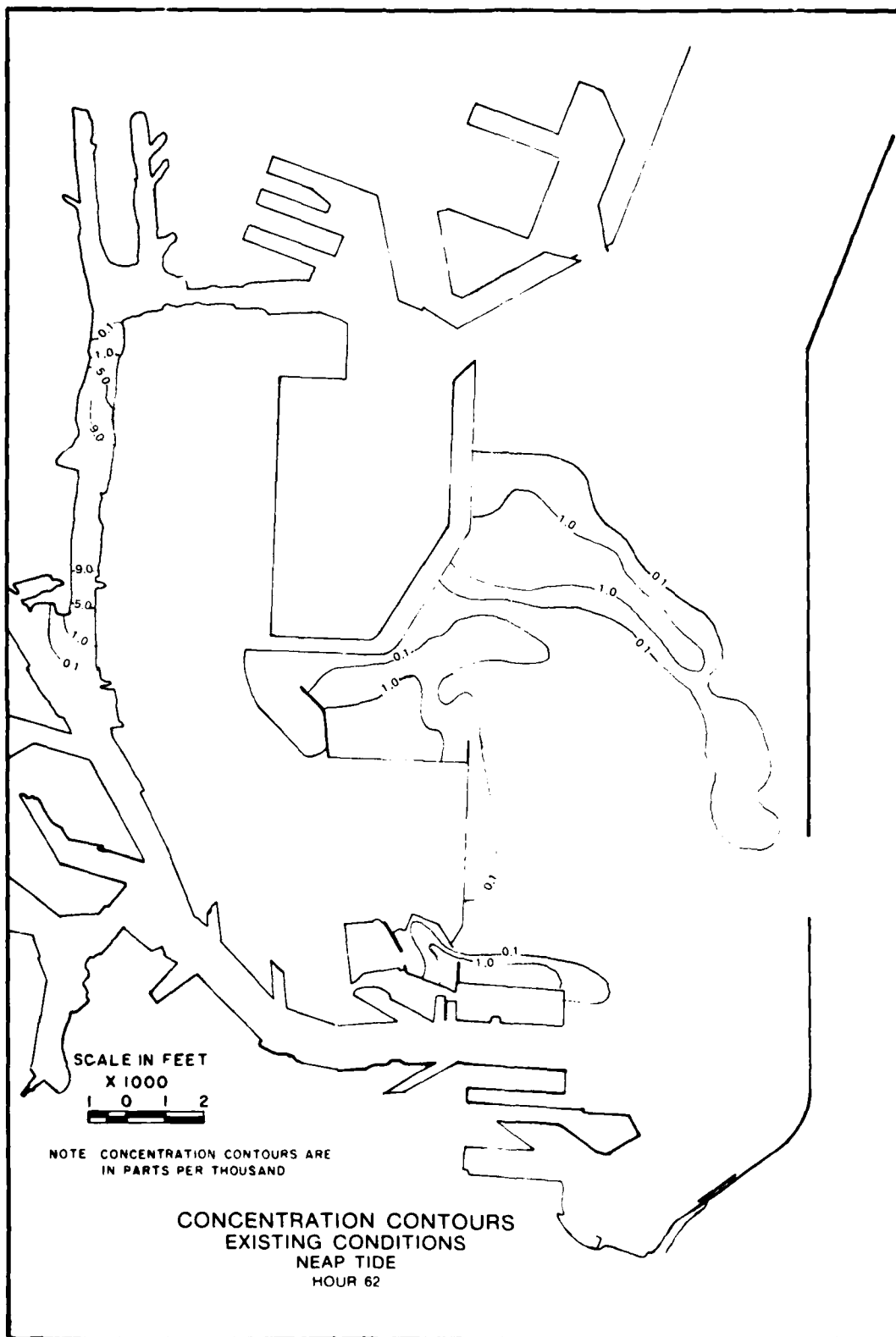


Plate 128



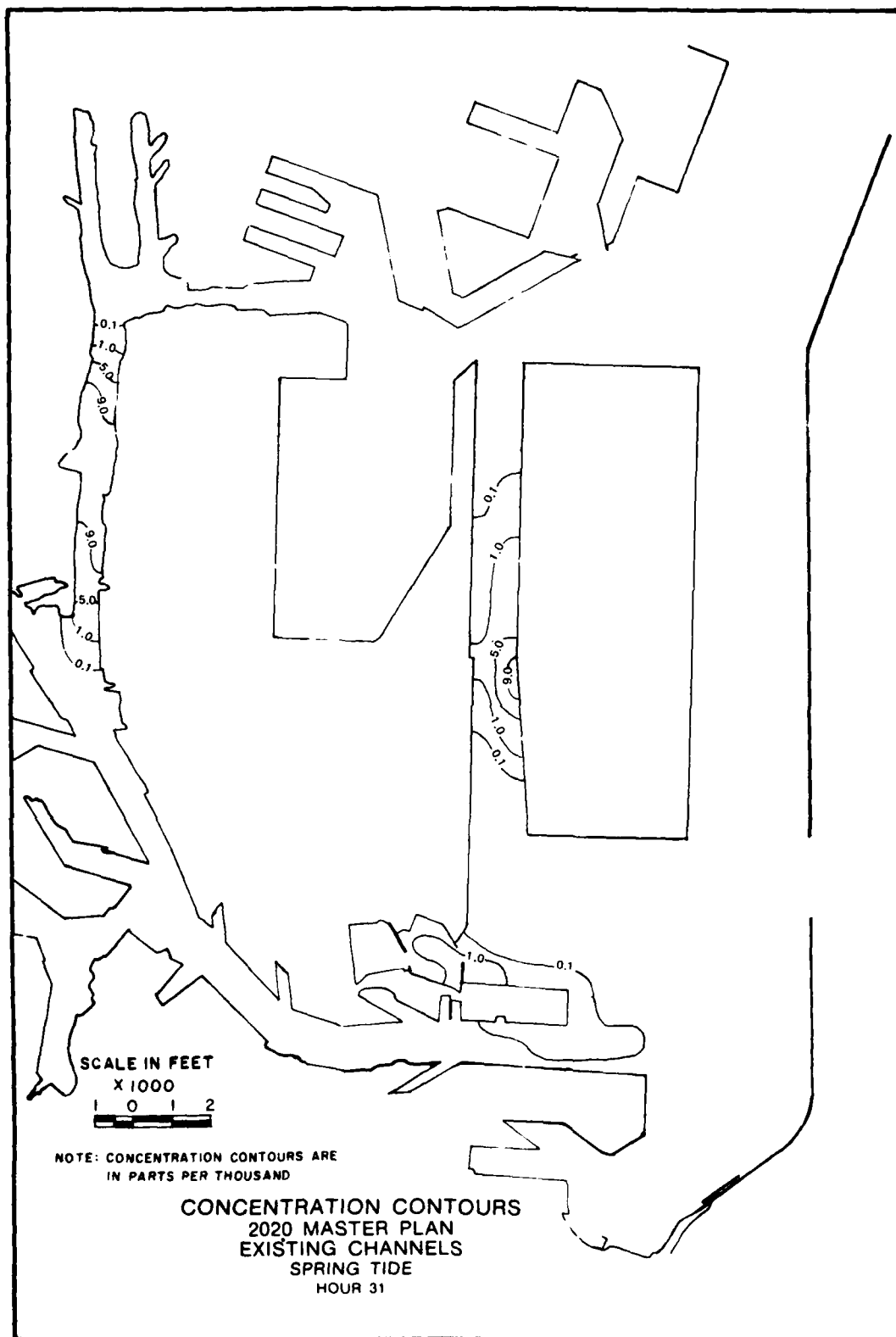
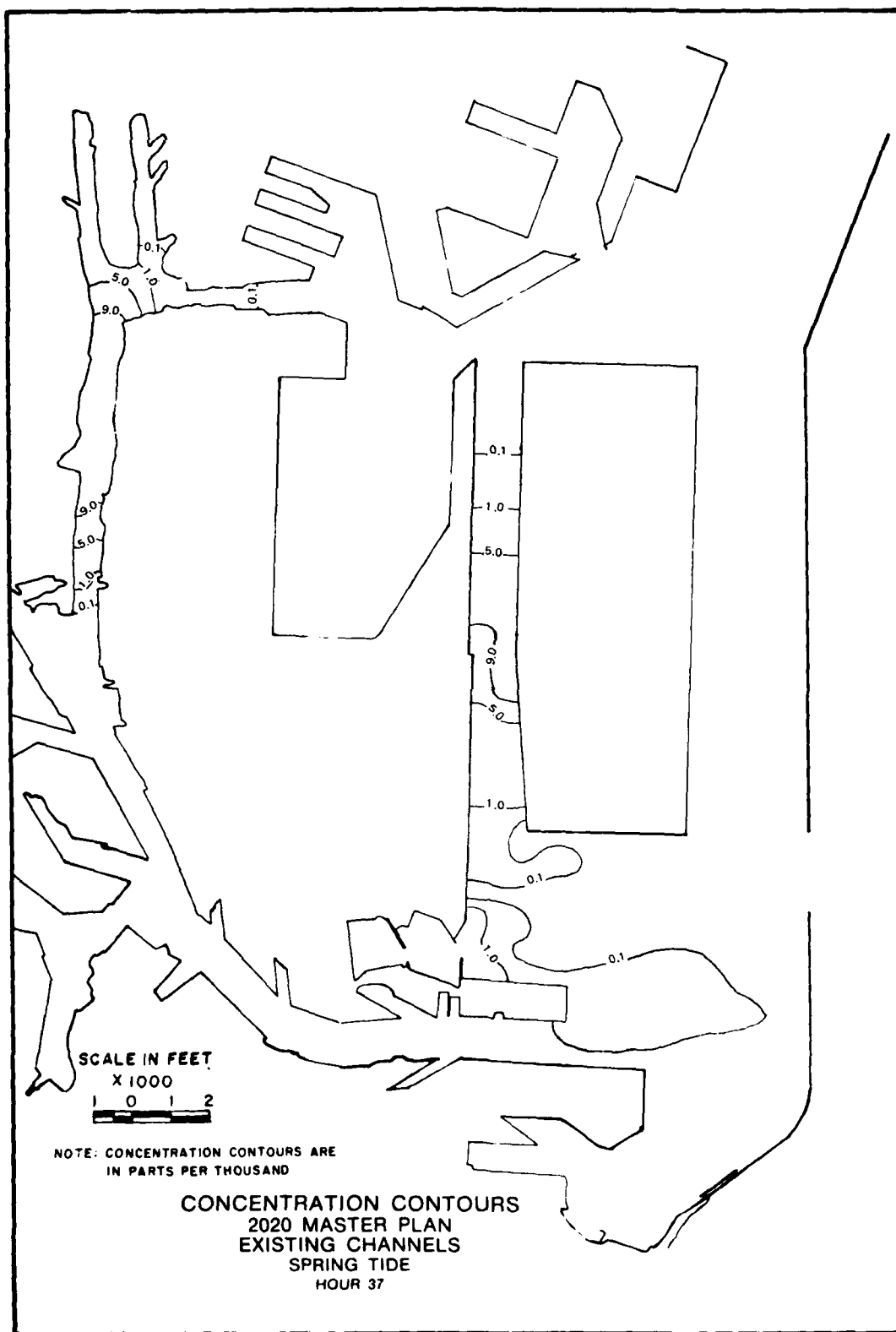
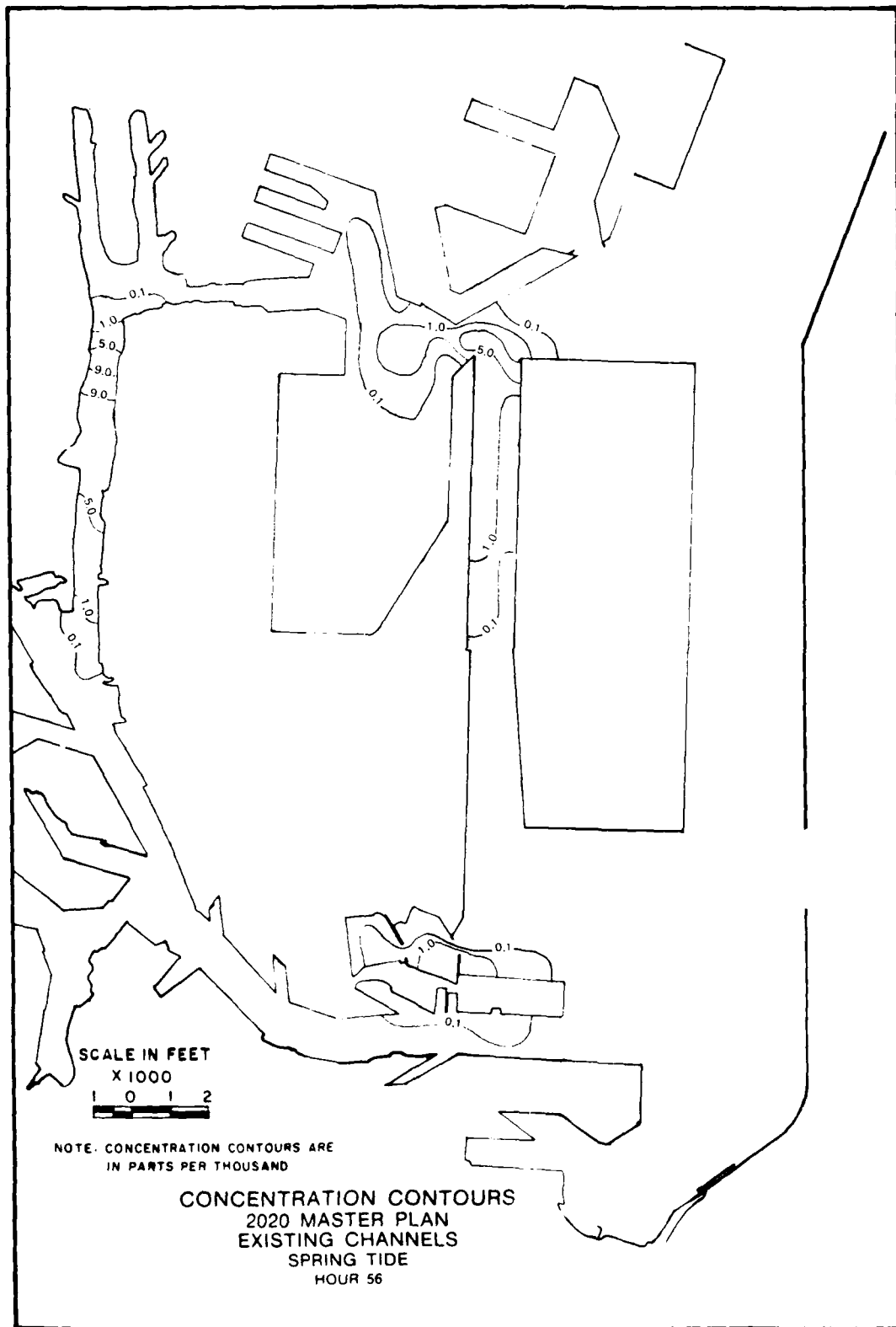


Plate 130





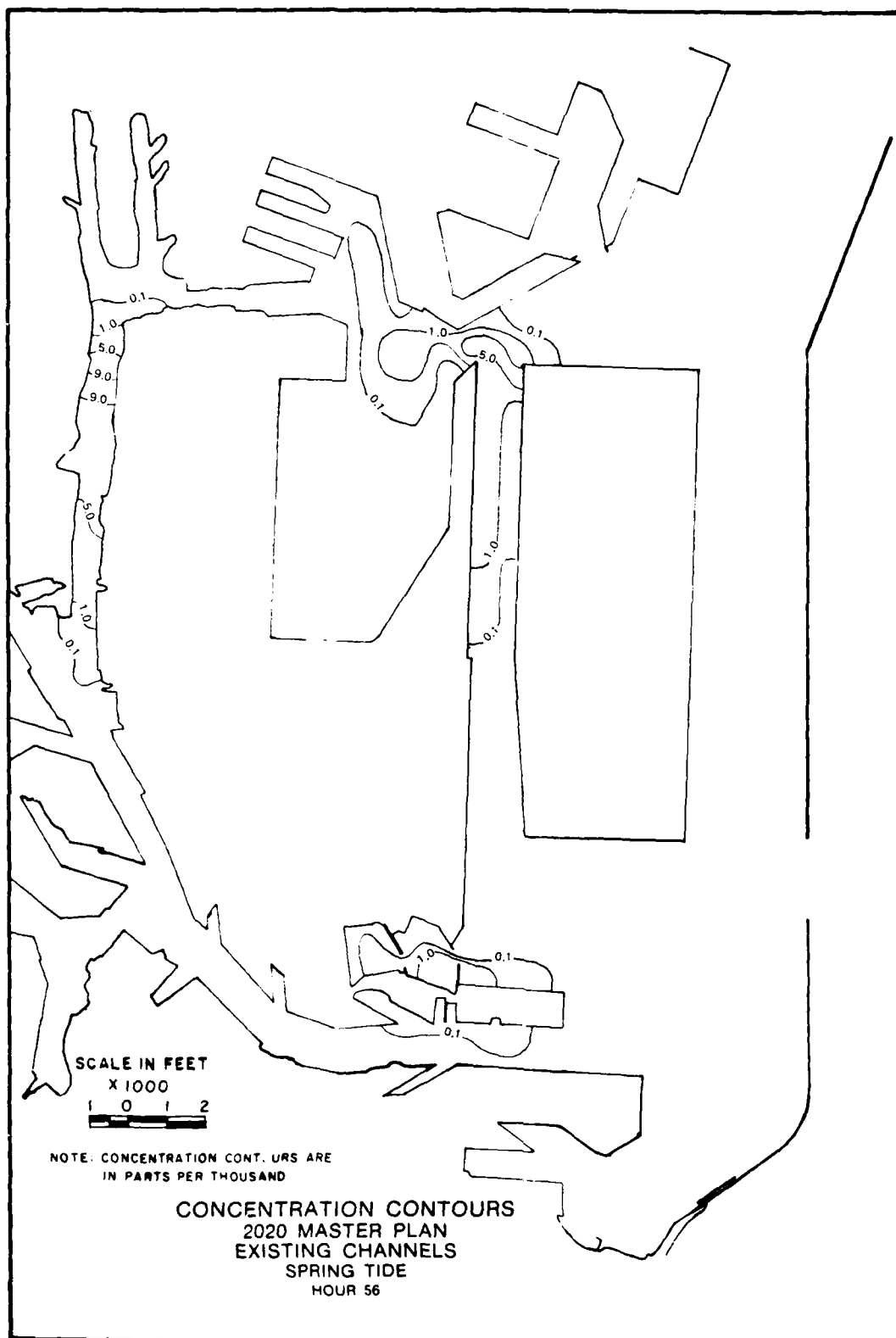
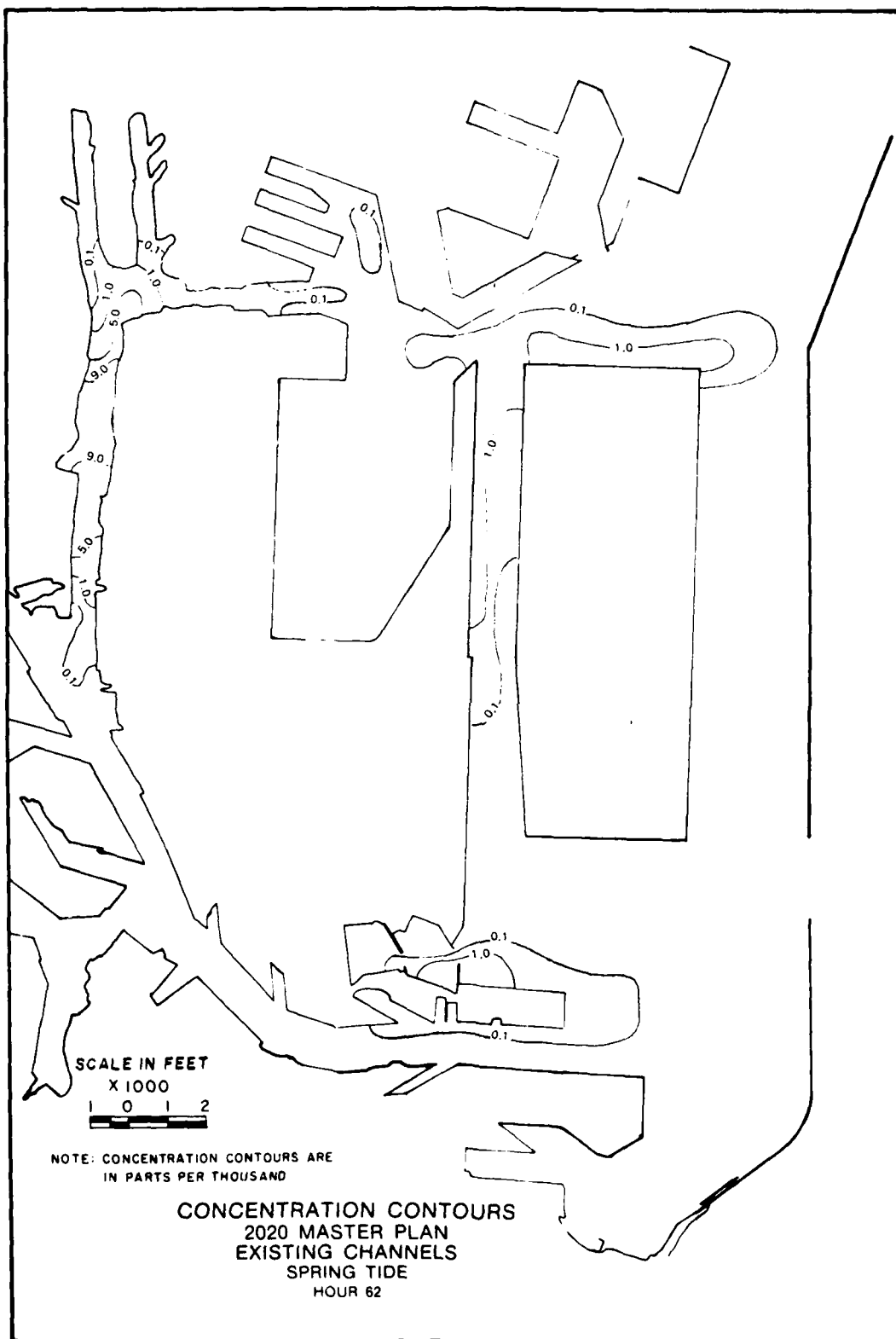


Plate 132



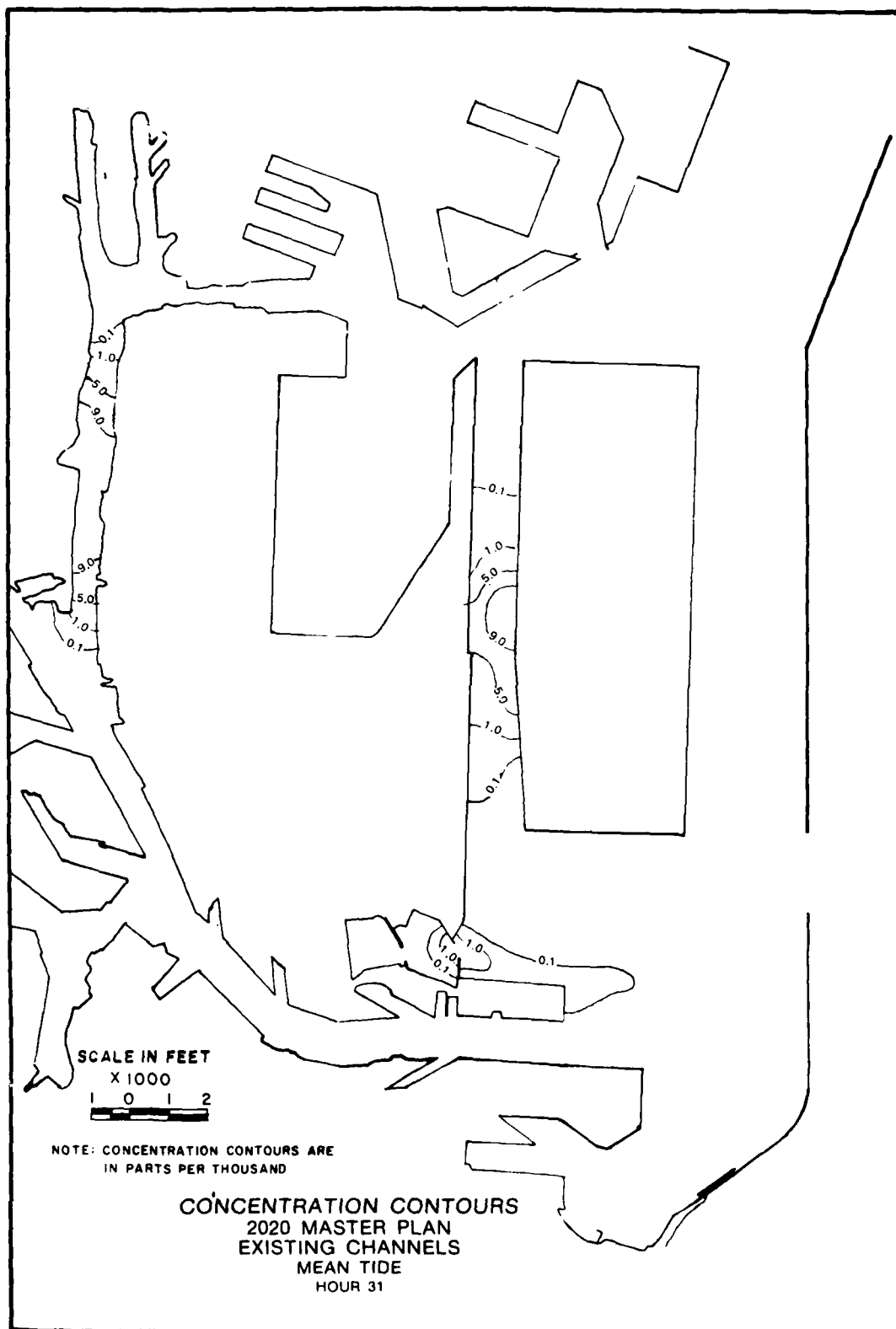
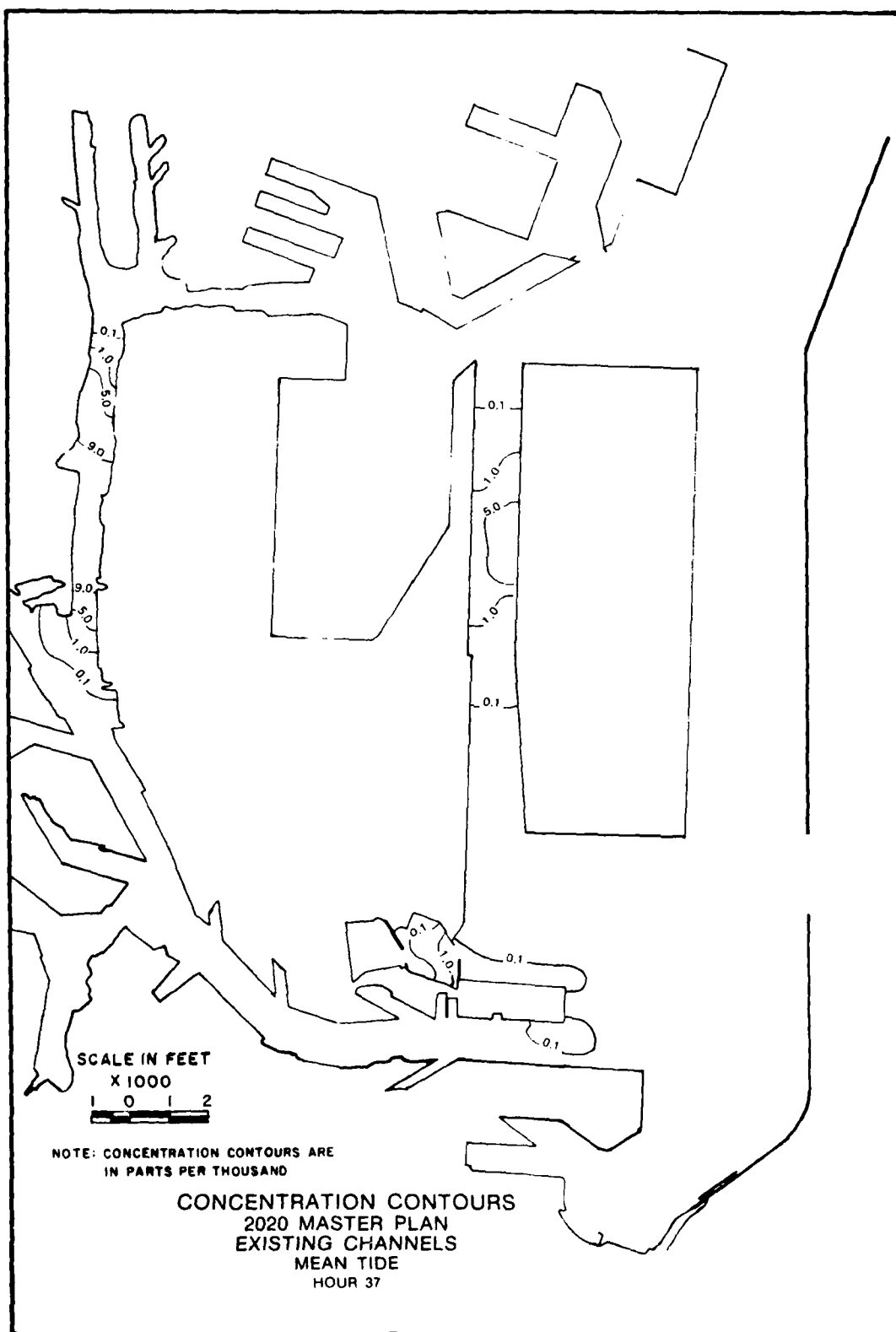
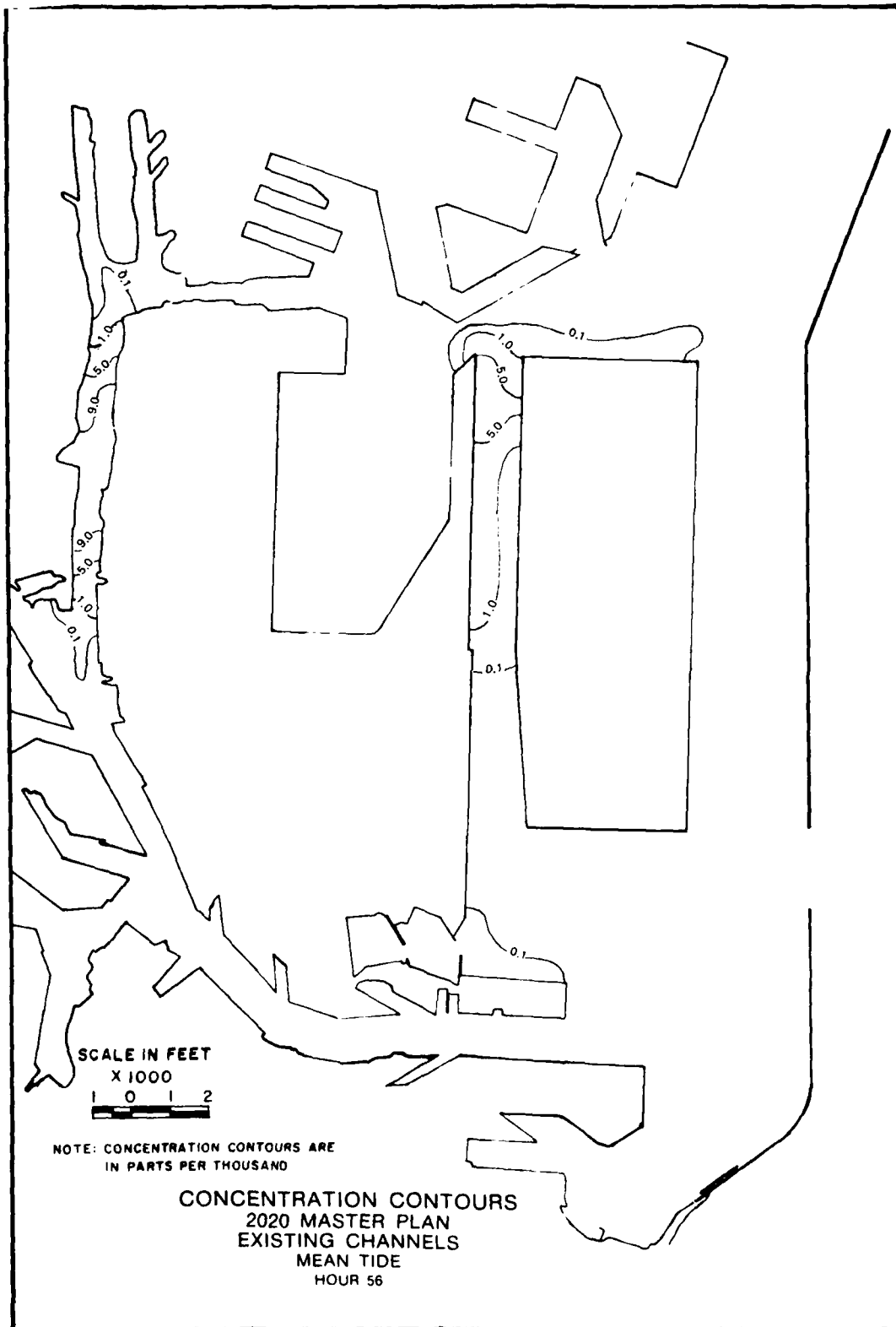
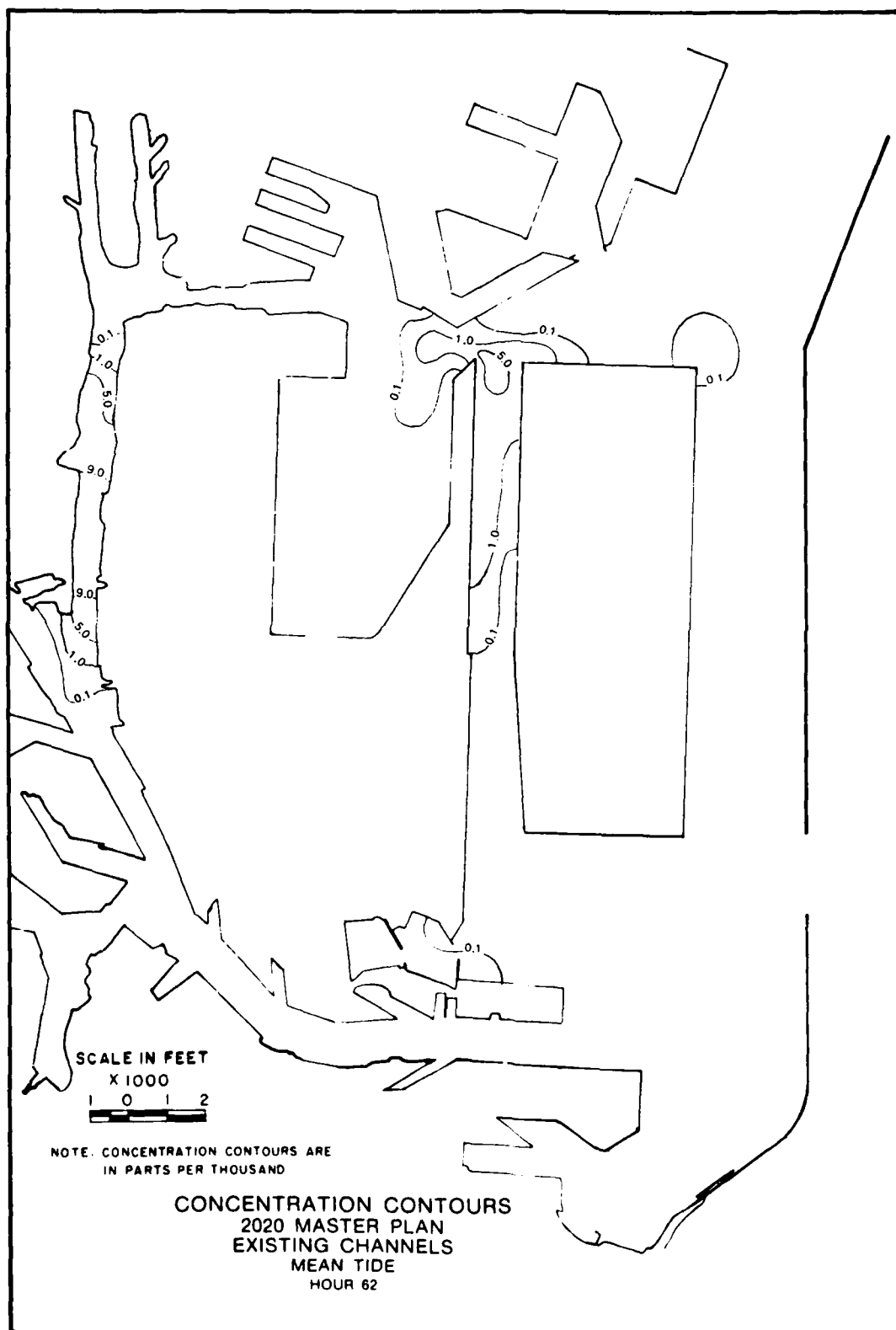


Plate 134







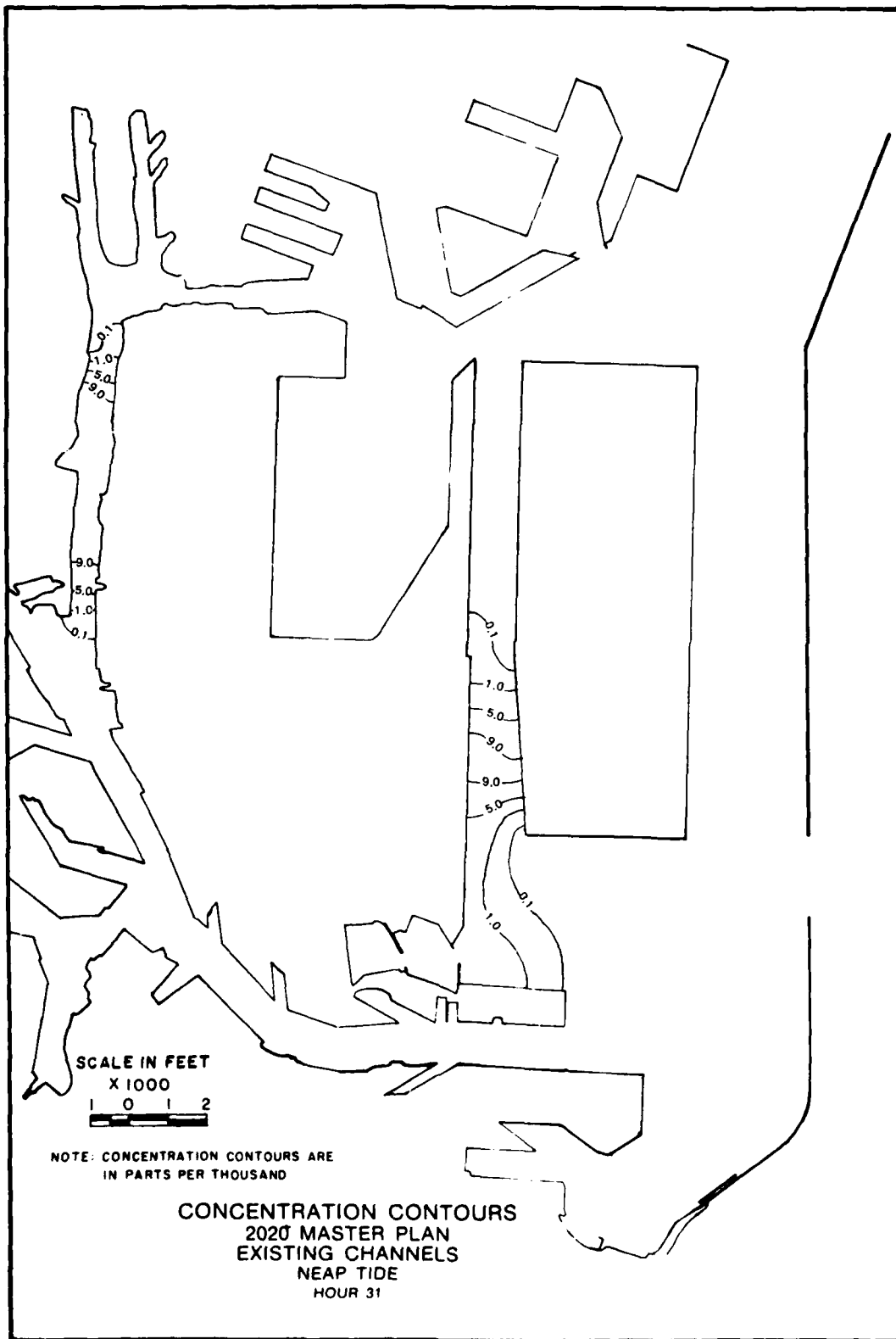
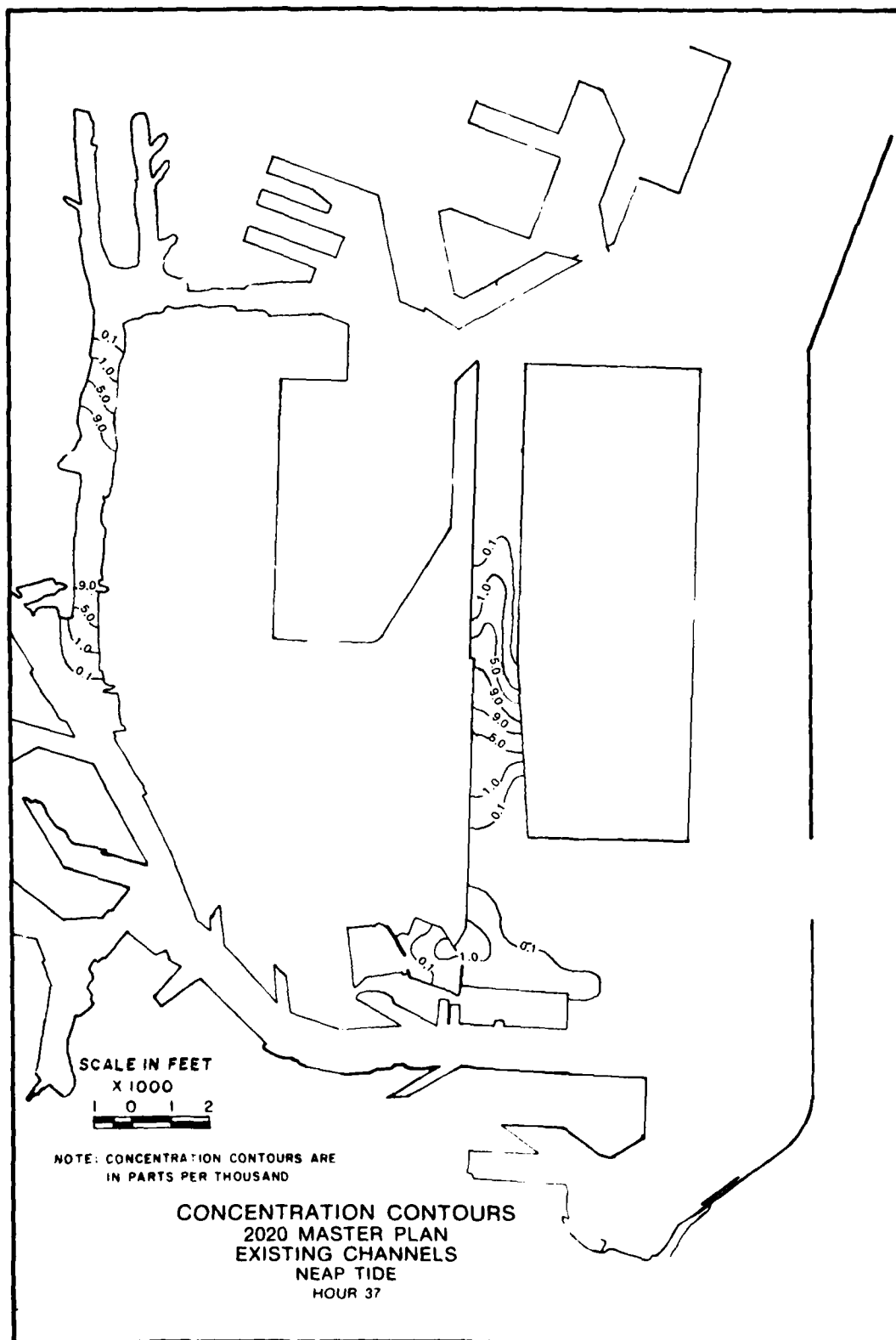


Plate 138



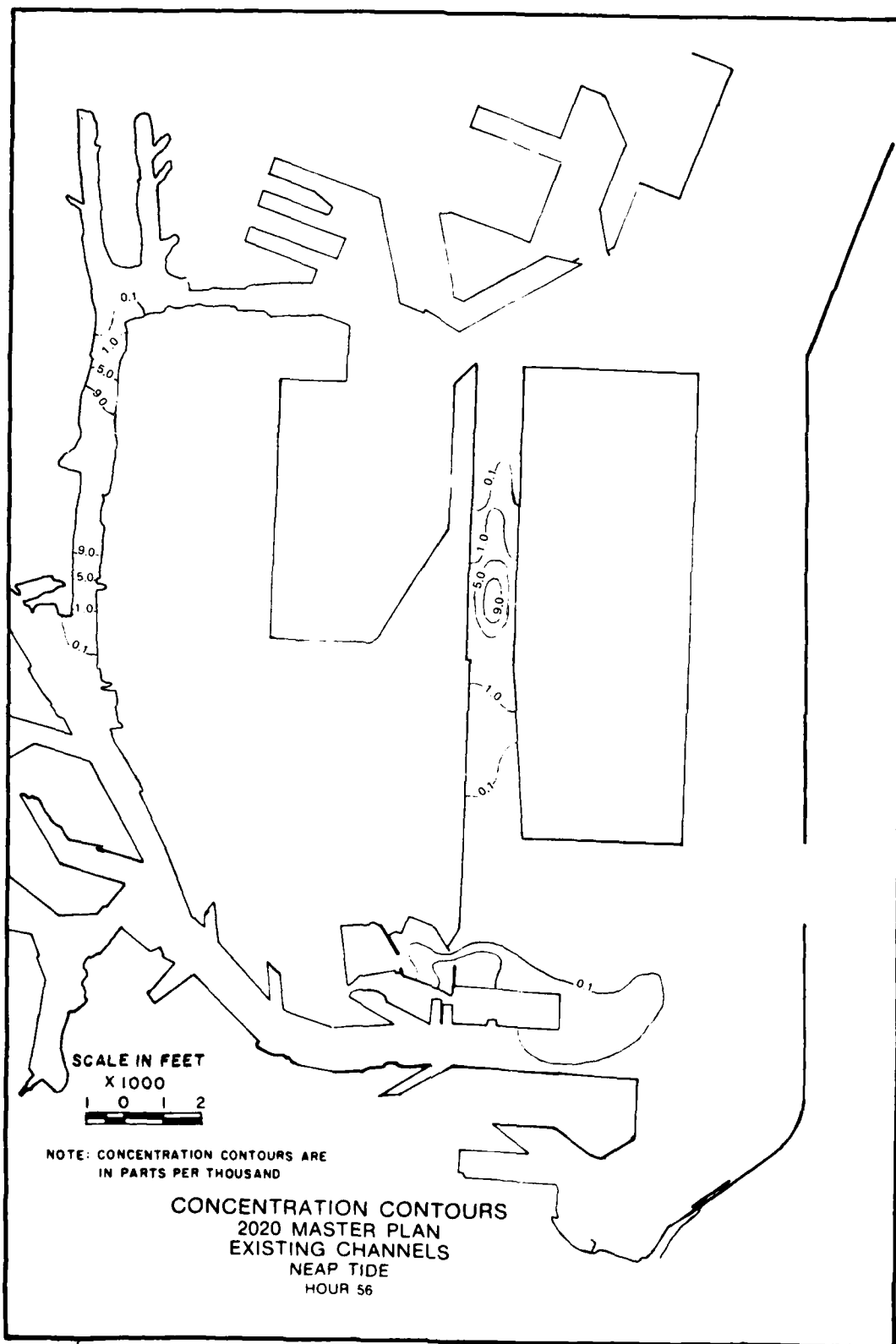
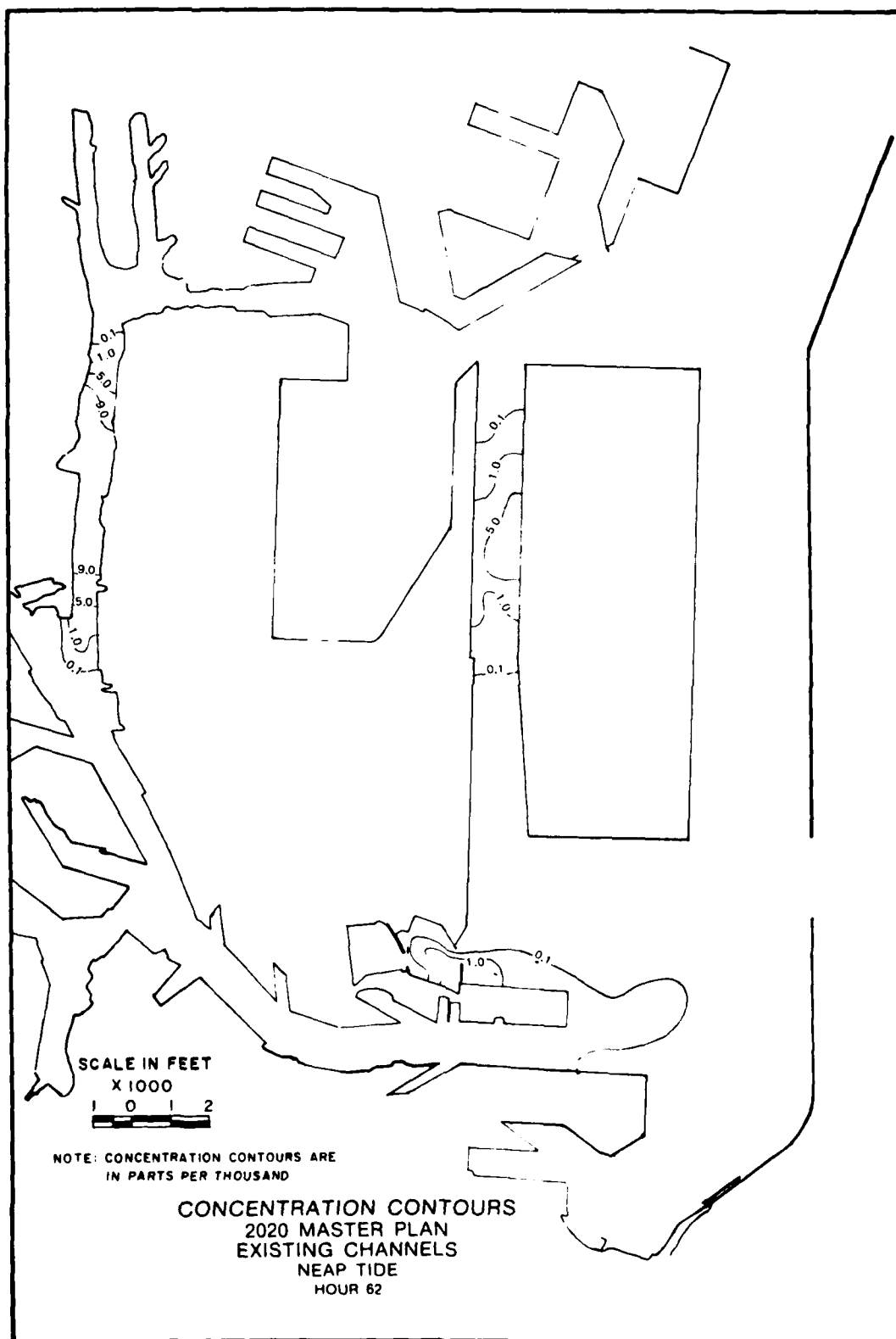


Plate 140



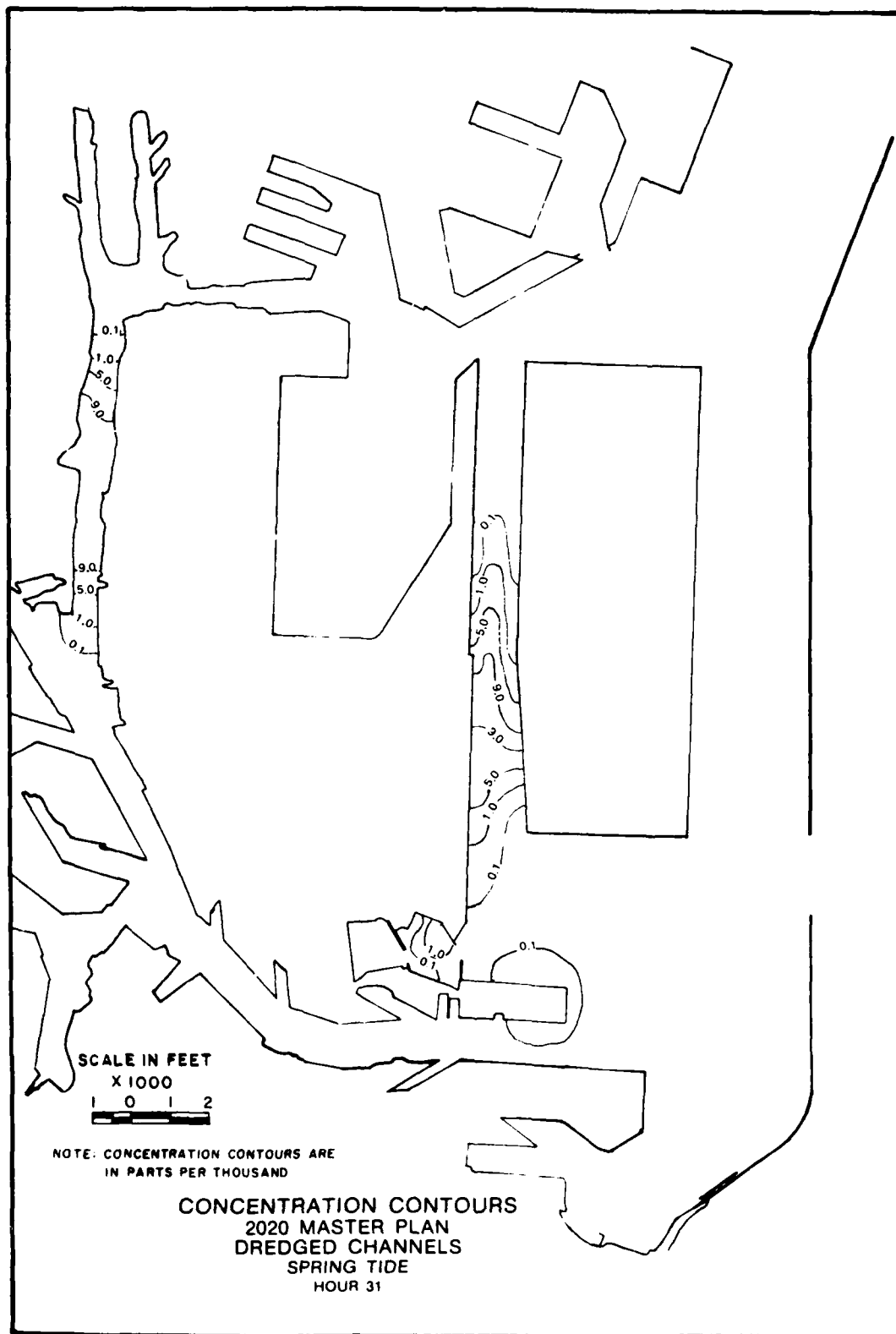
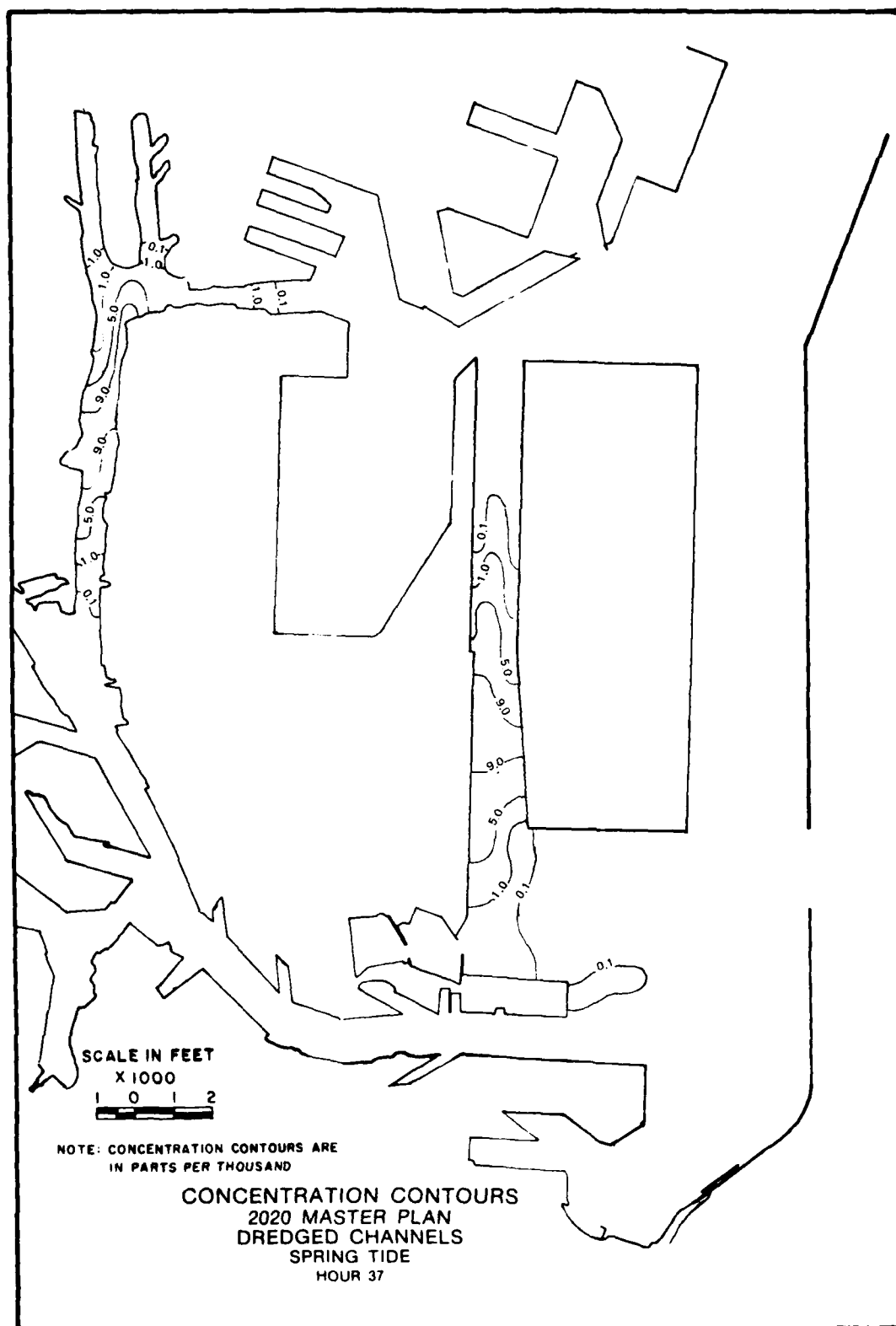
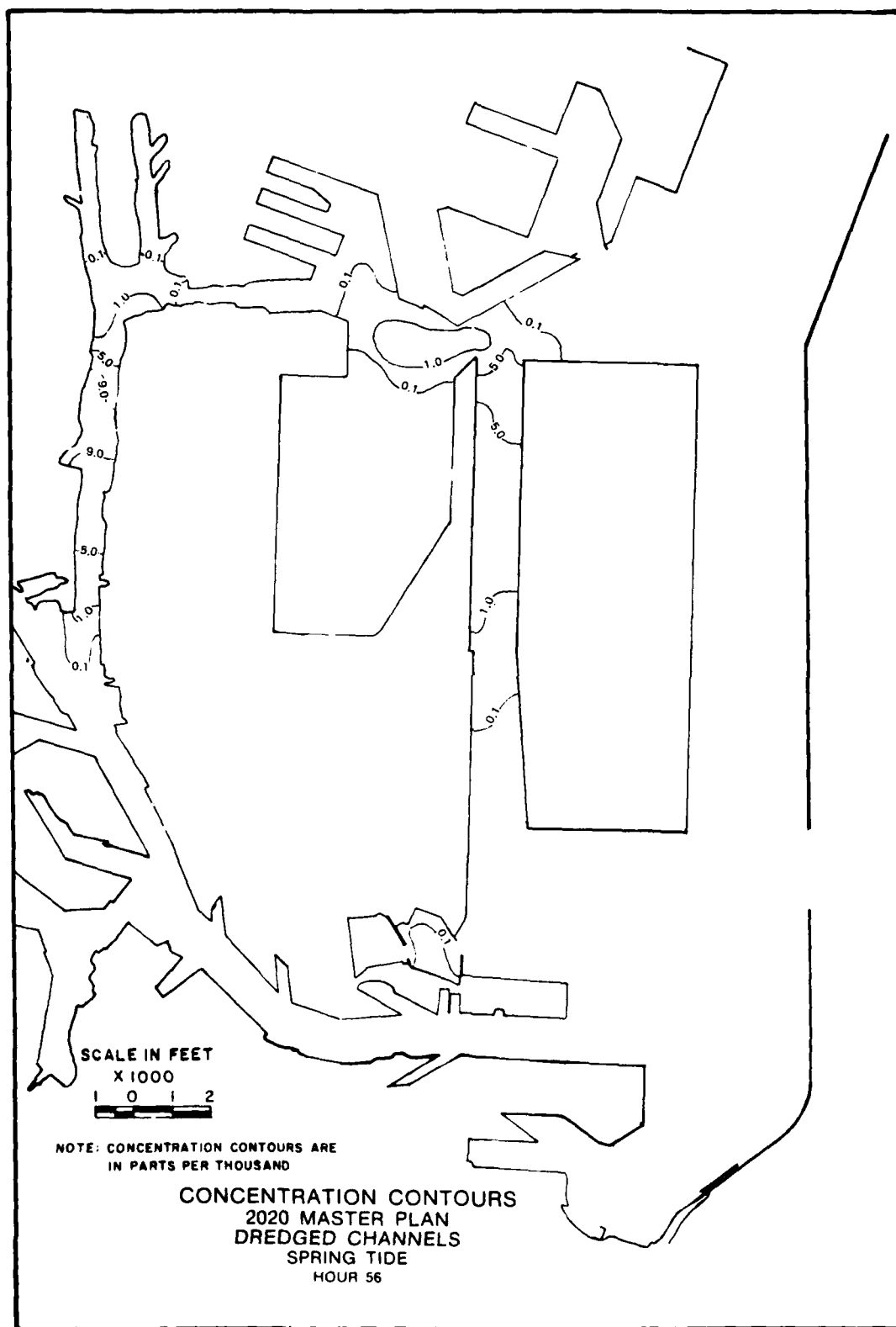
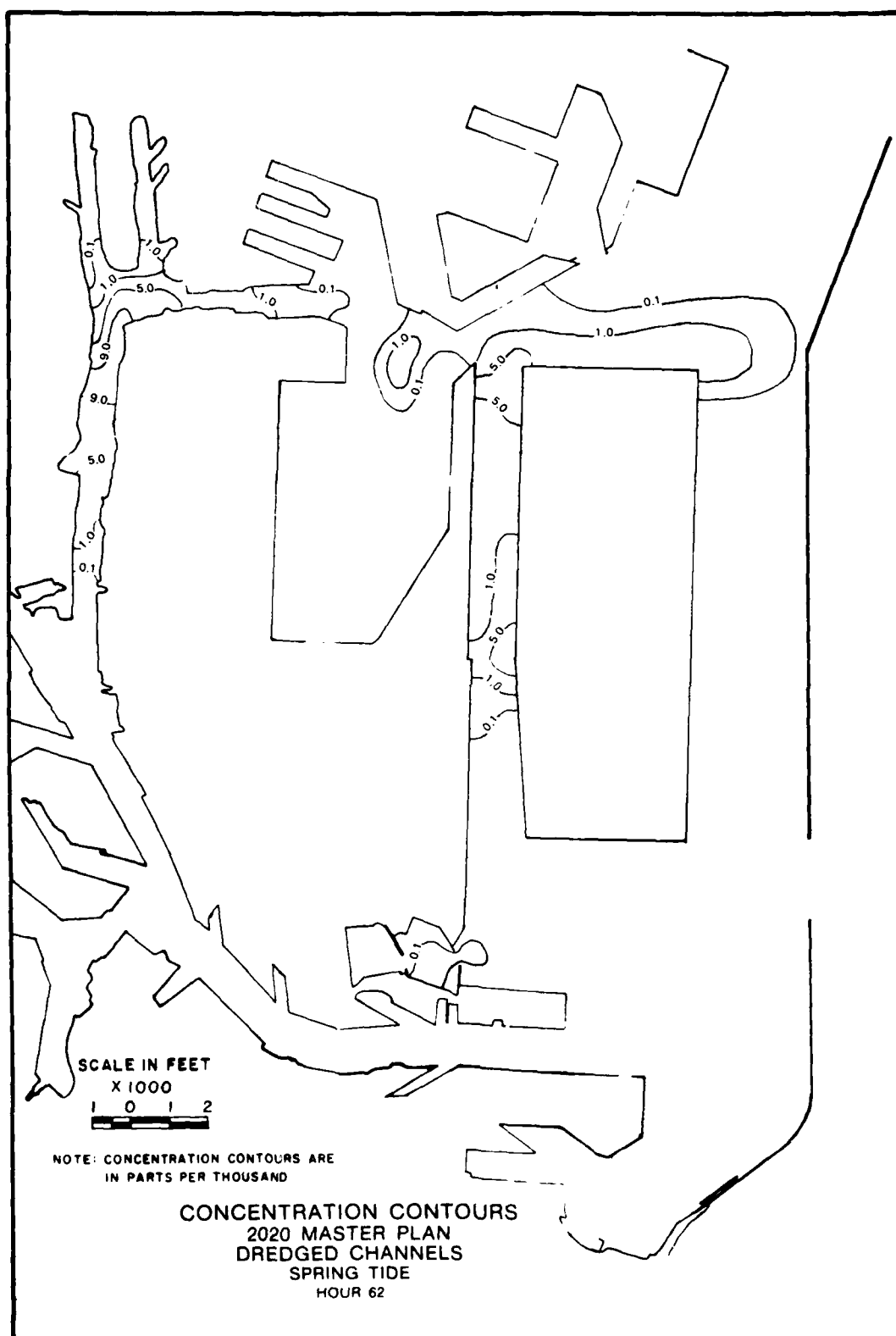


Plate 142







AD-A145 142 LOS ANGELES AND LONG BEACH HARBORS MODEL STUDY
NUMERICAL ANALYSIS OF TIDA..(U) COASTAL ENGINEERING
RESEARCH CENTER VICKSBURG MS W C SEABERGH ET AL.
UNCLASSIFIED JUN 84 CERC-MP-84-5 F/G 8/3

LOS ANGELES AND LONG BEACH HARBORS MODEL STUDY
NUMERICAL ANALYSIS OF TIDA..(U) COASTAL ENGINEERING
RESEARCH CENTER VICKSBURG MS W C SEABERGH ET AL.
JUN 84 CERC-MP-84-5 F/G 8/3

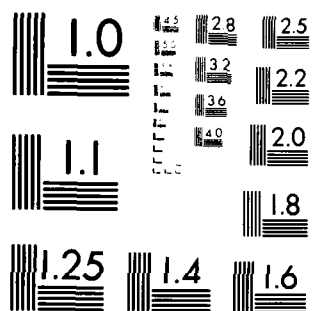
3/3

JUN 84 CERC-MP-84-5

F/G 8/3

NL

END
DATE
FILMED
10-84
DTIC



MICROCOPY RESOLUTION TEST CHART
NATIONAL BUREAU OF STANDARDS-1963-A

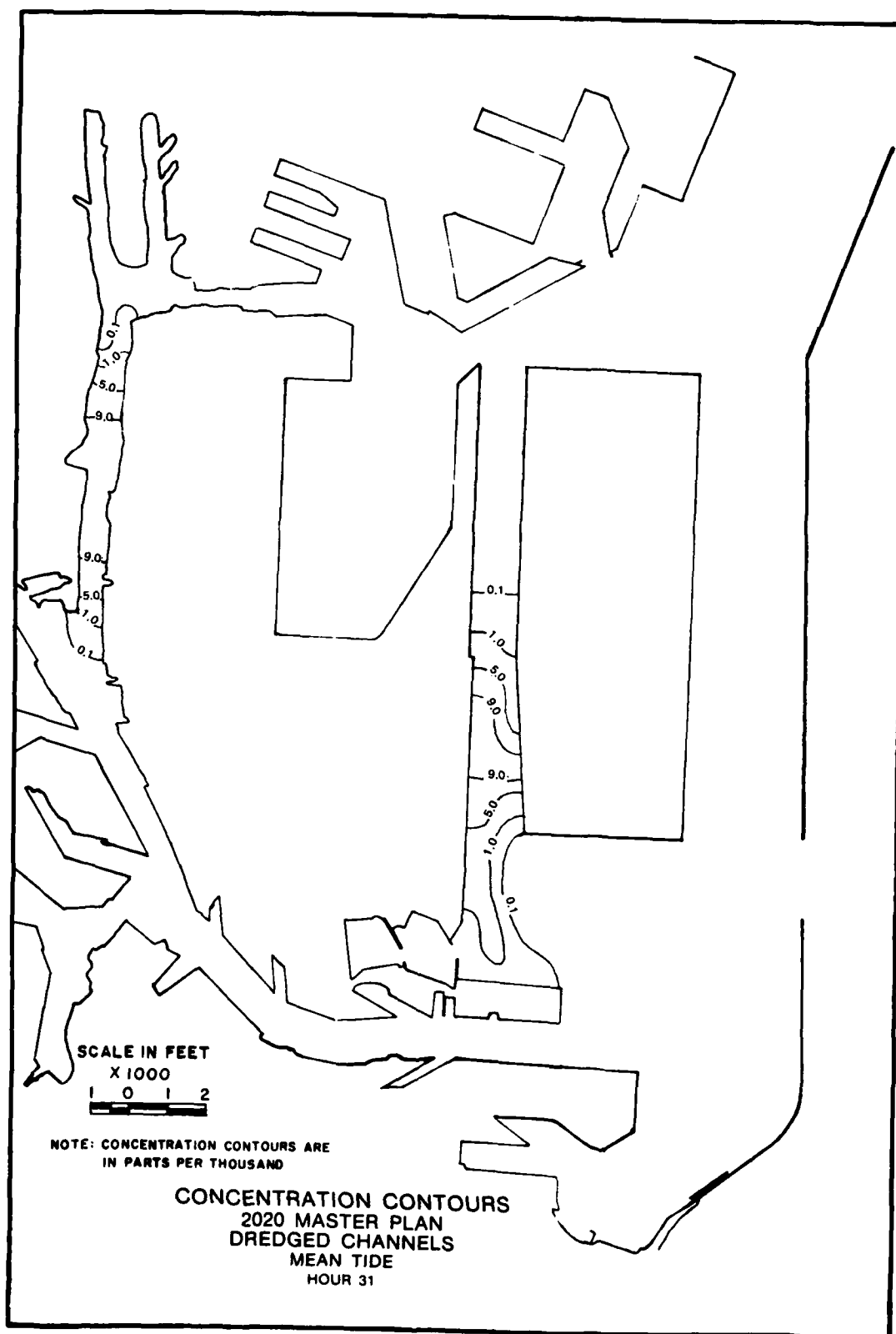
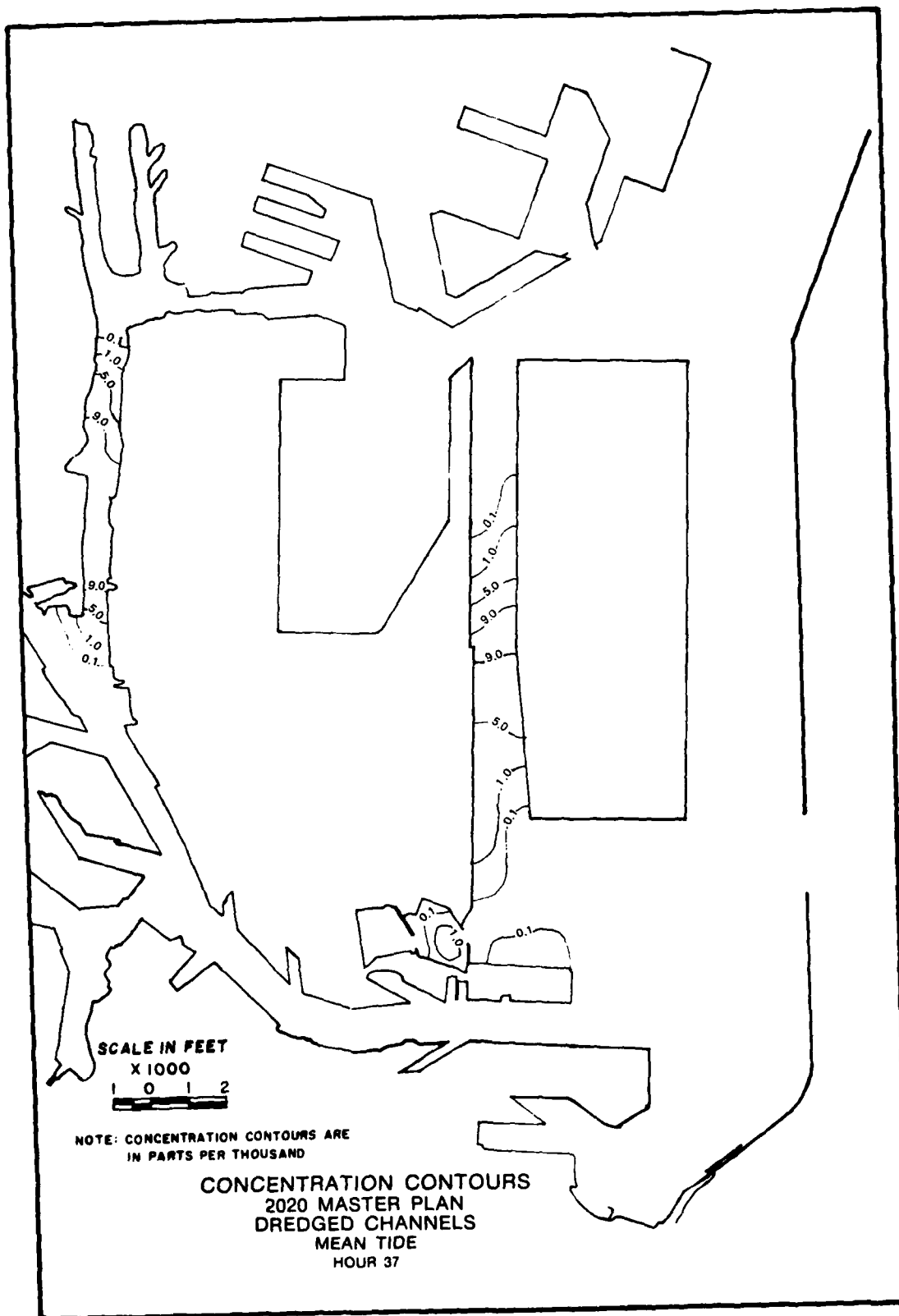


Plate 146



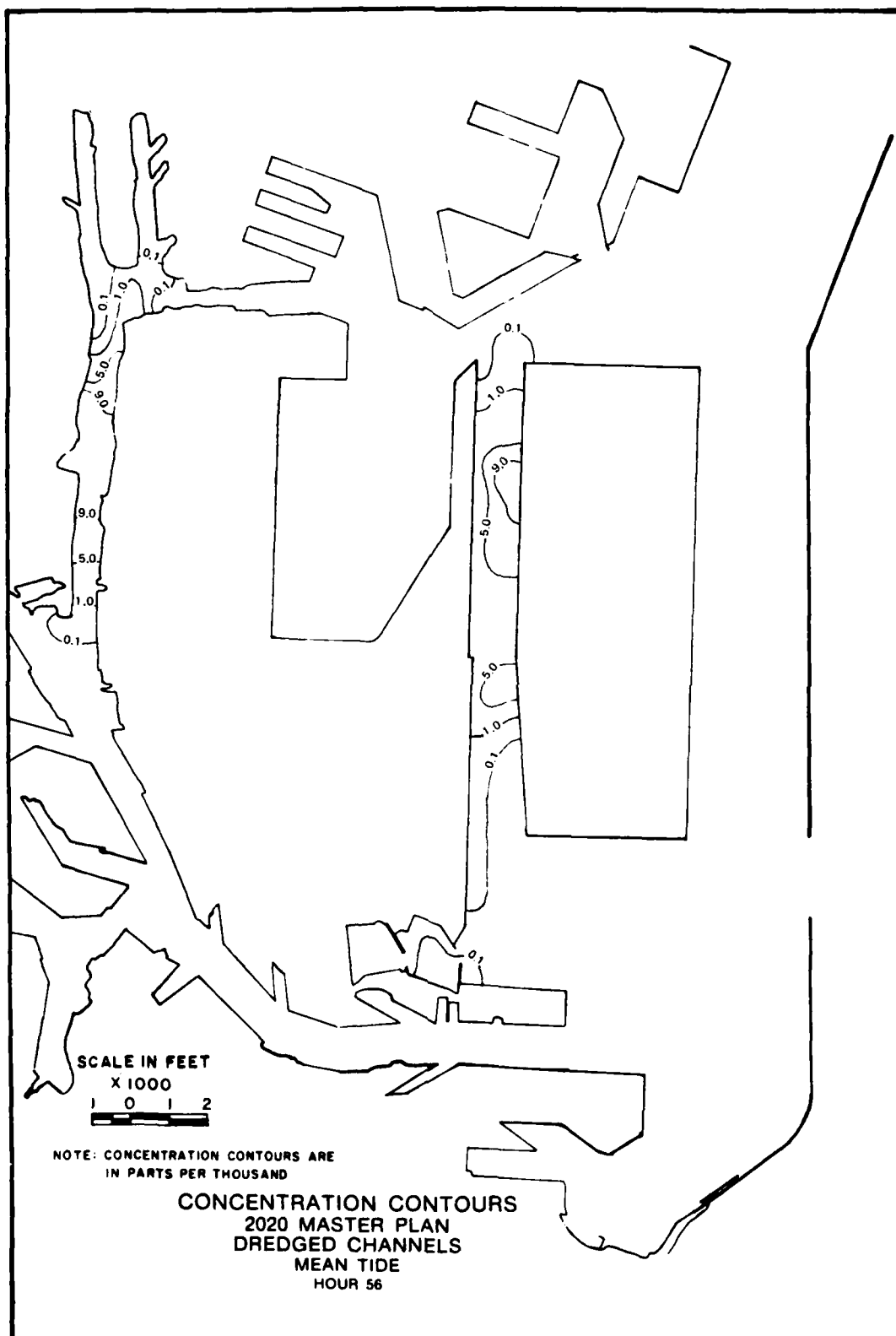
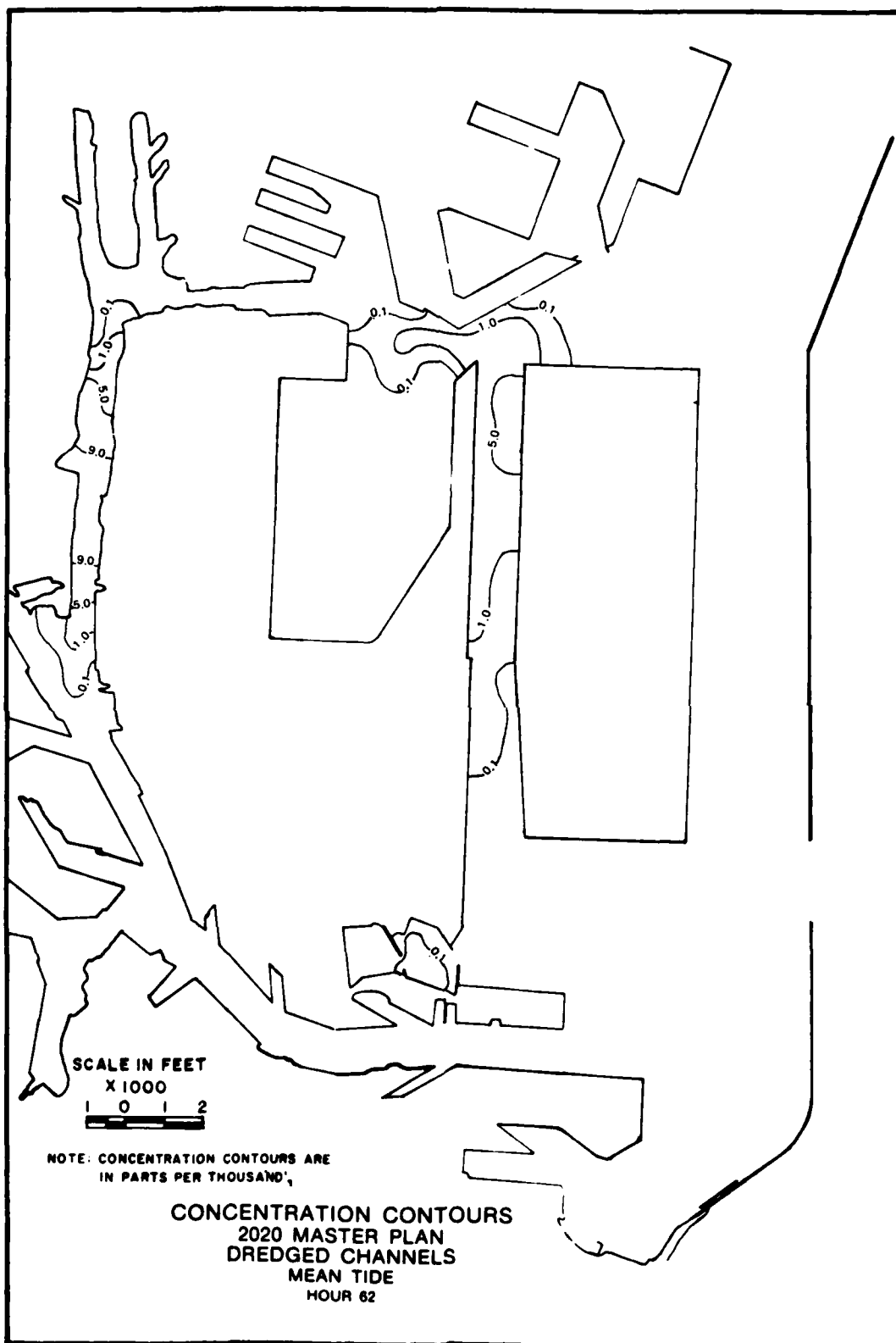


Plate 148



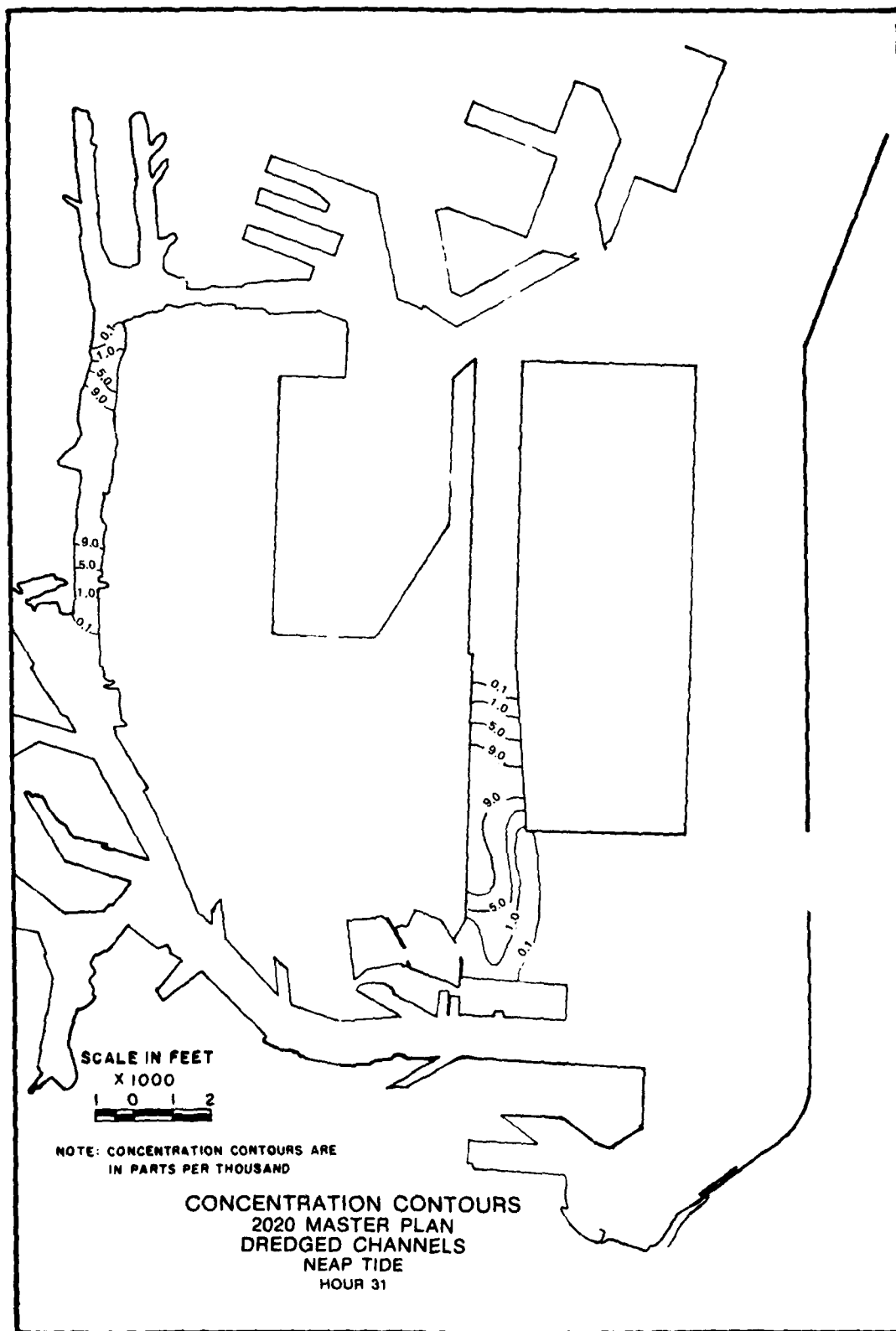
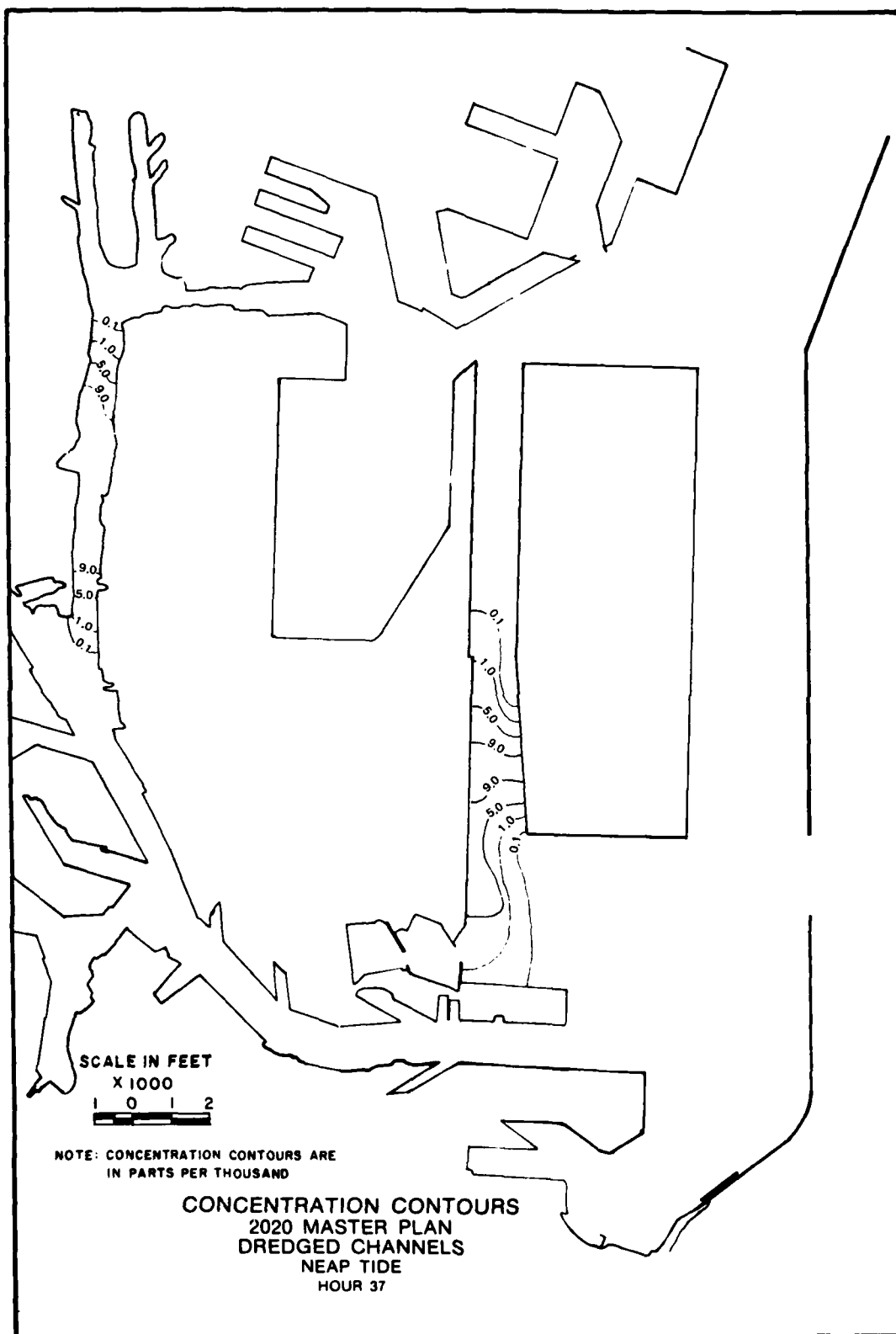


Plate 150



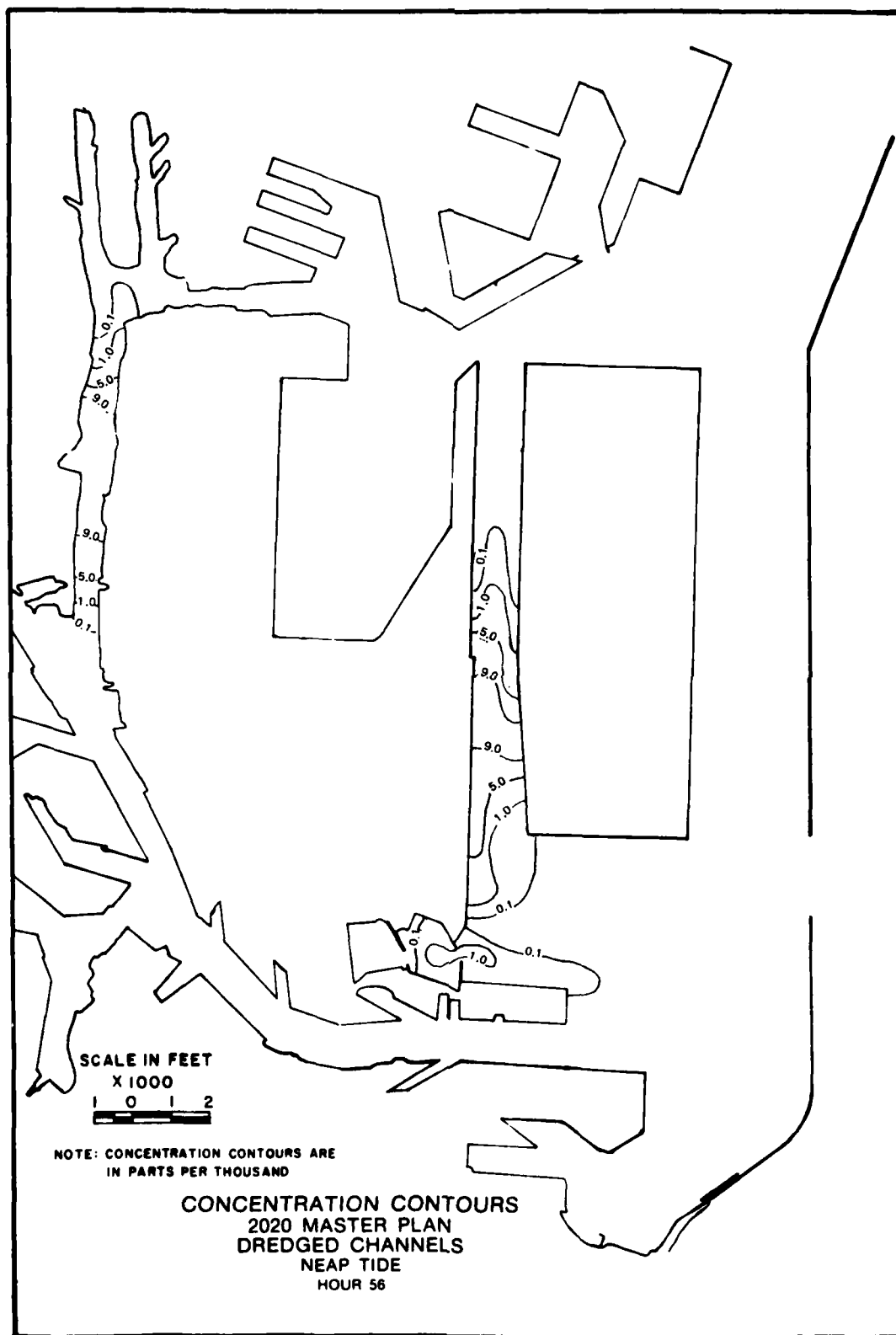


Plate 152

